Intrinsic Disorder and Coiled Coil formation in Prostate Apoptosis Response factor-4 (Par-4)

Submitted in fulfilment of the requirements
of the degree of Doctor of Philosophy

Institute of Fundamental Sciences
Massey University
New Zealand

Martin Schwalbe

2010

Abstract

Prostate apoptosis response factor-4 (Par-4) is a ubiquitously expressed pro-apoptotic and tumour suppressive protein. Par-4 contains a highly conserved coiled coil (CC) region at the C-terminus, particularly the distal 40 residues fulfil the criteria for a leucine zipper (LZ). This C-terminal domain serves as the primary recognition domain for a large number of binding partners. Par-4 is tightly regulated by the aforementioned binding partners and also by post-translational modifications. Biophysical data presented here describe Par-4 as primarily an intrinsically disordered protein (IDP). Bioinformatic analysis of the highly conserved Par-4 reveals low sequence complexity and enrichment in polar and charged amino acids. High proteolytic susceptibility and increased hydrodynamic radii are consistent with largely extended structures in solution. Spectroscopic measurements using circular dichroism (CD) and nuclear magnetic resonance (NMR) also reveal characteristic features of intrinsic disorder. Under physiological conditions, data show that Par-4 self-associates via the C-terminal domain possibly through coiled coil formation. Analysis of various constructs comprising the Par-4 LZ domain by NMR, CD, light scattering and other techniques reveals an environment-dependent conformational equilibrium between primarily disordered monomers and predominantly coiled coil dimers. Whereas the disordered monomers are easily observed by NMR, the coiled coil fraction is not amenable to NMR studies possibly due to intermediate exchange processes. Mutational approaches that stabilise the coiled coil fraction result in NMR spectra of lower quality compared to the wild-type form. The high degree of sequence conservation suggest that coiled coil formation and intrinsic disorder are essential for Par-4 to function as an effective regulator of apoptosis.

Acknowledgements

I would like to thank my Supervisor Dr. Steve Pascal for his patience with me. I further like to thank him and my Co-Supervisor Dr. Andrew Sutherland-Smith for invaluable advice on how to study Par-4, but also for never-ending ideas of what I could do next. I also wish to thank Dr. Pat Edwards for his brilliant assistance with the acquisition and analysis of NMR spectra. In this context I also like to thanks Dr. Stephen Headey and Dr. Jo Claridge. Dr. David Libich for pushing us on to the intrinsic disorder track and the amount of time he spent on helping to finish the publication. Trevor Loo for a phenomenal assistance with cloning and protein purification. Dr. Alice Clark, Dr. Greg Sawyer, Dr. Matt Bennett and Jan Richter for their help in teaching an NMR spectroscopist how to get crystals and everything related to crystallisation. Professor Geoff Jameson, Dr. Gill Norris and Dr. Mark Patchett for interesting discussions during the lab meetings. I wish to thanks Andrew and Alice again for turning a German grammar inspired thesis into proper English (at least I hope so). All members of the Centre for Structural Biology I forgot to mention for a great atmosphere in the group, for their assistance and for their advice. As I was not working all the time in the lab, I would like to thank all people I regularly met outside Massey for their friendship, encouragement and distraction. This includes the staff of the Celtic for the “Happy Hour” and all people of the Celtic Crowd, as enjoying a pint with friends is more fun than drinking it alone. In particular I have to say thanks to my golf flight, Nick Bennett, Jo Claridge, Greg Sawyer, Craig van Stratum and Raymond Illston for entertainment on the course (even when I enforced playing in the rain) and on the 19th hole. Finally, I wish to thank my family for their never-ending support, even though I was on the other side of the world.

Glossary of Abbreviations

A_{XXX}	**A**bsorption at **XXX** nm
AATF	**A**poptosis-**a**ntagonising **t**ranscription **f**actor
Apaf-1	**A**poptotic **p**rotease **a**ctivating **f**actor-1
Amp	**Amp**icillin
Aβ	**A**myloid **β**-peptide
aPKC	**a**typical **p**rotein **k**inase **C**
APP	**A**myloid **p**recursor **p**rotein
AR	**A**ndrogen **r**eceptor
AU	**A**nalytical **U**ltracentrifugation
BACE-1	**β**-site **A**PP **c**leaving **e**nzyme-1
BCA	**B**icin**c**honin**a**cid
CAD	**C**aspase **a**ctivated **D**Nase
Cam	**C**hlor**am**phenicol
CARD	**C**aspase **a**ctivation and **r**ecruitment **d**omain
CC	**C**oiled **c**oil
CD	**C**ircular **d**ichroism
cFLIP	**c**ellular **F**LICE-**l**ike **i**nhibitory **p**rotein
CHT1	**Ch**oline **t**ransporter 1
CM	**C**arboxy**m**ethyl
D2DR	**D**opamine **D2 r**eceptor
DAP	**D**eath-**a**ctivated **p**rotein kinase
DD	**D**eath **d**omain
DED	**D**eath **e**ffector **d**omains
DIABLO	**D**irect **I**AP-**b**inding protein with **lo**w pI
DISC	**D**eath-**i**nducing **s**ignalling **c**omplex
Dlk	**D**AP **l**ike **k**inase
DLS	**D**ynamic **l**ight **s**cattering
DOM	**D**is**o**rdered **m**onomer
DTT	**Di**thio**t**hreitol
EDC	1-**e**thyl-3-(3-**d**imethylaminopropyl)**c**arbodiimide
EDTA	**E**thylene**d**iamine**t**etraacetic **a**cid
ER	**E**ndoplasmatic **r**eticulum
ERK	**E**xtracellular signal **r**egulated **k**inase
FADD	**F**as **a**ssociated **d**eath **d**omain
FLICE	**F**ADD-**l**ike **i**nterleukin 1β **c**onverting **e**nzyme (= caspase 8)
GRP78	**G**lucose-**r**egulated **p**rotein-78
GST	**G**lutathione **S**-**T**ransferase

HCA	**H**ydrophobic **c**luster **a**nalysis
HMBP-3Cpro	**H**exa-histidine-**MBP**-tagged **3C** **pro**tease
HMQC	**H**eteronuclear **m**ultiple-**q**uantum **c**oherence
HSQC	**H**eteronuclear **s**ingle-**q**uantum **c**oherence
IAP	**I**nhibitors of **ap**optosis
ICAD	**I**nhibitor of **c**aspase **a**ctivated **D**Nase
ID	**I**ntrinsic **d**isorder
IDP	**I**ntrinsically **d**isordered **p**rotein
IEC	**I**on-**e**xchange **c**hromatography
IκB	**I**nhibitor of **κB** family
IKK	**Iκ**B **k**inase
IMAC	**I**mmobilised **m**etal ion **a**ffinity **c**hromatography
IPTG	**I**so**p**ropyl-β-D-**t**hio**g**alactopyranoside
Kan	**Kan**amycin
LB	**L**uria **B**ertani medium
LZ	**L**eucine **Z**ipper
MALLS	**M**ulti-**A**ngle **L**aser **L**ight **S**cattering
MAPK	**M**itogen-**a**ctivated **p**rotein **k**inases
MBP	**M**altose **b**inding **p**rotein
Mes	2-**Mo**rpholino**e**thane**s**ulfonic acid
MOPS	3-(N-**Mo**rpholino)**p**ropane**s**ulfonic acid
MS	**M**ass **s**pectrometry
MW	**M**olecular **w**eight
MWCO	**M**olecular **w**eight **c**ut **o**ff
NFκB	**N**uclear **f**actor **κB**
NLS	**N**uclear **l**ocalisation **s**equence
NMR	**N**uclear **m**agnetic **r**esonance
NOESY	**N**uclear **O**verhauser **E**ffect **S**pectroscop**y**
NRMSD	**N**ormalised **r**oot **m**ean **s**quare **d**eviation
NTA	**N**itrilo**tri**a**c**etic acid
OD_{XXX}	**O**ptical **d**ensity at **XXX** nm
Par-4	**P**rostate **a**poptosis **r**esponse factor-**4**
PAGE	**P**oly**a**crylamide **g**el **e**lectrophoresis
PBS	**P**hosphate **b**uffered **s**aline
PCD	**P**rogrammed **c**ell **d**eath
PCR	**P**olymerase **c**hain **r**eaction
PI3K	**P**hospho**i**nositide **3**-**k**inase
PKA, PKB or PKC	**P**rotein **k**inase **A**, **B** or **C**
PML	**P**ro**m**yelocytic **l**eukemia
POD	**P**redominantly **o**rdered **d**imer

PTEN	**P**hosphatase and **ten**sin homolog deleted on chromosome 10
RP-HPLC	**R**eversed **p**hase - **h**igh **p**erformance **l**iquid **c**hromatography
rpm	**R**evolutions **p**er **m**inute
rrPar-4	**r**ecombinant **r**at **P**rostate **a**poptosis **r**esponse factor-**4**
R_S	**S**tokes **r**adius
rTEV	**r**ecombinant **t**obacco **e**tch **v**irus protease
SAC	**S**elective **a**poptosis induction in **c**ancer cells
SAXS	**S**mall-**a**ngle **X**-ray **s**cattering
SEC	**S**ize **e**xclusion **c**hromatography
SDS	**S**odium **d**odecyl **s**ulphate
SMAC	**S**econd **m**itochondria-derived **a**ctivator of **c**aspase
SOC	**S**uper **o**ptimal broth with **c**atabolite repression
SP	**S**ulfo**p**ropyl
SSB1, 2, 4	**S**PRY-domain containing **S**OCS **b**ox proteins 1, 2, 4
TCEP	**T**ris(2-**c**arboxy**e**thyl)**p**hosphine
TFA	**T**ri**f**luoro**a**cetic acid
TFE	**T**ri**f**luoro**e**thanol
T_m	**M**elting **t**emperature
TNFα	**T**umour **n**ecrosis **f**actor **α**
TNFR1	**T**umour **n**ecrosis **f**actor **r**eceptor 1
TOP1	**Top**oisomerase 1
TRAIL	**T**NF-**r**elated **a**poptosis **i**nducing **l**igand
WT	**W**ild **t**ype
WT1	**W**ilm's **t**umour protein **1**
XIAP	**X**-linked **i**nhibitor of **ap**optosis

Contents

List of Figures

List of Tables

1. Introduction

1.1. The pro-apoptotic protein Par-4 - a tumour-suppressor with biological significance

1.1.1. Apoptosis and human disease

Cell proliferation and cell death are two cellular processes essential for the survival of multicellular organisms. Tight control of both these processes is necessary for the evolution of differentiated cell types, ensuring the proper balance between various cell lineages. Intricate regulation of both processes is required for organogenesis and formation of complex multi-cellular tissues during embryonic development. Strict regulation is also essential for tissue homeostasis throughout the life-span of adult organisms [1,2]. Dying cells are eliminated preferentially without causing an inflammatory response and damaging neighbouring cells. This type of regulated cell death is an active cellular suicide process termed programmed cell death (PCD) [3]. The most common form of PCD is a process called apoptosis. A detailed description of apoptosis and the involvement of Par-4 will be discussed in Chapter 1.3.

Disregulation of the intricate balance between cell proliferation and PCD contributes to the pathogenesis of a variety of human diseases. Defects in the suppression of PCD can result in an uncontrolled loss of essential cells as demonstrated for neurodegenerative disorders, immuno-deficiency, ischemia [1] and infertility [2]. In contrast, insufficient PCD may manifest in autoimmune diseases or cancer [1]. Tumour development is a multi-step process and results from the constitutive stimulation of cell proliferation, by active growth signalling factors called oncogenes [4-6]. In response to constitutively active oncogenes normal cells usually undergo apoptosis. However, cancer cells often evade apoptosis because of defects in the PCD machinery. A key step is the inactivation of the so called tumour-suppressor genes. Other important steps in carcinogenesis include angiogenesis and the problem of overcoming cell senescence [4]. Interestingly, some cancer cells still retain some molecular components of the apoptotic pathway [7]. Identification and characterisation of these components would allow the development of anti-cancer strategies that reinitiate the apoptotic response without killing normal cells [5]. One appealing candidate for this approach is the prostate apoptosis response factor-4 (Par-4) [8].

1.1.2. Discovery of Par-4

As the name implies, the *par-4* gene was initially identified as a gene specifically upregulated during apoptosis in rat prostate cancer cells. Metastatic prostate cancer is usually treated by androgen ablation as androgens are essential cell survival factors for the majority of prostate cancer cells. However, androgen ablation therapy is rarely curative as tumours are

heterogeneous, containing both androgen-dependent and -independent cancer cells. Whereas androgen-dependent cancer cells undergo apoptosis after androgen ablation, androgen-independent cancer cells are resistant to the therapy and can cause a relapse of prostate cancer [9]. Apoptosis in androgen-dependent cancer cells, after androgen ablation, is accompanied by intracellular calcium elevation [9], a common event in diverse apoptotic processes [10,11]. However, androgen-independent cancer cells lack elevated intracellular calcium levels after androgen ablation, probably due to dysfunctions in upstream pathways. Artificial intracellular calcium elevation by the calcium ionophore, ionomycin, was shown to cause apoptosis in androgen-independent rat prostate cancer cells (AT-3 cell line) [12]. This prompted the isolation of genes that are differentially induced after ionomycin treatment. The *par-4* gene was identified as one of five immediate-early response genes associated with ionomycin-induced apoptosis in AT-3 cells. Induction of *par-4* preceded later steps of apoptosis such as caspase activation, chromatin condensation and mitochondrial dysfunction. Upregulation of *par-4* was apoptosis specific and not induced by growth stimulation, growth arrest or, oxidative stress and necrosis [13]. Interestingly, induction of *par-4* was also detected in androgen-dependent rat prostate cancer cells after androgen ablation, indicating that Par-4 may be a common factor in the apoptosis program [13].

A common role for Par-4 in apoptosis is further indicated as it is evolutionary conserved in vertebrates (Chapter 1.2.1.) and ubiquitously expressed in almost all mammalian tissues [8,14-16]. Par-4 is expressed in healthy non-apoptotic cells of ecto-, endo- and mesodermal origin indicating that the pro-apoptotic function of Par-4 is inhibited in normal cells. Downregulation of Par-4 in normal cells has been proposed to be correlated with differentiation. Typical examples for cell types with low Par-4 expression levels are neurons, the medulla of the adrenal gland, lymphocytes, dense connective tissue and some smooth muscle cells [15].

1.1.3. Par-4 as tumour-suppressor

Tumour-suppressors play a critical in the development of tumours. Tumour-suppressors are defined as genes that (i) if inactivation *in vivo* leads to enhanced tumour initiation, growth or progression and (ii) if a loss of function is accompanied by carcinogenesis [17]. Consistent with this definition, Par-4 knock-out mice develop spontaneous tumours in various tissues such as the endometrium, liver and lung. Interestingly, heterozygous loss of Par-4 yields the same frequency of tumours as does homozygous loss [8].

Consistent with this tumour-suppressor definition, downregulation of Par-4 is detected in a variety of cancers such as renal-cell carcinomas [18], neuroblastomas [19], leukaemia [20], lung carcinomas [21] or endometrial cancers [22]. An involvement of Par-4 in Wilm's tumourigenesis is likely, as this tumour is marked by chromosome reorganisations in the 12q21 region and *par-4* locates to chromosome 12q21.2 [23]. Furthermore, the 12q21 region is unstable and often deleted in human male germ cell tumours [24], pancreatic [25] and gastric cancers [8,26]. For endometrial cancer it was shown that Par-4 is downregulated by promoter hypermethylation. The same study also identified a single base mutation in exon 3 (Arg 189 to Stop) that caused a premature termination of Par-4 and thus resulted in its inactivation [22]. Downregulation of Par-4 in other cancers is less well understood, but may be related to the Ras signalling pathway [27]. *Ras* genes are common oncogenes in a number of human cancers [28] and Ras (and also Raf or Src) mediated downregulation of Par-4 via the MEK-ERK pathway has been described previously [29]. As will be discussed in the following section, ectopic overexpression of Par-4 can be sufficient to induce apoptosis in **most** cancer cell types [8] highlighting Par-4 as a potential target for the development of anti-cancer therapies.

1.1.4. Par-4 in neurodegenerative disease

Apoptosis is an essential cellular process during organ development, in particular for neuronal development in the central and peripheral nervous system where it is crucial for controlling neuron and glial cell numbers [30]. Par-4 was proposed to prevent hyper-proliferation of neurons during embryonic development through asymmetric distribution of Par-4 during mitosis of neuronal progenitor cells. Daughter cells with high levels of Par-4 undergo apoptosis, while those cells lacking Par-4 differentiate into neurons [31]. However, excessive death of neuron populations in the adult brain has been correlated with neurodegenerative disorders such as Alzheimer's disease [32], Parkinson's disease [33], Huntington's disease [34], amyotrophic lateral sclerosis [35] or HIV encephalitis [36]. Apoptosis and other forms of PCD are relatively late events in neurodegenerative processes and are preceded by functional alterations and microanatomical deficits (e.g. synapse loss) [37]. Thus, the high levels of Par-4 detected in the aforementioned diseases, may not be the primary cause for the diseases, but may contribute significantly to the severity of the diseases. Similarly, high levels of Par-4 are detected in neurons of more acute neurodegenerative conditions such as stroke [38] or epileptic seizures [39]. Furthermore, an increase in Par-4 is detected in cultured neurons undergoing apoptosis after trophic factor withdrawal, oxidative stress or exposure to metabolic insults [38]. The increase in

Par-4 levels in almost all cases, preceded both caspase activation and mitochondrial dysfunction, implying an early function of Par-4 in apoptosis. It is interesting to note that inhibition of Par-4 by antisense oligodesoxynucleotides could rescue neuronal cells from apoptosis in most of the aforementioned disorder paradigms [40]. Inhibition of Par-4 may therefore open up new therapeutic approaches for acute and chronic neurodegenerative disorders.

1.1.5. Other cellular roles of Par-4

Despite the potential of Par-4 for the treatment of cancer or neurodegenerative disorders, Par-4 is also involved in a variety of other non-apoptotic cellular processes. Facilitation of vascular contraction in smooth muscle was demonstrated to be dependent on Par-4 [41]. Par-4 was also shown to regulate the secretion of immunomodulatory cytokines such as IL-2. This indicates that Par-4 is involved in the stimulation, proliferation and differentiation of B- and T-cells, and hence plays an important role in the modulation of the immune response [42]. Furthermore, Par-4 appears to be an essential part of synapses. It was shown that Par-4 is involved in the uptake of choline into cholinergic neurons and thus in cholinergic signal transmission [43]. Additionally, Par-4 has been detected in the postsynaptic density of synaptosomes, which form synaptic contacts among neurons. The postsynaptic density is rich in cytoskeletal proteins and signalling proteins, and is therefore believed to be a major site for modulation of neuronal signal transduction. Thus Par-4 may be involved in synaptic plasticity and remodelling regulating the outgrowth of neurites [27,44]. The non-apoptotic role of Par-4 in neurons is further supported by the observation that Par-4 is involved in the development of depressive symptoms in mice models [45]. Altering the activity of Par-4, be it activation or inhibition, may therefore negatively interfere with the above-mentioned non-apoptotic processes. Hence, a precise understanding of the function of Par-4 is therefore necessary for the development of new therapies against cancer or neurodegenerative diseases.

1.2. Structure and function of Par-4

1.2.1. Structure of Par-4

Par-4 is an evolutionary conserved protein in vertebrates. The protein sequences of five Par-4 orthologues deposited in the UniProt database (www.uniprot.org) are shown in Figure 1.1. The sequence identity of the rat orthologue relative to mouse and human is 92% and 76%, respectively, whereas African clawed frog and zebra fish share 52% and 47% sequence identity with rat, respectively [46]. As can be seen from Figure 1.1 the degree of sequence similarity is

even higher. This high degree of conservation suggests functional significance for Par-4 and thus resistance to evolutionary pressure. It further implies that Par-4 is conserved in other vertebrates as well. Not surprisingly the anti-rat Par-4 antibody was shown to recognise Par-4 from other species [27]. Sequence conservation on the DNA level is less well studied, but a high degree of conservation is expected as human and mouse par-4 genes share a similar gene structure containing the same number of exons and introns [23,47]. The best described *par-4* gene is that of the human orthologue. As mentioned above, the human *par-4* gene locates to chromosome 12q21.2 [23]. The gene encompasses 99.1 kb of DNA and consists of seven exons and six introns, with the initiation codon being localised to exon 2. Three Par-4 mRNAs of different lengths have been detected in human cells but their importance is currently unknown [14,16]. Interestingly, co-expression of two Par-4 splice variants was detected in mouse embryonic body cells [47]. One variant comprises the full-length Par-4 protein, whereas the second variant lacks exon 3. The latter splice variant will be discussed in detail in Chapter 3.6.

All sequence numbering in this document is made with reference to the rat Par-4 isoform, to reflect the recombinant rat (rrPar-4) constructs used here. Rat Par-4 is a 35.9 kDa protein and contains 332 amino acids. Sequence analysis predicts two nuclear localisation sequences (NLS) in the N-terminal region and a coiled coil (CC) domain at the C-terminus (Fig. 1.1). Both NLS (NLS1: residues 20-25; NLS2: residues 137-153) are absolutely conserved in all known Par-4 sequences. A high degree of conservation is also observed for the CC domain (residue 254-332). Especially the leucine zipper (LZ) domain (residues 292-330), which is a subset of the CC domain, is highly conserved in all known Par-4 sequences. Interestingly, the CC domain shows significant homology to the death domains of other apoptotic proteins such as Fas, RIP, FADD and TRADD [48,49]. The biological significance of this observation is unknown and will be discussed in Chapter 1.2.3. A nuclear export sequence within the LZ domain has been predicted [8], but no functional evidence has yet been shown. A further domain (residues 137-195) shows strict sequence conservation in mammals (Fig. 1.1) and due to its properties has been named selective apoptosis induction in cancer cells (SAC) [50]. Additionally, several more or less conserved phosphorylation sites for the protein kinases A (PKA), B (PKB) and C (PKC), and casein kinase II have been predicted [27]. Two functionally important phosphorylation sites are shown in Figure 1.1 for PKA (rat: Thr 155, human: Thr 163, mouse: Thr 156) and PKB (rat: Ser 249, human: Ser 231, mouse: Ser 231). Whereas the PKA phosphorylation site is highly conserved in mammals the PKB site is not conserved (Fig. 1.1). As will be discussed later on, the

presence of these motifs suggests that the function of Par-4 may be tightly regulated by localisation, post-translational modification and interaction with various binding partners [8].

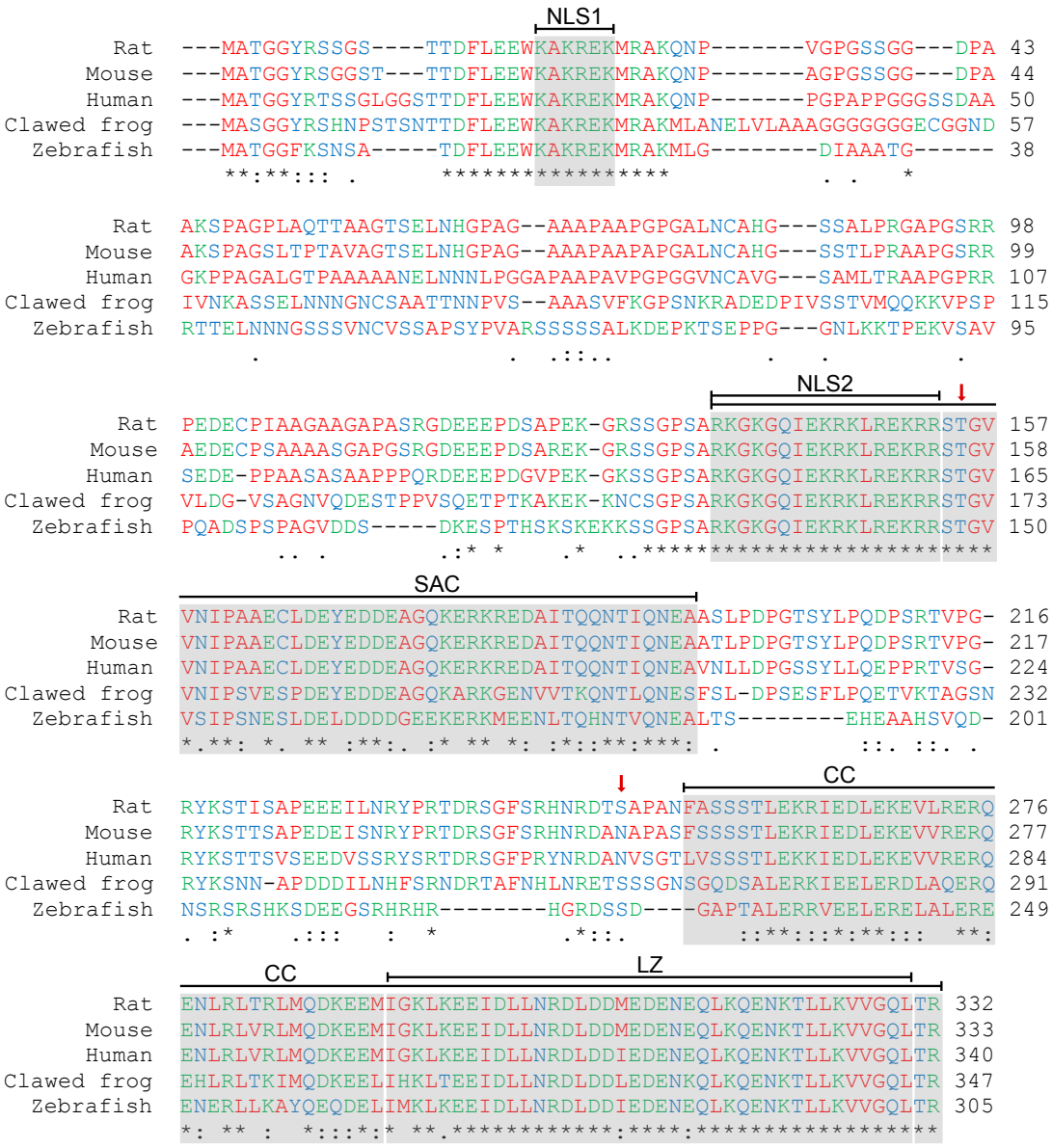

Figure 1.1 *– Sequence conservation in Par-4. A* BLASTP/CLUSTALW *[51,52] alignment of sequences of Par-4 from various species: rat (Rattus norvegicus), mouse (Mus musculus), human (Homo sapiens), African clawed frog (Xenopus laevis), and zebra fish (Danio rero). The amino acids are coloured as follows: red (non-polar side chains: Ala, Gly, Ile, Leu, Met, Phe, Pro, Trp and Val), blue (polar side chains: Asn, Cys, Gln, Ser, Thr and Tyr), green (polar, charged side chains: Arg, Asp, Glu, His and Lys). Symbols mean that (*) residues in that column are identical in all sequences, (:) substitutions are conservative, and (.) substitutions are semi-conservative. Referring to numbering of rat Par-4, several segments are of notable interest: two nuclear localisation sequences (NLS1 (20-25) and 2 (137-153)) which are completely conserved among all known Par-4s, the SAC domain (137-195) which includes NLS2 and is defined by being the absolute minimum fragment required for apoptosis induction [50]. The C-terminal domain (254-332) is a coiled coil (CC) motif that encompasses a leucine zipper (LZ, 292-330) as a subset. Two important phosphorylation sites Thr 155 and Ser 249 are denoted by red arrows. Figure and legend taken and adapted from Libich, Schwalbe et. al. [46].*

1.2.2. The pro-apoptotic function of Par-4

The apoptosis-inducing and -sensitising effects described for Par-4 in the literature are complex as they depend on various factors. The most critical factor is the cell type as different results are obtained with different cell types. Furthermore, it is important if endogenous Par-4 is analysed or if Par-4 is ectopically overexpressed. To summarise most of the results, ectopic overexpression of Par-4 selectively induces apoptosis in hormone-independent cancer cells. No apoptosis is induced in hormone-responsive, immortalised or normal cells, however, these cell types are sensitised to various pro-apoptotic stimuli such as chemotherapeutic agents, ionising radiation, serum deprivation or tumour necrosis factor to name a few. Similarly, endogenous Par-4 is not sufficient to induce apoptosis on its own, but sensitises cancer cells to the action of pro-apoptotic agents [8]. It is further important to note that the apoptosis-inducing function requires a different mechanism than the apoptosis-sensitising function. The first mechanism requires the SAC domain whereas the latter one relies on the presence of a functional LZ domain.

To identify the domains necessary for the pro-apoptotic function of Par-4, various N- and C-terminal Par-4 deletion mutants were created. As coiled coils and leucine zippers are common protein oligomerisation motifs, it was assumed that Par-4 exerts its pro-apoptotic function through protein-protein interactions via the CC and/or LZ domain. The Par-4 C-terminus was shown to be necessary for self-association of Par-4 [48,53,54] and as will be discussed in the following section, the majority of Par-4 binding partners interact with the CC region. However, it was shown that the CC domain is dispensable for the direct apoptosis-**inducing** function of Par-4 [50]. The CC domain is nonetheless essential for the apoptosis-**sensitising** function of Par-4. Cells that are resistant to apoptosis mediated by ectopically overexpressed Par-4 become sensitised to a variety of pro-apoptotic stimuli. In contrast, cells overexpressing a LZ deletion mutant (comprising residues 1-265) did not enhance apoptosis after exposure to pro-apoptotic stimuli [55]. It was further shown in the same study that co-expression of full-length Par-4 with a Par-4 CC construct (residues 240-332) rescued cancer cells from Par-4 mediated apoptosis. Likewise, neuronal cell lines overexpressing a construct comprising the LZ domain were resistant to apoptosis induced by various pro-apoptotic insults [40]. This indicates that the isolated CC domain can act in a dominant-negative manner abrogating the pro-apoptotic function of Par-4. It was proposed that the CC construct blocked the interaction of Par-4 with its interaction partners either by binding to the CC domain of full-length Par-4 or by direct binding to the interaction partners thereby inhibiting full-length Par-4 activity [55]. Experiments to

differentiate between both possibilities, such as immunoprecipitations or fluorescence techniques, have not been conducted yet.

In contrast to the apoptosis-**sensitising** function of Par-4 that mainly depends on a functional LZ domain, the apoptosis-**inducing** function is dependent on two distinct events (i) phosphorylation at Thr 155 by PKA and (ii) nuclear entry (Fig. 1.2) [26,50]. In normal and immortalised cells PKA activity is low and not sufficient for Par-4 to induce apoptosis and thus cells are resistant to Par-4 mediated apoptosis (Fig. 1.2A). Furthermore, in these cell types Par-4 is primarily located to the cytoplasm [14,26]. The mechanisms to retain Par-4 in the cytoplasm or for Par-4 inactivation will be discussed in Chapters 1.3.4. and 3.6. Conversely, in most cancer cells PKA isoform I is overexpressed and hence Par-4 is phosphorylated at Thr 155 [26]. However, in Par-4-insensitive cancer cells, Par-4 is retained in the cytoplasm and cells are resistant to Par-4 mediated apoptosis (Fig. 1.2B). In contrast, in Par-4-sensitive cancer cells overexpressed Par-4 localises both to the cytoplasm and the nucleus causing cancer cells to undergo apoptosis (Fig. 1.2C). Mutation of Thr 155 to alanine had no effect on the nuclear translocation of Par-4 in Par-4-sensitive cancer cells, however, this mutation abolished apoptosis induction. These results demonstrated that phospho-Thr 155 is essential for the apoptosis-inducing function of Par-4 [26]. Not surprisingly Thr 155 is absolutely conserved in vertebrates (Fig. 1.1).

Nuclear translocation of Par-4 is facilitated by the NLS motifs and precedes induction of apoptosis. Par-4 deletion mutants lacking both NLS motifs are incapable of nuclear entry and do not promote apoptosis [50]. As mentioned above, nuclear translocation does not depend on Thr 155. Interestingly, NLS2 is absolutely required for nuclear translocation of Par-4 [50], whereas NLS1 is not. This raises the question: Why is this motif strictly conserved in all known Par-4 sequences? (Fig. 1.1), as conserved motifs usually imply functional significance. It should be noted that the authors [50] failed to analyse a Par-4 construct only containing NLS1 but lacking NLS2. Therefore, no conclusions about the nuclear localisation potential of NLS1 can be made. Gao and co-workers recently proposed a role for the 36 N-terminal residues of Par-4 (including NLS1) as they demonstrated that this domain binds the Par-4 C-terminus in an intramolecular interaction. They suggested that the N-terminus may thereby function in a dominant-negative manner impairing homo- and hetero-oligomerisations via the C-terminus and thus interfering with the pro-apoptotic function [54].

Hormone-responsive cancer cells are resistant to nuclear translocation of overexpressed Par-4 and thus resistant to Par-4 induced apoptosis, even when Par-4 is phosphorylated at Thr 155.

Similarly, endogenous Par-4 is retained in the cytoplasm of hormone-independent cancer cells preventing apoptosis induction [26]. Cytoplasmic retention is achieved by phosphorylation of Par-4 at Ser 249 through PKB and subsequent binding and sequestration by the chaperone 14-3-3 [56]. This mechanism describes the best studied case, but other mechanisms may exist.

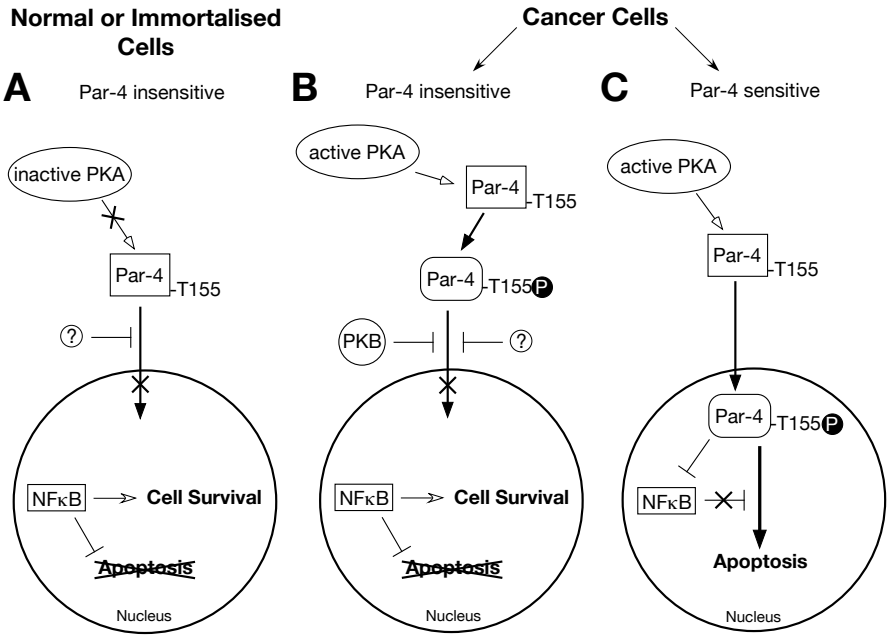

Figure 1.2 *– Model for the cancer-selective apoptosis by Par-4. The two important events, phosphorylation at Thr 155 and nuclear entry, necessary for apoptosis induction by Par-4 are schematically shown. (A) In normal or immortalised cells Par-4 is in an inactive non-phosphorylated state owing to low PKA activity. Furthermore, Par-4 is retained in cytoplasm by an unknown mechanism and cells are viable. (B) In Par-4-insensitive cancer cells despite phosphorylation at Thr 155 through PKA, Par-4 is retained in the cytoplasm. One possible sequestration mechanism involves phosphorylation through PKB, but other mechanism may exist. Cytoplasmic sequestration of Par-4 results in cell survival. (C) In Par-4-sensitive cancer cells phosphorylated Par-4 is able to translocate to the nucleus resulting in apoptosis induction. One of the important targets of Par-4 in the nucleus is the pro-survival factor NFκB. Figure adapted from Ranganathan & Rangnekar [57].*

1.2.3. Two cellular targets are essential for the apoptosis-inducing function of Par-4

An essential nuclear target of Par-4 is the transcription factor nuclear factor κB (NFκB). NFκB is a major pro-survival protein in the cell and regulates the expression of anti-apoptotic proteins such as XIAP (X-linked inhibitor of apoptosis), cFLIP (cellular FLICE-like inhibitory protein), Bcl-2 or Bcl-X_L [8] (Fig. 1.3). NFκB transcriptional activity is induced through various cell signalling pathways, including the Ras-pathway [58]. Par-4 is able to inhibit the NFκB transcriptional activity in the nucleus, which, depending on the cancer cell type, can be sufficient to induce apoptosis [50,59]; particularly oncogenic Ras expressing cells are sensitive to Par-4

induced apoptosis through inhibition of NFκB [60]. The mechanisms by which Par-4 regulates NFκB transcriptional activity are not well understood. Although, it is known that inhibition occurs without disruption of the NFκB DNA-binding capacity [60], and may be localised to the transactivation domain of NFκB [27]. It was further shown that the Par-4 LZ domain is dispensable for this inhibition [50].

Another essential cellular target of Par-4 is the Fas receptor. Par-4 was shown to induce the translocation of Fas and the Fas ligand (FasL) to the cell surface thereby activating the Fas-pathway (Chapter 1.3.3.). As inhibition of NFκB transcriptional activity is not sufficient to induce apoptosis in androgen-independent prostate cancer cells, parallel activation of the Fas-pathway is essential for the Par-4 mediated induction of apoptosis in these cells [59]. The mechanism of how Par-4 induces the Fas/FasL translocation is still elusive. As mentioned above, the C-terminus of Par-4 shows significant homology to the death domains of Fas, RIP, FADD and TRADD [48], which may indicate a possible interaction between Par-4 and Fas that could be necessary for trafficking Fas/FasL to the cell membrane. However, recent results demonstrate that Fas/FasL trafficking is independent of the Par-4 C-terminus [50]. Also, as will be shown in Chapter 4.6, the C-terminal Par-4 CC domain forms a coiled coil. A coiled coil is a rod-like α-helical structure that is distinct from the six-helical bundle structure of the death domains [61,62]. The sequence similarity of the Par-4 C-terminus with death domains may therefore be coincidental and of no physiological relevance. Taken together, both NFκB inhibition and Fas trafficking are required for the apoptosis-inducing function of Par-4. The fact that, for both proteins, no direct physical interaction with Par-4 has been described, suggests that the interaction is indirect through other proteins.

1.2.4. The importance of the SAC domain

Deletion analysis showed that the apoptosis-inducing function of Par-4 resides, as the name implies, in the SAC (selective apoptosis induction in cancer cells) domain (residues 137-195). This domain comprises all essential motifs for apoptosis induction such as Thr 155 and NLS2 (residues 137-153). Overexpression of the SAC domain is sufficient to induce apoptosis in cancer cells, regardless of their sensitivity or resistance to full-length Par-4, but not in normal or immortalised cells [50]. This is achieved by inhibition of NFκB transcriptional activity and translocation of Fas/FasL to the cell surface. As the SAC domain lacks the LZ domain, negative regulation through the LZ domain as observed for full-length Par-4 (Chapter 1.3.4.) is absent. This lack of negative regulation and its cancer cell selectivity make SAC a promising candidate

for molecular therapy. The SAC domain has so far only been described for the Par-4 proteins. To the knowledge of the author no studies have been conducted to identify SAC domains in other proteins. Also a simple attempt to identify similar domains in other proteins through the BLAST algorithm (au.expasy.org) has revealed no promising targets.

It has been reported that an artificial increase in tumour-suppressor activity may reduce the risk of carcinogenesis, but at the same time, compromise proliferation of stem cells, enhance apoptosis and/or increase senescence [63]. This was observed in a mouse model system expressing N-terminally truncated p53, which resulted in a shortened life span despite increased tumour resistance [64,65]. Conversely, SAC transgenic mice displayed normal development and life span. Additionally, SAC transgenic mice were protected from Ras or c-Myc induced oncogenic transformation. The authors could show that in murine embryonic fibroblasts this anti-transformation effect of the SAC domain was through the inhibition of oncogene induced NFκB activity and resulted in apoptosis. It was further shown that inhibition of the NFκB pathway is sufficient to induce apoptosis in the transformed cells. The anti-transformation effect of SAC transgenic mice also increased the resistance to spontaneous tumours during ageing. Interestingly, results indicate a stable inheritance of the SAC domain protecting the following generations of transgenic mice from spontaneous tumours [66]. Taken together, SAC induces apoptosis selectively in cancer cells upon transformation and thereby prevents tumour formation. Unlike classical chemo- or radiotherapy, SAC does not induce apoptosis in normal cells as it is inactive in these cells. These properties make SAC (unlike full-length Par-4) an ideal agent for anti-tumour therapy [66].

1.3. Par-4 interaction partners and their involvement in apoptosis

1.3.1. Programmed cell death

As mentioned above, apoptosis is the most common form of programmed cell death (PCD). PCD was termed in 1976 by Lockshin and Williams to describe a predetermined pattern by which specific cells die during insect development [3]. Two years later it was shown that in most cases PCD requires protein synthesis. This indicates that PCD represents an active cellular suicide process [67]. In 1972 the term apoptosis was introduced by Kerr and colleagues to describe a relatively uniform cell death process seen in a variety of situations from development to cell turnover to insult response [68]. It is important to note that apoptosis is not the only form of PCD and other non-apoptotic forms exist (Ref. [37] and references therein). Notably, some neurodegenerative disorders such as Huntington's disease, amyotrophic lateral sclerosis or

ischemia can show non-apoptotic cell deaths [69]. Currently, three forms of PCD are accepted in the scientific community: type I (nuclear or apoptotic PCD); type II (autophagic PCD); and type III (cytoplasmic PCD). Others forms have been described, however, due to insufficient data their relevance is controversial [37].

Apoptosis (Greek for 'falling away') is the best studied form of PCD. It is marked by typical morphological changes such as rounding up of cells, zeiosis or bleb formation, chromatin condensation and nuclear fragmentation, and budding off of so-called apoptotic bodies. Apoptotic bodies and other debris of the dying cell are removed by phagocytosis by nearby cells. In contrast to necrosis, apoptosis does not result in an immune response and thus a potential damage of neighbouring cells [2,70]. Furthermore, apoptosis is marked by mitochondrial membrane depolarisation and at the molecular level by a phospholipid asymmetry. Phosphatidyl-serine, which is usually located on the inside of the plasma membrane in living cells, faces inward and outward in apoptotic cells. Outward facing phosphatidylserine functions as a signal for phagocytosis of apoptotic bodies [37,71]. Great importance to these morphological changes is attributed to a set of cysteine proteases called caspases [70]. Activation of apoptosis, in particular activation of the caspase cascade, occurs through two main pathways: the extrinsic and intrinsic pathway. Both pathways will be discussed in more detail below.

In contrast to apoptosis, little is known about autophagic and cytoplasmic PCD. Autophagy (Greek for 'self eating') is a cellular stress response that allows cells to survive prolonged times of starvation. It represents a form of the lysosomal pathway and results in degradation of long-lived proteins, protein aggregates and (damaged) organelles. The targets of degradation are encircled in a biomembrane leading to morphologically visible 'autophagic vacuoles'. These 'vacuoles' then fuse with lysosomes resulting in degradation and thus recycling of amino acids and other molecular components. Autophagic PCD is observed in cases when the apoptotic machinery is dysfunctional. This is important to note, as anti-apoptotic therapies for neuro-degenerative disorders may carry the risk of inducing other forms of PCD [37]. Cytoplasmic PCD represents a necrosis-like form of cell death and is marked by swelling of mitochondria and the endoplasmatic reticulum (ER). It further lacks the typical morphological changes of apoptosis such as apoptotic bodies or nuclear fragmentation. However, even type III PCD is an active process requiring transcription and translation [37].

1.3.2. Caspases

Caspases are highly selective aspartyl-specific proteases that only cleave at a small subset of aspartic acid residues. They are synthesised in an inactive form, as zymogens, and are activated either by induced proximity or by proteolytic cleavage [72]. Caspases are classified into initiator and effector caspases. Initiator caspases such as caspase-8, 9 or 10, exist as inactive monomers in the cell. Initiator caspases are able to dimerise upon binding to other specific proteins through their death effector domains (DED) in caspase-8 and 10, or caspase activation and recruitment domains (CARD) in caspase-9. This dimerisation then results in initiator caspase activation. Contrary to earlier reports, no cleavage of the initiator caspase is necessary for its activation [72]. Cleavage occurs secondary to activation and partially stabilises the dimer. Activation is probably due to conformational changes upon dimerisation and/or binding to the adaptor protein. Once activated, initiator caspases activate the effector caspases (caspase-3, 6 or 7) through proteolytic cleavage. Note that this upstream/downstream relationship probably only exist in the early stages of the apoptotic cascade. Effector caspases exist as dimers in the cell, and cleavage produces a hetero-tetramer comprising two large and two small subunits. Effector caspases display a different and wider substrate specificity than initiator caspases and thus activate the apoptotic process by cleaving other protein substrates in the cell. More than 400 substrates are known and include structural proteins, other mediators of apoptosis, DNA repair proteins and cell cycle related proteins. An important target of the effector caspases is the inhibitor of caspase activated DNase (ICAD). Activated CAD together with DNase II is responsible for DNA fragmentation after the release from ICAD [71,72]. It is interesting to note here that caspases appear to contribute to some neurodegenerative disorders. Mutation of the caspase cleavage site in the amyloid precursor protein (APP) or polyglutamine-expanded huntingtin suppressed synapse loss and prevented neurodegeneration in Alzheimer's [73] and Huntington's disease [74] models, respectively.

Caspase activity is regulated via caspase inhibitors or through post-translational modification. Especially for caspase-9, phosphorylation by PKB, ERK (extracellular signal regulated kinase) or PKCζ has been shown to inhibit the proteolytic activity [70]. Active caspases are kept in control by the inhibitors of apoptosis (IAPs) such as XIAP and Survivin. IAPs function as caspase inhibitors and E3-ligases mediating caspase degradation. IAP inactivated caspases may be rescued by proteins such as OMI (HtrA2) or SMAC (second mitochondria-derived activator of caspase), which is also known as DIABLO (direct IAP-binding protein with low pI). Another caspase inhibitor, especially of caspase-8, is cFLIP, the expression of which is under control of

NFκB. Depending on the cytosolic adaptor proteins, NFκB can be activated by TNFR1 (tumour necrosis factor receptor 1) indicating a pro- and anti-apoptotic role for this death receptor (Fig. 1.3) [2,37,71].

1.3.3. The extrinsic and intrinsic pathways of apoptosis

The extrinsic or death receptor pathway originates from the activation of death receptors at the cell surface and results in activation of caspase-8 or 10. The extrinsic pathway will be explained here on the basis of the best characterised example the Fas receptor (Fig. 1.3, left hand side). The Fas ligand binds to Fas resulting in trimerisation of the receptor and thus the recruitment of FADD (Fas associated death domain) to the cytoplasmic site of the receptor. FADD is recruited through the so-called death domain (DD) of Fas. It is interesting to note here that DED, DD and CARD domains all adopt a similar fold indicating an evolutionary conserved structure in the assemblage of pro-apoptotic cascades. FADD is an adaptor protein that in turn binds caspase-8 via the DED domain. The resulting complex is called DISC (death-inducing signalling complex). DISC formation is also observed for the death receptor-ligand complexes TNFR1-TNFα (tumour necrosis factor α) and DR4/5-TRAIL (TNF-related apoptosis inducing ligand). Activated by induced proximity, the initiator caspase-8 cleaves and activates the effector caspases (e.g. caspase-3, 6 and 7). The effector caspases then initiate the apoptotic process [2,37,71].

The intrinsic or mitochondrial pathway is activated by diverse apoptotic stimuli such as DNA damage, oxidative stress or growth factor deprivation, and converges on the mitochondria. Depending on the relative balance between pro- and anti-apoptotic proteins of the Bcl-2 family, cytochrome c is released from mitochondria into the cytoplasm, which results in activation of caspase-9 (Fig. 1.3, right hand side) [2]. The anti-apoptotic proteins Bcl-2 and Bcl-X_L protect mitochondria from permeabilisation and cytochrome c release by the pro-apoptotic Bcl-2 family members. The pro-apoptotic Bcl-2 are classified into 3 groups based on structural properties. The first group contains the multidomain proteins BAX and BAK that can permeabilise the outer mitochondrial membrane. One model suggests that BAX and BAK polymerise on the outer mitochondrial membrane forming a pore. The second group includes the BH-3-only proteins such as BIM and tBID that activate BAX and BAK and may assist in membrane permeabilisation. The last group comprises the BH3-only derepressors such as PUMA, NOXA or BAD. These proteins sequester the anti-apoptotic Bcl-2 and Bcl-X_L proteins thereby freeing the BAX and BAK proteins [71]. Other proteins unrelated to the Bcl-2 family can influence the actions of

the Bcl-2 family members. Especially the BH3-only family members were shown to be controlled at a transcriptional level or via post-translational modification. For example, PUMA and NOXA are under transcriptional control of p53, whereas the activity of BAD is controlled by phosphorylation. Permeabilisation of the mitochondrial membrane releases various other pro-apoptotic proteins in the cytosol such as SMAC, OMI, AIF, endoG and cytochrome c. AIF and endoG translocate to the nucleus resulting in chromatin condensation and nuclear fragmentation. Once in the cytosol, cytochrome c induces heptamerisation of Apaf-1 (apoptotic protease activating factor), which then binds caspase-9 via the CARD domain leading to its activation. The complex of Apaf-1, cytochrome c, dATP/ATP and caspase-9 is called apoptosome. Following caspase-9 activation, the effector caspases-3, 6 and 7 are activated initiating the apoptotic process. Crosstalk between the extrinsic and intrinsic pathway is facilitated by BID. BID is cleaved by caspase-8 to produce tBID that then activates the intrinsic pathway and amplifies the apoptotic signal (Fig. 1.3) [2,37,71].

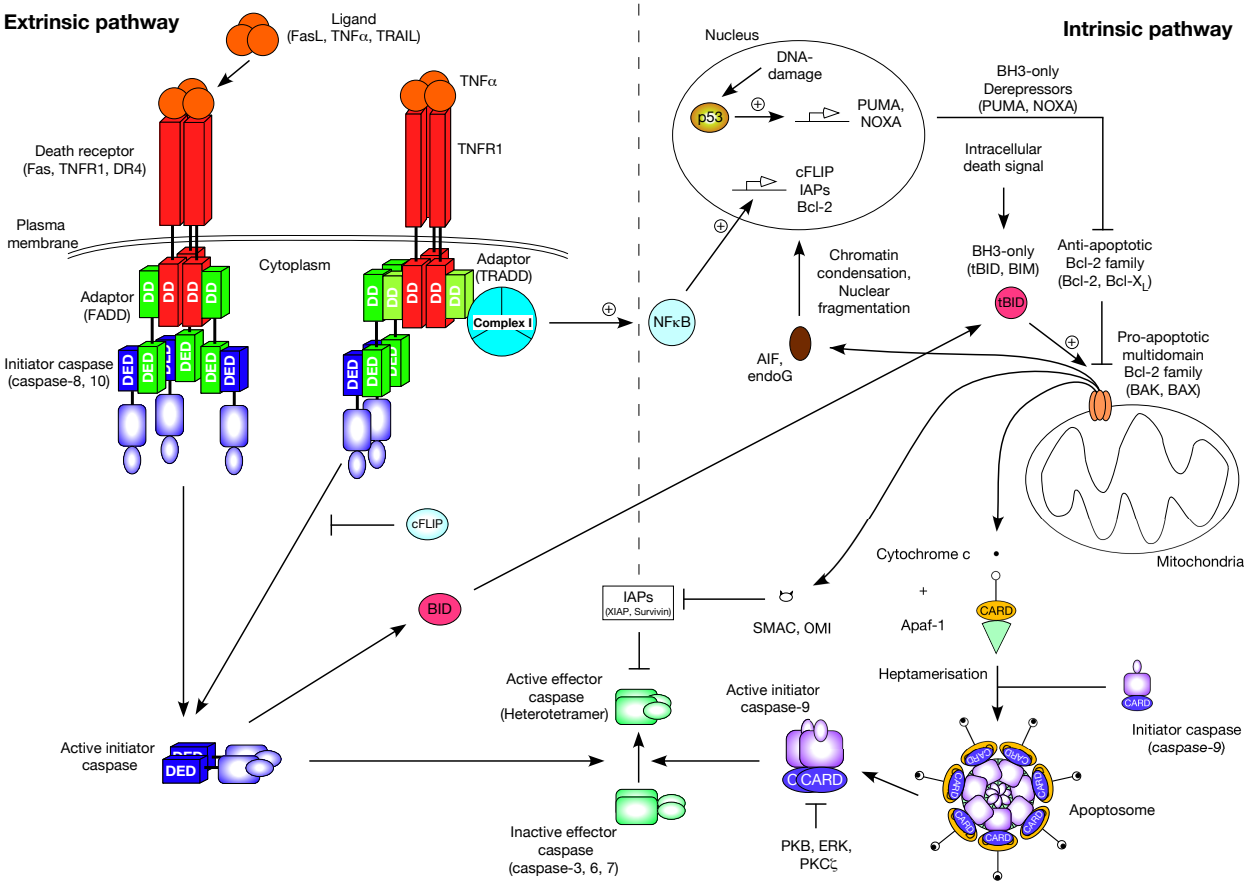

Figure 1.3 *– The extrinsic and intrinsic pathways of apoptosis. For details see text.*

A subset of the intrinsic pathway is sometimes discussed as a third pathway in the literature. It originates from the ER in response to stress such as accumulation of misfolded protein and results in the activation of caspase-9. This pathway is of particular interest as accumulation of

misfolded protein and protein aggregation are a common in some neurodegenerative disorders such as Alzheimer's or Huntington's disease [37]. It is interesting to note that Par-4 has been shown to be upregulated in response to ER stress [75], which may be related to the high levels of Par-4 detected in various neurodegenerative disorders. Also important for initiation of this second intrinsic pathway are the Bcl-2 family members. The best characterised example describes the binding of BAP31 (an ER-membrane protein) to Bcl-2 and a caspase-8 containing complex resulting in cleavage of BAP31. The cleavage product enhances among other effects cytochrome c release from the mitochondria. Other mechanisms for apoptosis induction in response to ER stress have been described, but are beyond the scope of this chapter [37].

It has long been hypothesised that acidification of the cytosol is necessary for apoptosis. Especially for neurons under ischaemic conditions it was shown that acidification of the cytosol induces neuronal injury and precedes nuclear fragmentation [76]. It is now commonly accepted that acidosis is not essential for apoptosis, however, it does contribute to some apoptotic processes. In particular, the translocation of BAX to mitochondria [77], apoptosome assembly and caspase activation were shown to be pH dependent and more efficient at acidic pH [78]. Acidosis can occur through the extrinsic pathway after activation by Fas in a caspase-dependent process. Alternatively, acidosis can be induced through the intrinsic pathway in a mitochondria-dependent, but caspase-independent manner. This process relies on BAX and can be inhibited by Bcl-2. As an important, but not the only factor, in this mitochondria-dependent acidosis the F_0F_1-ATPase was identified. The drop in pH that is commonly observed during apoptosis does not exceed 0.3-0.4 pH-units [11,76].

1.3.4. Interaction partners of Par-4

The pro-apoptotic function of Par-4 is achieved either by activation of molecular components of the apoptosis machinery or by inhibition of pro-survival factors. Par-4 was shown to interact with proteins involved both in the extrinsic and the intrinsic pathway. The most important Par-4 interaction partners and their implication in apoptosis will be discussed below. The interactions are schematically shown in Figure 1.4. Interactions with other proteins occur mainly through the LZ or the SAC domain, with the majority of proteins binding to the CC/LZ domain (Table 1.1). As will be described later on, the Par-4 LZ domain is a subset of the longer CC domain (Fig. 1.1). However, due to its homology the CC domain is often described as a DD in the literature and not as an extension of the LZ domain. Thus C-terminal Par-4 deletion mutants were often termed LZ deletion mutants even though they protruded N-terminally into the CC

domain. According to the nomenclature used in this document, these mutants would represent CC deletion mutants. For consistency, the term LZ deletion mutants will be kept for these mutants; however, the rat residue numbers will be given in brackets for clarity.

Inhibition of pro-survival function	Activation of pro-apoptotic function	Inactivation of Par-4	Other
protein kinase B (LZ)	DAP like kinase (LZ)	p62 (LZ)	CHT1 (?)
atypical protein kinase C λ/ι and ζ (LZ)	Actin filaments (residues 1-40)	protein kinase B (LZ)	SSB1, 2 and 4 (?)
WT1 (LZ)	Amida (LZ)	14-3-3 (phospho-Ser 249)	D2DR (LZ)
Androgen receptor (SAC)	β-site APP cleaving enzyme-1 (LZ)	Apoptosis-antagonising transcription factor (LZ)	
Topoisomerase 1 (LZ)	THAP (LZ)		
	E2F1 (LZ)		
	Glucose-regulated protein-78 (SAC)		
NFκB?	Fas/FasL?		

Table 1.1 *− Par-4 interaction partners. Par-4 binding partners are classified according to the effect of association with Par-4. Binding with Par-4 can inhibit pro-survival proteins, stimulate pro-apoptotic proteins or result in inactivation of Par-4. Molecules that have other effects or where the outcome of the interaction is unknown are listed in the last column. The interacting domain within Par-4 is given in brackets. LZ includes residues 240-332 and SAC includes residues 137-195. Question marks signify that the exact domain is not known. For NFκB and Fas/FasL a direct interaction with Par-4 has not been determined (Chapter 1.2.3.).*

a) Atypical protein kinase Cζ and λ/ι (aPKCζ and λ/ι)

The atypical PKC family consists of two isoforms: aPKCζ and λ/ι. aPKCλ is the mouse homolog of human aPKCι. All atypical PKCs (aPKC) share a high degree of homology across the catalytic and regulatory domains. In contrast to other PKC subgroups, the aPKCs are not regulated by calcium or diacylglycerol, but by other phospholipids such as ceramide and phosphatidylinositol-(3,4,5)trisphosphate. The latter, being a product of the phosphoinositide 3-kinase (PI3K), indicates an important role for aPKCs in cell proliferation and cell survival. Consistent with this role, aPKCs have been described as activators of NFκB and the mitogen-activated protein kinases (MAPK) such as ERK1 and 2 (Ref. [48] and references therein).

Both aPKC isoforms specifically interact with Par-4 through their regulatory domain, in particular the zinc-finger domain, resulting in an inhibition of their enzymatic activity. The LZ domain within Par-4 is necessary for binding to the zinc-finger domain. Thus, Par-4 LZ deletion mutants (residues 1-261) failed to bind the aPKC regulatory domain and therefore had no effect on the aPKC catalytic activity [48]. Inhibition of aPKC enzymatic activity results in a decrease in AP1-dependent promoter activity, which is likely to be related to aPKC-dependent activation of MAPK [48]. AP1 is an important transcription factor complex involved in cell proliferation, apoptosis and tumour development [79]. FADD is another substrate of aPKCζ and phosphorylation of FADD by aPKCζ in myeloid leukemic cells prevents DISC formation and subsequent activation of caspase-8 [80]. As mentioned above, caspase-9 is also inhibited by phosphorylation through aPKCζ (Fig. 1.3).

Furthermore, aPKCs are involved in the activation of NFκB. The classical form of NFκB is a heterodimer of p50 and p65 (RelA), but 5 other family members are known [81]. NFκB is sequestered in the cytoplasm by members of the inhibitor of κB family (IκB) [58,81]. Phosphorylation of IκB by IKKα (IκB kinase α) or IKKβ (IκB kinase β) results in IκB ubiquitination and proteasomal degradation. The free NFκB then translocates to the nucleus and exerts its anti-apoptotic activity (Ref. [82] and references therein). The anti-apoptotic activity of free NFκB is potentiated as it was also shown to act in a paracrine fashion thereby accelerating tumour growth [83]. NFκB activation by aPKCs is achieved at two different levels. First, aPKCs specifically phosphorylate and thus activate IKKβ, thereby promoting release of NFκB from IκB and allowing its translocation to the nucleus. Second, phosphorylation of NFκB in the p65 subunit by IKKβ [84] or aPKCζ [58] enhances the transcriptional activity of NFκB. Phosphorylation of p65 by aPKCζ is dependent on its release from IκB [85]. Hence, Par-4 prevents NFκB activation and nuclear translocation through inhibition of the aPKCs. Note that inactivation of NFκB, through inhibition of the aPKCs, is dependent on the Par-4 LZ domain, but it does not depend on nuclear translocation of Par-4 [82]. This indicates that regulation of aPKC activity is part of the apoptosis-sensitising function of Par-4. Consequently, inhibition of aPKC activity through ectopically overexpressed Par-4 was shown to promote apoptosis in immortalised mouse fibroblasts. Conversely, aPKC overexpression could rescue these cells from Par-4 mediated apoptosis [82]. The effects of Par-4/aPKC association are summarised in Figure 1.4.

b) p62

The p62 protein (also known as sequestosome 1) is an important adaptor protein and functions as hub protein in cell signalling [86]. It was originally identified as an adaptor protein for the aPKCs [87]. It was proposed that p62 recruits aPKCs to signalling complexes (e.g. complex-1 of TNFR1 in Fig. 1.3) in response to TNFα or interleukin-1 signalling mediating NFκB activation. Both p62 and Par-4 were shown to bind to the regulatory domain of aPKCs. However, the interaction was not competitive and all three proteins interact with each other and are involved in a ternary complex. Necessary for the interaction between p62 and Par-4 are the N-terminal residues 50-80 within p62 and the LZ domain (residues 296-332) of Par-4. Binding of p62 to a complex of aPKC and Par-4 restores the catalytic activity of the aPKC indicating an additional regulatory function for p62. Not surprisingly, co-expression of p62 and Par-4 in U2OS cells restored NFκB activity and rescued cells from Par-4 mediated apoptosis [88]. Consistent with these findings, it was recently shown that p62 is an important factor in Ras induced tumourigenesis [86]. The effects of Par-4/p62 association are summarised in Figure 1.4.

c) Protein kinase B (PKB)

PKB (or Akt kinase) is another downstream member of the PI3K pathway and is therefore involved in cell survival and transformation due to inhibition of apoptosis. As a serine/threonine kinase PKB phosphorylates and regulates a wide range of substrates including pro-apoptotic proteins. Elevated PKB activity has been detected in various cancers due to inactivation of PTEN (phosphatase and tensin homolog deleted on chromosome 10) and/or constitutive activity of PI3K. Phosphorylation of PKB by PDK1 (3-phosphoinositide dependent kinase 1) is essential for PKB activity, whereas the tumour suppressor PTEN as a phosphatase inactivates PKB. The importance of PTEN for PKB activity is demonstrated by the fact that the *pten* gene is often deleted in human cancers such as advanced prostate cancers (Ref. [56] and references therein).

Par-4 is one of the pro-apoptotic substrates of PKB and both proteins were shown to associate *in vivo* in a variety of cell lines including cancer and normal cells [56]. An active kinase domain within PKB and the Par-4 LZ domain (residues 289-332) are necessary for this interaction. Furthermore, PKB only associates with the phospho-Thr 155 form of Par-4. PKB phosphorylates Par-4 at Ser 249 (mouse: Ser 231, human Ser 231) [8] and thus prevents nuclear translocation of Par-4. Consistent with this role, co-expression of PKB and Par-4 in Par-4-sensitive cancer cells abrogated the Par-4 apoptosis-inducing function. However, inhibition of PKB activity by co-expression of PTEN or other PKB inhibitors resulted in apoptosis. Conversely, downregulation

of Par-4 through RNA interference, in cells expressing PTEN, abrogated apoptosis. This indicates that PTEN induces apoptosis primarily through Par-4.

Nuclear translocation of Par-4 is achieved through cytoplasmic sequestration by the chaperone 14-3-3, which selectively binds to the phospho-Ser 249 residue. It is interesting to note here that even though sequestration of Par-4 by 14-3-3 appears to be conserved in mammalian cells, the respective serine residues in Par-4 necessary for binding to 14-3-3 are not conserved relative to Thr 155. As can be seen in Figure 1.1, the serine residues Ser 249, Ser 231, and Ser 231 within rat, mouse and human, respectively, are at different positions within the Par-4 sequence. The reason for this observation is not clear, but may be due to different recognition sites of PKB and/or 14-3-3 in different mammalian species.

The mechanism described here explains why the active phospho-Thr 155 form of Par-4 does not induce apoptosis in Par-4-insensitive cells as the nuclear translocation is impaired (Fig. 1.2). Further, it becomes evident why the SAC domain is a more potent inducer of apoptosis than full-length Par-4 as it lacks the LZ domain necessary for binding to PKB [56]. Interestingly, a recent report demonstrated that Par-4 itself negatively regulates PKB. In the absence of Par-4, PKB was shown to be phosphorylated and thereby activated through aPKCζ in mouse lung cells. Conversely, expression of Par-4 abolished phosphorylation of PKB through inhibition of aPKCζ activity [21]. The effects of Par-4/PKB association are summarised in Figure 1.4.

d) DAP like kinase (Dlk)

Dlk is a serine/threonine kinase that shows homology to the DAP (death-activated protein) kinase. Sequence analysis shows the presence of a leucine zipper domain within Dlk. It was shown that this leucine zipper domain is necessary for homodimerisation and interaction with the transcription factor ATF-4 (a member of the ATF/CREB family). Thus Dlk is also termed zipper interacting protein kinase (ZIPK). *In vitro* substrates of Dlk are, for example, the core histones H2A, H3 and H4, and the myosin light chain (Ref. [16] and references therein). Interestingly, initial reports suggested that Dlk interacts with Par-4 through an arginine rich stretch (residues 338-417) but not through the leucine zipper domain. However, this observation has recently been challenged [89]. Association with Par-4 further depends on an active Dlk kinase domain. The interacting domain within Par-4 was mapped to the LZ domain (residues 262-332).

Co-expression of Par-4 and Dlk in rat embryonic fibroblasts results in translocation of nuclear Dlk to the cytoplasm, in particular to actin filaments. Note that Par-4 co-localises with Dlk in the cytoplasm but shows no nuclear localisation. However, this does not exclude Par-4 being

transiently located in the nucleus. Translocation of Dlk to actin filaments is followed by a reorganisation of the cytoskeleton and morphological changes indicative of apoptosis. Apoptosis is dependent on both Dlk and Par-4, and on the degree of cytoplasmic retention of Dlk. The exact way of apoptosis initiation by Dlk/Par-4 is not known. Localisation to actin filaments and phosphorylation of myosin light chain may be critical events as the latter is implicated in membrane blebbing. However, it has been shown that this actin localisation of the Par-4/Dlk complex has an important non-apoptotic role in facilitating contraction in vascular smooth muscle [41]. Alternatively, disruption of Dlk interactions with other proteins within the nucleus may further be another contributing factor in apoptosis induction [16]. Recent findings show that Dlk phosphorylates Par-4 at Thr 155 [90] and as described above this is an essential step in the apoptosis-inducing function of Par-4 [26]. Thus, co-localisation of Dlk and Par-4 to the actin cytoskeleton may be an alternate mechanism for the activation of Par-4.

A nuclear role for the Par-4/Dlk complex has also been determined. In response to the pro-apoptotic stimuli arsenic trioxide or gamma interferon, Par-4 enhances the interaction of Dlk with the pro-apoptotic protein Daxx in the nucleus of HeLa cells. This ternary complex then localises to PML nuclear bodies (see below) and induces apoptosis through the activation of the caspase cascade. Necessary for apoptosis induction in this system is the overexpression of all three proteins together, and downregulation of anyone of the three binding partners abolished apoptosis. The authors proposed that in this system Par-4 may function as a scaffold recruiting Dlk and Daxx [89]. The effects of Par-4/Dlk association are summarised in Figure 1.4.

e) Actin filaments (F-actin)

As mentioned above, the Dlk/Par-4 complex localises to actin filaments by an unknown mechanism. It could be shown for rat embryonic fibroblasts, rat immortalised fibroblasts and mouse fetal brain cells that endogenous Par-4 is directly bound to F-actin. Essential for this interaction is the N-terminal part of Par-4 (residues 1-266), in particular the first 40 N-terminal residues, but not the C-terminus. This indicates that Par-4 functions as scaffold recruiting other proteins to the actin cytoskeleton. Actin is bound by the Par-4 N-terminus while the C-terminus, in particular the LZ domain, can be involved in other protein interactions (e.g. Dlk, Amida). *In vitro* studies showed that Par-4 binding promotes actin bundling. Consistent with this role, significant cytoskeleton reorganisation, such as stress fibre formation, is observed in transformed cells upon Par-4 overexpression. Binding to F-actin is important for the Dlk/Par-4 mediated apoptosis, as a deletion of the first 40 N-terminal residues of Par-4 resulted in a decrease of Dlk/

Par-4 mediated apoptosis. Furthermore, disruption of the actin cytoskeleton by cytochalasin D also decreased the apoptotic rate. The localisation of the Dlk/Par-4 complex to F-actin appears to be necessary for the Dlk mediated phosphorylation of myosin light chain. This phosphorylation may be necessary for cytoskeletal reorganisations and thus essential for the progression of apoptosis [91]. The effects of Par-4/F-actin association are summarised in Figure 1.4.

f) Amida

Amida is a relatively poorly characterised protein. It was originally identified as an interaction partner of Arc (activity-regulated cytoskeleton-associated protein) and later found to associate with Par-4 in rat and mouse fibroblasts [53]. Critical for the interaction with Par-4 is the C-terminal domain of Amida (residues 113-259) and the LZ domain within Par-4 (residues 266-332). Interestingly, the authors could show that mutation of three leucine residues in *d* position of the Par-4 LZ domain to alanine (L295A, L316A, L330A) abrogated binding to Amida. This indicates that a functional LZ is required for the interaction with Amida. Primarily localised to the nucleus, Amida shows weak shuttling to the cytoplasm. Upon co-expression of Amida and Par-4, Amida translocates to the cytoplasm and associates with Par-4. As described for Dlk, Par-4 functions as a scaffold protein recruiting Amida to the actin cytoskeleton resulting in phosphorylation of the myosin light chain. Consistent with the observation for Dlk, co-expression of Amida and Par-4 induces apoptosis in rat fibroblast depending on an intact actin cytoskeleton and binding of Par-4 to F-actin [53]. The effects of Par-4/Amida association are summarised in Figure 1.4.

g) THAP1

Promyelocytic leukemia (PML) nuclear bodies are discrete sub-nuclear domains composed of various proteins. They are mainly organised by the PML protein, a pro-apoptotic protein involved in various apoptotic pathways. The exact mechanism by which PML promotes apoptosis is poorly understood, but it was proposed that PML might recruit other pro-apoptotic proteins, such as p53 and Daxx, into PML nuclear bodies. Consistent with this role, it was shown that PML acts as a transcriptional co-activator of p53 (Ref. [92] and references therein). Another pro-apoptotic factor associated with PML nuclear bodies is THAP1. THAP1 belongs to the THAP family that is characterised by a conserved DNA binding motif called THAP domain. Like Par-4, ectopic overexpression of THAP1 in mouse 3T3 fibroblasts was shown to sensitise cells to apoptotic stimuli such as serum deprivation or TNFα [92].

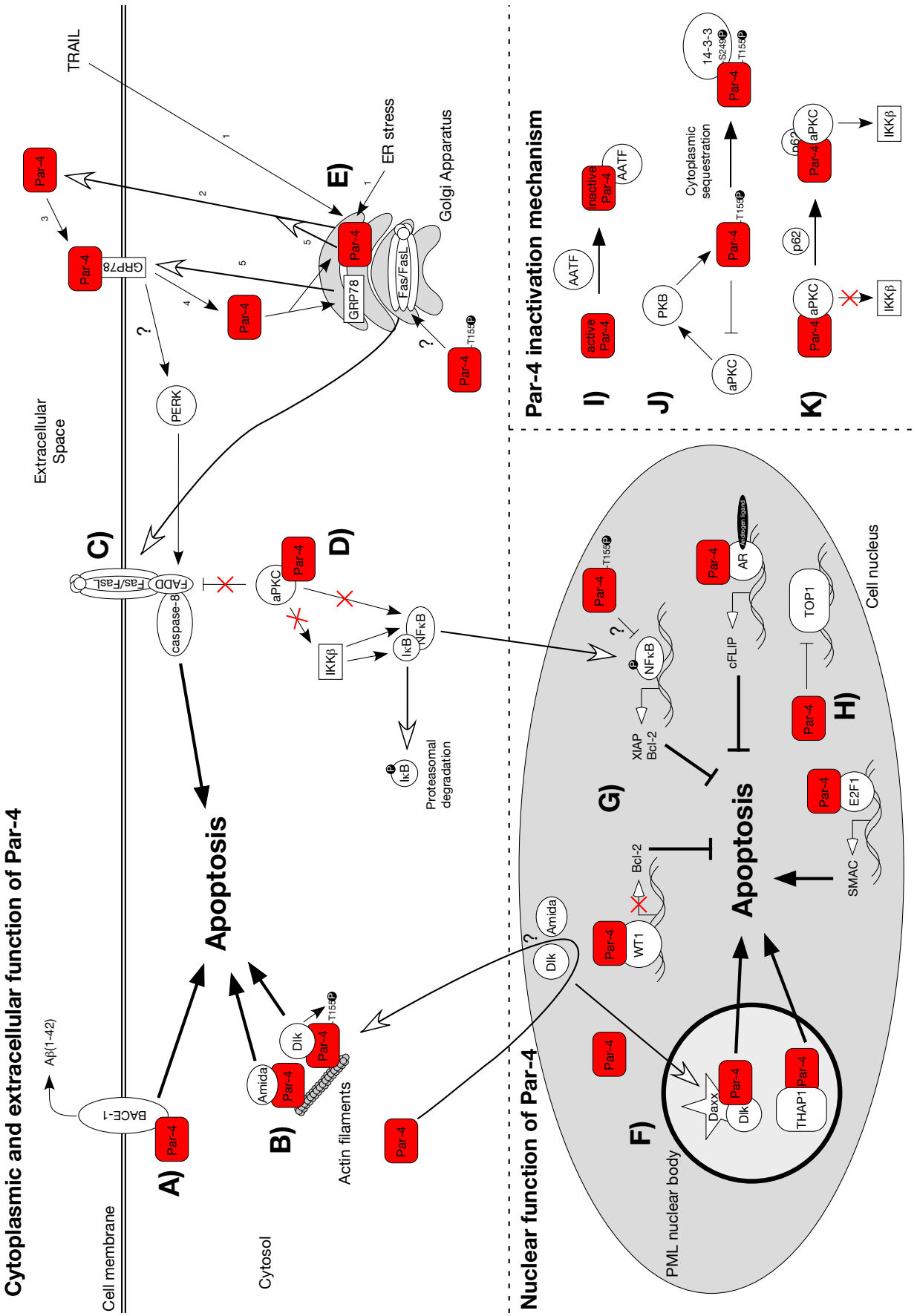
Cytoplasmic and extracellular function of Par-4
Cell membrane
Extracellular Space
Cytosol
Nuclear function of Par-4
Cell nucleus
Golgi Apparatus
ER stress
Actin filaments
PML nuclear body
Proteasomal degradation
Apoptosis
Par-4 inactivation mechanism
TRAIL
Aβ(1-42)
BACE-1
GRP78
PERK
FADD
caspase-8
Fas/FasL
aPKC
IKKβ
IκB
NFκB
Dlk
Amida
WT1
Bcl-2
XIAP
cFLIP
AR
TOP1
E2F1
SMAC
Daxx
THAP1
AATF
PKB
p62
14-3-3
Cytoplasmic sequestration
A)
B)
C)
D)
E)
F)
G)
H)
I)
J)
K)

Figure 1.4

The N-terminal THAP domain is essential for the pro-apoptotic function of THAP1, but dispensable for the localisation to PML nuclear bodies or binding to Par-4. The interaction between THAP1 and Par-4 is mediated through the CC domain of Par-4 and hence a Par-4 construct comprising residues 256-332 was sufficient for binding to THAP1. Co-localisation of endogenous Par-4 with THAP1 in PML nuclear bodies of primary endothelial cells and fibroblasts suggests that Par-4 is a component of PML nuclear bodies for these cell types. However, this localisation of Par-4 is cell type specific and is not observed in HeLa cells. It was proposed that THAP1 and Par-4 are recruited to PML by an unknown adaptor protein. Interestingly, for endogenous Par-4 that co-localised with THAP1 no apoptotic phenotype was described indicating that nuclear endogenous Par-4 is in an inactive state [92].

Figure 1.4 *− The pro-apoptotic function of Par-4. Schematic model for the different association partners of Par-4 and their involvement in apoptosis. Pro-apoptotic functions of Par-4 localised to the cytoplasm or extracellular space are shown in parts A-E. (A) Par-4 stimulates secretion of the neurotoxic Aβ(1-42) peptide. (B) Cytoplasmic translocation of the nuclear proteins Dlk or Amida and their Par-4 mediated interaction with the actin cytoskeleton results in apoptosis. If a nuclear translocation of Par-4 is necessary for this interaction is currently unknown. (C) Par-4 stimulates the trafficking of Fas/FasL to the cell membrane thereby promoting apoptosis. This is one of the essential apoptosis-inducing functions of Par-4 and is dependent on the phospho-Thr 155 form. However, the exact mechanism of Par-4 mediated Fas/FasL trafficking remains elusive. (D) Association of Par-4 and aPKC results in inhibition of aPKC activity thus preventing inactivation of FADD and activation of NFκB. (E) Activation of the ER stress response results in secretion of Par-4. Binding of Par-4 to GRP78 results in activation of PERK and subsequent activation of the Fas-FADD apoptotic pathway. The amplification loop for the Par-4/ GRP78 interaction is indicated with numbers from 1-5. Nuclear functions of Par-4 are displayed in parts F-H. (F) Association of Par-4 with Dlk, THAP1 or Daxx within PML nuclear bodies was shown to promote apoptosis by unknown mechanisms. (G) Nuclear Par-4 also functions as a transcriptional cofactor regulating the transcription of pro- and anti-apoptotic genes. Especially, downregulation of NFκB transcriptional activity is an essential apoptosis-inducing function of Par-4. The mechanism of NFκB downregulation by Par-4 is unknown, but depends on the phospho-Thr 155 form of Par-4. (H) Par-4 inhibits the DNA relaxation function of TOP1. Three inactivation mechanisms for Par-4 have been demonstrated thus far and are shown in parts I-K. (I) Par-4 is inhibited by binding to AATF. (J) The phospho-Thr 155 form of Par-4 is phosphorylated by PKB at Ser 249 resulting in cytoplasmic sequestration of Par-4 through the chaperone 14-3-3. PKB can be activated by the aPKCs, which themselves are under control of Par-4. (K) p62 can rescue Par-4 inactivated aPKC through formation of a ternary complex. The aPKC kinase activity is restored in this complex. For more details see text. Arrows with white heads indicate a translocation, whereas black arrows indicate a stimulation.*

The functional significance of the co-localisation of Par-4 and THAP1 to PML nuclear bodies is currently not known. It is possible that THAP1 acts as transcriptional regulator and Par-4 as a cofactor of THAP1, regulating expression of pro- and anti-apoptotic proteins. PML nuclear bodies may further serve as a depot for both proteins and/or may have a regulatory role by modulating post-translational modifications of both proteins. Taken together, these results suggest that recruitment of THAP1 and Par-4 represents another pathway by which PML exerts its pro-apoptotic function. As described above, another pathway might involve Dlk that was also shown to localise to PML nuclear bodies [92]. The effects of Par-4/THAP1 association are summarised in Figure 1.4.

h) Wilm's tumour protein 1 (WT1)

WT1 is a tumour-suppressor gene that encodes four alternatively spliced isoforms. The WT1 proteins function as transcription factors that can activate or repress genes depending on the promoter and the physiological context. WT1 was shown to promote growth arrest by negatively regulating growth related genes. Sequence analysis shows the presence of four zinc-finger domains that form the DNA binding domain of WT1 and are essential for the interaction with Par-4 (Ref. [14] and references therein). A second Par-4 interaction domain within WT1 has been described, however, is specific to a certain splice isoform [93]. All four WT1 isoforms were shown to bind Par-4 through its LZ domain (residues 268-332). In almost all cases, binding of Par-4 to WT1 inhibits the transcriptional activation function and augments the transcriptional repression function of WT1 [14,93]. This indicates that nuclear localised Par-4 can act as a transcription repressor, however, nuclear localisation depends on the cell type and physiological context [14,94].

One of the important targets of WT1 is *bcl-2,* an important proto-oncogene promoting cell survival. As described above, binding of the Par-4/WT1 complex to the *bcl-2* promoter resulted in transcriptional repression of the *bcl-2* gene. Downregulation of Bcl-2 is an essential step in the Par-4 mediated apoptosis of androgen-independent prostate cancer cell line LNln3 [94]. Consistently, a mutually exclusive expression pattern is observed for Par-4 and Bcl-2 in various prostate tumour types [95]. Additionally, for lymphatic cells it was shown that Bcl-2 downregulation is a necessary step in the Par-4 apoptosis-sensitising function [96]. However, unlike Par-4, WT1 displays a limited expression pattern and the described mechanism for Bcl-2 downregulation may not be a ubiquitous event [14]. The effects of Par-4/WT1 association are summarised in Figure 1.4.

i) Androgen receptor (AR)

The AR is another example for Par-4 acting as a transcription cofactor in the nucleus. As described above, androgens are important signalling molecules in maintaining prostate homeostasis. The androgen action is mediated by the AR that upon androgen binding translocates to the nucleus and regulates specific target genes. Association of Par-4 with the DNA binding domain of the AR resulted in an upregulation of the transcriptional activity of AR. In contrast to WT1, Par-4 acted in this context as a transcriptional co-activator. Transcriptional enhancement was dependent on bound androgen ligands and there was no upregulation in the absence of the androgen ligand. The zinc-finger DNA binding domain of the AR is highly conserved among other steroid nuclear receptors, and Par-4 was shown to enhance transcription from estrogen, progesterone and glucocorticoid receptor controlled promoters. The interaction domain within Par-4 was mapped to residues 137-193, which overlaps with the previously described SAC domain. One of the important targets of the AR/Par-4 complex is the cFLIP promoter. In response to androgen signalling this complex initiates transcription of cFLIP thereby promoting cell survival. Conversely, androgen ablation in androgen-responsive prostate cells results in downregulation of cFLIP and upregulation of Par-4 and thus in induction of apoptosis. This model therefore explains some of the results observed for prostate (cancer) cells in response to androgen ablation (Ref. [54] and references therein). The effects of Par-4/AR association are summarised in Figure 1.4.

j) E2F1

Neural cells undergo glutamate-induced apoptosis in ischaemic brain tissue. Using human-bone mesenchymal stem cells as a model system, it could be shown that the glutamate-induced apoptosis is dependent on increased Par-4 expression and SMAC release from the mitochondria (for the function of SMAC see Fig. 1.3). The results further showed that Par-4 associates with the transcription factor E2F1 through the LZ domain within Par-4 (residues 262-332). This complex targets the *smac* promoter and thereby stimulates SMAC expression. Par-4 does not bind to DNA itself, but is recruited to the *smac* promoter through E2F1. The transcription cofactor activity of Par-4 is dependent on the LZ domain and a LZ deletion mutant failed to increase SMAC expression. Nuclear association of Par-4 and E2F1, and binding of this complex to the SMAC promoter were further shown to be dependent on glutamate treatment of the mesenchymal stem cells. As glutamate is a common messenger for neural cells, these results may

have important implications for stem cell therapies in ischaemic brain injuries [97]. The effects of Par-4/E2F1 association are summarised in Figure 1.4.

k) Topoisomerase 1 (TOP1)

Regulation of DNA relaxation by TOP1 is critical for cellular processes such as DNA replication, transcription or recombination. Consistent with this cell-growth promoting function, TOP1 activity was shown to be elevated in various cancer cells and TOP1 inhibitors are used in anti-cancer therapies for small cell lung cancer or colon cancer (Ref. [98] and references therein). Endogenous Par-4 and TOP1 were shown to interact in the nucleus in a variety of normal, immortalised and cancer cells. Essential for this interaction is the LZ domain (residues 268-332) within Par-4. Binding of Par-4 to TOP1 resulted in TOP1 sequestration and abrogated the binding of TOP1 to DNA. Inhibition of the TOP1 DNA-relaxation function resulted in an S-phase arrest, however, no apoptosis was observed in the studied cell lines. It was further shown that TOP1 is essential for cellular transformation and that inhibition of TOP1 function by Par-4 prevents transformation [98]. The effects of Par-4/TOP1 association are summarised in Figure 1.4.

l) β-site APP cleaving enzyme-1 (BACE-1)

Amyloid plaques are characteristic lesions in Alzheimer's disease and are mainly extracellular deposits of the amyloid β-peptide (Aβ) (1-42). Increased production, secretion and aggregation of Aβ(1-42) has been shown to be a neurotoxic event that contributes to the pathogenesis of Alzheimer's disease. Aβ(1-42) is produced by cleavage of APP through β- and γ-secretases. The β-secretase BACE-1 is a membrane-bound aspartyl protease and is responsible for early APP processing events (Ref. [99] and references therein). Par-4 overexpression was previously shown to stimulate Aβ(1-42) secretion in human neuroblastoma cells, whereas inactivation of Par-4 activity by a dominant negative Par-4 LZ construct prevented Aβ(1-42) production. Aβ(1-42) production occurred in a caspase dependent way and only after trophic factor withdrawal. This indicates that apoptosis and aberrant APP processing may be intimately linked processes [100]. Furthermore, in human neuroblastoma cells and primary hippocampal neurons, Par-4 selectively binds to the cytosolic site of BACE-1 increasing APP cleavage and Aβ(1-42) secretion [99]. The C-terminal half of Par-4 was necessary for the interaction with BACE-1 suggesting that binding to BACE-1 is through the LZ domain. Conversely, silencing of Par-4 by RNA interference resulted in decreased APP cleavage by BACE-1. These findings indicate the importance of Par-4

in Alzheimer's disease pathogenesis and its implication in the development of new therapeutic strategies [99]. The effects of Par-4/BACE-1 association are summarised in Figure 1.4.

m) Apoptosis-antagonising transcription factor (AATF)

AATF was initially identified as an interaction partner of Dlk. It was shown to contain two putative nuclear localisation signals and a leucine zipper domain. AATF and Par-4 selectively interact through their respective leucine zipper domains and co-localise both in the cytoplasm and the nucleus of neural cells. A Par-4 LZ deletion mutant (residues 1-265) was unable to bind to AATF indicating the importance of the Par-4 LZ domain for this interaction. Binding of AATF to Par-4 antagonised Par-4 mediated apoptosis implying a functional inhibitor role for AATF. As mentioned above, Par-4 is involved in APP processing and stimulation of Aβ(1-42) production thus increasing intracellular and secreted Aβ(1-42) levels. Increased Aβ(1-42) production is observed in neuronal cells undergoing apoptosis and was shown to contribute to the development of the Alzheimer's disease. Consistent with this role, AATF inhibits Par-4 induced Aβ(1-42) production and secretion in Alzheimer's disease models (Ref. [101] and references therein). The effects of Par-4/AATF association are summarised in Figure 1.4.

n) Glucose-regulated protein-78 (GRP78)

Association of Par-4 with GRP78 represents the first example for an extracellular function of Par-4. Cell culture studies indicated a bystander effect of Par-4 overexpression as neighbouring cells not expressing Par-4 were shown to undergo apoptosis. Ectopic and endogenous Par-4 are spontaneously secreted through a brefeldin A-sensitive pathway in cultured normal and cancer cells. Secretion of Par-4 was independent of apoptosis, but could be stimulated in response to ER-stress. The cell surface receptor GRP78 is a stress protein of the HSP70 superfamily and may promote either apoptosis or growth stimulation. Binding of Par-4 to GRP78 was shown to induce apoptosis through activation of the FADD/caspase-8 pathway in diverse cancer cell lines but not in non-transformed cells. Activation of FADD occurred through PERK (PKR-like ER kinase) a proximal component of the ER stress response pathway (Ref. [75] and references therein). Binding of Par-4 to GRP78 further induced an ER stress response loop upregulating and trafficking GRP78 to the cell surface in an intracellular Par-4 dependent manner. Sufficient for the interaction of Par-4 with GRP78 were the N-terminus within GRP78 and the SAC domain within Par-4. The ectopically expressed SAC domain was secreted in a similar manner as full-length Par-4. The same study also showed that the extracellular ligand TRAIL induces secretion

of Par-4, and that TRAIL induced apoptosis is dependent on both extra- and intracellular Par-4 [75]. This is important as TRAIL, like Par-4, selectively induces apoptosis in diverse cancer cells [71]. The effects of Par-4/GRP78 association are summarised in Figure 1.4.

o) Choline transporter CHT1

CHT1 is a sodium and chloride dependent choline transporter that is specifically located in cholinergic neurons. Cholinergic neurotransmission is important for various physiological functions (e.g. motor, autonomic, behavioural or cognitive functions) and defects in the cholinergic system have been implicated in disorders like Alzheimer's disease. Choline uptake is believed to be the rate-limiting step in acetylcholine synthesis in cholinergic neurons and thus essential for cholinergic transmission (Ref. [43] and references therein). Par-4 was shown to interact with CHT1 in cholinergic neurons through its C-terminal half (residues 164-332) suggesting that the LZ domain may be critical for this interaction. Association of Par-4 with CHT1 resulted in cytoplasmic sequestration of CHT1. Reduced incorporation of CHT1 into the cell membrane resulted in reduced choline uptake. The affinity of CHT1 for choline was unaltered when bound or unbound by Par-4. The regulation of choline uptake by Par-4 may have important implications for the pathogenesis of Alzheimer's disease, but may also be of general importance for synapse physiology in non-apoptotic neuronal cells [43].

p) Dopamine D2 receptor (D2DR)

Interaction of Par-4 with D2DR represents another modulatory function of Par-4 in neuronal signalling. An interaction between the D2DR and Par-4 was demonstrated by yeast two-hybrid assays. Additional experiments indicated an association of the endogenous proteins in mouse brain lysates. Using cultured striatal neurons, a co-localisation of Par-4 and D2DR could be shown for the periphery of the cell soma and neuronal processes. The interaction domains were mapped to the calmodulin binding motif in the third cytoplasmic loop of D2DR and to the LZ domain (residues 235-332) within Par-4. Binding of Par-4 to D2DR is essential for the dopamine-mediated inhibition of cyclic adenosine monophosphate (cAMP) signalling. A physiological relevance of this interaction has been demonstrated in mouse models where inhibition of the Par-4/D2DR complex formation resulted in the development of depression-like behaviours [45].

q) SPRY-domain containing SOCS box proteins 1, 2 and 4 (SSB-1, 2 and 4)

Little is known about the SSB proteins except that they contain two conserved motifs, the SPRY domain and the SOCS-box domains. SOCS-box containing proteins have been described as E3-ligases involved in ubiquitination and proteasomal degradation of proteins. SPRY domains on the other hand have been described as protein-protein interaction modules. For SSB-1 a more detailed function has been described where it is involved in enhancing Ras/ERK signalling. All three proteins SSB-1, 2 and 4 were shown to bind to Par-4 through the SPRY domain. However, the biological significance of this interaction and the involved Par-4 domains are unknown (Ref. [102] and references therein).

These results indicate that Par-4 has a wide spectrum of binding partners and that different domains of Par-4 are involved these interactions. Even though the interaction studies between Par-4 and its partners were carried out carefully, there is still the possibility that some of the interactions are false positive results. It was also shown that Par-4 is involved in both the extrinsic and the intrinsic pathway. Whereas Par-4 was shown to directly activate the extrinsic pathway through trafficking of Fas/FasL to the cell membrane [59], it is mainly involved in inhibiting anti-apoptotic proteins of the intrinsic pathway. It is interesting to note here that Par-4 activates caspase-8, thereby promoting cleavage of BID. Processed tBID is then translocated into the mitochondria, promoting the release of cytochrome c and other pro-apoptotic proteins thus activating the intrinsic pathway in a Par-4-dependent manner [103].

The Par-4 CC/LZ domain was shown to be the major interaction domain of Par-4. It is possible that for complexes where the interaction is mediated by the CC/LZ domain, other domains of Par-4 or other proteins may be involved in the interaction and thus necessary for the pro-apoptotic function. If contacts are solely mediated by the CC/LZ domain, a construct comprising only the Par-4 CC or LZ domain should have a similar effect. However, such a construct comprising the Par-4 CC domain was demonstrated to have an opposite effect than full-length Par-4 acting in a dominant negative manner [55]. This hypothesis remains speculative as the information about Par-4 protein complexes is sparse and as it is not known how the Par-4 CC construct acts in a dominant negative manner. Taken together, as can be expected for a strictly regulated cellular process like apoptosis, the pro-apoptotic function of Par-4 depends on a variety of factors: sub-cellular localisation, phosphorylation state, availability of interaction partners or cell type to name a few.

1.3.5. The oligomeric state of homo- and heteromeric Par-4 complexes

The Par-4 CC domain has been described in the previous chapter as the binding domain for the majority of interaction partners. Sequence analysis of the Par-4 CC domain (Chapter 4.1.2.) further suggests that Par-4 is able to self-associate through formation of a dimeric coiled coil. Experimental evidence for *in vivo* self-association of Par-4 was initially gained from yeast two-hybrid assays [48]. Immunoprecipitation experiments further suggested that the CC domain is required for self-association of mouse full-length Par-4 and a 33 kDa splice variant of Par-4 [47]. Recently, *in vitro* pull-down experiments using Par-4 deletion mutants confirmed that the CC domain is essential for self-association [54]. However, non of the above described experiments could demonstrate that self-association is via coiled coil formation, nor that Par-4 dimerises as suggested by the amino acid sequence. Therefore, the *in vivo* oligomeric state of Par-4 is still elusive. Similarly the exact stoichiometry of complexes of Par-4 and its binding partners are unknown. Association of Par-4 and its effector proteins was analysed *in vivo* and *in vitro* using yeast two-hybrid assays (e.g. Dlk [16] or THAP1 [92]), immunoprecipitation (e.g. p62, aPKCζ [88] or AATF [101]), or pull-down assays (e.g. WT1 [14] or Amida [53]). It remains to be determined if Par-4 forms 1:1 complexes with its partners, or if self-association of Par-4 is a prerequisite to form 2:1 complexes with its partners. The often described homo- and heterodimeristion of Par-4 [54,57] is therefore a hypothetical assumption based on the amino acid sequence, which awaits experimental confirmation.

1.4. Coiled Coils and Leucine Zippers

Sequence analysis predicts the presence of a coiled coil domain within the C-terminus of Par-4 (Chapter 1.2.1.). Coiled coils are common oligomerisation motifs and are predicted in approximately 10% of all eukaryotic proteins [104]. These amphipathic α-helical motifs are able to form left-handed supercoiled structures by wrapping two or more helices around each other [105]. The amino acid sequence of coiled coils is characterised by a seven residue repeat designated $(abcdefg)_n$ [106]. The *a* and *d* positions of each heptad are generally hydrophobic and form the centre of the oligomeric interface. Amino acids at other positions are generally polar or charged. Despite these simple sequence requirements, or perhaps because of it, a large variety of coiled coil structures is observed. Dimers [107,108], trimers [109,110], tetramers [111,112], pentamers [113] and heptamers [114] with varying orientation have been described in the literature.

Coiled coils are associated with various functions and can occur either as homo- or hetero-complexes. Short coiled coils of six or seven heptad repeats often function as protein-protein interaction domains in signal transduction pathways [115-121]. Long coiled coils of several hundred residues can form fibres, meshworks or scaffolds due to their rod-like tertiary structures [105] and have various functions, most notably as components of the cytoskeleton [122], the extra cellular matrix [123] and cellular motor proteins [124].

Leucine zippers are a special case of coiled coils and are often found in the bZIP (basic leucine zipper proteins) [117] and b-HLH-LZ (basic helix-loop-helix leucine zipper proteins) [118] transcription factor families. They are characterised predominantly by leucine residues at position *d* of the heptad repeat [125,126]. Together with hydrophobic residues at position *a* they form the oligomeric interface. Residues at position *a* are more variable and define the oligomeric state of the leucine zipper, whereas leucine residues at position *d* contribute mainly to leucine zipper stability [127]. Due to its favourable properties the GCN4 leucine zipper has been used to study the relationship between the oligomeric state of coiled coils and the effect of amino acid type at various heptad positions [109,128]. The most important factors determining the oligomeric state and helix orientation are (i) the packing complementarity of residues at positions *a* and *d*, (ii) electrostatic interactions between residues at positions *e* and *g*, and (iii) hydrogen bonding of buried and partially buried polar residues [128].

The occurrence of β-branched hydrophobic residues such as isoleucine or valine at position *a* has been correlated with a dimeric state, particularly if *d* positions are occupied by leucine residues. Conversely, trimeric and tetrameric states are observed if β-branched residues predominantly occupy *d* positions and leucine residues position *a* [109]. A GCN4 leucine zipper variant with exclusively isoleucine at positions *a* and *d* adopts a parallel trimeric conformation [109]. Interestingly, a pentameric coiled coil has been described if both the *a* and *d* position are occupied by phenylalanine residues [113]. The occurrence of polar residues, in particular asparagine, within the hydrophobic interface is also common. Whereas residues such as threonine at position *a* usually indicate heterodimeric coiled coils, asparagine residues at the same position result in homodimeric conformations[117]. The polar asparagine side chain interacts preferentially with other asparagine residues rather than with non-polar or other polar residues [129]. This helps to define a parallel unstaggered conformation of the dimer by forming an interhelical hydrogen bond between opposing asparagines in position *a* [107]. In contrast, other polar residues, such as threonine, preferentially form heterotypic interactions with opposing residues in position *a* necessitating heterodimeric coiled coils [129]. The specificity in

interhelical orientation and register conferred by asparagine (and other polar residues at position *a*) comes, however, at the expense of leucine zipper stability [109,130]. The decrease in leucine zipper stability was in these cases compared to the stability contributions of hydrophobic residues, such as isoleucine, leucine or valine, at position *a*. Interestingly, a trimeric coiled coil structures has been described that has almost exclusively asparagine residues at position *d* [131]. It was proposed that this trimeric structure is due to sequence peculiarities of the coiled coil domain of *Salmonella* autotransporter adhesins. Next to asparagine at *d* position, these coiled coils are marked by having primarily isoleucine at position *a* and threonine at position *e*. The high abundance of polar residues is thought to facilitate the sequestration of anions within the central cavity of the coiled coil, which thereby stabilises the trimeric structure.

Further contributions to leucine zipper oligomerisation specificity and stability stem from residues in the *e* and *g* positions. Charged residues at these positions are able to form interhelical ion-pairs [132,133]. Whereas the contribution of attractive *e-g* electrostatic interactions to leucine zipper stability and specificity is case-dependent [134,135], repulsive *e-g* electrostatic interactions are important destabilising factors that can affect overall leucine zipper stability and specificity [117,136]. In addition to charged amino acids, uncharged amino acids are also important factors in determining the oligomeric state of the coiled coil. Substitution of all residues at position *e* and *g* of the GCN4 leucine zipper with alanine resulted in a switch from a dimeric to a heptameric coiled coil [114]. Residues at position *e* and *g* are further important for helix orientation within the coiled coil, particularly for parallel and antiparallel tetramers[128]. For a special GCN4 variant, mutation of a single glutamate to cysteine was sufficient to switch from a parallel tetramer to an antiparallel one [137]. A further level of specificity and stability control arises from van der Waals interactions between the side-chain methylene groups of residues at positions *e* and *g,* and the sidechains of hydrophobic residues at positions *a* and *d* [107].

Isolated α-helices are rarely observed in aqueous solutions [138,139] unless certain additives such as trifluoroethanol (TFE) are added that favour helix formation (see Ref. [140] and references therein). Furthermore, helix formation and interhelical association are tightly coupled events. It was therefore proposed that coiled coil formation occurs, in most cases, as a two-state process between unfolded monomers and the coiled coil oligomers (e.g. dimer) [138,139]. A typical experimental indication of a two-state process for coiled coil formation is observed by Circular Dichroism (CD) spectropolarimetry in the form of an isodichroic point near 203 nm [134,136]. A different CD parameter that indicates coiled coil formation is obtained from the

ratio of the ellipticities at 222 and 208 nm ($[\theta]_{222}/[\theta]_{208}$ ratio). For α-helical proteins deep negative transitions at 222 nm and 208 nm are observed. Supercoiling as observed in coiled coils results in an increase of the ellipticity at 208 nm to less negative values, however, does not affect the ellipticity at 222 nm. Thus ratios above 1.0 are interpreted as an indication for a stable coiled coil [141, whereas ratios below 0.9 indicate non-coiled helices [142]. Based on these criteria, a detailed analysis of the Par-4 CC and LZ domain will be given in Chapter 4.1.2.

1.5. Intrinsically disordered proteins

The ubiquitous expression of Par-4, its post-translational modifications and a plethora of binding partners are characteristics common to many intrinsically disordered proteins (IDPs) [143] and prompted the investigation if Par-4 indeed can be classified as an IDP. A short introduction explaining the importance and characteristics of IDPs is given below. Under physiological conditions IDPs either entirely lack a well defined secondary and/or tertiary structure or contain long regions without a well defined secondary and/or tertiary structure. In contradiction to the structure-defines-function paradigm, stating that an ordered 3D structure is required for effective protein functioning, IDPs are biologically active and functional [144-146]. Proteins particularly involved in cell regulation exhibit a high prevalence for ID with approximately 75% of these proteins predicted to contain disordered regions of 40 or more consecutive residues. Cell regulation involves processes such as cell division, transcription, translation, signal transduction, protein phosphorylation, and assembly/disassembly of multi-protein complexes [146]. Additionally, cytoskeletal, ribosomal and cancer-associated proteins (e.g. Par-4) show a high abundance of disordered regions [147] implying that ID may be important for their function. The cancer-associated protein class may be considered as an extension of the cell regulatory protein class as highly regulated processes such as cell proliferation or apoptosis often become dysregulated in cancer cells [4]. A prominent example for the relation of signalling proteins with cancerous processes is the well established IDP p53. Loss of its transcriptional control due to mutations has been shown to contribute to the development of tumours [148]. This suggests an important function for ID in human diseases [149,150]. Consistent with these observations, ID is more common in the eukaryotic proteome than in the prokaryotic. Approximately 35-51% of eukaryotic proteins contain disordered regions of 40 or more consecutive residues relative to 6-33% of prokaryotic proteins. It was proposed that this is because eukaryotes utilise a more complex protein network for signalling and regulation [151,152].

IDPs possess characteristics that are distinct from those of folded globular proteins. Relative to globular proteins, the sequences of IDPs display a low complexity. Furthermore, IDPs are depleted of hydrophobic amino acids (e.g. Ile, Phe, Trp, Tyr) and hence enriched in polar and charged amino acids, and proline (e.g. Glu, Gly, Lys, Pro) [153]. The depletion of hydrophobic residues has an important consequence, it prevents the formation of a hydrophobic core. Hence, IDPs adopt rather elongated structures with increased hydrodynamic radii relative to globular proteins of similar molecular weight. The protein backbone further displays increased structural flexibility resulting in rapid interconversion between multiple conformers [146]. Multiple conformers are thought to arise as residues in disordered segments display a distribution of Ramachandran phi and psi angles. However, it was noted that IDPs tend to transiently adopt polyproline II helices in solution [154,155].

While some IDPs completely lack secondary structure, others exhibit partial secondary structure that may be transient in nature. In most cases the residual secondary structure is of α-helical nature predominating over β-strands [146]. Based on their structural properties such as secondary structural content or compactness, IDPs can be classified into three non-exclusive groups: random coil, pre-molten globule and molten globule. The latter two groups are marked by varying degrees of fluctuating secondary structure and increasing compactness [145]. The Protein Quartet model proposes [145] that a protein may exist in any of the four thermodynamic states: ordered, molten globule, pre-molten globule and random coil [144]. The function of the protein may depend on any of the states or on a transition between two of the states [144,145]. Various examples for the Protein Quartet model have been reviewed in references [144-146] and some of the most prominent examples are given below. This list is not thought to be comprehensive, but to give an impression of the complexity of cellular processes IDPs are involved in.

Several cases have been described where the biological function of IDPs resides in the disordered state. Disordered segments, due to their inherent flexibility, have been described to serve as linkers between structured domains in multi-domain proteins such as p53 [156] or Calmodulin [157]. Another function of disordered segments involves the presentation of post-translational modification, or protease digestion sites as suggested for Bcl-X_L and Bcl-2 [158-161]. Furthermore, disordered regions were demonstrated to function as entropic bristles necessary for the separation of neighbouring neurofilaments, or to serve as entropic springs such as Titin in muscle filaments [162]. Biologic functions for pre-molten globules, molten globules or transitions between either of the two have been described for various proteins; such as myelin

binding protein [163], calsequestrin [164] or 1,25-dihydroxyvitamin D_3 receptor [165]; upon binding to metal ions or other non-protein metabolites.

A common feature for many IDPs is a disorder-to-order transition upon binding to their biologic targets, a process termed induced folding [152,166]. Examples for induced folding includes the binding of p21 to Cdk2 [146,167], formation of a functional ribosome by ribosomal proteins [168], or binding of transcription factors such as the Lac-Repressor to DNA [169,170]. However, binding to a biologic target does not necessarily induce structure and examples are known where ID regions retain disorder and a high degree of flexibility after binding. One such case has been described for p27 bound to the Cdk2-Cyclin A complex. Residual flexibility in some regions of p27 allow for phosphorylation of a buried tyrosine residue thus marking p27 for ubiquitination and proteasomal degradation [171].

These examples indicate that ID is more common then previously thought. It was therefore asked what functional advantages IDPs possess. (i) As disordered regions are solvent exposed they are easily accessible for post-translational modifications that help control function, localisation and turnover. (ii) Consistently, disordered segments are more susceptible to proteolysis, which may influence the lifetime of an IDP in the cell. Proteolytic degradation was shown to depend on the exposition of protease cut sites or certain regulatory sequences such as PEST sites. These sites may be buried upon complexation thus increasing the lifetime of a protein, whereas in the non-complexed state the protein is rapidly degraded. However, since protein degradation *in vivo* is a highly regulated process the generality of this concept has been challenged. (iii) Disordered regions confer increased structural plasticity overcoming steric restrictions that result in larger interaction surface areas per residue compared to folded globular proteins [166]. (iv) Furthermore, IDPs bind their targets with high specificity yet low affinity; (v) the latter increasing association/dissociation rates. The fly-casting mechanism has been proposed to describe how increased association rates are achieved [172]. Due to their extendedness disordered segments can sample a larger solution volume for interaction partners relative to globular proteins. Binding to the target surface is initially weak followed by folding to reel in the target thereby increasing the strength of the interaction. (vi) Another important functional advantage of IDPs is their ability to specifically bind to structurally different targets [144-146]. This promiscuous binding property sparked the idea that IDPs function as hubs in protein interaction networks [173]. However, recent studies have challenged the generality and validity of this concept [174,175]. As the number of studied IDP complexes is increasing, more definitive results can be expected.

1.6. Assessing intrinsic disorder

The methods listed below represent only a small number of available methods to study protein disorder. These methods can be considered as initial experiments to assess ID. More information about these methods and additional experiments are found in the review articles given in Ref. [150,155,176] and references therein.

1.6.1. Computational methods

Due to their unique structural characteristics computational algorithms have been developed to recognise ID. Two prominent examples are PONDR [177] and DisEMBL [178]. Hydrophobic cluster analysis (HCA) identifies the presence or absence of hydrophobic clusters and thus might indicate regions of order or disorder [179]. Additionally, charge-hydrophobicity plots can be used to identify IDPs. In contrast to globular folded proteins, IDPs occupy a distinct space marked by high mean net charge and low mean hydrophobicity [144,180].

1.6.2. Biochemical methods

A first indication for ID can be gained from sodium dodecyl sulfate - polyacrylamide gel electrophoresis (SDS-PAGE). As IDPs tend to bind less SDS compared to globular folded proteins due to a depletion in hydrophobic amino acids, IDPs are marked by an abnormal electrophoretic mobility resulting in high apparent molecular weights (*MWs*). The SDS-PAGE determined *MWs* are often 1.2-1.8 times larger than can be expected from the amino acid sequence. In contrast to IDPs, globular proteins tend to aggregate upon heat or acid denaturation due to exposure of buried hydrophobic residues. As IDPs are depleted in hydrophobic residues, they exhibit increased thermal and acid resistance that has been successfully used to purify IDPs. As mentioned above, IDPs are hypersensitive to protease digestion. Folded segments in contrast to disordered regions sequester their protease cut sites and are thus cleaved at a much lower rate. Limited proteolysis assays may therefore be used to identify possible regions of ID (optimally combined with the analysis of possible fragments by mass spectrometry) [155].

1.6.3. Methods to assess the protein dimension and shape

In contrast to globular proteins, IDPs are marked by varying degrees of extended conformations. A critical parameter that can be determined in this respect is the hydrodynamic radius or Stokes radius (R_S). Consistent with the above mentioned IDP characteristics, the hydrodynamic radius (and thus the hydrodynamic volume) increases from globular, over molten

globule, pre-molten globule to coil-like states. Based on their hydrodynamic properties it is therefore possible to discriminate between these states [181]. Size exclusion chromatography (SEC) for instance is a simple method to assess the hydrodynamic properties of proteins. Due to their increased hydrodynamic radii IDPs produce higher apparent *MWs* by SEC compared to globular proteins of similar chain length. However, similar high apparent *MWs* are also observed for well-ordered but asymmetrically (i.d. non-globular) shaped proteins. Similarly, R_S values can be obtained from dynamic light scattering (DLS) experiments that allow distinction between globular proteins and IDPs. An alternative method for the determination of R_S values has been described for pulsed-field-gradient nuclear magnetic resonance (PFG-NMR) diffusion experiments [176].

Hydrodynamic properties of proteins can also be assessed by analytical ultracentrifugation, which determines the apparent sedimentation coefficient. This value is related to the *MW* and shape of the molecule, allowing *MW* estimates for proteins or protein complexes. A more powerful method for assessing the dimension and shape of proteins is small-angle X-ray scattering (SAXS). The shape of a protein may be determined by SAXS if it is well defined. Otherwise, the maximum dimensions can be obtained from the distance distribution function, which is the histogram of all interatomic distances within the molecule. Furthermore, the forward scattering intensity is proportional to the *MW* of a protein and thus allows the determination of the oligomeric state. This, in conjunction with the experimentally determined radius of gyration (R_g), allows the discrimination between globular, pre-molten globule and coil-like states. The R_g value is the root-mean-square distance from the centre of gravity of the molecule weighted by the electron density. Typically large R_g values are obtained for IDPs [155].

1.6.4. Methods for the assessment of secondary structure

One of the simplest methods to determine the secondary structural content is provided by far-UV CD spectropolarimetry. The CD effect relies on the interaction of circular polarised light with chiral compounds. For protein spectroscopy the interaction with the peptide bond proved to be crucial. As the CD signal reflects the symmetry of the peptide bond, it is dependent on the conformation of the two participating residues and thus gives information about the secondary structure [182]. CD measures the overall secondary structural content and does not allow the localisation of certain secondary structural elements to specific regions in the protein sequence. Furthermore, the obtained spectrum represents the population-weighted average of all structures in the conformational ensemble. CD spectra of IDPs are typically marked by a large negative

ellipticity at 200 nm, a negligible negative ellipticity at 222 nm, and an ellipticity close to zero at 185 nm. Other optical analysis methods to assess residual secondary structure are provided by Raman spectroscopy [150,155].

Nuclear magnetic resonance (NMR) spectroscopy allows, unlike CD spectropolarimetry, the determination of secondary structure down to the atomic level. Thus, secondary structural elements can be located within the protein sequence. A detailed description of NMR would be beyond the scope of this section, therefore only important concepts will be provided. NMR measures the magnetic properties of susceptible atoms such as ^{1}H, ^{13}C and ^{15}N. As the latter two are not naturally occurring in biologic samples, proteins can be enriched in these atoms with specific labelling techniques (Chapter 2.5.). In strong external magnetic fields these atoms, or more accurate spins, can be excited through absorption of energy, a phenomenon called resonance. Energy is provided through irradiation of radio wave pulses. NMR follows the return of the excited spins to equilibrium, which yields characteristic resonance frequencies for each spin. These resonance frequencies depend on local magnetic fields and thus on the local chemical environment. As the local chemical environment is influenced by neighbouring atoms, resonance frequencies are therefore reflective of the local secondary structure [183].

Due to their flexibility and rapid interconversion between multiple conformers, residues in IDPs experience similar local chemical environments. This results in similar resonance frequencies, especially of protons, and thus in a narrow spectral dispersion. As mentioned for CD spectropolarimetry, the observed resonance frequencies therefore represent a population-weighted average over all structures in the conformational ensemble [155]. For comparison with residues in secondary structural elements, these resonance frequencies have been termed random coil chemical shifts. Secondary structure induces a deviation from the random coil shifts termed the secondary chemical shift. As a result of secondary structure, an increased dispersion of the resonance frequencies is usually observed. Especially, ^{13}C resonances such as the alpha and beta carbons (C^{α} and C^{β}), or the carbonyl of the peptide bond (C') are sensitive to the secondary structure induced shifts. Therefore, the secondary chemical shift values of these residues can be used for the identification of secondary structural elements. Secondary structure can further be identified from specific proton-proton distances. These distances are measured by NOE (nuclear Overhauser enhancement) experiments.

Measurements of amide proton exchange rates by NMR can further provide information about the compactness of a protein. In folded segments the amide exchange rate is reduced due to a possible involvement in hydrogen bonds or due to burial in a hydrophobic core, whereas in

disordered regions the rate is increased as the amides are solvent exposed and unprotected. Finally, NMR determined dynamics of a residue can provide information about secondary structure, with residues in flexible segments having distinct dynamics than residues in ordered regions [150,155,176].

1.6.5. Methods to assess tertiary structure

Various methods can be applied to gain information about the presence of tertiary structure and, under certain conditions, of residual secondary structure. Differential scanning microcalorimetry (DSC) produces heat absorption curves, which shape is characteristic for the presence or absence of tertiary structure. Alternatively, extrinsic fluorescence compounds such as ANS may be used to identify residual hydrophobic core-like structures in a given protein. ANS binds to hydrophobic pockets that may be present in molten globule or pre-molten globule states resulting in a fluorescence increase. In this way molten globule or pre-molten globule states can be easily discriminated from extended coil-like states. Various other fluorescence techniques have been described to assess the degree of tertiary structure in IDPs, most importantly Förster resonance energy transfer (FRET) techniques. Due to the low abundance of tryptophan in IDPs this residue type is commonly used as donor in fluorescence experiments [150,155]. Information about the local environment of aromatic amino acid residues, in particular the tertiary structure around them, can be gained by near-UV CD spectropolarimetry (250-350 nm). Near-UV CD spectra of IDPs typically display a low complexity and intensity due to a lack of ordered structure. The aforementioned limited proteolysis assay is another method useful for the identification of possible regions of order.

NMR spectroscopy can also provide useful information about the tertiary structure of a protein. Long range NOE contacts over distances up to ~10 Å can indicate the proximity of certain regions within an IDP. However, these NOEs may be difficult to detect in IDPs as the contacts may be to short lived due to the inherent flexibility of the molecule. Therefore, a different NMR technique has been proven more useful in the determination of tertiary contacts within IDPs. Paramagnetic relaxation enhancement (PRE) involves the introduction of a paramagnetic label, commonly by coupling to free cysteine groups, which drives the enhanced relaxation of nearby nuclei. This method is more sensitive and enables the detection of contacts up to ~20-25 Å apart [150,155,176].

As IDPs are marked by fast interconversion between various structures the gathered structural information has to be interpreted as ensemble-average values. Despite computational approaches

a unique representation of the conformational ensemble has seldom been achieved. This is, however, of great importance for the analysis of the biological function, as only a small population of the ensemble might represent the biologically active state [176].

1.7. Research Aims

Par-4 is an important regulatory protein of apoptosis and has been associated with various human diseases such as cancer or neurodegenerative disorders. The Par-4 CC/LZ domain has been described in the literature as the main protein interaction domain of Par-4 (e.g. binding to aPKCζ). As will be discussed in Chapter 4, this domain shows sequence peculiarities that are detrimental to coiled coil stability. It was previously shown that the Par-4 LZ domain displayed a pH dependent coiled coil formation allowing self-association at low pH and low temperature [184].

(1) Determination of the NMR solution structure of the Par-4 LZ domain at low pH and low temperature was the main objective of this thesis. Furthermore, these results were to be compared with structural data of the Par-4 LZ domain in its disordered state at neutral pH.
(2) Also the NMR solution structures of two basic mutants of the Par-4 LZ domain that form a coiled coil independent of pH [185] were main objectives.
(3) Determination of the NMR solution structure of the Par-4 LZ domain in complex with the zinc-finger domain of the aPKCζ.
(4) Determination if the LZ domain of Par-4 binds to the aPKCζ as an oligomeric coiled coil or as an unfolded monomer.

However, instabilities of the LZ constructs and the insolubility of the aPKCζ zinc-finger domain prevented the completion of these objectives (Appendix C). Coiled coil formation of the Par-4 CC domain was therefore analysed using full-length Par-4 and Par-4 LZ deletion mutants that were considered to be more stable than the LZ constructs. Initial NMR experiments of a Par-4 LZ deletion mutant suggested that Par-4 may be an IDP. This idea was further corroborated by the facts that the multitude of Par-4 interaction partners and stringent control by post-translational modifications are characteristic features commonly linked with the concept of intrinsic disorder. Based on this hypothesis, new research aims were formulated and the results are reported in Chapter 3.

(5) Is there evidence for intrinsic disorder in Par-4?

(6) If Par-4 is an IDP, does it or specific sub-domains (e.g. SAC) contain residual secondary and/or tertiary structure?

(7) If residual structure is detected, can it be localised to specific regions in Par-4?

In contrast to earlier reports [184], full-length Par-4 self-associated independent of pH most likely via coiled coil formation. As an understanding of the molecular details of coiled coil formation in Par-4 may be beneficial for developing Par-4 inhibitors, analysis of the Par-4 CC/ LZ domain was resumed. Due to the experience gained with the isolation of full-length Par-4 stable Par-4 LZ constructs could be purified that allowed further analysis by NMR spectroscopy and CD spectropolarimetry. Despite clear indications for coiled coil formation of the isolated Par-4 LZ domain by CD spectropolarimetry, no coiled coil state was observed by NMR spectroscopy. These results are reported in Chapter 4.

(8) Why is the coiled coil state of the isolated Par-4 LZ domain, or of two basic mutants, not observed by NMR?

(9) What is the oligomeric state of the Par-4 LZ coiled coil?

(10) What factors influence the coiled coil stability of the Par-4 LZ domain?

(11) Is the Par-4 CC domain, unlike the LZ domain, sufficient to form a coiled coil independent of pH, and is the formed coiled coil more stable than the LZ coiled coil?

2. Expression and Purification of Par-4

2.1. Basic microbiologic techniques

A list of suppliers for the used materials and enzymes is given in Appendix A. Unless stated otherwise the buffer recommended by the manufacturer was used for enzymatic reactions. Standard molecular biologic procedures were performed as described in Sambrook *et al.* [186]. All buffers were prepared with MilliQ grade water and were autoclaved before use.

2.1.1. Preparation of ultra-competent cells

Ultra-competent *E. coli* cells were made from TOP10 or DH5α *E. coli* strains for plasmid maintenance and from BL21(DE3) CodonPlus or Rosetta(DE3) *E. coli* strains for protein expression. Starting from a glycerol stock, cells were streaked out on a Luria-Bertani (LB) Agar plate and incubated overnight at 37 ºC. For BL21(DE3) CodonPlus and Rosetta(DE3) strains LB-Agar plates were supplemented with 34 µg/ml chloramphenicol (Cam). A single colony was picked and used to inoculate 50 ml of LB medium. The culture was agitated at 37 ºC until an OD_{600} = 0.3-0.4 and subsequently incubated on ice for 15 min. Cells were harvested by centrifugation for 15 min at 4 ºC and 3,300 g (Heraeus Multifuge 1 S-R, Rotor TTH400, Kendro, Langenselbold, Germany). The cell pellet was resuspended in 18 ml RF1 buffer, containing 100 mM RbCl, 50 mM $MnCl_2$, 10 mM $CaCl_2$ and 30 mM KAc, pH 5.8. The cell suspension was kept on ice for 30 min and then centrifuged again. The cell pellet was resuspended in 4 ml RF2 buffer, containing 10 mM RbCl, 75 mM $CaCl_2$, 10 mM MOPS. The cell suspension was divided into 100 µl aliquots and stored at -80 ºC.

2.1.2. Transformation of E. coli cells

Ultra-competent *E. coli* cells were thawed on ice for 10 min. Typically 10 ng of plasmid DNA (Chapters 2.3. and 2.4.) were added and the cell suspension was gently mixed. Cells were incubated on ice for 30 min, then put into a water bath kept at 42 ºC for 90 s and incubated again on ice for 120 s. After adding 400 µl of SOC medium the transformation reactions was agitated for one hour at 37 ºC in a shaking incubator. The transformation reaction was plated out on LB-Agar plates, which were supplemented with the necessary antibiotics for the plasmid and the *E. coli* strain, and left to dry for one hour on the bench close to a burning Bunsen burner. The LB-Agar plates were incubated at 37 ºC overnight, but no longer than 18 h.

2.1.3. Preparation of glycerol stocks

A single colony from the LB-Agar plate was picked and used to inoculate 25 ml of LB medium. Depending on the plasmid and *E. coli* strain used, the LB medium contained 0.1 mg/ml ampicillin (Amp) or 0.1 mg/ml Amp and 34 µg/ml Cam, respectively. The culture was agitated at 37 ºC up to an OD_{600} = 0.5-0.6. From that culture 10 ml were centrifuged for 15 min at 4 ºC and 3,300 g (Rotor TTH400). The cell pellet was resuspended in 1 ml LB medium with 25% glycerol ($^{v}/_{v}$) and stored at -80 ºC.

2.2. Expression and purification of recombinant proteases

2.2.1. Expression and purification of HMBP-3Cpro

The 3C protease from human rhinovirus 14 was expressed as a fusion protein with an N-terminal hexa-histidine and maltose binding protein-tag (HMBP) [187] and therefore denoted HMBP-3Cpro. A 25 ml preculture of LB, containing 0.1 mg/ml Amp and 34 µg/ml Cam, was inoculated with cell material from a glycerol stock and agitated overnight at 37 ºC. The OD_{600} value was measured and the preculture centrifuged for 15 min at 4 ºC and 3,300 g (Rotor TTH400). The cell pellet was resuspended in 3 ml fresh LB and then used to inoculate the main culture. The main culture had a volume of 500 ml LB containing 0.1 mg/ml Amp and 34 µg/ml Cam. The volume of the preculture used for inoculation was measured so that the main culture had a starting OD_{600} = 0.06. The main culture was agitated at 37 ºC up to an OD_{600} = 0.6. Expression was induced by the addition of isopropyl-β-D-thiogalactopyranoside (IPTG) to a concentration of 0.4 mM and cells were incubated overnight at 25 ºC with agitation. Cells were harvested by centrifugation at 4,400 g and 4 ºC (Sorvall Evolution RC, Rotor GS3, Kendro, Langenselbold, Germany).

The cell pellet was resuspended in 20 ml 100 mM NaCl, 25 mM imidazole, 0.5 mM TCEP and 50 mM Na_2HPO_4/NaH_2PO_4, pH 8.0 and 50 µl of the protease inhibitor cocktail were added. The cell suspension was passed three times through a French Press (AMINCO, Silver Spring, USA). The cell lysate was clarified by centrifugation for 30 min at 14,000 g and 4 ºC (Heraeus Multifuge 1 S-R, Rotor FA12.94 High*conic*, Kendro, Langenselbold, Germany). The supernatant was passed through a 0.8 µm syringe filter and the filtrate was rotated for 3 h with 2 ml (bed-volume) Chelating Sepharose, which had been charged with $NiCl_2$ and equilibrated to the lysis buffer. The Ni-NTA column was washed successively with 10 ml lysis buffer and 5 ml lysis buffer with 50 mM imidazole. The 64 kDa fusion protein was eluted with 10 ml 100 mM NaCl, 250 mM imidazole, 0.5 mM TCEP and 50 mM Na_2HPO_4/NaH_2PO_4, pH 8.0. HMBP-3Cpro

containing fractions were pooled and dialysed overnight at 4 ºC against 500 ml 200 mM NaCl, 1 mM DTT and 40 mM Na_2HPO_4/NaH_2PO_4, pH 7.8. The dialysate was concentrated to a protein concentration of approximately 5 mg/ml using a Vivaspin 20 device (*MWCO* = 10 kDa) at 3,000 g and 4 ºC (Rotor TTH400). After adding ice-cold glycerol to 25% ($^v/_v$), HMBP-3Cpro was divided into 1 ml aliquots and stored at -20 ºC. Cleavage reactions were usually performed for 10 h and 4 ºC at a HMBP-3Cpro to substrate ratio of 1:100.

2.2.2. Expression and purification of rTEV protease

The rTEV protease from tobacco etch virus was expressed as a fusion protein with an N-terminal hexa-histidine tag. The rTEV expressing *E. coli* strain was kindly provided by Dr. Gill Norris (Institute of Molecular Biosciences, Massey University, New Zealand). The rTEV expressing *E. coli* strain was streaked out on an agar plate, containing 0.1 mg/ml Amp and 30 µg/ml kanamycin (Kan), and incubated overnight at 37 ºC. A 25 ml preculture of LB, containing 0.1 mg/ml Amp and 30 µg/ml Kan was inoculated with a single colony from the agar plate and agitated overnight at 37 ºC. The OD_{600} value was measured and the preculture centrifuged for 15 min at 4 ºC and 3,300 g (Rotor TTH400). The cell pellet was resuspended in 3 ml fresh LB and then used to inoculate the main culture. The main culture had a volume of 500 ml LB, containing 0.1 mg/ml Amp and 30 µg/ml Kan. The volume of the preculture used for inoculation was measured so that the main culture had a starting OD_{600} = 0.06. The main culture was agitated at 37 ºC up to an OD_{600} = 0.6. Expression was induced by the addition of IPTG to a concentration of 0.1 mM and cells were incubated overnight at 25 ºC with agitation. Cells were harvested by centrifugation at 4,400 g and 4 ºC (Rotor GS3).

The cell pellet was resuspended in 20 ml 100 mM NaCl, 25 mM imidazole, 10% glycerol ($^v/_v$) and 50 mM Na_2HPO_4/NaH_2PO_4, pH 8.0 and 50 µl of the protease inhibitor cocktail were added. The cell suspension was passed three times through a French Press. The cell lysate was clarified by centrifugation for 30 min at 14,000 g and 4 ºC (Rotor FA12.94 High*conic*). The supernatant was passed through a 0.8 µm syringe filter and the filtrate was rotated for 3 h with 2 ml (bed-volume) Chelating Sepharose, which had been charged with $NiCl_2$ and equilibrated to the lysis buffer. The Ni-NTA column was washed successively with 10 ml lysis buffer and 5 ml lysis buffer with 50 mM Imidazole. The 27 kDa fusion protein was eluted with 10 ml 100 mM NaCl, 500 mM imidazole, 10% glycerol ($^v/_v$) and 50 mM Na_2HPO_4/NaH_2PO_4, pH 8.0. rTEV containing fractions were pooled and the buffer concentration adjusted to 1 mM EDTA and 1 mM DTT. The eluate was concentrated to a protein concentration of 1-2 OD_{280} using a Vivaspin 20 device

(*MWCO* = 10 kDa) at 3,000 g and 4 ºC (Rotor TTH400). The concentrate was dropped with a 1 ml pipette into liquid nitrogen. The formed balls were collected and stored in 1.5 ml reaction tubes (7-8 balls per tube) at -80 ºC. One ball with 2 OD_{280} usually cleaves 5 mg protein in 2 h at room temperature.

2.2.3. Summary

With the methods described above highly active HMBP-3Cpro and rTEV protease were purified. The proteases were stable and remained active for at least 9 months; for HMBP-3Cpro even 18 month old preparations showed very good cleavage activity. The use of proteases with an N-terminal hexa-histidine tag allowed the removal of the proteases by immobilised metal ion affinity chromatography (IMAC). In the case of HMBP-3Cpro separation by affinity chromatography with Amylose resin is possible as well. High purity of the proteases is not necessary and hence the purification time is very short. Since most of the impurities elute at imidazole concentrations of 250 mM, they are likely to be removed together with the protease by the second IMAC step used for the removal of the expression tag after cleavage of the Par-4 fusion proteins (see below). In case of the Par-4 constructs with a GST tag (Chapters 2.10. and 2.11.), these impurities are removed by the RP-HPLC (reversed phase-high performance liquid chromatography) step. Furthermore, the proteases are used at lower concentrations than the Par-4 fusion proteins and the impurities are therefore considerably diluted. This dilution effect also makes a buffer exchange step to reduce the imidazole concentration for rTEV obsolete.

2.3. Preparation of cell free expression vectors

2.3.1. Materials and Methods

Primer sequences, annealing temperatures and the templates used for the PCR reactions are listed in Table 2.1. PCR with KOD Polymerase was performed according to the manufacturers instructions with the following cycle:

1.) 2 min at 95 ºC
2.) 60 s at 95 ºC
3.) 45 s at X ºC (see Table 2.1)
4.) 60 s at 72 ºC
5.) 5 min at 72 ºC
steps 2.) to 4.) are repeated 30 times

The PCR products and the pET23a vector were cut with *Nde* I and *BamH* I according to the manufacturers instructions. The double digested PCR products and vectors were ligated with T4-DNA Ligase at 16 ºC according to the manufacturers instructions. The ligation reaction was used to transform TOP10 *E. coli* cells (Chapter 2.1.1.). Vectors with the correct sequence were identified by sequencing of the plasmid (Allan Wilson Centre for Molecular Ecology and Evolution, Massey University, New Zealand).

Construct Name	Forward Primer (5'-3')	Reverse Primer (5'-3')	Template	Annealing Temperature
pCFE-GST-3C	CTGGCATATGTCCCCTATACTAGGTTAT	CCGGGGATCCCAGGGGCCCCTGGAACAG	pGex-4T-3	55 ºC
pCFE-GST-TEV	CTGGCATATGTCCCCTATACTAGGTTAT	CCGGGGATCCCTGAAAATACAGGTTTTCATCCGATTTTGGAGGATG	pGex-4T-3	55 ºC
pCFE-GST-TEV2	CTGGCATATGTCCCCTATACTAGGTTAT	CCGGGGATCCCTGAAAATACAGGTTTTCGGTCGTTGGGATATCGTAATCATCCGATTTTGGAGGATG	pGex-4T-3	45 ºC
pCFE-HMal-TEV	GGGAATTCCATATGCATCACCATCACCATCACATGAAAACTGAAGAAGGTAAACTGG	CCGGGGATCCCTGAAAATACAGGTTTTCCCCGAGGTTGTTGTTATTGTT	HpMal-c2P	50 ºC
pCFE-HTEV	GAGCGGCCATATGTCGTACTACCATCACCATCACC	TGCCAAGCTTTCTAGAGGATCCGGATTGAAAATACAGGTTTTCGGTC	pET32TEV	55 ºC
pCFE-TrxH-TEV	CTGGCATATGAGCGATAAAATTATTCAC	CCGGGGATCCCTGAAAATACAGGTTTTCGGTCGTTGGGATATCGTAATCGTGATGGTGATGGTGATGCATATG	pET32a	55 ºC

Table 2.1 *– Preparation of cell free expression vectors. Primer sequences, DNA templates and annealing temperatures used for PCR amplification to prepare the cell free expression vectors.*

2.3.2. Results and Discussion

Cell free expression [188] is a method combining *in vitro* transcription and translation for rapid protein expression. Therefore, the time consuming fermentation of *E. coli* cell cultures is not necessary. This also allows the expression of proteins that would be toxic to the expression host. Additives such as ligands, detergents or chaperones can be added to increase the yield in folded protein [188]. Another advantage that this system allows is selective isotopic labelling. Using defined combinations of isotopically labelled and unlabelled amino acids, various labelling schemes can be achieved. As cell free expression is based on *in vitro* transcription with T7-RNA-Polymerase from plasmid DNA, co-expression of various proteins from different plasmids containing the T7-promoter is possible. Co-expression of Par-4 proteins with potential

binding partners, in particular with the zinc finger domain of aPKCζ, was considered as a potential expression method for Par-4, as complex formation might increase the solubility of full-length Par-4. The aPKCζ constructs and particularly full-length Par-4 (Chapter 2.6.) are mostly insoluble in native lysis buffer and different purification strategies had to be considered.

The requirements for a cell free expression vector are (i) a T7-promoter and T7-terminator for transcription initiation and termination, (ii) a ribosome binding site and an initiation codon for translation initiation and (iii) a multi cloning site for insertion of the protein sequence. These requirements are based on the cell free expression system used by our collaborator Dr. Andrew Kralicek (HortResearch, Auckland, New Zealand). It was further necessary to exclude a *lac* operator from the operon. Since *in vitro* translation systems use cell lysates [188], in particular from *E. coli*, endogenous *lac* repressor may prevent transcription from vectors containing a *lac* operator. Hence, the *lac* repressor coding *lacI* gene must be removed. Therefore, the pET23a vector was chosen as the backbone for all cell free expression vectors (pCFE-vectors) listed in Table 2.1. pET23a contains no *lac* operator and *lacI* gene, but instead it has a T7 promoter and a T7 terminator. Also the ribosome binding site and initiation codon are correctly spaced relative to each other. The multi cloning site offered the use of the same restriction enzymes as were already used by our group. This allows a simple transfer of Par-4 inserts from existing vectors to the new pCFE-vectors. Expression tags such as glutathione S-transferase (GST), maltose binding protein (MBP), thioredoxin or a hexa-histidine tag can easily be inserted into the *Nde* I and *BamH* I site without affecting the spacing between ribosome binding site and initiation codon.

The strong T7 promoter allows high level protein expression in *E. coli* cells containing the λDE3 lysogen. However, under certain circumstances, high level expression may be detrimental and lead to insoluble or improperly folded protein. In addition, due to the missing *lac* operator, transcription control is less stringent compared to other vectors, which may be problematic for cytotoxic proteins. More stringent control can be achieved using hosts carrying pLysS or pLysE genes (pET System Tutorial, Merck Biosciences, Darmstadt, Germany).

Various cell free expression vectors were created during the PhD offering the choice between different purification tags such as (i) **GST** (pCFE-GST-3C, pCFE-GST-TEV or pCFE-GST-TEV2), (ii) **MBP** (pCFE-HMal-TEV), (iii) **thioredoxin** (pCFE-TrxH-TEV) or (iv) a **hexa-histidine** tag (pCFE-HTEV). Plasmid maps of each vector are given in Appendix B. The pCFE-vectors with GST as purification tag further offer the choice between two different proteases (HMBP-3Cpro and rTEV) for the removal of the purification tag. pCFE-GST-TEV and pCFE-GST-TEV2 differ in the length of the spacer between GST and the rTEV cleavage site. The

longer spacer of pCFE-GST-TEV2 might be favourable if bulky proteins are fused to GST. MBP, thioredoxin and the hexa-histidine tag allow purification through standard IMAC purification protocols. In addition, the well established solubilising properties of MBP allow the expression of target proteins with limited solubility. rTEV is the protease of choice as it only leaves a two amino acid (pCFE-GST-TEV, pCFE-GST-TEV2 and pCFE-HMal-TEV) or three amino acid artefact (pCFE-HTEV and pCFE-TrxH-TEV) at the N-terminus of the target protein (see plasmid maps, Appendix B). rTEV has further advantages over HMBP-3Cpro as will be discussed in Chapter 2.12.1.

Sequencing showed that all cell free expression vectors listed in Table 2.1 had the correct sequence. The vectors pCFE-GST-TEV (Chapter 2.11.4.), pCFE-HMal-TEV (data not shown), and pCFE-TrxH-TEV (Chapter 2.8.2.) were used for protein expression in *E. coli* cells and showed good expression results. The expression levels are comparable to other vectors (pET32a, HpMal-c2P). In the case of pCFE-HMal-TEV with a human rhinovirus 14 3C protease insert, the over-expressed fusion protein accounted for approximately 30% of the total cell proteins as judged by SDS-PAGE (personal communication with Dr. J. Claridge). *In vitro* expression was tested by Dr. Andrew Kralicek with pCFE-GST-3C, pCFE-HMal-TEV and pCFE-TrxH-TEV. Protein expression is observed only for pCFE-TrxH-TEV and only with aPKCζ inserts. pCFE-TrxH-TEV constructs with inserts from Par-4 show no expression indicating a dependence of protein expression from the insert. The expressed aPKCζ proteins were, however, mostly insoluble (personal communication with H. Venugopal). It is not clear why other pCFE-vectors (pCFE-GST-3C and pCFE-HMal-TEV) or pCFE-TrxH-TEV vectors with Par-4 inserts, e.g. Par-4(1-290)G40G in pCFE-TrxH-TEV (Chapter 2.8.2.), show no expression. These vectors show good expression in *E. coli* cells indicating a functional operon.

Taken together, a new set of expression vectors was created allowing stable over-expression of heterologous recombinant proteins. Various expression tags are combined with cleavage sites for highly specific proteases allowing the removal of the expression tag. Due to the same multi cloning site in all vectors transfer of inserts between different vectors is simplified. Hence, different purification strategies can be selected depending on the kind of expression vector allowing an adaptation of the purification process to the properties of the target protein.

2.4. Preparation of Par-4 expression vectors

2.4.1. Materials and Methods

Table 2.2 contains a list of all prepared Par-4 expression vectors. It lists the PCR primer sequences and the templates used for the PCR reactions. The expression vector and restriction enzymes used for cloning are also given. PCR with *Pwo* or KOD Polymerase was performed according to the manufacturers instructions. The PCR cycles for the two used polymerases were:

***Pwo* Polymerase**	**KOD Polymerase**
1.) 5 min at 94 ºC	1.) 2 min at 95 ºC
2.) 60 s at 94 ºC	2.) 20 s at 95 ºC
3.) 45 s at 60 ºC	3.) 15 s at 60 ºC
4.) 75 s at 72 ºC	4.) 45 s at 72 ºC
5.) 5 min at 72 ºC	5.) 5 min at 72 ºC
steps 2.) to 4.) are repeated 30 times	steps 2.) to 4.) are repeated 30 times

The expression vectors and PCR products were digested with the corresponding restriction enzymes (Table 2.2) according to the manufacturers instruction. Cut vectors and inserts were ligated with T4-DNA Ligase according to the manufacturers instruction. The ligation reaction was used to transform TOP10 or DH5α *E. coli* cells (Chapter 2.1.1.). Correct insertion of the PCR product was assessed by sequencing of the plasmid (Allan Wilson Centre for Molecular Ecology and Evolution, Massey University, New Zealand). Plasmids with the correct sequence were used to transform the expression hosts *E. coli* BL21(DE3) CodonPlus or Rosetta(DE3).

pET32TEV is an in-house expression vector created by Dr. Rose Brown (Institute of Molecular Biosciences, Massey University, New Zealand) and is derived from pET32a. The hexa-histidine tag and TEV cleavage site from pProEX-HTb was PCR amplified using the Primers 5'-GGTTCTGGCCATATGTCGTACTACCATCACCATCA-3' (Fw) and 5'-TGCCAAG CTTTCTAGAGGATCCGGATTGAAAATACAGGTTTTCGGTC-3' (Rv). The PCR product was cut with *Msc* I and *BamH* I and then used to replace the original sequence, with a Thrombin and Enterokinase cleavage site, in pET32a. The vector name HpMal-c2P is used instead of HMBP-3C [187] to avoid any confusion with the hexa-histidine and MBP-tagged 3C protease (HMBP-3Cpro).

Construct Name	Forward Primer (5'-3')	Reverse Primer (5'-3')	Template	Restriction Enzymes	Expression Vector
Par-4(1-332)WT	CAGGAATTCCATGGCGACCGGCGGCTATCGGAGC	CAGGTCGACTTACCTTGTCAGCTGCCCAACAAC	rat Par-4 cDNA	*EcoR* I / *Sal* I	pGex-4T-3
Par-4(1-332)WT	CAGGAATTCAAATGGCGACCGGCGGCTATCGGAG	CAGGTCGACTTACCTTGTCAGCTGCCCAACAAC	rat Par-4 cDNA	*EcoR* I / *Sal* I	pProEX-HTb
Par-4(1-332)G40G	CAGGGATCCATGGCGACCGGCGGCTATCGGAG	CTTGGCGGCTGGATCTCCGCCGCTCGAAC	rat Par-4 cDNA	*BamH* I	pET32a
	GTTCGAGCGGCGGAGATCCAGCCGCCAAG	CAGGTCGACTTACCTTGTCAGCTGCCCAACAAC	rat Par-4 cDNA	*Sal* I	
Par-4(1-332)G40G	CAGGGATCCATGGCGACCGGCGGCTATCGGAG	CAGGTCGACTTACCTTGTCAGCTGCCCAACAAC	Par-4(1-332)G40G in pET32a	*BamH* I / *Sal* I	pET32TEV
Par-4(1-290)G40G	CAGGGATCCATGGCGACCGGCGGCTATCGGAG	CCGGAAGCTTTTATTCTTCTTTATCTTGCATCAG	Par-4(1-332)G40G in pET32a	*BamH* I / *Hind* III	pCFE-TrxH-TEV
Par-4(286-332)WT	GCACTAGGATCCCAAGATAAAGAAGAAATG	CAGGTCGACTTACCTTGTCAGCTGCCCAACAAC	rat Par-4 cDNA	*BamH* I / *Sal* I	pCFE-GST-3C
Par-4(286-332)WT	GCACTAGGATCCCAAGATAAAGAAGAAATG	CAGGTCGACTTACCTTGTCAGCTGCCCAACAAC	rat Par-4 cDNA	*BamH* I / *Sal* I	pCFE-GST-TEV
Par-4(286-332)WT	GCACTAGGATCCCAAGATAAAGAAGAAATG	CAGGTCGACTTACCTTGTCAGCTGCCCAACAAC	rat Par-4 cDNA	*BamH* I / *Sal* I	pGex-6P-3
Par-4(286-332)N313I	GCACTAGGATCCCAAGATAAAGAAGAAATG	CCTGCTTTAGTTGCTCGATTTCGTC	Par-4(286-332) WT in pGex-6P-3	*BamH* I	pGex-6P-3
	GACGAAATCGAGCAACTAAAGCAGGA	CAGGTCGACTTACCTTGTCAGCTGCCCAACAAC	Par-4(286-332) WT in pGex-6P-3	*Sal* I	

Table 2.2 *– Preparation of Par-4 expression vectors. Primer sequences and DNA templates for PCR amplification are given. Restriction enzymes and host vectors are also listed.*

2.4.2. Results and Discussion

The Par-4 constructs made for this study were designed so that they produce proteins, which are of biological significance (Chapter 1.2.). All sequence numberings refer to the rat isoform of Par-4. Note that the cDNA of rat Par-4 was used as a template for PCR reactions during the preparation of Par-4 expression vectors. Full-length constructs of Par-4 (Par-4(1-332)) were made as reference constructs to all other constructs comprising deletion mutants and single domains of Par-4. To take advantage of an N-terminal *BamH* I site, an internal *BamH* I site present in the rat Par-4 cDNA was removed by PCR (Table 2.2). Constructs with this silent point mutation are denoted G40G instead of WT (wild-type). Using a *BamH* I site at the N-terminus reduces the N-terminal cloning artefact for most expression vectors, especially for vectors of the pET series. Also transfer between different expression vectors is simplified as most *BamH* I sites

are in the same translation frame in various vectors. As mentioned in the Introduction, ectopic over-expression of Par-4 in PC3 or melanoma cells showed that the LZ domain is essential for the sensitivity to apoptotic stimuli [55]. Deletion mutants that lack the LZ domain, however, did not confer enhanced sensitivity [55]. Two such LZ deletion mutants were made (Par-4(1-265) and Par-4(1-290)). The Par-4(1-290) constructs contain 15 additional residues of the C-terminal CC region (residues 254-332) [46]. The rationale was to determine if coiled coil formation is possible without the LZ domain. The SAC domain is sufficient for apoptosis induction in cancer cells [50]. Therefore, a similar construct as used in this previous study comprising only the SAC domain was made (Par-4(137-195)). A construct comprising the CC domain (Par-4(240-332)) was made as it was shown that this domain is able to act in a dominant negative manner abrogating the pro-apoptotic function of Par-4 [55]. Various constructs of the LZ domain (Par-4 (286-332)) were made as these constructs show an interesting pH dependent folding behaviour [184]. However, a physiological function has not been described for this construct. The Par-4 (286-332)W285 mutant was created to determine the protein concentration by A_{280} measurements as the wild-type LZ domain does not contain aromatic residues. The rationale for the creation of the Par-4(286-332)D305K and E310K point mutants is described in Dutta *et. al.* [185]. In short, these two mutants adopt a coiled coil conformation independent of pH.

Sequencing confirmed correct insertion of the PCR products into the vectors and verified the right nucleotide sequence for almost all constructs. Only one Par-4 expression vectors listed in Table 2.2 could not be created during the PhD (see below). Some of the vectors used in this study were created by other researchers in a similar way and their acknowledgements are given below. The HpMal-c2P expression vectors of Par-4(286-332)WT, Par-4(286-332)W285, Par-4 (286-332)D305K and Par-4(286-332)E310K [184,185], and the pGex-6P-3 expression vector of Par-4(240-332)WT were kindly provided by Dr. Kaushik Dutta (New York Structural Biology Center, New York, USA). The HpMal-c2P expression vectors of Par-4(1-332)WT, Par-4(1-265) WT and Par-4(1-290)WT were prepared by Dr. Komala Ponniah (Institute of Molecular Biosciences, Massey University, Palmerston North, New Zealand). Par-4(137-195)WT in pET32TEV was created by Sachin Kate (Institute of Fundamental Sciences, Massey University, Palmerston North, New Zealand).

The only Par-4 expression vector that could not be created during the PhD was Par-4(1-332) WT in pGex-4T-3. Even though a similar vector is described in the literature [53], all attempts to create this vector resulted in recombination. Sequencing of several clones after transformation showed that both the pGex-4T-3 vector and the PCR product were cut properly at the 5' and 3'

end and that the PCR product and the vector ligated properly. However, in all sequenced constructs the central part of Par-4, approximately residues Ser 8 to Asp 308, was lost by recombination. Restriction digest, ligation and transformation were repeated, however, gave similar results. Additionally, different *E. coli* strains such as DH5α, TOP10 or BL21(DE3) CodonPlus were tested, but all gave similar results. As expression results of Par-4(1-332)G40G from pET32a were promising, preparation of the pGex-4T-3 vector was abandoned. Re-cloning of this construct was not tried as Par-4(1-332) can be purified in high purity from a different construct.

Due to improper cleavage of the 5'-end of the PCR insert for pCFE-GST-3C four additional nucleotides were included between the ribosome binding site and the initiation codon. In case of Par-4(286-332)WT in pCFE-GST-3C (Chapter 2.11.2.) this increased spacing between the ribosome binding site and the initiation codon still allowed expression. However, the protein expression levels were comparable to the pGex-6P-3 (Chapter 2.11.3.) vector suggesting that the increased spacing decreased the expression efficiency. pCFE-GST-3C has been re-cloned to remove these four additional residues, but it has not been tested for expression with new inserts.

2.5. Protein expression and labelling techniques

2.5.1. Expression of unlabelled Par-4

Par-4 was expressed either from BL21(DE3) CodonPlus or Rosetta(DE3) *E. coli* cells. A preculture, 20 to 50 ml LB containing 0.1 mg/ml Amp and 34 µg/ml Cam, was inoculated with cell material from a glycerol stock and agitated overnight at 37 ºC. The OD_{600} value was measured and the preculture centrifuged for 15 min at 4 ºC and 3,300 g (Rotor TTH400). The cell pellet was resuspended in 1-3 ml fresh LB and then used to inoculate the main culture. The main culture had a volume of 300-1000 ml LB, containing 0.1 mg/ml Amp and 34 µg/ml Cam. The volume of the preculture used for inoculation was measured so that the main culture had a starting OD_{600} = 0.06. The main culture was agitated at 37 ºC up to an OD_{600} = 0.6. Expression was induced by the addition of IPTG to a concentration of 0.4 mM and cells were agitated at 25 ºC for 8 h or overnight, respectively. Cells were harvested by centrifugation at 4,400 g and 4 ºC (Rotor GS3).

2.5.2. Expression of $^{13}C/^{15}N$-labelled Par-4

For isotopic labelling of proteins with ^{13}C and (or) ^{15}N, the initial steps are identical to the expression of unlabelled proteins (see above). When the main culture had reached an

OD_{600} = 0.6, cells were harvested by centrifugation for 15 min at 4,400 g and 4 ºC (Rotor GS3). The cell pellet was resuspended in half the starting volume of M9 minimal medium, i.d. 250 ml of M9-medium if the main culture had a volume of 500 ml. The culture was agitated for 30 min at 30 ºC with agitation. ^{15}N-ammonium chloride and uniformly ^{13}C-labelled D-glucose were dissolved in 10 ml M9 medium and added to the culture by sterile filtration through a 0.2 µm syringe filter to a final concentration of 1 g/l and 6 g/l, respectively. For proteins with only ^{15}N labelling, ^{13}C-labelled D-glucose was substituted by ^{12}C-D-glucose. After one hour incubation at 30 ºC, expression was induced by the addition of IPTG to a concentration of 0.4 mM and cells were agitated at 25 ºC for 8 h or overnight, respectively. Cells were harvested by centrifugation at 4,400 g and 4 ºC (Rotor GS3).

2.5.3. Deuteration of Par-4

Deuterated proteins were produced with M9 minimal medium utilising D_2O as solvent and with d^8-glycerol (final concentration 6 g/l) as sole carbon and ^{15}N-ammonium chloride (final concentration 1 g/l) as sole nitrogen source. A preculture; 20 to 50 ml LB containing 0.1 mg/ml Amp and 34 µg/ml Cam; was inoculated with cell material from a glycerol stock and agitated overnight at 37 ºC. The OD_{600} value was measured and the preculture centrifuged for 15 min at 4 ºC and 3,300 g (Rotor TTH400). The cell pellet was resuspended in 1 ml fresh M9 medium and then used to inoculate 25 ml of M9 medium to an OD_{600} = 0.06. The culture was agitated at 37 ºC up to an OD_{600} = 0.6 or higher. The culture was harvested by centrifugation for 15 min at 4 ºC and 3,300 g (Rotor TTH400), the cell pellet resuspended in 1 ml fresh M9 medium and the main culture of 250 ml M9 medium was then inoculated to an OD_{600} = 0.06. The main culture was agitated at 37 ºC up to an OD_{600} = 0.6. Expression was induced by the addition of IPTG to a concentration of 0.4 mM and cells were agitated at 25 ºC for 38 h. Cells were harvested by centrifugation at 4,400 g and 4 ºC (Rotor GS3).

2.5.4. REDPRO expression of Par-4

REDPRO (reduced protonation) [189] samples of Par-4 were produced with M9 minimal medium utilising D_2O as solvent and with uniformly ^{13}C-labelled D-glucose (final concentration 6 g/l) as sole carbon and ^{15}N-ammonium chloride (final concentration 1 g/l) as sole nitrogen source. Competent BL21(DE3) CodonPlus cells(Chapter 2.1.1.) were freshly transformed with plasmid DNA. A preculture; 20 to 50 ml LB containing 0.1 mg/ml Amp and 34 µg/ml Cam; was inoculated with a single colony and agitated overnight at 37 ºC. The OD_{600} value was measured

and the preculture centrifuged for 15 min at 4 ºC and 3,300 g (Rotor TTH400). The cell pellet was resuspended in 1 ml fresh LB medium and then used to inoculate the main culture; 500 ml to 2 l LB containing 0.1 mg/ml Amp and 34 µg/ml Cam; to an OD_{600} = 0.06. The culture was agitated at 37 ºC up to an OD_{600} = 2.0. The culture was harvested by centrifugation for 15 min at 4,400 g and 4 ºC (Rotor GS3), and the cell pellet resuspended in a quarter of the starting volume of M9 medium containing D_2O, e.g. 125 ml M9 medium if the main culture had a volume of 500 ml. The culture was incubated for one hour at 25 ºC with agitation, and expression was induced by the addition of IPTG to a concentration of 0.4 mM. After 5-8 h incubation at 25 ºC with agitation, cells were harvested by centrifugation at 4,400 g and 4 ºC (Rotor GS3). An adapted version of this protocol has been used in the later stages of the PhD for the production of ^{15}N-labelled samples.

2.6. Purification of Par-4(1-332)

2.6.1. Purification of Par-4(1-332)WT from HpMal-c2P

a) Materials and Methods

For conciseness, purification steps are described once in detail as a general protocol. For later protocols only differences to this general protocol will be described. Unless stated otherwise all Par-4 purifications were performed on ice or at 4 ºC. All purification methods are described for a culture volume of one litre.

The cell pellet was resuspended in 20 ml PBS and 100 µl of the protease inhibitor cocktail were added. The cell suspension was passed three times through a French Press. The cell lysate was clarified by centrifugation for 30 min at 14,000 g (Rotor FA12.94 High*conic*). The supernatant was passed through a 0.8 µm syringe filter and the filtrate rotated for 3 h with 2 ml (bed-volume) Chelating Sepharose, which had been charged with $NiCl_2$ and equilibrated to PBS. The Ni-NTA column was washed successively with 10 ml PBS, 15 ml PBS with 1 M NaCl and 10 ml PBS. For cleavage of the Par-4 fusion protein, the TCEP concentration was adjusted to 0.3 mM, HMBP-3Cpro was added and the Ni-NTA column was rotated overnight at 4 ºC. In case of incomplete cleavage of the Par-4 fusion protein more HMBP-3Cpro was added and the cleavage reaction continued till more than 90% of the fusion protein was cleaved. Cleaved Par-4 (1-332)WT was eluted from the column with 10 ml PBS. Par-4(1-332)WT containing fractions were pooled and concentrated to 2 ml using a Vivaspin 20 device (*MWCO* = 10 kDa) at 3,000 g (Rotor TTH400). To remove traces of residual MBP, the concentrate was applied to 2 ml Amylose resin and the flow-through collected.

b) Results

Par-4(1-332)WT in HpMal-c2P was expressed in an unlabelled form with a final OD_{600} = 4 after overnight expression. The Par-4 fusion protein was mostly soluble, but 40-50% remained in the insoluble fraction after clarification of the cell lysate. The IMAC purified Par-4 fusion protein was 70-80% pure and was cleaved on the column with HMBP-3Cpro. Adding TCEP to a concentration of 0.3 mM improved the cleavage performance of HMBP-3Cpro and nearly 90% of the Par-4 fusion protein was cleaved. Due to the same electrophoretic mobility of MBP and Par-4(1-332)WT, only one band corresponding to a 45 kDa protein is visible by SDS-PAGE. Amylose resin purification showed that all eluted protein bound to the Amylose resin, indicating that only MBP eluted from the Ni^{2+}-Sepharose column. Cleaving the Par-4 fusion protein in solution, resulted in protein precipitation, suggesting that Par-4(1-332)WT without the MBP tag is mostly insoluble in solution. Hence no Par-4(1-332)WT could be purified with this method.

2.6.2. Purification of Par-4(1-332)WT from pProEX-HTb

a) Materials and Methods

The cell pellet was resuspended in 20 ml 100 mM NaCl, 25 mM imidazole and 50 mM Na_2HPO_4/NaH_2PO_4, pH 8.0 and 100 µl of the protease inhibitor cocktail were added. Cell lysis and incubation with Chelating Sepharose are described in Chapter 2.6.1. The Ni-NTA column was washed successively with 10 ml lysis buffer and 5 ml lysis buffer with 50 mM imidazole. The Par-4 fusion protein was eluted with 10 ml 100 mM NaCl, 250 mM imidazole and 50 mM Na_2HPO_4/NaH_2PO_4, pH 8.0. Par-4 fusion protein containing fractions were pooled and dialysed overnight against 500 ml 100 mM NaCl, 25 mM imidazole, 0.3 mM TCEP and 20 mM Tris, pH 8.0. The Par-4 fusion protein was cleaved for 4 h at room temperature with rTEV (Chapter 2.2.2.).

b) Results

Par-4(1-332)WT in pProEX-HTb was expressed in an unlabelled form with a final OD_{600} = 5 after overnight expression. A protein of the correct size (~45 kDa), as estimated by SDS-PAGE, was purified by IMAC. Dialysis of this protein against rTEV cleavage buffer (100 mM NaCl, 25 mM Imidazole, 0.3 mM TCEP and 20 mM Tris, pH 8.0) resulted in protein precipitation. Cleavage of the remaining soluble protein with rTEV showed no cleavage activity, suggesting that the isolated protein is a bacterial protein without rTEV cleavage site. Optimising induction of protein expression with various IPTG concentrations (final concentrations 0-0.5 mM) showed

no upregulated protein relative to the non-induced cell culture, indicating that Par-4(1-332)WT is not expressed from pProEX-HTb.

2.6.3. Purification of Par-4(1-332)G40G from pET32a

a) Materials and Methods

Cell lysis and IMAC purification are described in Chapter 2.6.2. Par-4 fusion protein containing fractions were pooled and dialysed overnight against 500 ml 150 mM NaCl, 0.5 mM EDTA, 0.3 mM TCEP and 50 mM Tris, pH 7.5. The Par-4 fusion protein was cleaved overnight with 1 mg Thrombin.

b) Results

Par-4(1-332)G40G in pET32a was expressed in an unlabelled form with a final OD_{600} = 4 after overnight expression. A 60 kDa protein, as estimated by SDS-PAGE, was isolated by IMAC and was more than 90% pure after elution. As described in Chapter 2.6.1, over 50% of the Par-4 fusion protein remained in the insoluble fraction after clarification of the cell lysate. Cleavage of the Par-4 fusion protein with Thrombin resulted in the degradation of the Par-4 fusion protein as was indicated by SDS-PAGE with protein bands below 20 kDa.

2.6.4. Native purification of Par-4(1-332)G40G from pET32TEV

a) Materials and Methods

Cell lysis and IMAC purification are described in Chapter 2.6.2. Par-4 fusion protein containing fractions were pooled and dialysed overnight against 500 ml 100 mM NaCl, 25 mM imidazole, 0.3 mM TCEP and 20 mM Tris, pH 8.0.

b) Results

Par-4(1-332)G40G in pET32TEV was expressed in an unlabelled form with a final OD_{600} = 4 after overnight expression. Using a standard lysis buffer with 100 mM NaCl, approximately 90% of the Par-4 fusion protein remained in the insoluble fraction after clarification of the cell lysate. Lysis conditions were optimised with six different buffers, testing two NaCl concentrations (250 and 500 mM) at three different pH values (pH 6.0, 7.0 and 8.0). The imidazole and Na_2HPO_4/ NaH_2PO_4 concentration were the same in all six lysis buffers. Using a lysis buffer containing 500 mM NaCl at pH 8.0, almost 90% of the Par-4 fusion protein remained in the soluble fraction after clarification of the cell lysate. Note that at pH 6.0 the Par-4 fusion protein was virtually

insoluble, with intermediate solubility at pH 7.0. The IMAC purified Par-4 fusion protein was ~80% pure after elution and had an apparent *MW* of 60 kDa as judged by SDS-PAGE (Fig. 2.1, lane 7). Dialysis against rTEV cleavage buffer resulted in an almost complete precipitation of the Par-4 fusion protein. Hence, no Par-4(1-332)G40G could be purified by this method.

2.6.5. Denaturing purification of Par-4(1-332)G40G from pET32TEV − Purification of rrPar-4FL

a) Materials and Methods

Unless stated otherwise, all steps of the denaturing purification were carried out at room temperature. The cell pellet was resuspended in 20 ml 8 M urea, 1 M NaCl, 25 mM imidazole, 100 mM NaH_2PO_4 and 10 mM Tris, pH 8.0 and 100 µl of the protease inhibitor cocktail were added. The cell suspension was passed three times through a French Press. The cell lysate was clarified by centrifugation for 30 min at 14,000 g and 4 ºC (Rotor FA12.94 High*conic*). The supernatant was passed through a 0.8 µm syringe filter and the filtrate rotated for 3 h with 2 ml (bed-volume) of Chelating Sepharose, which had been charged with $NiCl_2$ and equilibrated to the lysis buffer. The Ni-NTA column was washed successively with 10 ml lysis buffer and 5 ml lysis buffer with 50 mM imidazole. The Par-4 fusion protein was eluted with 10 ml 8 M urea, 500 mM NaCl, 250 mM imidazole, 100 mM NaH_2PO_4 and 10 mM Tris, pH 8.0. Par-4 fusion protein containing fractions were pooled and dialysed for 6 h against 500 ml 4 M urea, 250 mM NaCl, and 50 mM Tris, pH 8.0, followed by an overnight dialysis against 500 ml cleavage buffer, containing 1 M urea, 100 mM NaCl, 25 mM imidazole, 0.3 mM TCEP and 50 mM Tris, pH 8.0. The Par-4 fusion protein was cleaved for 6 h with rTEV. After more than 90% of the Par-4 fusion protein was cleaved, the cleavage reaction was applied again to the Ni-NTA column, which had been equilibrated to the cleavage buffer. The flow through was collected and the Ni-NTA column washed with 5 ml cleavage buffer. Par-4(1-332)G40G containing fractions were pooled and concentrated to 2 ml using a Vivaspin 20 device (*MWCO* = 10 kDa) at 3,000 g and 25 ºC (Rotor TTH400).

Par-4(1-332)G40G was further purified either by ion-exchange chromatography (IEC) or RP-HPLC. Ion-exchange chromatography was performed using a HiTrap Q FF column connected to the BioLogic DuoFlow System (BioRad, Hercules, USA). Par-4(1-332)G40G was purified on a linear gradient of 0-60% high salt buffer over 20 min. The low salt buffer contained 1 M urea, 50 mM NaCl and 20 mM Tris, pH 7.5; the high salt buffer contained 1 M urea, 1 M NaCl and 20 mM Tris, pH 7.5. Par-4 was purified at 4 ºC with a flow rate of 0.8 ml/min. Par-4(1-332)

G40G containing fractions that were free of impurities, were pooled and concentrated using a Vivaspin 20 device (*MWCO* = 10 kDa) at 3,000 g and 4 ºC (Rotor TTH400). Buffer exchange was achieved by successive 1:1 dilution with 20 mM NaCl, 10 mM Tris, pH 7.0 and subsequent re-concentration. After 8 steps the buffer exchange was to 99.6% complete.

RP-HPLC was performed with a Delta Pak C18-300Å column connected to an Ultimate 3000 HPLC (Dionex Corporation, Sunnyvale, USA). Par-4(1-332)G40G was purified at 25 ºC with a flow rate of 1.5 ml/min using a linear water-acetonitrile gradient of 20-45% over 20 min in the presence of 0.1% TFA ($^{v}/_{v}$). Par-4(1-332)G40G containing fractions that were free of impurities were lyophilised and then resolubilised in 20 mM NaCl, 10 mM Tris, pH 7.0. The protein concentration was determined by A_{280} and A_{205} absorbance measurements using the extinction coefficient 13,075 $M^{-1}cm^{-1}$ and the relationship described by Scopes [190].

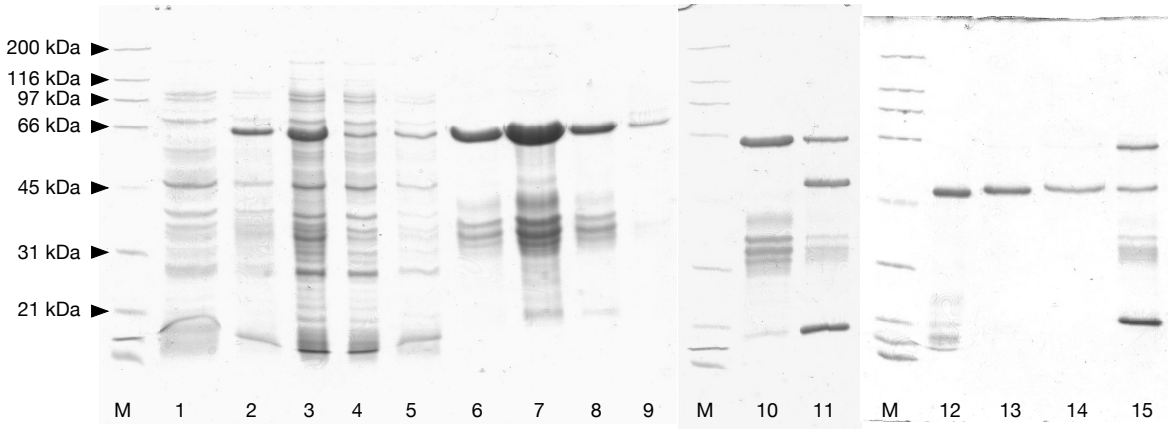

Figure 2.1 *− Denaturing purification of rrPar-4FL. A typical purification of Par-4 by IMAC is shown for rrPar-4FL using a denaturing purification protocol. Similar results are obtained for other Par-4 constructs using native protocols. All fractions were analysed by 11% SDS-PAGE. Expression of the thioredoxin-Par-4(1-332)G40G fusion protein is evident from the comparison of (1) non-induced and (2) induced E. coli cells. Note that the size of the Par-4 proteins as judged by SDS-PAGE is greater than what is expected from the amino acid sequence (66 kDa relative to 51 kDa for the fusion protein and 46 kDa relative to 36 kDa for rrPar-4FL). The cell lysate was clarified by centrifugation (3) and applied to a Ni-NTA column. After 3 h incubation the flow-through (4) was collected and the column washed successively with buffers containing 25 mM (5) and 50 mM (6) imidazole. The fusion protein was eluted from the column with 250 mM imidazole (7,8) and the Ni-NTA column assessed for remaining fusion protein (9). The fusion protein was dialysed against cleavage buffer containing 1 M urea (10) and incubated for 6 h with rTEV protease at room temperature (11). The cleavage reaction was applied again to a Ni-NTA column to remove the thioredoxin tag. After 3 h incubation the flow-through (12) was collected and the column washed with cleavage buffers (13,14). The Ni-NTA column was assessed for remaining rrPar-4FL (15). rrPar-4FL was then further purified by RP-HPLC (data not shown). Lanes with molecular weight (MW) markers are labelled with (M). Approximate molecular weights are shown on the left edge.*

b) Results

Using a denaturing purification protocol almost all Par-4 fusion protein remained in the soluble fraction after clarification of the cell lysate. The IMAC purified Par-4 fusion protein was 70-80% pure after elution. Reducing the urea concentration for the cleavage reaction resulted in precipitation of ~10% of the Par-4 fusion protein. The cleaved Par-4(1-332)G40G after the second IMAC purification was ~90% pure (Fig. 2.1, lane 12). Buffer exchange of the IEC-purified Par-4(1-332)G40G with a Vivaspin 20 device resulted in a complete loss of Par-4 (1-332) due to precipitation. Alternatively, dialysing the IEC-purified Par-4(1-332)G40G and then concentrating it, also lead to a complete loss due to precipitation.

Using RP-HPLC for final purification, improved the purity of Par-4(1-332)G40G (rrPar-4FL) to > 98% as judged by mass spectrometry (MS, Centre for Protein Research, University of Otago, Dunedin, New Zealand). Resolubilising the lyophilised rrPar-4FL in 20 mM NaCl, 10 mM Tris, pH 7.0 gave a concentrated (0.43 mM) soluble protein. Storage of this solution at 4 ºC resulted in protein precipitation after a few days. The protein yield using the denaturing purification protocol and RP-HPLC was ~20 mg rrPar-4FL per litre cell culture. Par-4(1-332) G40G purified by this protocol (denaturing purification, RP-HPLC) will be denoted as **rrPar-4FL** throughout the remainder of this text.

2.7. Purification of Par-4(1-265)

2.7.1. Purification of Par-4(1-265)WT from HpMal-c2P

a) Materials and Methods

Cell lysis and IMAC purification are described in Chapter 2.6.2. Par-4 fusion protein containing fractions were pooled and dialysed overnight against 500 ml 150 mM NaCl, 25 mM imidazole, 0.3 mM TCEP and 20 mM Tris, pH 7.5. The Par-4 fusion protein was cleaved overnight with HMBP-3Cpro. After more than 90% of the Par-4 fusion protein was cleaved, the cleavage reaction was applied again to the Ni-NTA column, which had been equilibrated with the cleavage buffer. The flow through was collected and the Ni-NTA column washed with 5 ml 1 M NaCl. Traces of residual MBP were removed by applying the Par-4(1-265)WT containing fractions to 2 ml Amylose resin and collecting the flow-through.

b) Results

Par-4(1-265)WT in HpMal-c2P was expressed in an unlabelled form with a final OD_{600} = 4.5 after overnight expression. More than 95% of the Par-4 fusion protein remained in the soluble

fraction after clarification of the cell lysate. The IMAC purified Par-4 fusion protein was 70-80% pure after elution and appeared as a 80 kDa protein as judged by SDS-PAGE. After HMBP-3Cpro cleavage two bands of 45 kDa (MBP) and 40 kDa (Par-4(1-265)WT) were visible by SDS-PAGE. Separation of MBP and Par-4(1-265)WT by a second IMAC step resulted in retention of Par-4(1-265)WT on the Ni-NTA column together with the majority of MBP. The flow through only contained MBP. Applying the cleavage reaction to Amylose resin also failed to separate MBP from Par-4(1-265)WT. The purification was stopped after most of Par-4(1-265) WT had degraded.

2.8. Purification of Par-4(1-290)

2.8.1. Purification of Par-4(1-290)WT from HpMal-c2P

a) Materials and Methods

The purification of Par-4(1-290)WT from HpMal-c2P is identical to the protocol described in Chapter 2.7.1. for Par-4(1-265)WT from HpMal-c2P.

b) Results

Par-4(1-290)WT in HpMal-c2P was expressed in an unlabelled form with a final OD_{600} = 5 after overnight expression. The results for the purification are virtually identical to the results described above for the purification of Par-4(1-265)WT from HpMal-c2P and no Par-4(1-290) WT could be purified due to degradation.

2.8.2. Purification of Par-4(1-290)G40G from pCFE-TrxH-TEV − Purification of rrPar-4ΔLZ

a) Materials and Methods

Cell lysis and IMAC purification are described in Chapter 2.6.2. Par-4 fusion protein containing fractions were pooled and dialysed overnight against 500 ml 100 mM NaCl, 25 mM imidazole, 0.3 mM TCEP and 20 mM Tris, pH 8.0. The Par-4 fusion protein was cleaved for 4 h at room temperature with rTEV. After more than 90% of the Par-4 fusion protein was cleaved, the cleavage reaction was applied again to the Ni-NTA column, which had been equilibrated with the cleavage buffer. The flow through was collected and the Ni-NTA column washed with 5 ml cleavage buffer. Par-4(1-290)G40G containing fractions were pooled and concentrated using a Vivaspin 20 device (*MWCO* = 10 kDa) at 3,000 g (Rotor TTH400).

The concentrate was further purified by IEC on a HiTrap Q FF column connected to the BioLogic DuoFlow System. Par-4(1-290)G40G was purified at 4 ºC with a flow rate of 0.8 ml/

min using a linear gradient of 0-60% high salt buffer over 20 min. The low salt buffer contained 50 mM NaCl and 20 mM Na_2HPO_4/NaH_2PO_4, pH 7.5; the high salt buffer contained 1 M NaCl and 20 mM Na_2HPO_4/NaH_2PO_4, pH 7.5. Par-4(1-290)G40G containing fractions that were free of impurities, were pooled and concentrated using a Vivaspin 20 device (*MWCO* = 10 kDa) at 3,000 g and 4 ºC (Rotor TTH400). Buffer exchange was achieved by successive 1:1 dilution with 20 mM NaCl, 10 mM Tris, pH 7.0 and subsequent re-concentration. After 8 steps the buffer exchange was to 99.6% complete. The protein concentration was determined as described in Chapter 2.6.5.a.

b) Results

Par-4(1-290)G40G in pCFE-TrxH-TEV was expressed in unlabelled and ^{15}N-labelled form with final OD_{600} = 4.0 and OD_{600} = 6.0, respectively, after overnight expression. More than 95% of the Par-4 fusion protein remained in the soluble fraction after clarification of the cell lysate. The IMAC purified Par-4 fusion protein was 70-80% pure after elution and appeared as a 55 kDa protein as judged by SDS-PAGE. The purity of the cleaved Par-4(1-290)G40G after the second IMAC step was ~90% and improved to > 95% after the IEC step as judged by MS. The protein yield was ~22 mg Par-4(1-290)G40G per litre cell culture. Par-4(1-290)G40G purified by this protocol will be denoted as **rrPar-4ΔLZ** throughout the remainder of this text.

2.9. Purification of Par-4(137-195)

2.9.1. Purification of Par-4(137-195)WT from pET32TEV − Purification of rrPar-4SAC

a) Materials and Methods

Purification of Par-4(137-195)WT from pET32TEV is virtually identical to the protocol described above for Par-4(1-290)G40G from pCFE-TrxH-TEV except for the IEC step (Chapter 2.8.2.a). IEC was performed at 4 ºC with a flow rate of 0.8 ml/min using a HiTrap SP FF column and a linear gradient of 0-60% high salt buffer over 25 min. The low salt buffer contained 50 mM NaCl, 20 mM Na_2HPO_4/NaH_2PO_4, pH 6; the high salt buffer contained 1 M NaCl, 20 mM Tris, pH 7.5. Par-4(137-195)WT containing fractions that were free of impurities, were pooled and concentrated using a Vivaspin 20 device (*MWCO* = 3 kDa) at 3,000 g and 4 ºC (Rotor TTH400). Buffer exchange was achieved by successive 1:1 dilution with 20 mM NaCl, 10 mM Tris, pH 7.0 and subsequent re-concentration. After 8 steps the buffer exchange was to 99.6% complete. The protein concentration was determined by A_{280} and A_{205}

absorbance measurements as described in Chapter 2.6.5.a with an extinction coefficient of 1,490 $M^{-1}cm^{-1}$.

b) Results

Par-4(137-195)WT in pET32TEV was expressed in ^{15}N-labelled form with a final OD_{600} = 4.0 after overnight expression. More than 95% of the Par-4 fusion protein remained in the soluble fraction after clarification of the cell lysate. The IMAC purified Par-4 fusion protein was 80-90% pure after elution and appeared as a 25 kDa protein as judged by SDS-PAGE. The purity of the cleaved Par-4(137-195)WT after the second IMAC step was ~95% and improved to > 98% after the IEC step as judged by MS. Concentration of Par-4(137-195)WT in 20 mM NaCl, 10 mM Tris, pH 7.0 resulted in minor precipitation. The protein yield was ~8 mg Par-4(137-195) WT per litre cell culture. Par-4(137-195)WT purified by this protocol will be denoted as **rrPar-4SAC** throughout the remainder of this text.

2.10. Purification of Par-4(240-332)

2.10.1. Denaturing purification of Par-4(240-332)WT from pGex-6P-3 − Purification of rrPar-4CC

a) Materials and Methods

The cell pellet was resuspended in 20 ml PBS and 100 µl of the protease inhibitor cocktail were added. The cell suspension was passed two times through a French Press. The cell lysate was clarified by centrifugation for 30 min at 16,000 g and 4 ºC (Sorvall Evolution RC, Rotor SS34, Kendro, Langenselbold, Germany). The supernatant was stored overnight at 4 ºC. To increase protein yields the centrifugation pellet was resuspended in 15 ml 6 M urea, 250 mM NaCl, 5 mM DTT and 50 mM Tris, pH 8.0. The suspension was passed again through a French Press and clarified as described above. The supernatant was dialysed for 3 h at room temperature against 500 ml 2 M urea, 250 mM NaCl, 1 mM DTT and 50 mM Tris, pH 8.0, followed by 3 h at room temperature against 500 ml 0.5 M urea, 250 mM NaCl, 1 mM DTT and 50 mM Tris, pH 8.0, and finally overnight at 4 ºC against 500 ml 250 mM NaCl, 1 mM DTT and 50 mM Tris, pH 8.0. Any precipitate occurring during dialysis was removed by centrifugation at 14,000 g (Rotor FA12.94 High*conic*). The dialysate was then united with the clear supernatant from the first lysis (see above), passed through a 0.8 µm syringe filter, and the filtrate was rotated for 3 h with Glutathione Sepharose, which had been equilibrated with PBS. The Glutathione Sepharose was washed with 10 ml 1 M NaCl, 20 mM Na_2HPO_4/NaH_2PO_4, pH 7.0 followed by 5 ml PBS.

The Par-4 fusion protein was eluted with 6 ml 10 mM reduced glutathione, 50 mM Tris, pH 8.0. Par-4 fusion protein containing fractions were pooled and dialysed for 1 h at 4 ºC against 500 ml 150 mM NaCl, 1 mM DTT and 20 mM Tris, pH 7.5. The Par-4 fusion protein was cleaved at 4 ºC with HMBP-3Cpro and dialysis was continued overnight. The resulting precipitate was spun down for 15 min at 14,000 g (Rotor FA12.94 High*conic*) and the pellet was resolubilised in a minimal volume of 7 M urea.

The urea resolubilised Par-4(240-332)WT was further purified by RP-HPLC using a Delta Pak C18-300Å column connected to the Ultimate 3000 HPLC system. The protein was purified at 25 ºC with a flow rate of 1.0 ml/min using a linear water-acetonitrile gradient of 30-50% over 25 min in the presence of 0.1% TFA ($^{v}/_{v}$). Par-4(240-332)WT containing fractions that were free of impurities, were lyophilised and then resolubilised in H_2O. The protein concentration was determined by A_{205} absorbance measurements as described by Scopes [190].

b) Results

Par-4(240-332)WT in pGex-6P-3 was expressed in unlabelled form with a final OD_{600} = 4.3 after overnight expression. Using a denaturing protocol, more than 95% of the Par-4 fusion protein remained in the soluble fraction after clarification of the cell lysate. Reducing the urea concentration of the cell lysate by dialysis, resulted in protein precipitation of approximately 20% of the Par-4 fusion protein. The purified Par-4 fusion protein was more than 90% pure after elution and appeared as 37 kDa protein as judged by SDS-PAGE. During the cleavage reaction the majority (> 95%) of Par-4(240-332)WT precipitated. Resolubilisation in 7 M urea allowed purification by RP-HPLC. The purity of Par-4(240-332)WT after the RP-HPLC step was more than 98% as judged by SDS-PAGE. The H_2O-resolubilised lyophilisate was stable and showed no signs of precipitation. The protein yield was ~8 mg Par-4(240-332)WT per litre cell culture. Par-4(240-332)WT purified by this protocol will be denoted as **rrPar-4CC** throughout the remainder of this text.

2.11. Purification of Par-4(286-332)

2.11.1. Purification of Par-4(286-332)WT from HpMal-c2P

a) Materials and Methods

This purification protocol is described in Alexandrov *et. al.* [187]. Cells were lysed and the resulting lysate clarified as described in Chapter 2.6.1.a The supernatant was passed through a 0.8 µm syringe filter and the filtrate rotated for 3 h with 5 ml (bed-volume) of TALON cobalt

affinity resin, which had been equilibrated to PBS. The TALON resin was washed successively with 10 ml PBS, 15 ml PBS with 1 M NaCl and 10 ml PBS. The Par-4 fusion protein was cleaved with HMBP-3Cpro on the column and the TALON resin was rotated overnight at 4 ºC. In case of incomplete cleavage of the fusion protein, more HMBP-3Cpro was added and the cleavage reaction continued till more than 90% of the fusion protein was cleaved. Cleaved Par-4 (286-332)WT was eluted from the column with 15 ml PBS. Par-4 containing fractions were pooled and concentrated using a Vivaspin 20 device (*MWCO* = 3 kDa) at 3,000 g (Rotor TTH400).

For the removal of residual MBP that co-eluted with Par-4(286-332)WT, five different strategies were tested:

i) The Par-4(286-332)WT concentrate was passed over two columns that were used in series. Each column contained 1.5 ml bed-volume of Maltoheptaose Agarose or Amylose resin, respectively, that had been equilibrated to PBS. The columns were washed with further 10 ml of PBS. Aliquots of 1 ml were collected and Par-4(286-332)WT containing fractions were identified by SDS-PAGE analysis.

ii) The Par-4(286-332)WT concentrate was rotated for one hour with 1 ml bed-volume of Chelating Sepharose, that had been charged with $NiCl_2$ and equilibrated to PBS. The column was washed successively with 5 ml PBS and 5 ml PBS with 1 M NaCl. Aliquots of 1 ml were collected and Par-4(286-332)WT containing fractions were identified by SDS-PAGE analysis.

iii) The Par-4(286-332)WT concentrate was passed over a column with 3 ml bed-volume of CM-sephadex that had been equilibrated to PBS. The column was washed successively with 5 ml PBS and 5 ml PBS with 1 M NaCl. Aliquots of 1 ml were collected and Par-4 (286-332)WT containing fractions were identified by SDS-PAGE analysis.

iv) The Par-4(286-332)WT concentrate was passed over a column with 3 ml bed-volume of QAE-sephadex that had been equilibrated to PBS. The column was washed successively with 5 ml PBS, 5 ml 200 mM NaCl and 5 ml 500 mM NaCl. Aliquots of 1 ml were collected and Par-4(286-332)WT containing fractions were identified by SDS-PAGE analysis.

v) Par-4(286-332)WT and MBP were separated by size exclusion chromatography (SEC). The concentrate was applied to a Superdex 75 column. Separation was achieved by an isocratic flow of 0.4 ml/min using the BioLogic DuoFlow System. The buffer contained

50 mM KCl, 20 mM Na_2HPO_4/NaH_2PO_4, pH 7.5. Aliquots of 1 ml were collected and Par-4(286-332)WT containing fractions were identified by SDS-PAGE analysis.

Par-4(286-332)WT fractions that were free of impurities, were pooled and concentrated using a Vivaspin 20 device (*MWCO* = 3 kDa) at 3,000 g and 4 ºC (Rotor TTH400). Buffer exchange to NMR buffer was achieved as described in Chapter 2.8.2.a The protein concentration was determined by BCA-assays [191]. As a reference, Par-4(286-332)WT was buffer exchanged to H_2O and subsequently lyophilised. The lyophilisate was weighed and then used to establish a BCA-assay calibration curve.

b) Results

Par-4(286-332)WT in HpMal-c2P was expressed in unlabelled (final OD_{600} = 6 after 8 h expression), ^{15}N-labelled (final OD_{600} = 6 after 8 h expression), ^{13}C,^{15}N-labelled (final OD_{600} = 4.5 after overnight expression) and ^{2}H,^{15}N-labelled form (final OD_{600} = 3 after 38 h expression). Approximately 50% of the Par-4 fusion protein remained in the insoluble fraction after clarification of the cell lysate. The Par-4 fusion protein bound to the TALON resin was ~90% pure and appeared as a 50 kDa protein as judged SDS-PAGE (Fig. 2.2A, lane 12). Cleavage of the Par-4 fusion protein on the column took on average three to six days. The cleavage performance of HMP-3Cpro was improved by adding TCEP to a concentration of 0.3 mM. Elution of cleaved Par-4(286-332)WT resulted in co-elution of MBP (Fig. 2.2B, lane 13). The majority of the impurities were removed using an IEC step with QAE sephadex (Fig. 2.2C, lanes 22-24). Repeating the IEC improved the purity of Par-4(286-332)WT to > 98%, however, high molecular weight impurities (> 45 kDa) were still visible on the corresponding acrylamide gels (Fig. 2.2D). Concentration and buffer exchange using a Vivaspin 20 device resulted in protein precipitation of 10-20% of Par-4(286-332)WT. The protein yield for unlabelled, ^{15}N-labelled and ^{13}C,^{15}N-labelled Par-4(286-332)WT was ~6-7 mg per litre cell culture and ~8 mg per litre cell culture for ^{2}H,^{15}N-labelled Par-4(286-332)WT, respectively.

Separation of Par-4(286-332)WT from HMBP using Amylose resin was inefficient. Some HMBP could be removed, but the majority co-eluted with Par-4(286-332)WT. Using SEC 80-90% of the HMBP could be removed, but due to the close retention times (~29 and ~32.5 min) the Par-4(286-332)WT fraction still contained MBP. Samples with traces of HMBP had shorter life times than samples purified as above with QAE sephadex. No separation of HMBP and Par-4(286-332)WT was achieved with CM-sephadex or Chelating sepharose.

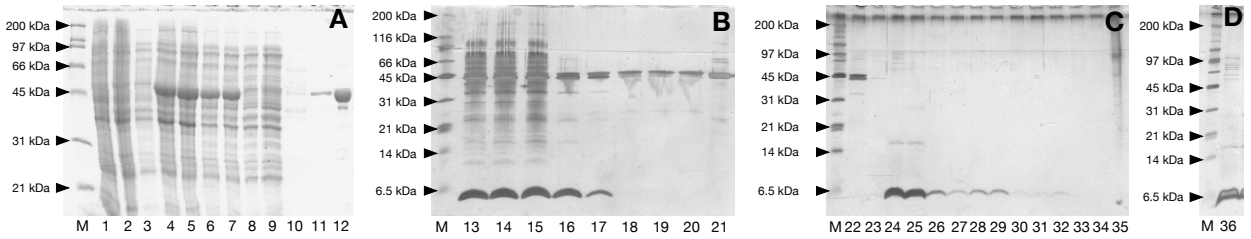

Figure 2.2 *− Purification of Par-4(286-332)WT as MBP fusion protein. The purification of {^{2}H,^{15}N}-Par-4(286-332)WT is shown as a typical example for the purification method described in Chapter 2.11.1. (A) Over-expression of the HMBP-Par-4(286-332)WT fusion protein is evident by 12% SDS-PAGE comparing non-induced (1-3) and induced (4,5) E. coli cells. The cell lysate (6) was clarified by centrifugation (7) and applied to TALON resin. After 3 h incubation at 4 ºC the flow-through (8) was collected and the column washed successively with PBS (9), PBS + 1M NaCl (10) and PBS (11). The purity of the fusion protein on the column is shown in lane 12. (B) The 16.5% Tricine-PAGE [192] displays co-elution of MBP with Par-4(286-332)WT from the TALON resin after cleavage with HMBP-3Cpro. The eluate was collected in 1.5 ml fractions (13-20) and the TALON resin (21) was assessed for complete elution of Par-4(286-332)WT. (C) Typical result of an IEC purification with QAE-sephadex analysed by 16.5% Tricine-PAGE. Pooled Par-4(286-332)WT containing fractions were applied to a QAE-sephadex column and the flow-through (22) was collected. The column was washed with PBS (23) and Par-4(286-332)WT was eluted from the column with increasing concentrations of NaCl (24-34). The QAE-sephadex was assessed for remaining Par-4(286-332)WT (35). (D) After repeating the IEC step, Par-4(286-332)WT containing fractions were concentrated (36) and the purity was analysed by 16.5% Tricine-PAGE. Lanes with molecular weight markers are labelled with (M). Approximate MWs are shown on the left edge of each gel. Note that the gel shown in panel A is stained with Coomassie Blue, whereas all other gels were silver stained. The apparent increase in impurities in lanes 13-15 relative to lane 12 is a result of the silver staining process. Visualisation of the 6 kDa peptide Par-4(286-332)WT by silver staining resulted in an overstaining of the larger proteins such as MBP (~45 kDa).*

2.11.2. Purification of Par-4(286-332)WT from pCFE-GST-3C

a) Materials and Methods

The cell pellet was resuspended in 20 ml 100 mM NaCl, 1 mM DTT and 50 mM Na_2HPO_4/NaH_2PO_4, pH 8.0 and 100 µl of the protease inhibitor cocktail were added. The cells were lysed and the cell lysate clarified as described in Chapter 2.6.1.a. The supernatant was passed through a 0.8 µm syringe filter and the filtrate was rotated for 3 h with 2 ml (bed-volume) of Glutathione Sepharose, which had been equilibrated to PBS. The Glutathione Sepharose was washed with 10 ml 1 M NaCl, 20 mM Na_2HPO_4/NaH_2PO_4, pH 7.0 followed by 5 ml PBS. The Par-4 fusion protein was eluted with 6 ml 10 mM reduced glutathione, 50 mM Tris, pH 8.0. Par-4 fusion protein containing fractions were pooled and dialysed overnight against 500 ml 150 mM NaCl, 1 mM DTT and 20 mM Tris, pH 7.5. The Par-4 fusion protein was cleaved at 4 ºC with

HMBP-3Cpro. After more than 90% of the Par-4 fusion protein was cleaved, the cleavage reaction was rotated for 3 h with 2 ml Glutathione Sepharose. The flow through was collected and the Glutathione Sepharose washed with 5 ml PBS. Par-4(286-332)WT containing fractions were pooled and concentrated using a Vivaspin 20 device (*MWCO* = 3 kDa) at 3,000 g (Rotor TTH400).

Par-4(286-332)WT was further purified by RP-HPLC as described in Chapter 2.10.1.a using a linear water-acetonitrile gradient of 30-50% over 25 min. Par-4(286-332)WT containing fractions that were free of impurities, were lyophilised and then resolubilised in 50 mM KCl, 100 mM Na_2HPO_4/NaH_2PO_4, pH 7.5. The protein concentration was determined as described in Chapter 2.10.1.a.

b) Results

Par-4(286-332)WT in pCFE-GST-3C was expressed in unlabelled and ^{15}N-labelled form with final OD_{600} = 3.5 and OD_{600} = 5.0 after 6 h expression. After clarification of the cell lysate, 40-50% of the Par-4 fusion protein remained in the insoluble fraction. The purified Par-4 fusion protein was more than 95% pure after elution and appeared as 30 kDa protein as judged by SDS-PAGE (Fig. 2.3A, lane 8). Separation of cleaved Par-4(286-332)WT from GST by applying the cleavage reaction again to Glutathione Sepharose failed and resulted in co-elution of GST and Par-4(286-332)WT. Separation was only achieved using a RP-HPLC step. The purity of Par-4 (286-332)WT was > 98% after RP-HPLC purification as judged by MS. Resuspending the lyophilisate in buffers at pH 6.0 or dialysing resolubilised Par-4(286-332)WT to buffers at pH 6.0 resulted in precipitation of approximately 50% of Par-4(286-332)WT. At pH values above 6.0 Par-4(286-332)WT was mostly soluble. The protein yield was ~8.5 mg Par-4(286-332) WT per litre cell culture.

2.11.3. Denaturing purification of Par-4(286-332)WT from pGex-6P-3 − Purification of rrPar-4LZ

a) Materials and Methods

Par-4(286-332)WT from pGex-6P-3 was purified as described in Chapter 2.10.1.a. The cleavage reaction containing soluble Par-4(286-332)WT was concentrated, then RP-HPLC purified and the protein concentration determined as described in Chapter 2.11.2.a.

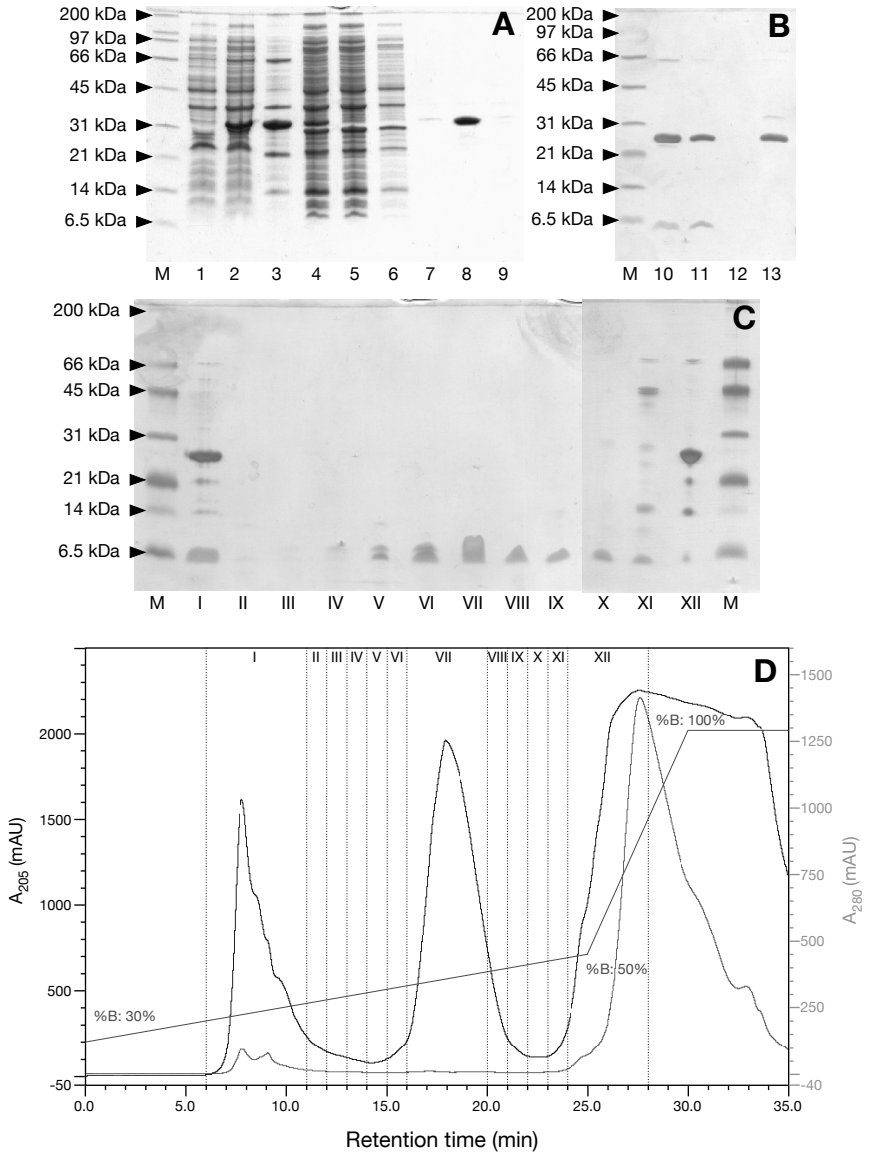

Figure 2.3 *– Purification of Par-4(286-332)WT as GST fusion protein. The purification of {^{15}N}-Par-4(286-332)WT is shown as a typical example for the purification method described in Chapter 2.11.2. (A) Over-expression of the GST-Par-4(286-332)WT fusion protein is evident from the comparison of non-induced (1) and induced (2) E. coli cells. Under native conditions 70% of the fusion protein remains in the insoluble fraction after clarification of the cell lysate (3). The soluble fraction of the cell lysate (4) was applied to a Glutathione Sepharose column. After 3 h incubation at 4 ºC the flow-through (5) was collected and the column washed successively with PBS + 1M NaCl (6) and PBS (7). The fusion protein was eluted (8) and the column (9) assessed for remaining fusion protein. (B) The eluted fusion protein was cleaved with HMBP-3Cpro (not shown) and GST was removed by re-purification with Glutathione Sepharose. After 3 h incubation at 4 ºC, the flow-through (10) was collected and the column washed with PBS (11,12). However, only a minority of GST was bound to the column (13), the majority of GST co-eluted with rrPar-4LZ. Uncleaved GST-Par-4 fusion protein is indicated by a 31 kDa band. (C) rrPar-4LZ containing fractions were concentrated and purified by RP-HPLC (I-XII). The corresponding RP-HPLC chromatogram is shown in panel (D). The collected fractions (I-XII) are indicated by vertical dotted lines. For analysis, 10% Tricine-PAGE was used in (A), (B) and (C). Lanes with molecular weight markers are labelled with (M). Approximate MWs are shown on the left edge of each gel.*

b) Results

Par-4(286-332)WT in pGex-6P-3 was expressed in ^{15}N-labelled form with a final OD_{600} = 5.0 after overnight expression. Using a native protocol 60-70% of the Par-4 fusion protein remained in the insoluble fraction after clarification of the cell lysate (Fig. 2.3A, lane 3). In contrast, with a denaturing protocol an almost complete solubilisation was achieved. Reducing the urea concentration of the cell lysate by dialysis, resulted in protein precipitation of 10-20% of the Par-4 fusion protein. The subsequent steps of the purification gave similar results as described above for Par-4(286-332)WT in pCFE-GST-3C (Chapter 2.11.2.b). The protein yield was ~10 mg Par-4(286-332)WT per litre cell culture. Par-4(286-332)WT purified by this protocol will be denoted as **rrPar-4LZ** throughout the remainder of this text.

2.11.4. Purification of Par-4(286-332)WT from pCFE-GST-TEV

a) Materials and Methods

Purification of Par-4(286-332)WT from pCFE-GST-TEV is identical to the protocol described above for Par-4(286-332)WT from pCFE-GST-3C (Chapter 2.11.2.a). However, the Par-4 fusion protein after elution was not cleaved with rTEV, but dialysed against 50 mM NaCl, 1 mM DTT and 20 mM Na_2HPO_4/NaH_2PO_4, pH 7.0. The protein concentration was determined by A_{280} absorbance measurements using an extinction coefficient of 44,600 $M^{-1}cm^{-1}$.

b) Results

Par-4(286-332)WT in pCFE-GST-TEV was expressed in ^{15}N-labelled form with a final OD_{600} = 3.0 after overnight expression. After clarification of the cell lysate 60-70% of the Par-4 fusion protein remained in the insoluble fraction. The purified Par-4 fusion protein was more than 95% pure after elution The protein yield was ~4 mg GST-Par-4(286-332)WT fusion protein per litre cell culture.

2.11.5. Purification of Par-4(286-332)W285 from HpMal-c2P

a) Materials and Methods

Purification of Par-4(286-332)W285 from HpMal-c2P is identical to the protocol described in Chapter 2.11.1.a for Par-4(286-332)WT from HpMal-c2P. Residual MBP was removed with two Amylose resin columns.

b) Results

Par-4(286-332)W285 in HpMal-c2P was expressed in ^{15}N-labelled form with a final OD_{600} = 6 after 8 h expression. The purification results were similar as described above for Par-4 (286-332)WT from HpMal-c2P (Chapter 2.11.1.b). Traces of MBP after IMAC purification were almost completely removed by affinity chromatography using Amylose resin columns.

2.11.6. Purification of Par-4(286-332)D305K from HpMal-c2P − Purification of rrPar-4LZD305K

a) Materials and Methods

Par-4(286-332)D305K in HpMal-c2P was purified as described above in Chapter 2.6.2.a. Par-4 fusion protein containing fractions were pooled and dialysed for 4 h against 500 ml 150 mM NaCl, 25 mM imidazole, 0.3 mM TCEP and 20 mM Tris, pH 7.5. The Par-4 fusion protein was cleaved overnight with HMBP-3Cpro, while dialysis was continued against 500 ml fresh cleavage buffer. After more than 90% of the Par-4 fusion protein was cleaved, the cleavage reaction was applied again to the Ni-NTA column, which had been equilibrated to the cleavage buffer. The flow through was collected and the Ni-NTA column washed successively with 5 ml lysis buffer and 5 ml 1 M NaCl, 20 mM Tris, pH 7.0. Par-4(286-332)D305K containing fractions were pooled, concentrated, RP-HPLC purified and the protein concentration determined as described in Chapter 2.11.2.a.

b) Results

Par-4(286-332)D305K in HpMal-c2P was expressed in ^{15}N-labelled form with a final OD_{600} = 2 after overnight expression. Approximately 50% of the Par-4 fusion protein remained in the soluble fraction after clarification of the cell lysate. The IMAC purified Par-4 fusion protein was 70-80% pure after elution and appeared as a 50 kDa protein as judged by SDS-PAGE. Elution of cleaved Par-4(286-332)D305K resulted in co-elution of MBP after the second IMAC step. The purity of Par-4(286-332)D305K after RP-HPLC purification was > 98%. The protein yield was ~2.5 mg Par-4(286-332)D305K per litre cell culture. Par-4(286-332)D305K purified by this protocol with RP-HPLC will be denoted as **rrPar-4LZD305K** throughout the remainder of this text.

2.11.7. Purification of Par-4(286-332)E310K from HpMal-c2P – Purification of rrPar-4LZE310K

a) Materials and Methods

Par-4(286-332)E310K in HpMal-c2P was purified as described in Chapter 2.11.6.

b) Results

Par-4(286-332)E310K in HpMal-c2P was expressed in ^{15}N-labelled form with a final OD_{600} = 2 after overnight expression. Purification results are similar to the results described in Chapter 2.11.6.b. The protein yield was ~3 mg Par-4(286-332)E310K per litre cell culture. Par-4 (286-332)E310K purified by this protocol will be denoted as **rrPar-4LZE310K** throughout the remainder of this text.

2.11.8. Denaturing purification of Par-4(286-332)E310K from HpMal-c2P

a) Materials and Methods

To further improve the yields of Par-4(286-332)E310K, especially of insoluble Par-4 (286-332)E310K that remains in the pellet after cell lysis, a denaturing protocol was applied. Initial cell lysis steps are as described in Chapter 2.6.2.a. The supernatant was stored at 4 ºC until further use. The cell lysis pellet was resuspended in 20 ml 6 M urea, 250 mM NaCl, 25 mM imidazole and 50 mM Tris, pH 8.0. The suspension was passed again through a French Press and clarified by centrifugation for 30 min at 16,000 g and 4 ºC (Rotor SS34). This supernatant was united with the first supernatant and passed through a 0.8 µm syringe filter. The filtrate was rotated for 3 h with 2 ml (bed-volume) of Chelating Sepharose, which had been charged with $NiCl_2$ and equilibrated to 6 M urea, 250 mM NaCl, 25 mM imidazole and 50 mM Tris, pH 8.0. The Ni-NTA column was washed successively with 10 ml 6 M urea, 250 mM NaCl, 25 mM imidazole and 50 mM Tris, pH 8.0 and 5 ml 6 M urea, 250 mM NaCl, 50 mM imidazole and 50 mM Tris, pH 8.0. The Par-4 fusion protein was eluted with 10 ml 6 M urea, 250 mM NaCl, 250 mM imidazole and 50 mM Tris, pH 8.0. Par-4 fusion protein containing fractions were pooled and dialysed for 6 h at room temperature against 500 ml 1 M urea, 250 mM NaCl, 25 mM imidazole 0.3 mM TCEP and 50 mM Tris, pH 7.5. Dialysis was continued overnight at 4 ºC against 500 ml fresh buffer. Any precipitate occurring during dialysis was removed by centrifugation at 14,000 g (Rotor FA12.94 High*conic*). The Par-4 fusion protein was cleaved for 4 h at room temperature with HMBP-3Cpro. After more than 90% of the Par-4 fusion protein was cleaved, the cleavage reaction was applied again to the Ni-NTA column, which had been

equilibrated with cleavage buffer. The flow through was collected and the Ni-NTA column washed with 10 ml cleavage buffer. Par-4(286-332)D305K containing fractions were pooled and concentrated as described in Chapter 2.11.2.a.

RP-HPLC purification of Par-4(286-332)E310K was achieved using a Jupiter 5u C18 300Å column connected to a Ultimate 3000 HPLC system. The protein was purified at 25 ºC with a flow rate of 5.0 ml/min using a linear water-acetonitrile gradient of 30-40% over 25 min in the presence of 0.1% TFA ($^{v}/_{v}$). Par-4(286-332)E310K containing fractions that were free of impurities, were lyophilised and then resolubilised in H_2O. The protein concentration was determined as described in Chapter 2.10.1.a.

b) Results

A REDPRO sample of Par-4(286-332)E310K in HpMal-c2P was expressed as described in Chapter 2.5.4. with a final OD_{600} = 6.3 after 6 h expression. Using a denaturing protocol, almost no Par-4 fusion protein was detected in the pellet after cell lysis. Furthermore, retention of cleaved Par-4(2686-332)E310K on the Ni-NTA column was reduced in the presence of 1 M urea. Other purification results were similar as described in Chapter 2.11.7.b. Using a preparative C18-column for RP-HPLC greatly reduced the purification time and also reduced the amount of Par-4 peptide that was not retained on the column. The protein yield was ~2 mg Par-4(286-332)E310K per litre cell culture. Par-4(286-332)E310K purified by this protocol will be denoted as **REDPRO rrPar-4LZE310K** throughout the remainder of this text.

2.11.9. Denaturing purification of Par-4(286-332)N313I from pGex-6P-3 − Purification of rrPar-4LZN313I

a) Materials and Methods

Par-4(286-332)N313I in pGex-6P-3 was purified as described in Chapter 2.10.1.a. The cleavage reaction containing soluble Par-4(286-332)N313I was concentrated as described in Chapter 2.11.2.a. RP-HPLC purification of Par-4(286-332)N313I was achieved as described in Chapter 2.11.8.a using a linear water-acetonitrile gradient of 40-47% over 25 min. The protein concentration was determined as described in Chapter 2.10.1.a.

b) Results

Par-4(286-332)N313I in pGex-6P-3 was expressed in ^{15}N-labelled form with a final OD_{600} = 8.2 after 5 h expression. Including a second lysis step under denaturing conditions gave

an almost complete solubilisation of the Par-4 fusion protein. Note that 60% of the total Par-4 fusion protein was in the denaturing lysate. Reducing the urea concentration of the cell lysate by dialysis, resulted in protein precipitation of 20-30% of the total Par-4 fusion protein. The purified Par-4 fusion protein was more than 95% pure after elution and appeared as a 30 kDa protein as judged by SDS-PAGE. Separation of cleaved Par-4(286-332)WT from GST was achieved using a RP-HPLC step. The protein yield was ~11 mg Par-4(286-332)N313I per litre cell culture. Par-4 (286-332)N313I purified by this protocol will be denoted as **rrPar-4LZN313I** throughout the remainder of this text.

2.12. Summary

2.12.1. General purification problems of Par-4

Of the various purification protocols described above (Chapters 2.6. to 2.11.) only a few result in pure soluble Par-4 protein. The Par-4 proteins that were successfully isolated are the full-length construct rrPar-4FL (Chapter 2.6.5.), the leucine zipper-less construct rrPar-4ΔLZ (Chapter 2.8.2.), the SAC domain comprising rrPar-4SAC (Chapter 2.9.1.), the coiled coil domain comprising rrPar-4CC (Chapter 2.10.1.), the LZ domain comprising rrPar-4LZ (Chapter 2.11.3.) and the three LZ domain point mutants rrPar-4LZD305K (Chapter 2.11.6.), rrPar-4LZE310K (Chapters 2.11.7. and 2.11.8.) and rrPar-4LZN313I (Chapter 2.11.9.). Par-4 (1-265)WT and Par-4(286-332)W285 could not be purified due to degradation of the proteins. Since Par-4(1-265)WT is almost identical to rrPar-4ΔLZ no further purifications were attempted. For almost all Par-4 constructs the ID nature and/or self-association complicate the purification process and make it more difficult. General problems observed during the purification are discussed below.

Par-4 constructs containing the LZ domain (Par-4(1-332) and Par-4(286-332) constructs) are less soluble than Par-4 constructs without the LZ domain (Par-4(1-265), Par-4(1-290) and Par-4 (137-195) constructs). The later group shows very little Par-4 fusion protein in the insoluble fraction after clarification of the cell lysate. The decreased solubility of the LZ containing constructs is probably due to self-association linked to the presence of the LZ domain. MBP, as is established in general, shows a greater solubilising effect as purification tag (~50% soluble Par-4(1-332) and Par-4(286-332) constructs) than GST (~40% soluble Par-4(286-332)WT) or thioredoxin (~10% soluble Par-4(1-332)G40G) (Chapters 2.6.1, 2.11.1, 2.11.2. and 2.6.5, respectively). The solubility of the Par-4 fusion proteins could be improved in most cases if cells were fermented at 25 ºC after induction with IPTG. Even though MBP has a favourable

solubilising effect, effective separation of cleaved Par-4 proteins such as Par-4(1-265)WT (Chapter 2.7.1.) or Par-4(286-332)WT (Chapter 2.11.1.) from the MBP tag could seldom be achieved. This is probably due to non-specific interactions between Par-4 and MBP. Residual MBP further affects the stability of the Par-4 proteins (see below). MBP was therefore replaced by other purification tags that allowed a more effective purification of the Par-4 proteins. Solubility problems are greatly overcome using denaturing purification protocols resulting in the solubilisation of most of the Par-4 fusion proteins (e.g. Chapter 2.6.5.). This allows the use of GST and thioredoxin as fusion tags, which are easier to separate from the Par-4 proteins. This further benefits the stability of the Par-4 proteins (see below). Importantly, urea as a denaturant is essential for the purification of rrPar-4FL. If not kept in urea containing buffers until it has been purified by RP-HPLC, rrPar-4FL is almost completely lost due to precipitation (Chapter 2.6.5.).

Due to their extended coil-like conformations (Chapter 3.2.2.) Par-4 proteins contain hydrophobic residues that are not buried and are accessible for non-specific interactions. Such interactions could occur with other hydrophobic residues and may result in aggregation. Alternatively, such interactions could lead to non-specific binding to surfaces of consumables (e.g. storage tubes). Freely accessible residues other than hydrophobic residues may be involved as well. In particular for rrPar-4FL and rrPar-4ΔLZ, significant protein losses were observed using Vivaspin devices or dialysis tubings, probably due to non-specific binding to the membrane. Protein losses of rrPar-4FL were greatly reduced in the presence of urea (see above). The use of Vivaspin devices and dialysis tubing should therefore be kept to a minimum and only when absolutely necessary to prevent greater protein losses. Furthermore, storage of Par-4 proteins in non-siliconised reaction tubes resulted in the loss of Par-4 protein. In case of rrPar-4ΔLZ no protein was detectable after three days if the sample was left on the bench at room temperature in a standard 1.5 ml reaction tube (Fig. 2.4A). Storage of the same protein under identical conditions in a siliconised 1.5 ml reaction tube showed virtually no decrease in protein concentration after three (Fig. 2.4B) or more days (data not shown). Non-specific binding of Par-4 was also observed by other research groups [91].

Time and concentration dependent aggregation is another critical factor especially at higher protein concentration. For nearly all Par-4 proteins, except rrPar-4SAC, precipitates were observed after a few days in concentrated storage solutions kept at 4 ºC. In particular LZ domain containing constructs were prone to aggregation and precipitation at 4 ºC. This is not surprising as concentration dependent aggregation is not unusual for amphipathic helices [142]. An example for the aggregation of the Par-4 LZ mutant Par-4(286-332)E310K is shown in

Figures 2.4C and D. Native PAGE analysis of freshly purified Par-4(286-332)E310K produces one major band (Fig. 2.4C). Similarly, only a single band is observed For Par-4(286-332)WT under the conditions of the native PAGE (pH 8 and 20 ºC). These results indicate predominantly single oligomeric species for both proteins. The difference in the electrophoretic mobility of Par-4(286-332)E310K relative to Par-4(286-332)WT is probably related to different oligomeric states for both proteins (Chapter 4.2.2.) and to the charge difference between both proteins. Par-4 (286-332)E310K has one glutamate residue mutated to a lysine residue resulting in a charge difference of two relative to Par-4(286-332)WT. A control experiment a week later under similar conditions, but after the Par-4(286-332)E310K stock solution showed precipitation, produced completely different result. Multiple bands of low electrophoretic mobility are visible for Par-4 (286-332)E310K indicating the existence of aggregates (Fig. 2.4D). Similarly, Gao *et. al.* reported that full-length Par-4, heterologously expressed in bacteria, was prone to polymerise, and was thus not suitable for some of their *in vitro* assays [54]. Precipitation and non-specific binding are therefore likely factors contributing to the relatively low Par-4 protein yields.

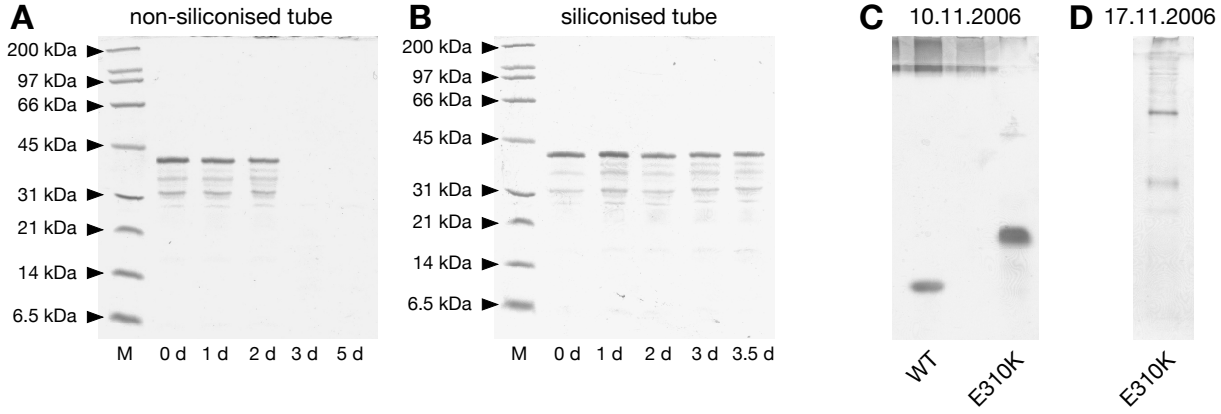

Figure 2.4 *– Non-specific binding and aggregation of Par-4 constructs. Analysis of the stability of rrPar-4ΔLZ by 10% Tricine-PAGE. (A) An aliquot of rrPar-4ΔLZ is transferred to a standard non-siliconised 1.5 ml reaction tube and left on the bench at room temperature. Aliquots are taken after five minutes (0 d), one day (1 d), two days (2 d), three days (3 d) and five days (5 d). (B) For comparison, an aliquot of rrPar-4ΔLZ is transferred into a siliconised 1.5 ml reaction tube and left on the bench at room temperature. Aliquots are taken after five minutes (0 d), one day (1 d), two days (2 d), three days (3 d) and three and a half days (3.5 d). No protein loss is observed with siliconised tubes, even after five days (data not shown). Lanes with molecular weight markers are labelled with (M). Approximate MWs are shown on the left edge of each gel. (C,D) Native PAGE analysis of Par-4(286-332)E310K. The 12% native PAGE is run as a standard Laemmli SDS-PAGE but without SDS [186]. (C) Freshly purified Par-4 (286-332)E310K (10.11.2006) is analysed together with Par-4(286-332)WT. (D) A week later, after the Par-4(286-332)E310K stock solution showed precipitation, the clarified supernatant is analysed again displaying various bands with low electrophoretic mobility.*

Increased proteolytic susceptibility due to extended conformations is another typical property of IDPs (Chapters 1.5. and 1.6.2.). The degradation of Par-4(1-332)G40G in pET32a by Thrombin (Chapter 2.6.3.) is therefore interesting, as it can be considered as another indication for the extended conformation of Par-4(1-332)G40G. In addition to the Thrombin cleavage site between thioredoxin and Par-4(1-332)G40G, a second internal Thrombin cleavage site is predicted for Par-4(1-332)G40G. Cleavage at this site would result in Par-4(1-332)G40G fragments of 9 and 27 kDa. However, only fragments below 21 kDa are observed suggesting non-specific cleavage at other sites. This non-specific cleavage is probably enhanced by the extended structure that exposes other cleavage sites, which are then more accessible for the protease. Degradation is a great problem during the purification of Par-4 and was observed several times for various Par-4 constructs, especially rrPar-4FL and rrPar-4ΔLZ. This was probably due to proteolysis resulting from protein impurities. Therefore, fast work, careful preparation of buffers and non-contaminated consumables are required to prevent degradation of Par-4 during the purification process. Degradation was the major reason that prevented purification of Par-4(1-265)WT (Chapter 2.7.1.). The separation of MBP from Par-4(1-265)WT was inefficient and time consuming therefore allowing enough time for proteolytic degradation. A protease inhibitor could have been included in the buffers making the purification more expensive. However, fast working and efficient removal of any impurities made this step unnecessary for most other Par-4 constructs. Especially RP-HPLC purified Par-4 proteins show increased stability relative to other purification methods. For example, Par-4(286-332) constructs containing traces of MBP and other impurities (Fig. 2.2D) at the end of the purification process had decreased life times relative to RP-HPLC purified Par-4(286-332) proteins. Therefore, to prevent protein losses due to precipitation and proteolytic degradation, purified Par-4 solutions are kept at -20 ºC. Even though it is not the best way to store proteins in general, it greatly contributed to the stability of the Par-4 samples.

The cell densities after overnight expression are fairly low with OD_{600} of approximately 4. To increase the protein yield future cultures may be induced at higher cell densities as described in Chapter 2.5.4. for the REDPRO growth. However, this may result in more insoluble Par-4 fusion protein and should be tested before trying isotopically labelled growths. In the case of rrPar-4LZN313I (Chapter 2.11.9.) this expression protocol did contribute to an increased cell density and in the end to an increased protein yield. For three Par-4 constructs, Par-4(286-332) WT in pCFE-GST-TEV (Chapter 2.11.4.), rrPar-4LZD305K (Chapter 2.11.6.) and rrPar-4LZE310K (Chapter 2.11.7.) significantly lower cell densities were obtained ($OD_{600} \approx 2$).

These were due to problems with the M9 medium. After discarding the old M9 medium and using a freshly made M9 medium, higher cell densities (~4 OD_{600}) were obtained. The low cell densities are therefore responsible for the reduced yields of these three proteins.

The use of rTEV protease is favoured over HMBP-3Cpro. A virtually complete removal of the thioredoxin tag after cleavage with rTEV is easily achieved by an additional IMAC purification step. In contrast, cleavage with HMBP-3Cpro reduced the efficiency of the removal of the purification tag. This resulted in co-elution of HMBP (Fig. 2.2B, lane 13) or GST (Chapter 2.11.2.b) with the Par-4 protein. Removal of GST was so inefficient that the cleavage reaction was directly purified by RP-HPLC (Chapter 2.11.3.). A second Glutathione Sepharose affinity purification step was not necessary.

Taken together, recombinant expression of Par-4 proteins was achieved in *E. coli* systems. However, the ID nature of Par-4 and self-association due to the LZ domain, made this purification process non trivial. These difficulties are further worsened by the inherent "instability" of the Par-4 proteins. Effective separation of impurities is therefore necessary to prevent proteolytic degradation. The non-specific binding of Par-4 to surfaces is an additional factor contributing to the "instability" of the Par-4 proteins and great care should be taken when handling Par-4 proteins to minimise protein losses. The time dependent aggregation, especially at higher protein concentration, requires further optimisation to determine suitable long term storage conditions. Considering these factors, it is not surprising that development of effective purification protocols for Par-4 and finding conditions increasing the stability of the proteins was (and still is) a time consuming process.

2.12.2. Purification problems of Par-4(286-332)

The Par-4(286-332) constructs were the first Par-4 proteins to be purified during the PhD. Hence the greatest modifications to an existing protocol [184,187] were made (Chapter 2.11.). These modifications and the reasons for them will be given below. The term Par-4(286-332) includes the WT construct as well as the mutants W285, D305K, E310K and N313I.

The specificity of the TALON resin is higher relative to a Ni-NTA matrix (Talon manual) and Par-4 fusion proteins of greater purity were therefore obtained (compare Figures 2.1, lane 7 and 2.2A, lane 12). However, due to the above mentioned problems with HMBP-3Cpro this advantage was nullified by co-elution of MBP. Using a Ni-NTA based system increased the protein yields due the higher affinity of the Ni-NTA matrix and therefore minimised Par-4 fusion protein losses. Cleaving Par-4 constructs on the column was abandoned as this method was

inefficient and time consuming. Even though initially less HMP-3Cpro was used, adding more protease did not resulted in complete cleavage of the fusion protein. The cleavage efficiency was increased by adding TCEP. Cleavage reactions performed in this way took on average three to six days. In contrast, almost complete cleavage was achieved by eluting the fusion protein off the column and cleaving it overnight in solution (e.g. Chapter 2.11.6.a).

IEC with QAE-sephadex reduced the amount of protein impurities, but was not very efficient. IEC with QAE-sephadex was nonetheless superior in removing MBP to all other methods described in Chapter 2.11.1. It was generally necessary to perform the IEC step twice. Note that separation of Par-4(286-332) constructs form MBP using a Vivaspin 20 device (*MWCO* = 30 kDa) as described in Ref. [187] was not possible. Par-4(286-332) constructs were efficiently retained in the Vivaspin 20 device. Taken together, even with the changes introduced, purification by this method was time consuming and took 15 to 30 days, depending on the efficiency of the cleavage reaction and IEC purification. The long purification times, that may favour proteolytic degradation, and repeated purification by IEC were detrimental to protein yields. Also impurities were not completely removed (Fig. 2.2D) and most Par-4(286-332) samples only remained stable for a short time. This is based on stability analysis by Tricine-PAGE [192] that showed decreasing band intensities for the Par-4(286-332) constructs. This decrease may have been caused by degradation or non-specific binding to the storage tube.

As is well established, GST binds with high affinity and high specificity to glutathione. Indeed, very pure GST-Par-4(286-332)WT fusion protein was obtained (Fig. 2.3A, lane 8). It was therefore thought that this method would allow complete removal of GST after cleavage with HMBP-3Cpro. However, less than 30% of GST was removed after cleavage in this way (Fig. 2.3B, lanes 10-13). The reason for the decreased binding of GST to the glutathione sepharose matrix after cleavage with HMBP-3Cpro is not clear. Efficient removal of GST was achieved by RP-HPLC (see below). As mentioned above, more GST-Par-4(286-332)WT fusion protein (~60-70%) (Chapter 2.11.2.b) was found in the insoluble fraction after clarification of the cell lysate relative to a similar HMBP-Par-4(286-332)WT fusion protein (40-50%) (Chapter 2.11.1.b). Most of the GST-Par-4(286-332)WT fusion protein was resolubilised with a denaturing purification protocol and only 10-20% of the fusion protein remained insoluble in native buffer (Chapter 2.11.3.b). Reducing the urea concentration by dialysis appears to increase the total purification time, however, this method is still faster than the Ni-NTA-based purification of HMBP-tagged Par-4(286-332) constructs (Chapter 2.11.6.). Elution of cleaved Par-4(286-332) constructs from a Ni-NTA column required two to three times the volume needed for the elution

of cleaved rrPar-4LZ from a Glutathione column (compare Chapters 2.11.6.a and 2.11.3.a). Hence, for the RP-HPLC purification more eluate coming from the IMAC column needed to be concentrated. This was then the most time consuming step and took one to two days. Additionally, concentration allowed for degradation and non-specific binding to the Vivaspin 20 device (see above), thus reducing the protein yields. As mentioned earlier, separation of rrPar-4LZ from GST by a second affinity chromatography step was not worthwhile and thus less volume needed to be concentrated reducing the protein losses. Elution of Par-4(286-332) from the Ni-NTA column was increased using high salt buffers (Chapter 2.11.6.a) as Par-4(286-332) was most likely retained because of ionic interactions between the negatively charged Par-4 (286-332) (pI ~ 4.4-4.5) and the positively charged Ni-NTA-matrix.

RP-HPLC greatly improved the purity of Par-4(286-332) constructs and contributed to an increased stability. The Delta Pak C18-300Å column was used due to budget restrictions as it was available and saved the need of buying a new column. Approximately 30% of rrPar-4LZ did not bind to the C18-300Å column, due to overloading, and eluted in the flow through together with excess GST (Fig. 2.3C, lane I). Due to the low binding capacity of the column, the RP-HPLC purification took in most cases several days. As these results showed that RP-HPLC purification is the better way to purify Par-4(286-332), a preparative scale C18-column was bought. The increased binding capacity reduced the purification time down to one day in the case of rrPar-4LZN313I (Chapter 2.11.9.). Furthermore, no protein was observed in the flow through indicating that all applied protein was retained by the column. Decreasing the pore size of the column matrix further contributed to a better resolution.

Lyophilisation removed the need to concentrate the RP-HPLC eluates and hence protein losses due to precipitation and non-specific binding were minimised. Lyophilised rrPar-4LZ constructs were easily dissolved in H_2O allowing concentration measurements by the A_{205} method without interference from buffer components. These measurements allowed an easier determination of the protein concentration than the initially used BCA-assay (Chapter 2.11.1.a). The H_2O-dissolved Par-4 protein solutions were strongly acidic (pH ~ 3-4) after lyophilisation. To some extent, this was probably due to residual TFA that could not be removed by lyophilisation. Also the low pI of the rrPar-4LZ proteins may have contributed to the low pH. Residual TFA is likely to have interfered with the A_{205} absorbance measurements and may have skewed the results to a higher apparent concentration. A more accurate concentration determination would be achieved by amino acid analysis, which should be used for comparison with the results from the A_{205} measurements. However, appropriate institutions that offer amino

analysis are not easily accessible in New Zealand. The Par-4(286-332)W285 construct (extinction coefficient 5,500 $M^{-1}cm^{-1}$) was created to allow easy concentration determination from A_{280} measurements. With this information a calibration curve for the BCA-assay was attempted. However, rapid degradation of Par-4(286-332)W285 prevented any concentration determination. Dissolving lyophilised rrPar-4LZ in H_2O allowed higher protein concentrations (> 1 mM) relative to centrifugal concentration devices. The H_2O-dissolved Par-4(286-332) was easily diluted with appropriate buffers for CD or NMR spectroscopy at the desired ionic strength and pH. Because the RP-HPLC purified Par-4(286-32) were acidic when dissolved in H_2O, neutralisation was required before use. Especially the low salt buffers used for CD spectropolarimetry were not able to compensate for this low pH.

The switch from HMBP-tagged fusion proteins to GST-tagged fusion proteins, and particularly using RP-HPLC for Par-4(286-332) purification, became necessary as the initial NMR results of the Par-4(286-332) peptides (Chapter 2.11.1.) were not consistent. Additionally, using GST-tagged Par-4(286-332) fusion proteins and RP-HPLC resulted in higher purity, an increased stability and higher yields in a shorter amount of time. This instability of the Par-4 (286-332) peptides was probably due to problems associated with the original purification protocol of HMBP-fusion proteins (Chapter 2.11.1.). NMR spectra of the Par-4(286-332) peptides displayed more peaks than were expected from the amino acid sequence (Appendix C). The peak number increased as the pH was decreased and it was therefore thought that this increase in peak number is correlated with an increase in secondary structure (Chapter 4.). A significant amount of time was spent on analysing these spectra and also with trying to improve the spectral quality. For conciseness, only representative NMR spectra of Par-4(286-332)WT under various pH conditions are shown in Appendix C. As a CD spectrometer was not available at this time, an increase in secondary structure could not be confirmed. However, mounting evidence from SEC, ^{15}N-relaxation measurements and backbone assignments suggested that the increase in peak number is not correlated with an increase in secondary structure, but an indication of peptide degradation (data not shown). This was consistent with results from 16.5% Tricine-PAGE showing a decrease in the intensity of the band representing the intact Par-4 (286-332) constructs (data not shown). However, no low molecular weight bands (indicating degradation products) could be detected. With the availability of a CD spectrometer it was proven that the increase in peak numbers is associated with protein disorder (data not shown). It is likely that degradation is related to the insufficient purity and the presence of contaminants in the Par-4 protein samples. Attempts to increase the stability of the Par-4 LZ domain are shown in

Appendix D. In short the Par-4 LZ domain was analysed as a GST fusion protein (Chapter 2.11.4.), which increased the stability, but did not allow structural characterisation. Apart from the need of highly pure Par-4(286-332) peptides, great care should also be taken when preparing the NMR samples as this was identified as another source contributing to Par-4 (286-332) instability. However, with the use of highly pure protein stock solutions obtained by RP-HPLC and extensively cleaned NMR tubes an increased protein stability was achieved. The risk of contamination was further reduced by avoiding dialysis and instead diluting H_2O-dissolved Par-4(286-332) peptides in buffer with the desired ionic strength and pH. Using pH paper instead of a pH probe for pH adjustment and minimising transfers in and out of the NMR tube also minimised the possibility for contamination. With these measures higher quality spectra were obtained and the life times of the NMR samples could be prolonged.

3. Intrinsic Disorder in Par-4

Most parts of this section have been published recently by *Libich, Schwalbe et. al.* [46] and is given here in an adapted form to fit the style of this thesis. This publication is a joint first authorship between Dr. David Libich (Institute of Fundamental Sciences, Massey University, Palmerston North, New Zealand) and Martin Schwalbe. Computational analysis of Par-4 (DisEMBL, GOR4 etc. and R_S calculation) was performed by Dr. Libich and all figures were created by Dr. Libich as well. All experimental results such as protein expression, limited proteolysis, CD, DLS and NMR spectroscopy were carried out by Martin Schwalbe. SEC results for the Par-4 proteins and TFE studies of rrPar-4SAC have not been published, but are given here to further illustrate the extent of ID in Par-4.

3.1. Bioinformatic analysis

Many proteins lack a well defined secondary or tertiary structure in their biologically active state questioning the 'classical' structure-defines-function paradigm [193-195]. A short introduction to this phenomenon called intrinsic disorder was given in Chapter 1.5. As mentioned in this section, Par-4 exhibits several characteristics of intrinsically disordered proteins (IDP) that prompted the investigation if Par-4 can be classified as an IDP. For structural characterisation several constructs were created that comprise different domains of Par-4, most notably the domains with a high degree of sequence conservation. Sequence conservation in the SAC (selective apoptosis induction in cancer cells), CC (coiled coil) and in particular the LZ (leucine zipper) domain (Fig. 1.1) has been discussed in Chapter 1.2.1. Due to their distinct structural properties the CC and LZ domain containing constructs (except rrPar-4FL) will be discussed in Chapter 4. The extent of ID in Par-4 was therefore mainly analysed with three constructs shown in Figure 3.1A. Note that all sequence numbering will be in reference to rat Par-4, to reflect the recombinant rat (rrPar-4) constructs used in these studies. As mentioned in Chapter 2.4, rrPar-4FL comprises the full-length Par-4 (residues 1-332), rrPar-4ΔLZ (residues 1-290) lacks the LZ domain, but still contains N-terminal parts of the CC domain, and rrPar-4SAC comprises the SAC domain including NLS2 (residues 137-195) (Fig. 3.1A).

The results of the analysis of full-length Par-4 by various bioinformatic methods are shown in Figure 3.1. DisEMBL analysis [178] predicts more than 70% of Par-4 to be disordered (Fig. 3.1B). The putative ordered regions (indicated by grey bars in Figure 3.1B) align with highly conserved and functionally important regions of Par-4 such as NLS1 and 2, the SAC domain and the CC domain (Fig. 3.1A). These putative ordered regions further align with regions showing the highest helical propensity as indicated by the GOR4 plot [196] (Fig. 3.1C)

and with the most hydrophobic regions as indicated by the hydrophobic cluster analysis (HCA [179]) (Fig. 3.1D).

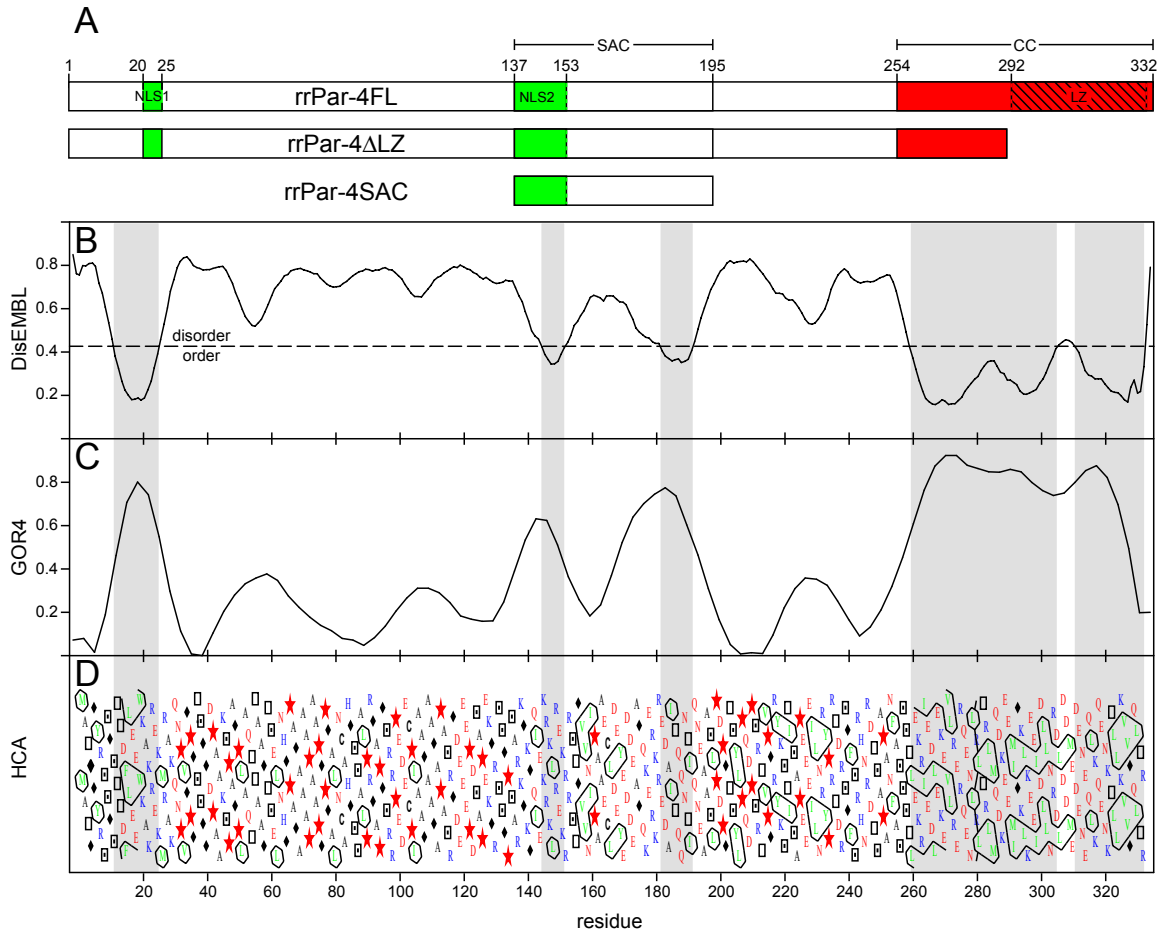

Figure 3.1 *– Computational analysis of Par-4. (A) A block diagram of the three constructs of rrPar-4 mainly used in this chapter. Marked on each construct are the primary regions of functional importance including the nuclear localisation sequences 1 (NLS1, 20-25) and 2 (137-153), coloured green, the region necessary for selective apoptosis induction in cancer cells (SAC, 137-195), the coiled coil C-terminal domain (CC, 254-332, coloured red) and the leucine zipper (LZ, 292-330, shown with hatching). The rrPar-4ΔLZ construct lacks residues 291-332 which is approximately half of the coiled-coil and the entire leucine zipper. The rrPar-4SAC construct represents residues 137-195 of Par-4 including NLS2. All three constructs used in this study have an N-terminal GGS tag, a remnant from the cleavage of the purification tag, which is omitted here for simplicity. (B)* DisEMBL *predicts regions of order/disorder in proteins using neural networks trained on multiple definitions of disorder [178]. The dashed line in panel B represents a threshold value separating order and disorder. (C) Secondary structure prediction (only α-helix shown) using* GOR4 *[196], and (D) hydrophobic cluster analysis (HCA) [179], a visually enhanced representation of the amino acid sequence that highlights clustering of hydrophobic residues using symbols for Thr (open squares), Ser (open squares with black dot), Gly (filled diamonds) and Pro (red stars); and colours (red – Pro, Asn, Asp, Gln, Glu; blue – basic residues Arg, His, Lys; green – hydrophobic residues Ile, Leu, Met, Phe, Trp, Tyr, Val; and black for all other residues – Ala, Cys, Gly, Ser, Thr). The grey bars indicate the predicted regions of order in panel B and for comparison are extended over panels C and D. Figure and legend taken and adapted from Libich, Schwalbe et. al. [46].*

A plot of mean net charge ($\overline{R}$) against mean hydrophobicity ($\overline{H}$) determined from a protein's primary structure allows differentiation between folded and intrinsically disordered proteins as folded proteins occupy different spaces than intrinsically disordered proteins. Intrinsically disordered proteins typically fall into spaces marked by low mean hydrophobicity and high net charge [144]. Based on an analysis by *Uversky et. al* [180] an empirically determined line ($\overline{R} = 2.785\overline{H} - 1.151$) divides the plot space into regions typical for folded and intrinsically disordered proteins (Fig. 3.2A). The three rrPar-4 constructs used in this study are plotted in Figure 3.2A. For comparison several well established folded ('classically folded') proteins are plotted too. Clearly rrPar-4FL, rrPar-4ΔLZ and rrPar-4SAC fall into disordered space. Not surprisingly, the rrPar-4SAC construct with 14 positively charged and 13 negatively charged residues, but few hydrophobic residues, lies further in the disordered region.

The percent difference between the amino acid usage of a set folded (globular) proteins versus a set of known IDPs is shown in Figure 3.2B (black bars). Relative to folded proteins positive values indicate a depletion in the corresponding amino acid while negative bars indicate an enrichment. The sequence complexity of rrPar-4FL can be described by comparison to this reference set. The amino acid usage of a set folded proteins versus rrPar-4FL is shown in Figure 3.2B (grey bars). The observed pattern is similar to what is observed for IDPs [144,193] namely a depletion of order-promoting amino acids (Asn, Cys, Ile, Leu, Phe, Trp, Tyr) and enrichment of disorder-promoting residues (Gln, Glu, Lys, Pro, Ser) [153]. A similar amino acid usage pattern is observed for rrPar-4ΔLZ and rrPar-4SAC (data not shown).

The HCA plot shows a low abundance of hydrophobic residues and only few regions with hydrophobic clusters (Fig. 3.1D). A depletion in hydrophobic residues is further indicated by charge/hydrophobicity plots and sequence complexity analysis (Fig. 3.2). These results speak against the formation of a hydrophobic core and thus provides a strong argument against the formation of stable global tertiary structure [193]. Interestingly, the highly conserved and functionally important regions of Par-4 correlate well with the predicted regions of order (Fig. 3.1B), with the predicted regions of secondary structure (Fig. 3.1C), and with the predicted regions of greatest hydrophobic clustering (Fig. 3.1D). As disorder prediction in Par-4 does not exclude formation of short regions of structure, or of larger but transient secondary structure elements, highly conserved regions of rrPar-4FL (and possibly other regions) may be capable of forming α-helices either independently or upon association with binding partners. This would suggest that Par-4's function may be associated with structure stabilisation in the functionally important regions. Induced folding upon binding to interaction partners has been described for

various proteins. In the absence of binding partners the interaction domain of ACTR (activator for thyroid hormone and retinoid receptors) is unfolded in solution [197]. Similarly, the kinase-inducible transcriptional-activation domain (KID) of CREB (cAMP-responsive element-binding protein) is disordered in solution and adopts an α-helical fold upon association with CBP [198,199]. Interestingly, the ID nature and the CBP-induced helical residues could be predicted from the primary structure [194].

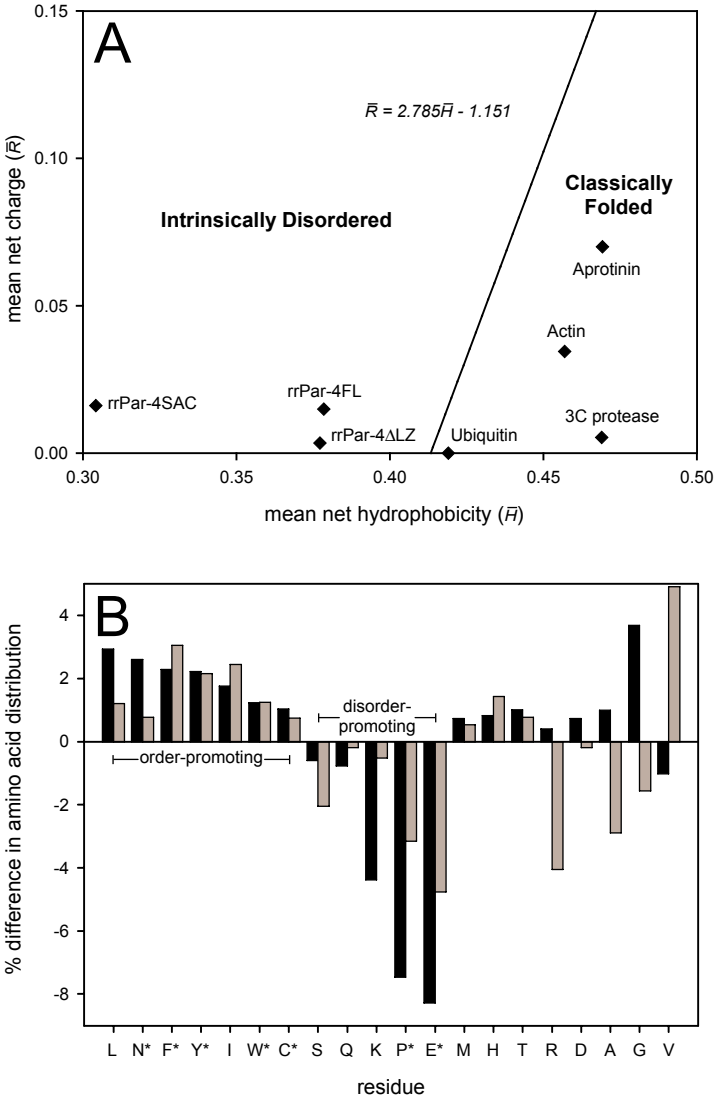

Figure 3.2 *– Charge/hydrophobicity plot and sequence complexity of Par-4. (A) Charge/hydrophobicity plot of rrPar-4 proteins. The dividing line ($\overline{R}$ = 2.785$\overline{H}$ – 1.151) represents an empirically determined divisor between intrinsically disordered (high charge, low hydrophobicity) and structured (low charge, high hydrophobicity) space. Proteins such as aprotinin [200], actin [201], ubiquitin [202] and 3C protease [203] are plotted as examples of 'classically folded' proteins. (B) Sequence complexity of rrPar-4FL (grey bars) compared with the average amino acid distribution of IDPs (black bars) relative to the average amino acid distribution of globular proteins. The relative distributions were sampled from proteins (both IDPs and folded) deposited in the Protein Data Bank. Positive and negative values indicate an enrichment or depletion, respectively, of a particular residue relative to globular proteins. Residues marked with an asterisk occur two times more or less frequently on average in IDPs than in globular proteins [193]. Figure and legend taken from Libich, Schwalbe et. al. [46].*

In summary, bioinformatic analysis of Par-4 displays characteristic features of IDPs including high net charge, low mean hydrophobicity and low sequence complexity. Further a depletion in order-promoting amino acids and an enrichment in disorder-promoting residues could be shown. The lack of hydrophobic residues suggests that the formation of a hydrophobic core is unlikely

and thus the formation of stable tertiary structure. However, next to the primarily ID nature of Par-4 potential α-helical regions are predicted that may be stabilised upon binding to interaction partners.

3.2. Electrophoretic mobility, hydrodynamic and proteolytic analysis

3.2.1. Materials and Methods

a) Dynamic Light Scattering (DLS)

The rrPar-4 proteins rrPar-4FL, rrPar-4ΔLZ and rrPar-4SAC were expressed and purified as described in Chapters 2.6.5, 2.8.2. and 2.9.1. The apparent Stokes radii (R_S) of the rrPar-4 constructs were analysed using a Zetasizer Nano ZS (Malvern Instruments, Malvern, United Kingdom). Sample concentrations were 0.3 mg/ml (8 µM rrPar-4FL, 10 µM rrPar-4ΔLZ and 43 µM rrPar-4SAC) in native buffer (20 mM NaCl, 10 mM Tris, pH 7.0) or native buffer + 1 M urea. An additional sample of 8 µM rrPar-4FL was prepared in native buffer + 6 M urea. DLS data was obtained at 25 ºC using a low-volume disposable 1 cm pathlength plastic cuvette. Five successive scans were collected and averaged for each protein sample. Samples were prepared a day in advance and allowed to sit overnight at 4 ºC to permit bubbles to dissipate, and then allowed to equilibrate to 25 ºC before measurements. The diffusion coefficients were extracted from the correlation curve and the hydrodynamic radius was calculated using the Stokes-Einstein equation. The highest peak of the resulting histogram recorded for each sample was taken as the mode diameter for that particular sample. R_S values obtained from measurements in urea were corrected using the Dispersion Technology Software 5.1 (Malvern Instruments, Malvern, United Kingdom) to account for the increased solvent viscosity and the increased refractive index.

b) Limited Proteolysis

BSA and the rrPar-4 proteins were incubated with trypsin for 15 min at 37 ºC at a protein to protease ratio of 280:1 ($^{w}/_{w}$) in 50 mM NaCl, 20 mM Na_2HPO_4/NaH_2PO_4, pH 7.5. Aliquots were taken after 1, 2, 5, 10 and 15 min and the reaction was quenched by the addition of Laemmli sample buffer and boiling for 5 min. The proteolysis reaction was analysed by 10% Tricine-PAGE and the extent of digestion was measured from the relative intensities of the polyacrylamide gel band representing the non-digested band by densitometry using the Gel Doc Imager and Quantity One software package (BioRad, Hercules, USA).

3.2.2. Results and Discussion

MALDI-TOF mass spectrometry (Centre for Protein Research, University of Otago, Dunedin, New Zealand) was used to assess the purity and to determine the sizes of the recombinant Par-4 constructs. As described in Chapter 2.12.1, all three proteins were isolated in high purity. After accounting for ^{15}N-labelling of the samples used for MS analysis, the sizes determined for rrPar-4ΔLZ (44.5 Da difference between expected and observed) and rrPar-4SAC (6.6 Da difference between expected and observed) agree within error (approx. 0.1%) with the sizes predicted from sequence analysis (Table 3.1). Interestingly, MS indicates that the rrPar-4FL construct is approximately 0.2 kDa larger than expected. The source of the size difference is currently unknown and matter of ongoing research. A possible source may be that rrPar-4FL is modified by the *E. coli* based expression system. However, no greater mass differences are observed for rrPar-4ΔLZ and rrPar-4LZ. Both proteins comprise, to a certain extent, the same residues as rrPar-4FL.

Aberrant electrophoretic mobility in denaturing PAGE systems can be an indication of ID in proteins. Due to their unique amino acid composition relative to globular proteins the amount of SDS that is able to bind to IDPs is reduced [155,193,204]. Therefore, the reduced mass/charge ratio relative to globular proteins results in a reduced migration in denaturing polyacrylamide gels and thus in higher apparent molecular weights (*MWs*). Aberrant mobility was detected for rrPar-4FL, rrPar-4ΔLZ and rrPar-4SAC (Fig. 3.3, lanes 1-3) but not for rrPar-4LZ (Fig. 3.3, lane 4). Consistently, the LZ point mutants rrPar-4LZD305K, rrPar-4LZE310K, rrPar-4LZN313I and the CC construct rrPar-4CC show normal electrophoretic mobility (data not shown). The later four constructs have a higher content in hydrophobic residues (Fig. 3.1D) and may therefore bind SDS to similar amounts as globular proteins. The apparent *MWs* are summarised in Table 3.1.

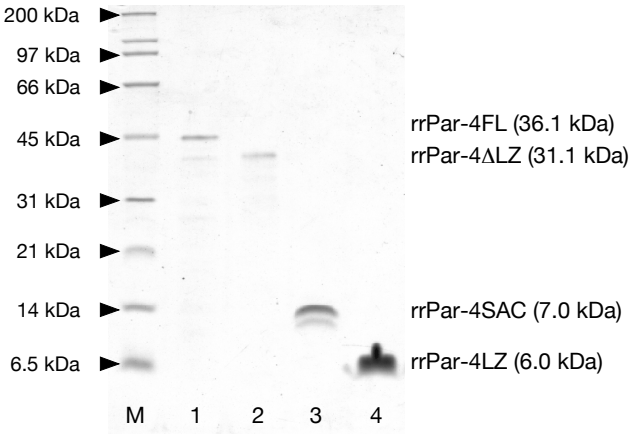

Figure 3.3 *− Electrophoretic mobility of Par-4. Displayed is the electrophoretic mobility of four Par-4 constructs using 10% Tricine-PAGE. The approximate MWs for various globular proteins (M) are shown on the left edge. The from the amino acid sequence expected sizes of the Par-4 constructs rrPar-4FL (1), rrPar-4ΔLZ (2), rrPar-4SAC (3) and rrPar-4LZ (4) are shown on the right edge. Clearly, aberrant electrophoretic mobility is observed in lanes 1-3.*

Table 3.1 compares the experimentally determined *MWs* from Tricine-PAGE for rrPar-4FL, rrPar-4ΔLZ and rrPar-4SAC to other experimentally (MS and DLS) determined *MWs*, and from sequence calculated *MWs*. The amino acid sequence predicts *MWs* of 36.1, 31.1 and 7.0 kDa for rrPar-4FL, rrPar-4ΔLZ and rrPar-4SAC, respectively. The experimentally determined apparent *MWs* from Tricine-PAGE of 49.1, 41.5 and 12.4 kDa for rrPar-4FL, rrPar-4ΔLZ and rrPar-4SAC, respectively, are 36%, 33%, and 77% larger than the *MWs* predicted from sequence or measured using MS (Table 3.1). Aberrant electrophoretic mobility of Par-4 and Par-4 constructs (i.e. deletion mutants) has been previously shown by other research groups although there is little indication that the authors considered the effects of IDP amino acid composition on their results (e.g. Refs. [88,91,98]). It is interesting to note here that Par-4 is repeatedly reported as a 38 kDa protein in the literature when expressed in **mammalian** cells (e.g. Refs. [47,99]). It is possible that this rather normal electrophoretic behaviour is due to post-translational modifications such as phosphorylation, which may be absent in *E. coli* cells.

		Method of analysis		
Construct	**Sequence**	**MS**	**PAGE**	**DLS**
rrPar-4FL	36.1 (26.5)	36.2 (26.5)	49.5 (29.6)	8899 (189)
rrPar-4ΔLZ	31.1 (25.1)	31.2 (25.1)	41.5 (27.8)	64.1 (32.5)
rrPar-4SAC	7.0 (14.8)	7.1 (14.8)	12.5 (18.1)	18.7 (20.9)

Table 3.1 *− Hydrodynamic properties of rrPar-4 constructs using various biophysical techniques. MW (kDa) and hydrodynamic radius R_S (Å) are shown in the format MW (R_S) for three constructs using four techniques. R_S and MW were calculated from the amino acid sequence in reference to a folded conformation using $\log(R_S) = 0.357*\log(MW) - 0.204$. Results are taken from Libich, Schwalbe et. al. [46].*

For comparison with the PAGE and MS results, the DLS obtained Stokes radii (R_S) for rrPar-4FL, rrPar-4ΔLZ and rrPar-4SAC are converted to *MWs* using the equation $\log(R_S) = 0.357*\log(MW) - 0.204$ [181,205]. It should be noted that this equation is strictly valid only for globular proteins as it assumes a spherical shape of the particle. However, it is used here to illustrate the degree of extended structure ('unfoldedness') in the rrPar-4 proteins. The R_S values measured for rrPar-4FL, rrPar-4ΔLZ and rrPar-4SAC correspond to *MWs* of 8.9 x 10^3, 64.1 and 18.7 kDa, respectively. Consistent with the proposed ID nature, these experimentally determined values are much larger (713, 129 and 141%) than the expected values for a globular

protein of the same size (Table 3.1). It further shows that the degree of 'unfoldedness' of the rrPar-4 proteins is very high.

ID in proteins is not synonymous with the term random coil. ID is better described as ensembles of rapidly interchanging conformers that sample varying regions of secondary structure space [193]. As mentioned in Chapter 1.5, IDPs are usually categorised into three non-exclusive groups: random coil, pre-molten globule or molten globule [149]. For comparison with the DLS results under denaturing and non-denaturing conditions, the theoretical R_S values for the rrPar-4 proteins as either monomeric globular (folded), molten globule, pre-molten globule, random coil or urea-denatured states are given in Table 3.2. As can be seen from these results, the observable R_S values of a protein increase in proportion to its degree of 'unfoldedness' with random coil conformations producing larger observable R_S values than folded globular proteins of the same *MW* [205,206] (for examples see *Uversky et. al.* [145].

		Measured R_S (Å)		Calculated R_S (Å)				
Construct	***MW* (kDa)**	**0 M urea**	**1 M urea**	**G**	**MG**	**PMG**	**RC**	**U**
rrPar-4FL	36.1	189	78.4	26.5	29.4	37.7	49.6	53.1
rrPar-4ΔLZ	31.1	32.5	43.6	25.1	28.0	35.6	46.1	49.2
rrPar-4SAC	7.0	20.9	28.1	14.8	17.1	19.9	22.2	22.7

Table 3.2 *– Comparison of experimental and theoretical Stoke's radii (R_S). The R_S was measured in 20 mM NaCl, 10 mM Tris, pH 7.0, in the presence or absence of 1 M urea. Calculated R_S values were obtained using the mean values from equations given in Ref. [181] for globular (folded) (G), molten globule (MG), pre-molten globule (PMG), random coil (RC) and urea-denatured (U) states. Results are taken from Libich, Schwalbe et. al. [46].*

The experimentally determined R_S values for rrPar-4ΔLZ (32.5 Å) and rrPar-4SAC (20.9 Å) in native buffer (20 mM NaCl, 10 mM Tris, pH 7.0) are smaller than the calculated random coil values (46.1 and 22.2 Å, respectively) for either protein (Table 3.2). This suggests that both proteins exist in an unfolded yet monomeric form under these conditions. The high degree of 'unfoldedness' for rrPar-4ΔLZ and rrPar-4SAC suggests that the conformation of the ensembles is best described by random coil-like ensembles rather than molten globule or pre-molten globule ensembles [205]. IDPs such as CREB (cAMP response element binding protein) and p27Kip1 (cyclin- dependent kinase inhibitor) have been shown to exist as structurally interconverting populations. The relatively broad distributions for rrPar4ΔLZ and rrPar-4SAC

(Figs. 3.4B and C) are consistent with such conformational exchange. It was further shown that under physiological conditions IDPs contain nascent secondary structure to varying degrees [146]. The subtle, but significant, increase in R_S for rrPar4ΔLZ and rrPar-4SAC (Table 3.2) suggests that upon addition of 1 M urea some folding elements get disrupted. While conformational exchange continues, the conformation of the ensemble is, however, shifted closer to a random coil.

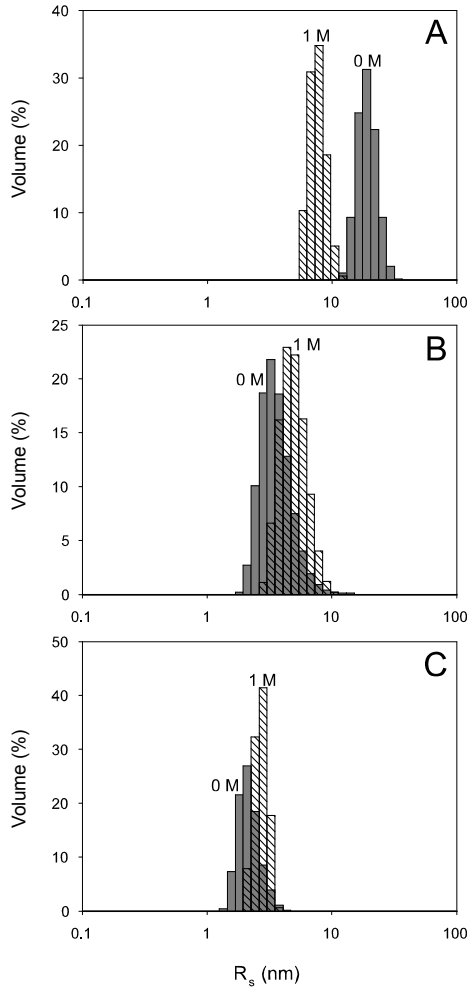

Figure 3.4 *– DLS analysis of rrPar-4FL, rrPar-4ΔLZ and rrPar-4SAC. Volume distribution representation of DLS results showing the apparent hydrodynamic radius of (A) rrPar-4FL, (B) rrPar-4ΔLZ and (C) rrPar-4SAC dissolved in either native buffer (20 mM NaCl, 10 mM Tris, pH 7.0) (grey bars) or in native buffer + 1 M urea (hatched bars). These results are summarised in Table 3.2. Upon the addition of 1 M urea the R_S for rrPar-4FL is significantly decreased (A). Both rrPar-4ΔLZ (B) and rrPar-4SAC (C) exhibit a slight increase in R_S upon addition of 1 M urea. Figure and legend taken and adapted from Libich, Schwalbe et. al. [46].*

Interestingly, the measured R_S value for rrPar-4FL in native buffer with 189 Å is much larger than what would expected for a monomeric random coil (49.6 Å) suggesting a polymeric state under these conditions (Table 3.2). Upon addition of 1 M urea to rrPar-4FL the R_S value decreases to 78.4 Å, which is still larger than the calculated R_S value of a random coil protein. However, it indicates the disruption of a non-covalent complex suggesting that rrPar-4FL is able to self-associate. Self-association of rrPar-4FL will be discussed in more detail in Chapter 3.6. and the DLS results in 6 M urea will also be given there. As discussed for rrPar4ΔLZ and rrPar-4SAC, the relatively broad volume weighted distributions for rrPar-4FL indicate ensembles of interconverting conformations (Fig. 3.4A), and the high degree of 'unfoldedness' for rrPar-4FL is best described by a random coil-like ensemble.

Limited proteolysis is a useful method for distinguishing ordered and disordered proteins, and for the mapping of disordered regions in proteins [207]. Due to protection of protease cleavage sites by tertiary folding [208,209] globular proteins are less susceptible to proteolysis than IDPs

[144,210]. The results of a limited tryptic digest of rrPar-4FL, rrPar-4ΔLZ, rrPar-4SAC and BSA are shown in Figure 3.5. BSA was chosen for comparison, as it contains a comparable percentage of predicted trypsin cut sites as the rrPar-4 constructs. After 15 minutes incubation with trypsin, rrPar-4ΔLZ was more than 95% digested, whereas rrPar-4FL and rrPar-4SAC were over 80% digested. In contrast, BSA was only 10% digested. This indicates that, unlike BSA, the Par-4 constructs lack protection by folded stable tertiary structure and are for the greater part solvent exposed. Furthermore, rrPar-4ΔLZ is somewhat less stable than rrPar-4FL and rrPar-4SAC suggesting a less compact conformation.

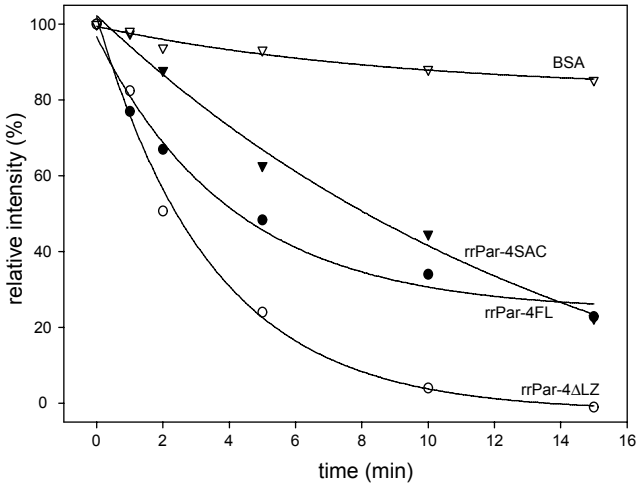

Figure 3.5 *– Limited proteolysis of rrPar-4FL, rrPar-4ΔLZ and rrPar-4SAC. BSA (open triangles), rrPar-4FL (filled circles), rrPar-4ΔLZ (open circles) and rrPar-4SAC (filled triangles) were incubated with trypsin at a ratio of 280:1 ($^{w}/_{w}$) in 50 mM NaCl, 20 mM Na_2HPO_4/NaH_2PO_4, pH 7.5. Figure and legend taken and adapted from Libich, Schwalbe et. al. [46].*

Taken together, MS indicates that the isolated rrPar-4 proteins had the expected masses. This implies that the apparent high molecular weights for the rrPar-4 proteins are caused by aberrant electrophoretic mobility. Aberrant mobility is due to the unique amino acid composition of the rrPar-4 proteins. Additional DLS and limited proteolysis experiments for the rrPar-4 proteins suggest extended coil-like conformations and the lack of stable tertiary structure in solution. For rrPar-4ΔLZ and rrPar-4SAC, DLS suggests the existence of folding elements that get disrupted upon addition of 1 M urea. DLS further shows that rrPar-4FL unlike rrPar-4ΔLZ and rrPar-4SAC is polymeric in native buffer.

3.3. Characterisation of Par-4 by size exclusion chromatography

3.3.1. Materials and Methods

For SEC, proteins were separated by an isocratic flow of 0.4 ml/min at 4 ºC using a Superdex 200 column connected to the BioLogic DuoFlow System. Calibration curves to convert retention times to *MWs* were established using the commercially available Molecular Weight Marker Kit (12-200 kDa) from Sigma-Aldrich and results are shown in Appendix E. The SEC buffer used for calibration contained 50 mM NaCl, 20 mM Na_2HPO_4/NaH_2PO_4, pH 7.5. The buffer for the

analysis of rrPar-4FL, rrPar-4ΔLZ and rrPar-4SAC contained 20 mM NaCl, 10 mM Tris, pH 7.0. Buffers distinct from this composition will be given in the Results section. All samples were filtered using an Ultrafree-MC Centrifugal Filter device (pore size 0.22 μm) prior to application to the SEC column. Collected fractions were analysed by SDS-PAGE.

3.3.2. Results and Discussion

As mentioned above, IDPs have different hydrodynamic properties compared to globular proteins [155]. The calibration curves used for conversion of retention time to *MW* are therefore only strictly valid for globular proteins like the molecular weight standards. However, for comparative purposes the apparent *MW* will be used rather than the retention time. As can be expected for IDPs, the SEC results are suggestive of extended confirmations for the rrPar-4 proteins. Extended structures are indicated by higher *MW* values than are expected from the amino acid sequence [155]. The broad and non-symmetric peaks observed for the rrPar-4 proteins relative to the peaks observed for the molecular weight standards (data not shown) further suggest the existence of interconverting ensembles [211,212].

Analysis of rrPar-4FL by SEC was not possible. Upon injection of rrPar-4FL (at concentrations of 55 μM and 15 μM) into the sample loop a faint precipitate was visible. The resulting chromatogram showed no signs of proteins indicating that all rrPar-4FL precipitated. Precipitation of rrPar-4FL upon dilution was observed various times, but the reason for precipitation is unknown. Concentrated rrPar-4FL solutions are stable, but below concentrations of ~10 μM precipitation occurs. Unlike DLS, an accurate control of the concentration was not possible as the protein solution was diluted upon injection. Collection of useful SEC data for rrPar-4FL was therefore not possible. Recently, the SEC analysis of a full-length Par-4 construct has been published by Gao *et. al.* [54]. In this study full-length Par-4 displayed a broad peak. Elution of Par-4 started at retention times corresponding to *MWs* of approximately 500-600 kDa and ended at retention times corresponding to 43 kDa with a maximum around 360 kDa. Using the maximum value of 360 kDa, an R_S value of ~60.2 Å can be approximated [181]. This value is not as large as the value obtained by DLS in the previous chapter (Table 3.1), but still larger than what can be expected for a coil-like conformation of rrPar-4FL (Table 3.2). The size difference between these two data sets may be attributed to the fact that Gao *et. al.* used full-length Par-4 isolated from LNCaP prostate cancer cells. Possible post-translational modifications in mammalian cell may affect the self-association of Par-4. Consistent with the analysis of the DLS data of rrPar-4FL (Chapter 3.2.2.), Gao *et. al.* concluded that full-length Par-4 is polymerising

[54]. Considering the extent of ID in Par-4, an octameric state as proposed by the authors is unlikely. The high apparent *MW* is probably, to some extent, due to ID in Par-4 as shown above.

Analysis of rrPar-4ΔLZ (31.1 kDa) at a concentration of ~0.5 mM (stock solution) was performed using a buffer containing 100 mM NaCl, 1 mM DTT and 20 mM Na_2HPO_4/NaH_2PO_4, pH 7.0. Application of 50 µl of the stock solution to the SEC column produced a chromatogram displaying two peaks (Fig. 3.6A, dashed line) with retention times corresponding to *MWs* of ~41 kDa and ~29 kDa. Applying seven times more sample, but otherwise identical conditions, a chromatogram with three peaks was obtained (Fig. 3.6A, solid line), indicating a dependence of the SEC results on the concentration of the Par-4 protein. The retention times correspond to *MWs* of approximately 207 kDa, 47 kDa and 30 kDa. Analysis of the collected fractions by SDS-PAGE showed that the peak corresponding to 207 kDa contained the majority (70-80%) of the applied rrPar-4ΔLZ.

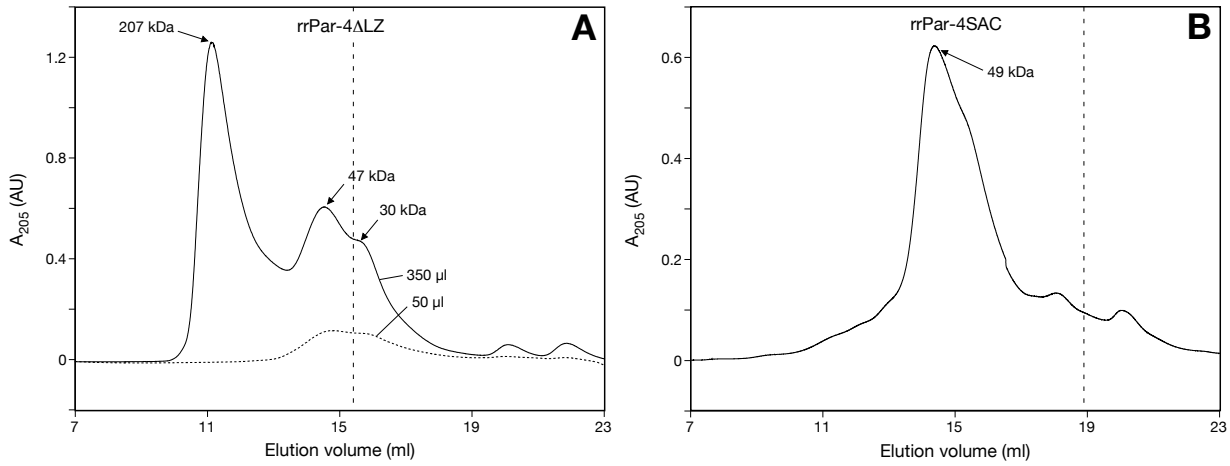

Figure 3.6 *– Size exclusion chromatography of Par-4. (A) Chromatograms of 0.5 mM rrPar-4ΔLZ using a Superdex 200 column at 4 ºC and 100 mM NaCl, 1 mM DTT and 20 mM Na_2HPO_4/NaH_2PO_4, pH 7.0 as buffer. Different results are obtained depending on the protein concentration. The chromatogram marked by a solid line is obtained if 350 µl of 0.5 mM rrPar-4ΔLZ are applied to the column; the chromatogram marked by a dashed line if 50 µl are applied. (B) Chromatogram of 0.21 mM rrPar-4SAC using a Superdex 200 column at 4 ºC and a low salt buffer containing 20 mM NaCl, 10 mM Tris, pH 7.0. Dashed vertical lines in both chromatograms indicate the expected elution times if both proteins were globular. Both proteins elute at earlier time points suggesting a non-globular conformation.*

An apparent *MW* of 207 kDa corresponds to an R_S value of ~49.4 Å [181]. This value is close to the value that can be expected for a coil-like conformation of rrPar-4ΔLZ (Table 3.2). In contrast, the R_S value of 29.1 Å calculated for the second peak corresponding to 47 kDa (or 41 kDa) is close to what can be expected for a molten globule state of rrPar-4ΔLZ (Table 3.2). The last peak (30 and 29 kDa, respectively) would correspond well with the expected value for a

globular protein of 31 kDa, however, a globular conformation is not to be supported by other experiments (Chapter 3.4.2.). It is currently not known what causes the different peaks and the concentration dependent behaviour. The 207 kDa peak suggests a coil-like conformation for rrPar-4ΔLZ, consistent with the DLS and limited proteolysis results (Chapter 3.2.2.). Consistent with DLS results, the non-symmetric peak shape further suggests the existence of an ensemble of interconverting structures. It is also possible that the 207 kDa peak represents aggregated rrPar-4ΔLZ. Protein aggregation was not detected by DLS experiments (Chapter 3.2.2.), however, for DLS the protein concentration was significantly lower than for SEC. Applying seven times less protein to the SEC could have resulted in the dissolution of the rrPar-4ΔLZ aggregates, and therefore no high molecular weight peak is seen in the corresponding chromatogram (Fig. 3.6A, dashed line). The other two peaks (47 kDa and 30 kDa) may represent retarded fractions that are interacting with the gel matrix thereby reducing the apparent *MW*. The reduction in the apparent *MW* of these two peaks is not due to protein degradation, as no degradation products were detected by SDS-PAGE.

For comparison with the DLS, CD and NMR results of rrPar-4ΔLZ and rrPar-4SAC, SEC was repeated using 20 mM NaCl, 10 mM Tris, pH 7.0 as buffer (Fig. 3.6B, only rrPar-4SAC is shown). The stock solutions were at a concentration of 10 µM (rrPar-4ΔLZ) and 210 µM (rrPar-4SAC). For both proteins broad peaks were obtained suggesting structural interconversion under these conditions. Peak maxima corresponded to ~38 kDa (rrPar-4ΔLZ) and ~49 kDa (rrPar-4SAC). The results obtained for rrPar-4ΔLZ (data not shown) are similar to the results at higher salt concentration (Fig. 3.6A). The high apparent *MW* (49 kDa) observed for the 7.0 kDa rrPar-4SAC protein (Fig. 3.6B) corresponds to an R_S of ~ 29.5 Å. This is slightly larger than the expected value for a coil-like conformation (Table 3.2). In contrast to the DLS results (Chapter 3.2.2.), this would suggest a higher oligomeric state for rrPar-4SAC or could indicate aggregation. DLS results show no indication for aggregation or oligomerisation, but were carried out at lower concentration. It should be noted that calibration of the Superdex 200 column using the low salt buffer was problematic and may have affected the accurate calculation of the apparent *MW*. The results for rrPar-4SAC may have therefore been skewed to higher *MWs*. According to manufacturer instructions the recommended NaCl concentration for SEC should be 150 mM to avoid non-specific interactions with the gel matrix. Slightly different retention times were observed for the molecular weight standards in buffers containing 50 mM NaCl, 20 mM Na_2HPO_4/NaH_2PO_4, pH 7.5 relative to 20 mM NaCl, 10 mM Tris, pH 7.0 (data not shown). This suggests that non-specific interactions with the matrix occur under low salt conditions.

Therefore, non-specific interactions may, to some extent, affect retention time and also the peak width. Due to the increased surface area of Par-4 proteins, or IDPs in general [166], non-specific interactions with the matrix may be even more pronounced for Par-4 than for globular proteins. Taken together, the SEC results were consistent with proposed ID nature for the rrPar-4 proteins. Probably due to the incompatibility of the SEC column matrix with the used low salt buffer conditions the results were inferior to DLS results. Additionally, no results could be obtained for rrPar-4FL.

3.4. Secondary structure assessment by CD and NMR spectroscopy

3.4.1. Materials and Methods

a) Circular Dichroism (CD)

CD spectra were recorded on a Chirascan CD spectropolarimeter (Applied Photophysics, Leatherhead, United Kingdom) equipped with a recirculating water bath. CD data was obtained using a quartz cuvette with 1 mm pathlength. Samples were at a concentration of 0.3 mg/ml (8 µM rrPar-4FL, 10 µM rrPar-4ΔLZ and 43 M rrPar-4SAC) in native buffer (20 mM NaCl, 10 mM Tris, pH 7.0). Additional samples of 8 µM rrPar-4FL were prepared in native buffer + 1 M or 6 M urea. Spectra were recorded in 0.5 nm steps from 260 to 190 nm with an integration time of 1 s at each wavelength. Further acquisition parameters are given in Appendix F. Three successive scans were recorded, the sample blank subtracted and the scans averaged and smoothed using a sliding window function (Chirascan Software, Applied Photophysics). Thermal stability was determined by acquiring CD spectra as a function of temperature at 5 ºC intervals from 5 ºC to 75 ºC with 2 minutes equilibration time at each temperature point. Melting curves were obtained by monitoring the ellipticity at 222 nm ($[\theta]_{222}$) as a function of temperature. Melting temperatures (T_m) were estimated by evaluating the maximum of $d[\theta]_{222}/dT$. Spectral deconvolution was performed using the CONTIN-LL algorithm [213] through the DICHROWEB server interface [214,215].

b) NMR spectroscopy

NMR experiments were recorded on a Bruker Avance 700 MHz spectrometer equipped with a cryoprobe, four rf-channels and gradient pulse capabilities. All spectra were acquired at 5 ºC on 300 µl samples containing 5% D_2O ($^v/_v$) in Shigemi NMR tubes. The rrPar-4FL sample concentration was 0.48 mM in 20 mM NaCl, 10 mM Tris, pH 7.0. The rrPar-4ΔLZ construct was uniformly ^{15}N-labelled with a protein concentration of 0.09 mM in 100 mM NaCl, 1 mM DTT,

20 mM Na_2HPO_4/NaH_2PO_4, pH 7.5. Similarly, rrPar-4SAC was uniformly ^{15}N-labelled at a concentration of 0.34 mM in 20 mM NaCl, 10 mM Tris, pH 7.0. In all cases the carrier frequency was set to the frequency of the water resonance in the ^1H dimension. Further acquisition parameters are listed in Appendix G. All data sets were linear predicted (32 prediction coefficients), apodised using a shifted (π/6) squared sinusoidal bell function and zero-filled once in the indirect dimension before Fourier transformation and final processing. Spectra were processed using TopSpin 2.1 (Bruker BioSpin GmbH, Rheinstetten, Germany). The ^1H and ^{15}N chemical shifts were referenced to the water signal [216].

3.4.2. Results and Discussion

The CD spectra for rrPar-4FL, rrPar-4ΔLZ and rrPar-4SAC are shown in Figure 3.7. Significant α-helical character is evident in the spectra of rrPar-4FL that remains stable up to 65 ºC (Fig. 3.7A). In contrast, rrPar-4ΔLZ (Fig. 3.7C) and rrPar-4SAC (Fig. 3.7E) display IDP characteristic CD spectra with a deep transition at 200 nm and a minor transition at 222 nm [155]. It was previously demonstrated that CD spectra of IDPs show minor contributions from secondary structure elements such as alpha or poly-proline type II helices [217]. Spectral deconvolution of the 25 ºC spectra estimates an α-helical content (combined regular and distorted α-helix [218]) of 32%, 17% and 18% for rrPar-4FL, rrPar-4ΔLZ and rrPar-4SAC, respectively. The results of rrPar-4FL in 1 M or 6 M urea will be discussed in Chapter 3.6. The CD traces from 5 ºC through to 65 ºC display similar features indicating that all three constructs are relatively stable throughout the heating cycle. Interestingly, an isodichroic point at 210 nm is observed for rrPar-4SAC (Fig. 3.7C) indicating a two-state transition [134,136]. Although the overall temperature-induced conformational changes are minor, this two-state transition could be due to secondary and/or tertiary structure that gets thermally disrupted. Thus in addition to the CC region of rrPar-4FL (Chapter 3.6.), other regions of the rrPar-4 proteins may transiently populate α-helical or other secondary structures.

As mentioned earlier, the secondary structural content of IDPs can be assessed by NMR with atomic resolution [155]. However, most residues in IDPs experience a similar chemical environment as they are solvent exposed and inherently flexible. This results in similar NMR frequencies and hence significant spectral overlap (particularly for ^1H resonances) [155,219]. Furthermore, population-weighted average chemical shifts are observed for IDPs [220]. The inherent flexibility also results in sharp peaks due to increased T_2 values [221].

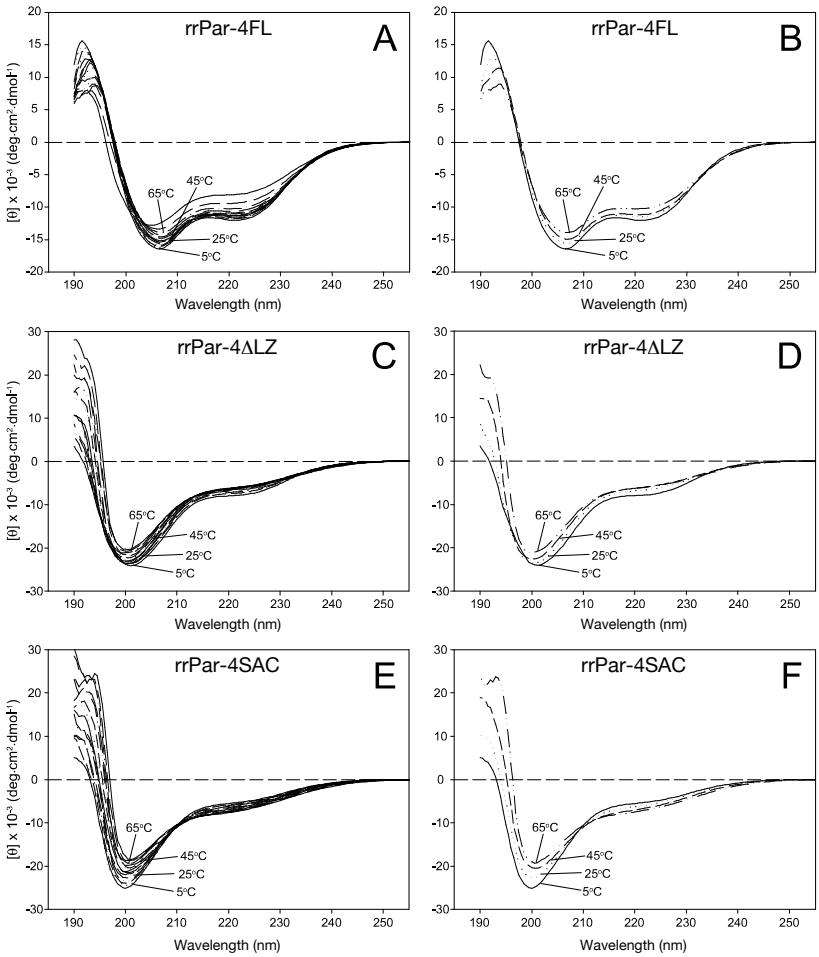

Figure 3.7 *– CD spectropolarimetry indicates ID in Par-4. Temperature dependence of the CD spectra of rrPar-4FL (A, B), rrPar-4ΔLZ (C, D) and rrPar-4SAC (E, F). Data for all constructs were recorded in 20 mM NaCl, 10 mM Tris, pH 7.0 over a temperature range of 5-75 ºC. Panels A, C and E show the traces for each temperature recorded in the experiment. For clarity panels B, D and F show four equally spaced temperatures from the sampled range. Acquisition parameters are given in Appendix F. Figure and legend taken and adapted from Libich, Schwalbe et. al. [46].*

Pairwise overlays of $^{1}H,^{15}N$-HSQC spectra for rrPar-4FL, rrPar-4ΔLZ and rrPar-4SAC are shown in Figure 3.8. The spectra of all three proteins exhibit the aforementioned characteristic features of ID, such as narrow ^{1}H chemical shift dispersion and sharp peaks. Interestingly, some structural similarity between rrPar-4FL and rrPar-4ΔLZ is indicated by chemical shift similarities (Fig. 3.8A). The constructs differ by the presence of the LZ domain (residues 292-332) in rrPar-4FL (Fig. 3.1A). This indicates that some residues (most likely at the N-Terminus) share a similar local environment and probably a similar conformation in both constructs. Residues closer to the C-terminus (hence closer to the LZ domain) probably experience different chemical environments due to the presence of the LZ domain resulting in chemical shift differences of the corresponding peaks for each construct. Fewer chemical shift similarities are observed for

rrPar-4FL or rrPar-4ΔLZ with rrPar-4SAC (Figs. 3.8B and C). This suggests that the majority of residues in rrPar-4SAC experience a different local environment and thus probably a different conformation than the SAC domain in the context of either rrPar-4FL or rrPar-4ΔLZ.

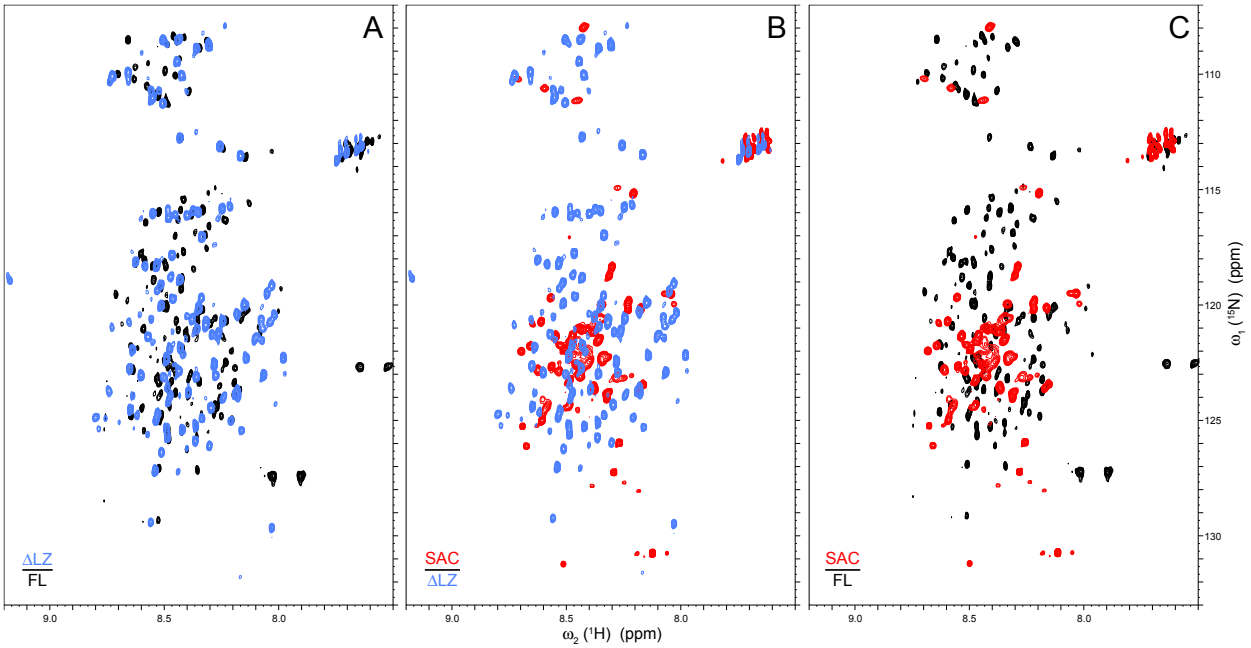

Figure 3.8 *– NMR spectroscopy displays typical features of ID in Par-4. Pairwise overlays of $^{1}H,^{15}N$-HSQC spectra of (A) rrPar-4FL (black contours) and rrPar-4ΔLZ (blue contours), (B) rrPar-4ΔLZ (blue contours) and rrPar-4SAC (red contours) and (C) rrPar-4FL (black contours) and rrPar-4SAC (red contours). Sample conditions were: 0.34 mM rrPar-4SAC in 20 mM NaCl, 10 mM Tris, pH 7.0 and 5% D_2O (v/v); 0.48 mM rrPar-4FL in 20 mM NaCl, 10 mM Tris, pH 7.0 and 5% D_2O (v/v); and 0.09 mM rrPar-4ΔLZ in 100 mM NaCl, 1 mM DTT, 20 mM Na_2HPO_4/NaH_2PO_4, pH 7.5 and 5% D_2O (v/v). The rrPar-4ΔLZ and rrPar-4SAC proteins were uniformly ^{15}N-labelled. All spectra were recorded at 5 °C. Acquisition parameters are given in Appendix G. Figure and legend taken and adapted from Libich, Schwalbe et. al. [46].*

For rrPar-4FL only approximately 160 of the 308 peaks expected (335 – N-terminal residue - 26 prolyl residues) and for rrPar-4ΔLZ only approximately 152 of the 266 expected peaks (293 – N-terminal residue - 26 prolyl residues) are readily identifiable in the $^{1}H,^{15}N$-HSQC (Figs. 3.8A and C). Due to missing assignments it is not clear if the same residues (or residues from the same regions) are unobservable in both constructs. Possible explanations for the low peak count include significant spectral overlap and/or intermediate exchange processes of currently unknown nature [183]. Further studies, including sequential assignment and ^{15}N-relaxation analysis, may help to identify the unobservable peaks or regions and to elucidate the time scales of motion for the visible peaks of rrPar-4FL and rrPar-4ΔLZ [222]. In contrast, the spectrum of rrPar-4SAC (Figs. 3.8B and C) is much more complete. Of the expected 60 peaks (62 – N-

terminal residue - 1 prolyl residue) 58 peaks were readily picked and only two glycyl residues remained unobservable. The small size of rrPar-4SAC (7 kDa), relative to rrPar-4FL and rrPar-4ΔLZ (> 30 kDa), is beneficial in the observance of almost all resonances as the chance of spectral overlap and the likelihood of slow to intermediate exchange is reduced due to fewer residues. Nonetheless, the sharp peak shape and poor chemical shift dispersion suggest a similar degree of disorder relative to rrPar-4FL and rrPar-4ΔLZ.

In summary, both CD and NMR spectroscopy indicate that rrPar-4FL, rrPar-4ΔLZ and rrPar-4SAC are mostly disordered. An isodichroic point in the CD data suggests the presence of transient secondary and/or tertiary structure in rrPar-4SAC. CD spectropolarimetry also indicates residual α-helical structure in rrPar-4FL that remains stable up to 65 ºC. However, the residual α-helical structure in rrPar-4FL is not readily identifiable in the corresponding NMR spectra. The NMR spectra of all three proteins display typical features of IDPs. The situation is further complicated as approximately 52% of the expected peaks for rrPar-4FL and rrPar-4ΔLZ are not readily observed.

3.5. Influence of pH and TFE on the conformation of the Par-4 SAC domain

3.5.1. Materials and Methods

a) Circular Dichroism

An aliquot containing 2 mg ^{15}N-labelled rrPar-4SAC (Chapter 2.9.1.) was dialysed overnight at 4 ºC against 500 ml H_2O and the protein concentration was determined. CD samples of rrPar-4SAC were prepared at four different pH values from 4-7 by dilution of this rrPar-4SAC stock solution with appropriate buffers (Table 3.3). Additionally, a CD sample containing 30% d^3-TFE ($^v/_v$) was prepared from this stock solution (Table 3.3, sample e). In all cases, the final rrPar-4SAC concentration was 43 µM (0.3 mg/ml). CD spectra were recorded in 1 nm steps from 260 to 190 nm as described in Chapter 3.4.1.a. Acquisition parameters are given in Appendix F. Spectral deconvolution was performed using the CONTIN-LL algorithm through the DICHROWEB server interface.

b) NMR spectroscopy

An aliquot containing 4 mg ^{15}N-labelled rrPar-4SAC (Chapter 2.9.) was dialysed overnight at 4 ºC against 500 ml PBS. The dialysate was concentrated to ~500 µl using a Vivaspin 20 device (*MWCO* = 3 kDa) and the concentration determined (~0.5 mM). After adding D_2O to 5% ($^v/_v$), the sample was used for NMR. Furthermore, the 43 µM rrPar-4SAC sample in 20 mM NaCl,

10 mM Tris + 30% d^3-TFE ($^v/_v$), pH 5 (Table 3.3, sample e) was analysed by NMR after adding D_2O to 5% ($^v/_v$). NMR spectra were recorded and processed as described in Chapter 3.4.1.b using a shifted ($\pi/2$) squared sinusoidal bell function for apodisation. Acquisition parameters are given in Appendix G.

	rrPar-4SAC concentration	Buffer composition
a)	43 µM	20 mM NaCl, 10 mM NaAc, pH 4.0
b)	43 µM	20 mM NaCl, 10 mM NaAc, pH 5.0
c)	43 µM	20 mM NaCl, 10 mM Mes, pH 6.0
d)	43 µM	20 mM NaCl, 10 mM Tris, pH 7.0
e)	43 µM	20 mM NaCl, 10 mM Tris + 30% d^3-TFE ($^v/_v$), pH 5

Table 3.3 − *Sample conditions of rrPar-4SAC at various pH values.*

3.5.2. Results and Discussion

The CD series of rrPar-4SAC as a function of temperature at four different pH values are shown in Figure 3.9. A CD series of rrPar-4SAC at pH 7.0 under almost identical conditions is shown in Fig. 3.7E. It was repeated here for consistency with the CD results at pH 6.0, 5.0 and 4.0, and to exclude the formation of artefacts during the buffer exchange to H_2O. To save time, the thermal stability at pH 7.0 was assessed in 10 ºC intervals instead of 5 ºC intervals. The obtained CD spectrum is almost identical to the previous spectrum (Fig. 3.7E) indicating the reproducibility of the results. The slight difference in the *[θ]* values relative to the results of Figure 3.7E is probably due to minor uncertainties in the concentration determination by A_{280} measurements and is within the error range expected. Note that rrPar-4SAC only contains one tyrosine residue resulting in only minor absorption at 280 nm The spectra at pH 6.0, 5.0 and 4.0 are virtually identical to the spectrum at pH 7.0 and indicative of ID with deep transitions at 200 nm (Fig. 3.9). Due to buffer absorption, no reliable data was obtained below 200 nm in most cases. Since no greater structural changes were observed over the pH range from 4.0 to 7.0 (Fig. 3.9), it was concluded that it is not worthwhile to acquire NMR spectra of these samples.

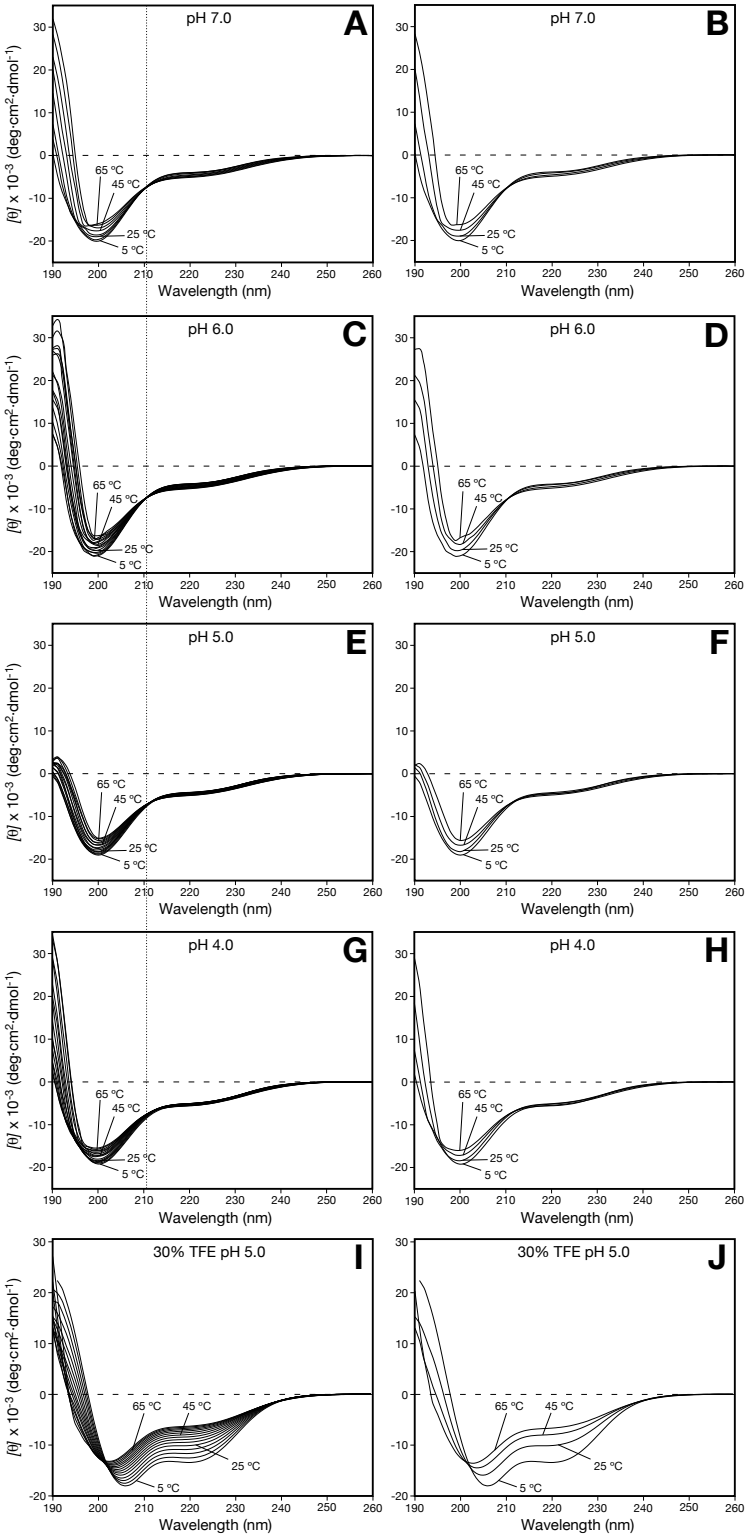

Figure 3.9 *− pH and TFE dependence of the CD spectra of rrPar-4SAC. Influence of pH on the CD spectra of 43 µM rrPar-4SAC as a function of temperature; (A, B) at pH 7.0, (C, D) at pH 6.0, (E, F) at pH 5.0 and (G, H) at pH 4.0. (I, J) Temperature dependence of the CD spectra of 43 µM rrPar-4SAC in 30% TFE (%v). Sample conditions are given in Table 3.3. All spectra were acquired in 5 ºC intervals (10 ºC for panel A) over a temperature range of 5-75 ºC. Traces for each temperature are shown in panels A, C, E, G and I, and for clarity panels B, D, F, H and J show traces of four evenly spaced temperatures. The dotted line through panels A, C, E and G is used as reference to show the shift of the isodichroic point at 210 nm to longer wavelengths. Acquisition parameters for each spectrum are given in Appendix F.*

A notable difference in the CD spectra at different pH values is the position of the isodichroic point. At pH 7.0 and 6.0 an isodichroic point at 210 nm is visible (Figs. 3.9A-D). With decreasing pH this isodichroic point shifts to longer wavelengths of approximately 212 nm (pH 5.0, Fig. 3.9E) and 214 nm (pH 4.0, Fig. 3.9G), respectively. The isodichroic point at 210 nm has been discussed as an indication of secondary and/or tertiary structure that gets disrupted upon thermal denaturation (Chapter 3.4.2.). The shift of the isodichroic point to higher wavelengths may indicate minor structural changes induced with decreasing pH. At pH 4.0 the isodichroic point is less well defined (Fig. 3.9G) and one may argue that it is lost altogether. This may be interpreted that less secondary and/or tertiary structure is present at pH 4.0 relative to pH 7.0 and hence that the transient secondary and/or tertiary structure is disrupted with decreasing pH.

^{1}H,^{15}N-HSQC spectra of rrPar-4SAC were acquired to asses if rrPar-4SAC adopts a similar conformation under low salt conditions as used for CD spectropolarimetry relative to physiological buffer conditions. The ^{1}H,^{15}N-HSQC spectra of rrPar-4SAC under low salt conditions (20 mM NaCl, 10 mM Tris, pH 7.0) and under physiological salt conditions (PBS, 140 mM NaCl) are shown in Figure 3.10A. Comparison of these two spectra shows almost no difference, indicating that rrPar-4SAC residues are in a similar local environment and probably in a similar conformation under both conditions. This further suggests that no artefacts are introduced using a low salt buffer for CD, DLS and NMR spectroscopy. Minor differences in the spectra may be due to the different concentration of rrPar-4SAC in low salt buffer (0.34 mM) and PBS (0.5 mM).

Secondary structure prediction of the SAC domain shows a propensity for α-helix (Chapter 3.1, Fig. 3.1B). TFE is well known to stabilise α-helical conformations in proteins [140]. Furthermore, TFE has been used to stabilise molten globule structures to allow NMR spectroscopic studies [223]. The rationale was therefore to use TFE to stabilise an α-helical state that may be similar to the conformation of the biological active SAC domain. The TFE-induced helix formation levels off above concentrations of 25% TFE [224]. Therefore, a TFE concentration of 30% was used as the starting concentration to induce a significant conformational change and analyse this by CD spectropolarimetry and NMR spectroscopy. CD spectropolarimetry shows significant α-helical character for rrPar-4SAC in 30% TFE, as is indicated by transitions near 208 and 222 nm (Fig. 3.9I). This α-helical character is stable up to approximately 35 ºC and with further increasing temperature gradually converts to a spectrum indicative of protein disorder. Note that the addition of d^{3}-TFE to the 20 mM NaCl, 10 mM Tris,

pH 7.0 buffer results in a pH drop to approximately pH 5. Spectral deconvolution estimates 39% α-helicity for rrPar-4SAC in 30% TFE at 5 ºC and pH 5 relative to 8% for rrPar-4SAC without TFE at 5 ºC and pH 5.0. This indicates that 30% TFE does not induce a complete conversion of rrPar-4SAC to an α-helix, and that rrPar-4SAC remains to a certain degree disordered.

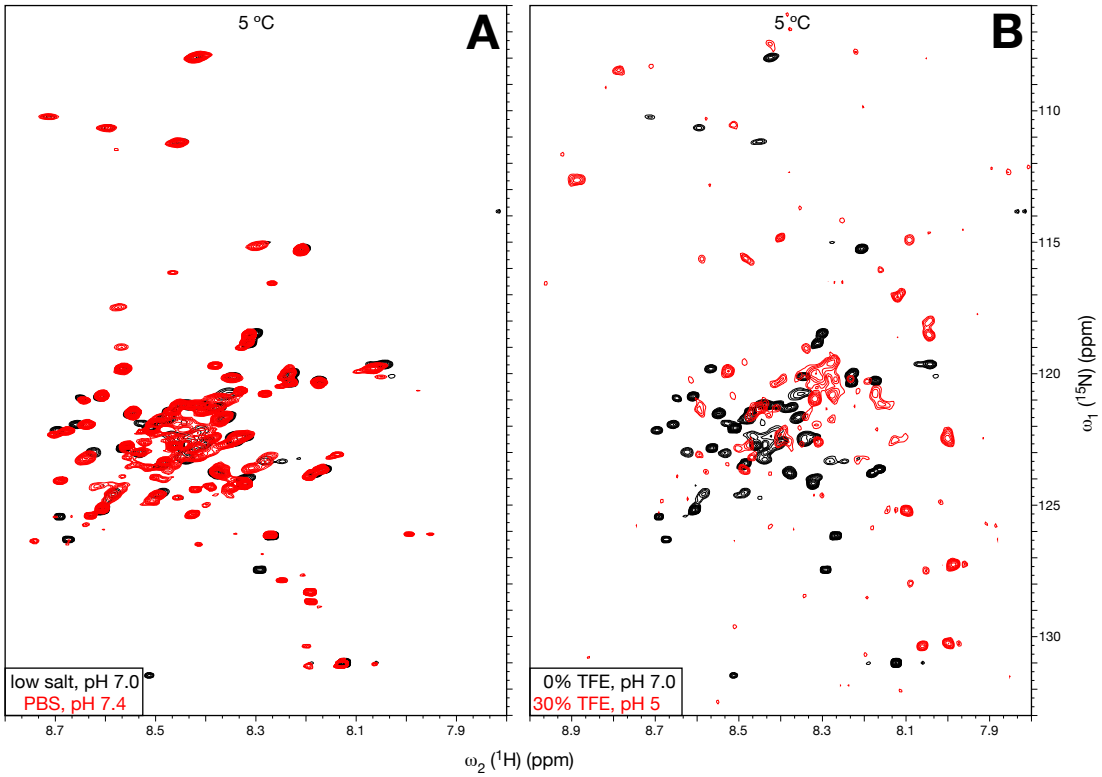

Figure 3.10 *− Influence of ionic strength and TFE on the NMR spectra of rrPar-4SAC. (A) Pairwise comparison of the $^{1}H,^{15}N$-HSQC spectra of rrPar-4SAC under low salt (black contours) and physiological salt conditions (red contours). Sample concentrations were 0.34 mM rrPar-4SAC in 20 mM NaCl, 10 mM Tris, pH 7.0 and 5% D_2O (v/v) (black contours) and 0.5 mM rrPar-4SAC in PBS, pH 7.4 and 5% D_2O (v/v) (red contours). (B) Overlay of the $^{1}H,^{15}N$-HSQC spectrum of 0.34 mM rrPar-4SAC in 20 mM NaCl, 10 mM Tris, pH 7.0 and 5% D_2O (v/v) (black contours) with the $^{1}H,^{15}N$-SOFAST-HMQC [225] spectrum of 43 µM rrPar-4SAC in 20 mM NaCl, 10 mM Tris + 30% d^3-TFE (v/v), pH 5 and 5% D_2O (v/v) (red contours). For preparation of the 0.34 mM rrPar-4SAC sample in 20 mM NaCl, 10 mM Tris, pH 7.0 and 5% D_2O (v/v), see Chapter 3.4.1.b. All spectra were acquired at 5 ºC. All samples were uniformly ^{15}N-labelled. Acquisition parameters for each spectrum are given in Appendix G.*

The TFE-induced increase in α-helicity observed by CD spectropolarimetry is also reflected in the corresponding NMR spectrum (Fig. 3.10B). Compared to the spectrum acquired without TFE an increased ^{1}H chemical shift dispersion is observed for the spectrum with 30% TFE (Fig. 3.10B). Notably is further the decreased intensity of the peaks in the centre of the spectrum compared to the peaks with lower ^{1}H ppm values. Furthermore, only 50 of the expected 60 peaks (62 − N-terminal residue − one prolyl residue) are visible in the presence of TFE. This may be

partly due to spectral overlap, but together with the decreased intensity of some of the peaks this is suggestive of intermediate exchange. Intermediate exchange resulting in peak broadening in the presence of TFE is not uncommon [140]. However, without residue specific assignments and assessment of the dynamics of rrPar-4SAC no more definitive statements can be made. Future experiments should be performed at higher concentration to reduce limitations arising from low signal intensity.

Taken together, no greater conformational changes in rrPar-4SAC are induced with decreasing pH. A significant increase in α-helicity is induced by TFE, which is observed by CD spectropolarimetry and NMR spectroscopy. However, due to the poor NMR spectroscopic properties of rrPar-4SAC, even in the presence of TFE, structural characterisation was suspended in favour of more promising experiments with other Par-4 constructs. However, rrPar-4SAC may adopt a stable secondary and/or tertiary structure upon binding to a target protein [152]. Once such a binding partner has been identified and expressed, structural characterisation of rrPar-4SAC may be resumed. It may then be worth testing other TFE concentrations for comparative purposes.

3.6. Evidence for self-association through coiled coil formation

The putative CC domain (residues 254-332, Fig. 1.1) is the main interaction domain for the majority of the known Par-4 binding partners (Chapter 1.3.4.). C-terminal deletion mutants (comprising the whole CC domain or only the LZ domain) of Par-4 were shown to be sufficient to prevent binding of Par-4 to proteins such as WT1, aPCKζ, Dlk, or PKB (for more examples see Table 1.1). As described in Chapter 1.4, coiled coils are characterised by the heptad repeat $(abcdefg)_n$ with hydrophobic residues at the *a* and *d* positions [109].

To assess the degree of α-helicity at 25 ºC in the Par-4 C-terminus, especially the LZ domain, a CD difference spectrum between rrPar-4FL and rrPar-4ΔLZ was created and is shown in Figure 3.11A. Both constructs differ in the presence of the LZ domain that is deleted in rrPar-4ΔLZ (Fig. 3.1A). The difference spectrum is characteristic of a coiled coil with a ratio of $[\theta]_{222}/[\theta]_{208} > 1$ [141], suggesting that at least two rrPar-4FL monomers are involved in self-association. As was shown in Chapter 3.2.2, a large R_S value of 189 Å is measured for rrPar-4FL in native buffer (Table 3.1 and Fig. 3.11C). Coiled coils are rod-like structures that are known to produce larger R_S values than globular proteins of the same *MW* [226]. Examples of various coiled coils (e.g. chromogranin A [227] or SAP1 [226]) and rod-shaped proteins (e.g. winter flounder anti-freeze protein [228], hydrophobin SC3 [229]) with larger R_S values have been

described in the literature. However, the apparent R_S value of rrPar-4FL is much larger than the calculated R_S value for a random coil monomer (Table 3.2) suggesting self-association of at least two monomers. In contrast, the rrPar-4 proteins lacking the LZ domain (rrPar-4ΔLZ and rrPar-4SAC) did not have appreciably large R_S values relative to the estimated random coil values (Table 3.2). It was also shown above that addition of 1 M urea resulted in a reduction of the R_S from 189 to 78 Å suggesting the disruption of a non-covalent interaction. However, this R_S value is still larger than the expected value for a random coil monomer (Table 3.2). A further increase in the urea concentration to 6 M urea produces an R_S value (58 Å) that is close to the calculated value for a urea denatured protein of the same *MW* (Table 3.2 and Fig. 3.11C). Melt curves obtained by CD spectropolarimetry under similar conditions show an increase in T_m from 25 ºC (6 M urea), 55 ºC (1 M urea) to 75 ºC (0 M urea) with decreasing urea concentrations (Fig. 3.11B). Thus as the concentration of urea is increased, a polymeric state of rrPar-4FL is disrupted resulting in decreased thermal stability of the complex. The stability of the coiled coil in rrPar-4FL in relation to other rrPar-4 constructs will be discussed in more detail in Chapter 4.6.

As mentioned before, the α-helical character detected by CD spectropolarimetry for rrPar-4FL (Fig. 3.7A) is not readily identifiable in the corresponding $^{1}H,^{15}N$-HSQC spectrum (Fig. 3.8A). It was further noticed that only 52% of the expected peaks are observed. Recently, it was demonstrated that the observable signals in a $^{1}H,^{15}N$-HSQC of a GST-fusion peptide arose almost exclusively from the target protein and the linker region but not from the GST-tag [230]. As GST forms a 52 kDa dimer, *Liew et. al.* proposed that the signals arising from GST are broadened beyond observable limits and thus the observable peaks are from the flexible linker and target protein [230]. In an analogous way the elongated and highly self-associated CC domain of rrPar-4FL may form a large core that behaves as a much larger protein and thus resonances arising from the CC domain may be unobservable due to line broadening. In contrast, signals of attached ID regions of rrPar-4FL are observable due to their inherent flexibility. Consistent with this proposal, comparison of the $^{1}H,^{15}N$-HSQC spectra of rrPar-4FL and rrPar-4ΔLZ show approximately 50 resonances that have identical or reasonably close chemical shifts suggesting similar local environments in both proteins (Fig. 3.8A). Non-overlap of the remaining peaks suggests that a significant portion of rrPar-4FL may be affected by coiled coil formation, through direct or relayed interactions. However, due to missing assignments it is not clear if the missing peaks correspond to the CC domain. Other contributions to line broadening may come from intermediate conformational exchange processes such as interconversion

between monomeric and oligomeric states. All data presented in this study are consistent with this hypothesis.

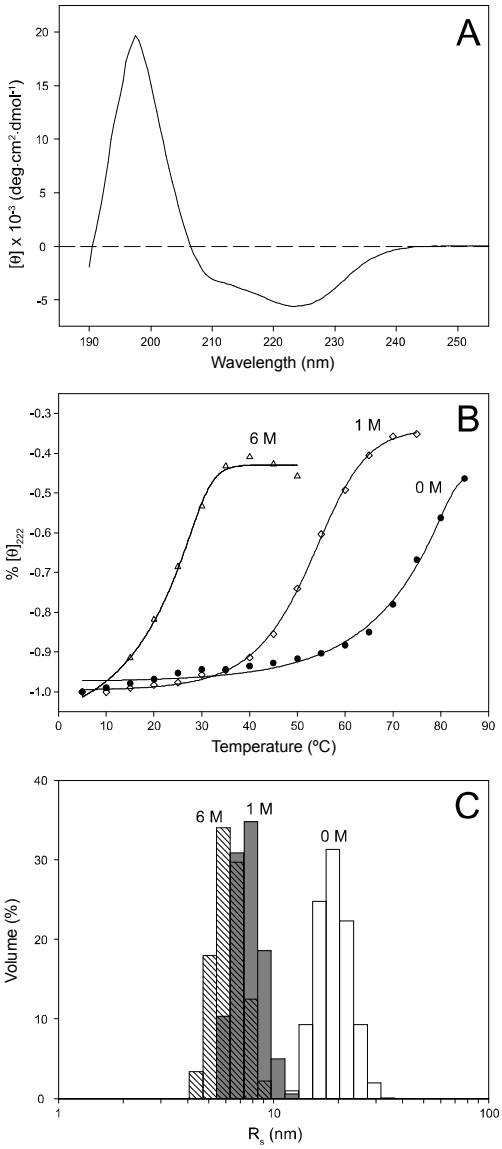

Figure 3.11 *– Influence of increasing concentrations of urea on rrPar-4FL. (A) Difference between the 25 ºC traces of rrPar-4FL and rrPar-4ΔLZ (Fig. 3.7). The difference spectrum is characteristic of a well defined coiled-coil displaying a* $[\theta]_{222}/[\theta]_{208}$ *ratio greater than one. (B) Temperature dependence of the molar ellipticity measured at 222 nm for rrPar-4FL in native buffer (20 mM NaCl, 10 mM Tris, pH 7.0) only (filled circles), native buffer + 1 M urea (open diamonds) and native buffer + 6 M urea (open triangles). (C) Volume distribution of DLS measurements of rrPar-4FL showing the apparent hydrodynamic radius of the particles in native buffer (white bars), native buffer + 1 M urea (grey bars) and native buffer + 6 M urea (hatched bars). The reduction of the apparent* R_S *upon increasing urea concentration suggests the disruption of a polymeric complex. Sample preparation and data acquisition are described in Chapters 3.2.1.a and 3.4.1.a Figure and legend taken and adapted from Libich, Schwalbe et. al. [46].*

The functional importance of homo-oligomeric coiled coil formation in Par-4 is currently unknown. Recently a 33 kDa splice variant of Par-4 was described by Wang *et. al*. This variant lacks exon 3 that comprises C-terminal residues of the SAC domain (residues 166-209), but retains the coiled coil region [47]. Residues 191-195 are necessary for the nuclear translocation of Par-4 [50] and hence this variant is retained in the cytoplasm. It was proposed that this variant has a dominant negative function and inhibits the pro-apoptotic activity of Par-4 by binding to and sequestering Par-4 in the cytoplasm [47]. Due to the presence of the CC domain in the 33 kDa splice variant, self-association of Par-4 may be physiologically relevant as an additional layer of regulation for its pro-apoptotic activity.

A further physiological implication of the presented data is that Par-4 may be an efficient linker protein binding one interaction partner through the coiled coil, while the ID regions comprising the majority of Par-4 are available for simultaneous interactions with another partner

or partners. Most interacting partners of Par-4 were shown to bind to the C-terminus, but a few were shown to bind N-terminally of the CC domain (e.g. F-actin [91], the androgen receptor [54], or GRP78 [75]). Ternary complexes of this kind have been described for Par-4 in Chapter 1.3.4. Par-4 binds to Dlk or Amida through the LZ domain and then translocates to actin filaments, which are bound by the Par-4 N-terminus. This translocation of Dlk and Amida to actin filaments was shown to be essential for their pro-apoptotic function [53,91]. Furthermore, ternary complexes have been demonstrated between Par-4, aPKCζ and p62 [88], and between Par-4, Dlk and Daxx[89].

Taken together, CD (Fig. 3.11A) and DLS results (Fig. 3.11C) suggest that rrPar-4FL self-associates through the CC domain. The LZ domain is of critical importance for self-association as no self-association (Fig. 3.4) or strong α-helical character (Fig. 3.7C) are observed for rrPar-4ΔLZ. This indicates that the LZ domain is necessary for self-association and that the majority of the α-helical character observed in rrPar-4FL (Fig. 3.7A) may be attributed to this domain. It is further proposed here that self-association occurs through coiled coil formation, and that self-association may be of physiological importance for the pro-apoptotic function of Par-4 [173].

3.7. The advantage of disorder in regulatory processes

Apoptosis is a highly dynamic cellular process that is dependent on the localisation, functional activity and stability of pro- and anti-apoptotic proteins [2,70,71]. ID may therefore impart several advantages for the pro-apoptotic role of Par-4. The solvent exposed disordered regions are easily accessible for post-translational modifications (e.g. phosphorylation, ubiquitination or Ubl-conjugation), which enable the precise control of localisation, function and turnover rate [143,231]. Notably, two phosphorylations were shown to be important for the function and localisation of Par-4. Phosphorylation of Thr 155 (Fig. 1.1) is required for the initiation of apoptosis [26], while phosphorylation of Ser 249 results in sequestration of Par-4 in the cytoplasm [56]. It was further proposed that ID is essential for the recognition of NLS by their respective receptors. NLS comprise a basic stretch of lysines or arginines that is flanked by acidic residues and helix breakers such as proline or glycine. Otherwise NLS are poorly conserved yet bind the same receptor. ID is proposed to facilitate the exposure of the signal stretch and the adaptation to the receptor [144]. An additional layer of cellular control is offered by the extreme proteolytic sensitivity of IDPs enabling rapid and controlled turnover [232].

Three human and two mouse Par-4 splice variants have been described in Chapter 1.2.1. Alternate splicing is a regulatory process that increases the complexity of the signalling network by producing different proteins with distinct functions from the same gene. Splicing within ordered domains of a protein could potentially disrupt the tertiary structure of a protein. It was therefore proposed that alternate splicing occurs in intrinsically disordered regions of a protein thereby reducing the risk of disrupting existing structure in a protein [233]. Consistently, for the 33 kDa splice variant of mouse Par-4, which lacks exon 3 (residues 166-209) [47], the spliced region localises to a sequence that was shown to be disordered in Chapter 3.4.2.

ID in proteins also confers an increased structural plasticity that allows IDPs to bind multiple targets with high specificity yet in a readily reversible manner. Promiscuous binding through primarily disorder containing regions has been shown for several proteins (e.g. p53 or high mobility group protein A (HMGA)) [147]. Similarly, Par-4 could contain multiple specific binding sites enabling the simultaneous interaction with different binding partners as demonstrated for the several ternary complexes of Par-4 (see above). Beneficial for the promiscuous binding ability of IDPs might be their increased amount of accessible surface area per residue that is available for intermolecular interactions [166]. It is interesting to note here that all 26 prolines present in Par-4 occur in the first 255 residues (Fig. 1.1). Proline has been discussed to favour open conformations and extended structures such as polyproline-type II helices. Polyproline-type II helices are an interesting type of secondary structure as they were shown to convert to other conformational states [234]. Additionally, prolyl residues are thought to promote inter-molecular recognition due to the absence of intra-residue hydrogen bonds [235].

As mentioned in the Introduction (Chapter 1.5.), IDPs are often found to form hubs or nodes in cellular pathways as they are tightly regulated through post-translational modifications and due to their promiscuous binding, that serves to link the functions of several proteins and/or cofactors together [173]. The extensively studied IDP HMGA, a chromosome and chromatin modulator, functions as a hub in cancer and other related pathological processes [236,237]. Considering the ubiquitous expression, tight temporal and spatial regulation, rapid turnover, the multitude of interaction partners and the inherent flexibility of Par-4, a similar role is likely for Par-4. Therefore, it is proposed here that due to the above mentioned properties, Par-4 is uniquely situated as a control factor hub for apoptosis integrating the signals of various pro- and anti-apoptotic pathways.

4. Order-disorder Equilibria in the Coiled Coil region of Par-4

It has been suggested in Chapter 3.6. that the full-length Par-4 protein self-associates through coiled coil formation. The Par-4 LZ domain was shown to be essential for this self-association. As was discussed in Chapter 1.3.4, the LZ domain is also important for binding to Par-4 interaction partners. It was previously shown by CD spectropolarimetry that a peptide comprising the Par-4 LZ domain displays a pH and temperature dependent coiled coil formation [184]. Mutation of key acidic residues abolished the pH dependency and resulted in an increased thermal stability of the coiled coil [185]. In this chapter the NMR spectroscopic characterisation of various Par-4 LZ peptides is shown, and together with other biophysical methods an environment-dependent folding behaviour for these peptides is described. Furthermore, the contributions of internal asparagine residues to coiled coil stability will be shown. A comparison of the thermal stabilities of various coiled coil forming Par-4 constructs and their possible implications for the physiological function of Par-4 will be given at the end of this chapter.

4.1. Sequence analysis of the Par-4 C-terminus

As mentioned in Chapter 1.4, coiled coils are amphipathic α-helical structures that are able to form left-handed supercoils by winding two or more helices around each other [105]. To summarise the most important characteristics, the amino acid sequence of coiled coils is characterised by a seven residue repeat designated $(abcdefg)_n$ [106]. The *a* and *d* positions of each heptad are generally hydrophobic and form the centre of the oligomeric interface. Leucine zippers as a coiled coil subset are typified by a predominance of leucine residues at position *d* of the heptad repeat [125,126]. Leucine residues at this position contribute mainly to leucine zipper stability, whereas residues at position *a* are more variable and define the oligomeric state of leucine zippers [127]. The occurrence of β-branched hydrophobic residues such as isoleucine or valine, and of polar asparagine residues at position *a* has been correlated with a dimeric state [109,117]. Asparagine residues further help to define a parallel unstaggered conformation of the dimer by forming an interhelical hydrogen bond between opposing asparagines in position *a* [107]. The specificity in interhelical orientation and register conferred by asparagine comes, however, at the expense of leucine zipper stability [109,130]. Amino acids at all other positions are generally polar or charged. Especially residues in the *e* and *g* positions contribute further to leucine zipper dimerisation specificity and stability. In particular, avoidance of repulsive *e-g* electrostatic interactions is an important factor in leucine zipper stability [117,136]. Based on these criteria a detailed discussion of the Par-4 CC and LZ domains will be given below.

4.1.1. Materials and Methods

Potential coiled coil regions in Par-4 were predicted using the program COILS [238]. A homology model of the C-terminal 41 residues of Par-4 (Met 291-Arg 332) was created with Swiss Model [239], using the GCN4 leucine zipper (PDB-code: 2zta) [107] as the template. Pymol (DeLano Scientific LLC) was used for visualisation and generation of the electrostatic surface.

4.1.2. Results and Discussion

It was shown earlier (Chapter 1.2.1.) that the C-terminal residues 254-332 of Par-4 are highly conserved within mammals (Fig. 1.1) suggesting functional significance for these amino acids. The program COILS predicts a high probability of coiled coil formation for this domain (Fig. 4.1A) and hence this domain has been termed the coiled coil domain (CC) of Par-4. The C-terminal 79 residues of Par-4 are shown in a helical wheel representation in Figure 4.1B. Residues 292-330 fulfil the criteria for a leucine zipper with 5 out of 6 *d* positions occupied by leucine residues (Fig. 4.1B). For clarity the 6 heptad repeats of the Par-4 leucine zipper (LZ) domain (residues Ile 292-Arg 332) are displayed in bold, whereas all other residues of the CC domain are shown in grey. From a didactic point of view the isolated LZ domain will be discussed first and the discussion will then be extended to the full CC domain. As can be seen from Figure 4.1B, three out of six *a* positions of the LZ domain are occupied by β-branched hydrophobic residues (two isoleucines and one valine) and two positions are occupied by asparagine residues, Asn 313 and Asn 320. Each of these characteristics is consistent with the formation of a parallel dimer, hence the representation of the helical wheel in a parallel dimeric conformation (Fig.4.1B). The *e* and *g* positions of the LZ domain further show the possibility for a salt bridge between Glu 312 and Lys 317, and more importantly a repulsive electrostatic interaction between Asp 305 and Glu 310. This repulsive interaction has been proposed to prevent coiled coil formation of a 51-residue peptide comprising the C-terminal 47 residues of rat Par-4 under physiological conditions [184].

A homology model of the C-terminal 41 residues (Met 291-Arg 332) in a parallel dimeric conformation is shown in Figure 4.1C. As can be seen from this model, the repulsive electrostatic interaction between Asp 305 and Glu 310 is located near the centre of the dimer. It is therefore not surprising that coiled coil formation of the isolated Par-4 LZ is prevented under physiological conditions [184]. This repulsive interaction appears to be further enhanced by a patch of acidic residues surrounding Glu 310 (Figs. 4.1D and E). In addition to this destabilising

interhelical interaction, this LZ segment (Asp 308-Glu 314) exhibits only a low abundance of potential intrahelical salt bridges (Fig. 4.1E). Intrahelical salt bridges have been proposed to stabilise the helical conformation and thereby contribute, to some extent, to leucine zipper stability [240]. Figure 4.1E also shows the presence of four aspartate residues in this segment. Statistical analysis showed that due to its low helix-forming propensity [241], aspartate is less frequently found in salt bridges than glutamate [240]. The high local concentration of aspartate may therefore be another factor detrimental to Par-4 LZ stability.

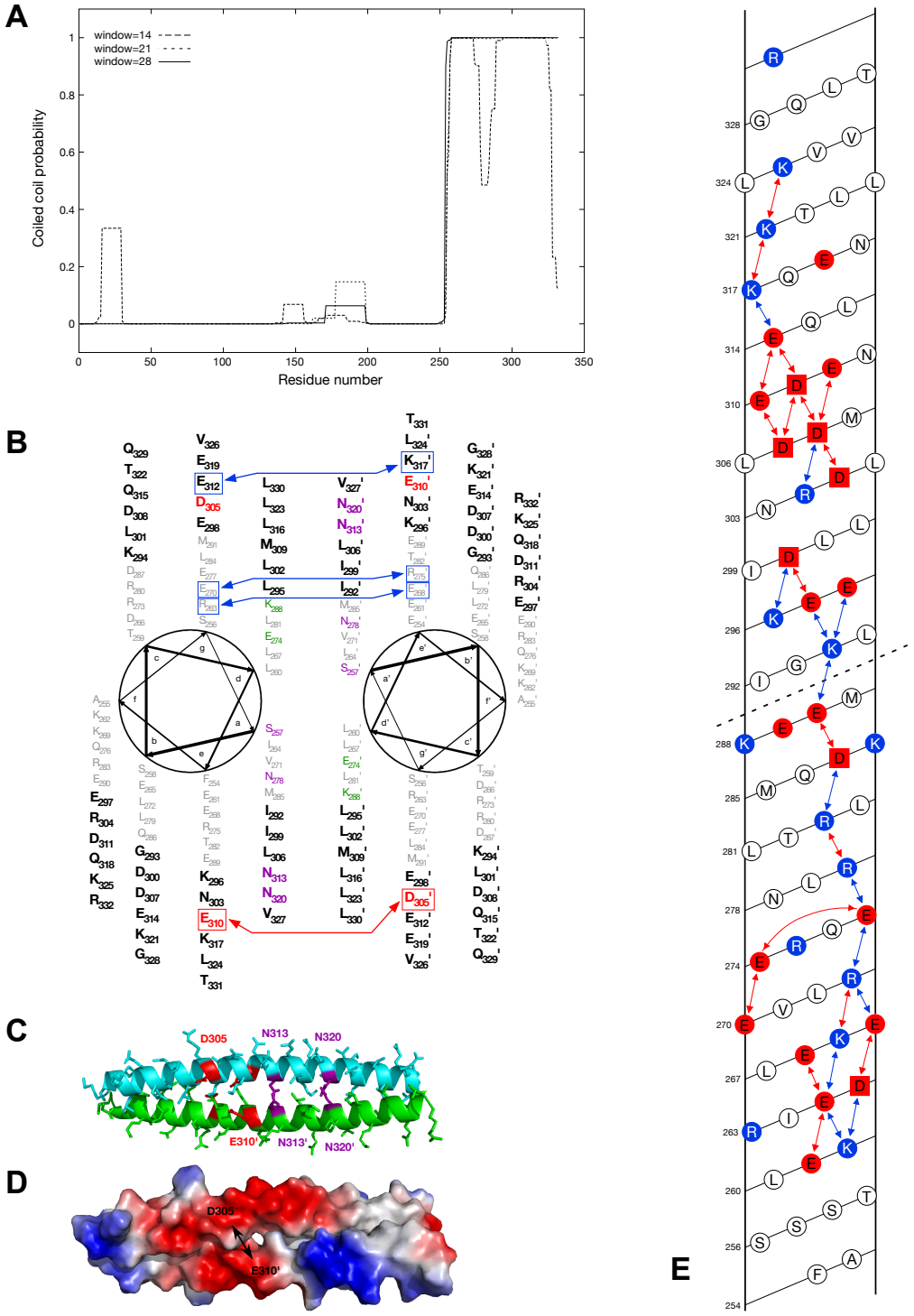

Figure 4.1

As mentioned above, asparagine residues at position *a* define the dimerisation specificity of a coiled coil at the expense of coiled coil stability. It could be shown that asparagine residues increase the dissociation rate of the coiled coil resulting in enhanced strand exchange [138,242]. Interestingly, unlike most other LZ-families (except for the Oasis family), the Par-4 LZ contains two asparagine residues at position *a* within its heptad repeats [117] (Figs. 4.1B and C). The influence of asparagine residues on coiled coil stability was shown to be position-dependent and coiled coils were found to be more stable with asparagine residues at the C-terminus relative to more N-terminally located asparagines [243]. Both Asn 313 and Asn 320 are located in the centre of the dimer (Fig. 4.1C) indicating that both residues may be critical for Par-4 LZ stability.

Figure 4.1 *− Coiled coil formation and stability - sequence analysis of Par-4. (A) Full-length Par-4 (residues 1-332) was analysed using the program COILS [238]. The probability for coiled coil formation for three window sizes is displayed on the y-axis, with increasing values indicating an increased likelihood for coiled coil formation. (B) Helical wheel representation of the Par-4 CC domain (residues Phe 254-Arg 332). Positions in the heptad repeat are denoted by abcdefg. Residues that are part of the LZ domain are shown in black bold letters. All other letters of the CC domain are shown in grey. Polar residues at position a of the heptad repeats are shown in purple (Ser 257, Asn 278, Asn 313 and Asn 320), charged residues at position d of the heptad are shown in green (Glu 274 and Lys 288). The acidic residues Asp 305 and Glu 310 at position e and g are shown in bold red, with the potential repulsive electrostatic interactions between these two residues indicated by a red double arrow. For clarity only one of the two possible interactions within the dimer is shown in the lower half of the model. Possible salt bridges between residues in e and g position are indicated by blue double arrows (upper half). Primes (') are used to distinguish between the two molecules of the dimer. (C) Homology model of the Par-4 LZ domain (residues Met 291-Arg 332) as a parallel dimer based on the GCN4 structure [107]. Proposed residues that may affect coiled coil stability are coloured and labelled as in part (B). (D) Electrostatic surface of the Par-4 LZ domain homology model showing negatively and positively charged surfaces in red and blue, respectively. The orientation is as in (C). The potential repulsive interaction between Asp 305 and Glu 310' is indicated by a black double arrow. (E) Helical net analysis of the Par-4 CC domain. The predicted coiled coil segment (residues Phe 254-Arg 332) was flattened into two dimensions by splitting the helix lengthwise. The display starts in the lower left corner with Phe 254. The first full helical turn is initiated by Ser 256 and completed with Thr 259. Thus the second full turn is initiated by Lys 260 and so on till Arg 322. The split bisects four residues (Glu 270, Lys 283, Leu 306 and Leu 324) such that each of these residues is displayed in duplicate. Potential complementary and repulsive electrostatic interactions (i to i + 3 or i to i + 4) within the helix are indicated by blue and red double arrows. Positively charged residues (Arg, Lys) are shown as blue circles, whereas negatively charged glutamate and aspartate residues are shown as red circles or squares, respectively. The dashed line indicates the start of the LZ domain. Figure D is adapted from Landschulz et. al. [125].*

Expanding the sequence analysis to the full Par-4 CC domain reveals further interesting features. In addition to the 6 heptad repeats predicted for the LZ domain 5 more repeats are likely to form (Fig. 4.1B). Increasing the chain length was demonstrated to increase coiled coil stability [224], and it appears that this is sufficient to overcome some of the destabilising factors noted in the Par-4 LZ domain (Chapter 3.6.). However, a closer analysis of residues in position *d* of the additional heptads shows the presence of three leucine residues and more importantly two charged residues (Glu 274 and Lys 288). As residues in *d* position are part of the oligomeric interface and determine coiled coil stability, these residues have generally long hydrophobic sidechains such as leucine[127]. Charged residues in this position are rare [240] and detrimental for coiled coil stability [117]. However, both Glu 274 and Lys 288 are flanked N-terminally (Arg 273, Asp 287) and C-terminally (Arg 275, Glu 289) by oppositely charged residues (Figs. 4.1B and E). It is possible that these residues mitigate some of charge introduced by Glu 274 and Lys 288. In position *a* of the heptad repeats of the CC domain three additional hydrophobic residues are observed. Especially the β-branched residues Ile 264 and Val 271 are a further indication for a parallel dimeric conformation of the Par-4 CC domain. This is further strengthened by another asparagine (Asn 278) residue in position *a* (Fig. 4.1B). The involvement of the *a* position polar residue Ser 257 in CC formation is questionable as this residue and all other residues N-terminal to Ser 257 are predicted with a low coiled coil forming probability (Fig. 4.1A). Occurrence of polar residues, such as serine or threonine, at *a* position has been proposed as a characteristic feature for heterodimerisation. Hence Ser 257 may be necessary for hetero-oligomerisation of Par-4 with effector proteins, which however remains to be determined.

Analysis of potential interhelical electrostatic interactions in the Par-4 CC domain between residues in *e* and *g* positions exhibits two additional complementary interactions but no further repulsive interactions (Fig. 4.1B). The salt bridges between Arg 263 and Glu 268’ (the prime indicating the second molecule of the proposed dimer) and between Glu 270 and Arg 275’ may have a stabilising effect on the CC domain. A recent study showed that parallel coiled coils rely more on intrahelical salt bridges than interhelical for stability [240]. The potential complementary and repulsive electrostatic interactions within the Par-4 CC domain are listed in Table 4.1 and are displayed in Figure 4.1E. Statistical analysis showed that not all potential salt bridges between residues in *i* to *i + 3* or *i* to *i + 4* position occur (e.g. 3RD, 3RE or 4DK). Such interactions are therefore omitted in this analysis. 3RD for example denotes a potential interaction between arginine at position *i* and aspartate at position *i + 3*. In contrast, other interactions are found more frequently (e.g. 3ER, 4ER or 4RE) and were thus proposed to be

important for coiled coil stability [240]. Salt bridges between neighbouring residues (*i* to *i + 1*) probably do not increase coiled coil stability [240] (and are therefore not listed in Table 4.1). As *i* to *i + 1* interactions of unlike charge are more common than of like charge [240], this may indicate that prevention of repulsive interactions may be critical for coiled coil stability. The same study proposed that formation of a salt bridge network is more stabilising than isolated interactions [240]. An almost uninterrupted network is evident for the N-terminus of the CC domain (Fig. 4.1E), which may stabilise this region. Conversely, this network is interrupted in the LZ domain between residues Asp 308-Glu 314 suggesting destabilisation of the coiled coil in this segment (see above). It is further evident from Figure 4.1E that some of the repulsive intrahelical electrostatic interactions may be mitigated by neighbouring residues of unlike charge.

Attractive *i* to *i + 3* interaction	**Attractive *i* to *i + 4* interaction**	**Repulsive *i* to *i + 1* interaction**	**Repulsive *i* to *i + 3* interaction**	**Repulsive *i* to *i + 4* interaction**
Lys 262 − Glu 265	Lys 262 − Glu 266			Glu 261 − Glu 265
	Glu 265 − Lys 269	Glu 265 − Asp 266	Glu 265 − Glu 268	Asp 266 − Glu 270
				Lys 269 − Arg 273
Glu 270 − Arg 273				Glu 270 − Glu 274
	Arg 273 − Glu 277		Glu 274 − Glu 277	
Glu 277 − Arg 280			Arg 280 − Arg 283	
	Arg 283 − Asp 287		Asp 287 − Glu 290	
	Glu 290 − Lys 294	Glu 289 − Glu 290		
Lys 294 − Glu 297	Lys 294 − Glu 298	Glu 297 − Glu 298	Glu 297 − Asp 300	
	Lys 296 − Asp 300			
	Arg 304 − Asp 308	Asp 307 − Asp 308	Asp 305 − Asp 308	
			Asp 307 − Glu 310	Asp 307 − Asp 311
		Glu 310 − Asp 311	Asp 308 − Asp 311	Asp 308 − Glu 312
		Asp 311 − Glu 312	Asp 311 − Glu 314	Glu 310 − Glu 314
Glu 314 − Lys 317				Lys 318 − Lys 321
				Lys 321 − Lys 325

Table 4.1 *− Potential electrostatic interactions within the Par-4 CC domain. Only those possible salt bridges (i to i + 3 and i to i + 4) are listed that were shown to occur with statistical significant frequency [240]. Additionally, repulsive electrostatic interactions (i to i + 1, i to i + 3 and i to i + 4) are shown. A graphical display of these interactions is given in Figure 4.1E. The dashed line indicates the start of the LZ domain.*

Taken together, sequence analysis strongly suggests the presence of a coiled coil at the Par-4 C-terminus. Furthermore, a parallel dimeric conformation is suggested. In addition to various potentially stabilising factors, the Par-4 CC domain contains residues that may be detrimental for coiled coil stability. Consistent with these findings, the isolated LZ domain was shown to be unfolded under physiological conditions [184]. Interestingly, data suggest that full-length Par-4 forms a coiled coil under physiological conditions (Chapter 3.6. and Ref. [46]). Possible reasons for the different coiled coil-forming properties of Par-4 constructs will be discussed in the following chapters.

4.2. Coiled coil formation of the Par-4 LZ domain - Assessing the oligomeric state

The coiled coil-forming potential of the Par-4 LZ domain (residues 292-330) is analysed using the Par-4(286-332) constructs. As was discussed above, this Par-4 domain contains a potential repulsive interhelical electrostatic interaction between residues Asp 305 and Glu 310'. This interaction was proposed to prevent coiled coil formation of the Par-4(286-332)WT construct under physiological conditions. Decreasing the pH allowed coiled coil formation at low temperature presumably due to partial protonation of Asp 305 and/or Glu 310 sidechains [184]. Based on an isodichroic point near 203 nm [134,136] a two-sate transition between a largely disordered and an α-helical state was proposed [184]. Concentration dependence studies and $[\theta]_{222}/[\theta]_{208}$ ratios near 1.1 indicated the formation of an intermolecular coiled coil. Mutation of either Asp 305 or Glu 310 to lysine (constructs called in this document Par-4 (286-332)D305K or Par-4(286-332)E310K) abolished the pH-dependence of the constructs and increased the thermal stability of the coiled coil [185]. The D305K mutant was found to be somewhat more thermally stable than the E310K mutant, possibly due to the introduction of an additional methylene group that becomes involved in van der Waals interactions with the hydrophobic core [185].

4.2.1. Materials and Methods

a) Combined sample preparation for CD and DLS

rrPar-4LZ, rrPar-4LZD305K and rrPar-4LZE310K were expressed and purified as described in Chapters 2.11.3, 2.11.6. and 2.11.7. Samples of rrPar-4LZ were prepared at four different pH values by diluting the H_2O-dissolved rrPar-4LZ with the appropriate sample buffer (Table 4.2). For samples with pH values below or equal to pH 6.0 the solubility of rrPar-4LZ is reduced and

precipitation occurred. The precipitate was removed by centrifugation in a tabletop centrifuge and the protein concentration was remeasured. In contrast, the H_2O-dissolved rrPar-4LZ stock solution was acidic but stable. No precipitation occurred when it is further diluted with H_2O. The pH of this sample was assessed with pH paper to avoid contamination and found to be approximately 4. The point mutants rrPar-4LZD305K and rrPar-4LZE310K were prepared at pH 7.0 in the same way as rrPar-4LZ. Four additional samples of both mutants were prepared in the presence of increasing concentrations of urea (Table 4.2). The same samples were used for CD spectropolarimetry and DLS.

	Par-4 LZ peptide concentration	**Buffer composition**
a)	75 µM rrPar-4LZ	20 mM NaCl, 10 mM Tris, pH 7.0
b)	75 µM rrPar-4LZ	20 mM NaCl, 10 mM Mes, pH 6.5
c)	40 µM rrPar-4LZ	20 mM NaCl, 10 mM Mes, pH 6.0
d)	50 µM rrPar-4LZ	H_2O, pH 4
e)	75 µM rrPar-4LZD305K	20 mM NaCl, 10 mM Tris, pH 7.0
f)	75 µM rrPar-4LZE310K	20 mM NaCl, 10 mM Tris, pH 7.0
g)	75 µM rrPar-4LZD305K	20 mM NaCl, 10 mM Tris, pH 7.0 + 1M urea
h)	75 µM rrPar-4LZE310K	20 mM NaCl, 10 mM Tris, pH 7.0 + 1M urea
i)	75 µM rrPar-4LZD305K	20 mM NaCl, 10 mM Tris, pH 7.0 + 6M urea
j)	75 µM rrPar-4LZE310K	20 mM NaCl, 10 mM Tris, pH 7.0 + 6M urea

Table 4.2 *− Sample conditions of Par-4 LZ peptide used for CD spectropolarimetry and DLS*

b) Circular Dichroism

CD spectropolarimetry was used to assess the proportion of stable secondary structure and the thermal stability of rrPar-4LZ, rrPar-4LZD305K and rrPar-4LZE310K. Spectra were recorded as described in (Chapter 3.4.1.a) in 1 nm steps from 260 to 190 nm. Acquisition parameters are given in Appendix F. Spectral deconvolution was performed using the Selcon3 [218] algorithm through the DICHROWEB server interface

c) Dynamic Light Scattering

The apparent Stokes radii (R_S) of rrPar-4LZ, rrPar-4LZD305K and rrPar-4LZE310K were measured as described in Chapter 3.2.1.a. R_S values obtained from measurements in urea were

corrected using the Dispersion Technology Software 5.1 (Malvern Instruments, Malvern, United Kingdom) to account for the increased solvent viscosity and the increased refractive index.

d) Size Exclusion Chromatography

SEC was performed at 4 ºC using a Superdex 75 SEC column connected to the BioLogic DuoFlow System with a flow rate of 0.4 ml/min. Calibration curves to convert retention times to *MWs* were established using the commercially available Gel Filtration Calibration Kit (6.5-75 kDa) from GE-Healthcare and results are shown in Appendix E. The running buffer contained 50 mM NaCl, 20 mM Na_2HPO_4/NaH_2PO_4, at pH 7.0 or pH 6.0. Sample concentrations were (i) 75 µM rrPar-4LZ in 20 mM NaCl, 10 mM Tris, pH 7.0; (ii) 40 µM rrPar-4LZ in 20 mM NaCl, 10 mM Mes, pH 6.0; and (iii) 75 µM rrPar-4LZD305K in 20 mM NaCl, 10 mM Tris, pH 7.0. All samples were filtered using an Ultrafree-MC Centrifugal Filter device (pore size 0.22 µm) prior to application to the SEC column.

e) Size Exclusion Chromatography - Multi Angle Laser Light Scattering (SEC-MALLS)

SEC-MALLS analysis was performed by Dr. David Gell (School of Molecular and Microbial Biosciences, University of Sydney, Australia). Samples were prepared by dissolving the lyophilised rrPar-4LZ and rrPar-4LZD305K in 20 mM NaCl, 10 mM Tris, pH 7.0 to a final peptide concentration of 0.33 mM (2 mg/ml). Each sample was passed over a 0.45 µM pore filter prior to loading 200 µg of peptide onto a Superdex 75 gel filtration column, running at ambient temperature (~22 ºC) with a flow rate of 0.6 ml/min. The SEC buffer contained 50 mM NaCl, 20 mM Na_2HPO4/NaH_2PO4, pH 7.0.

The eluate from the column was subject to in-line laser-light scattering and refractive index measurements. Light scattering intensity was measured with a mini-DAWN (Wyatt Technology Corp., Santa Barbara, USA) equipped with a 690 nm laser at three independent angles (41.5º, 90.0º and 138.5º). Voltages for the three detectors were normalised using BSA monomer as a standard isotropic scatterer. Absolute scattering intensity was calibrated against a standard sample of HPLC grade toluene. Protein concentrations were obtained from in-line refractive index measurements (Optilab differential refractometer, Wyatt), calibrated against standard salt solutions and a refractive index increment, with respect to mass concentration (*dn/dc*), of 0.19 ml g^{-1} for protein. A weight-average molecular weight (*MW*) was calculated every 5 µl across each eluting peak (data “slice”) according to the Rayleigh-Debye-Gans scattering model

for a dilute polymer solution, as implemented by the ASTRA software [244]. Molecular weights reported for each sample are a weight average calculated over the peak 0.2 ml fraction.

f) Crosslinking

For crosslinking reactions, 4.5 µl Par-4 LZ peptide were incubated with 0.5 µl 400 mM EDC (1-ethyl-3-(3-dimethylaminopropyl)carbodiimide) for 1 h on ice. The reaction was quenched with 0.3 µl 3 M NaAc, pH 5.2. Control reactions were performed without EDC. The crosslinked Par-4 LZ peptides were analysed by 10% Tricine-PAGE. Sample conditions for rrPar-4LZ at pH 7.0, rrPar-4LZ at pH 6.0 and rrPar-4LZD305K at pH 7.0 were identical to the SEC study described above.

4.2.2. Results and Discussion

a) CD spectropolarimetry

Expression of Par-4(286-332)WT as a GST-fusion (= rrPar-4LZ) (Chapter 2.11.3.) produced higher yields in a shorter time relative to HMBP-fusions (Chapter 2.11.1.). Using the pGex-6P-3 vector for expression introduced an additional leucine residue at the N-terminus of rrPar-4LZ that Par-4(286-332)WT expressed as a HMBP-fusion lacks. The HMBP-fusion construct was used in an earlier study demonstrating an increase in coiled coil formation of the Par-4 LZ domain with decreasing pH [184]. For this document, CD spectropolarimetry was repeated for consistency with DLS and NMR spectroscopy results. The pH dependence of coiled coil formation for rrPar-4LZ was found to be virtually identical to the aforementioned results of Dutta *et. al.* [184].

The CD spectra of rrPar-4LZ at four different pH values are shown in Figure 4.2 and indicate an increase in α-helicity with decreasing pH. Consistent with the previous study, rrPar-4LZ is mostly disordered between pH 7.0 and 6.5 (Figs. 4.2A and B). Contrary to previous results [184], using similar peptide concentrations (~40 µM) the α-helical content of rrPar-4LZ at pH 6.0 and 5 ºC is decreased from 75% to 56%. Also in contrast with the earlier study, a $[\theta]_{222}/[\theta]_{208}$ ratio of 0.89 at 5 ºC is observed (Fig. 4.2C) suggesting the absence of stable supercoiling. Consistent with these results, the thermal stability is decreased relative to previous results with a reduction in the T_m value from 24 ºC to 18 ºC (Fig. 4.3A). These results together indicate that the additional leucine residue in the N-terminus of rrPar-4LZ may interfere with coiled coil formation at decreasing pH.

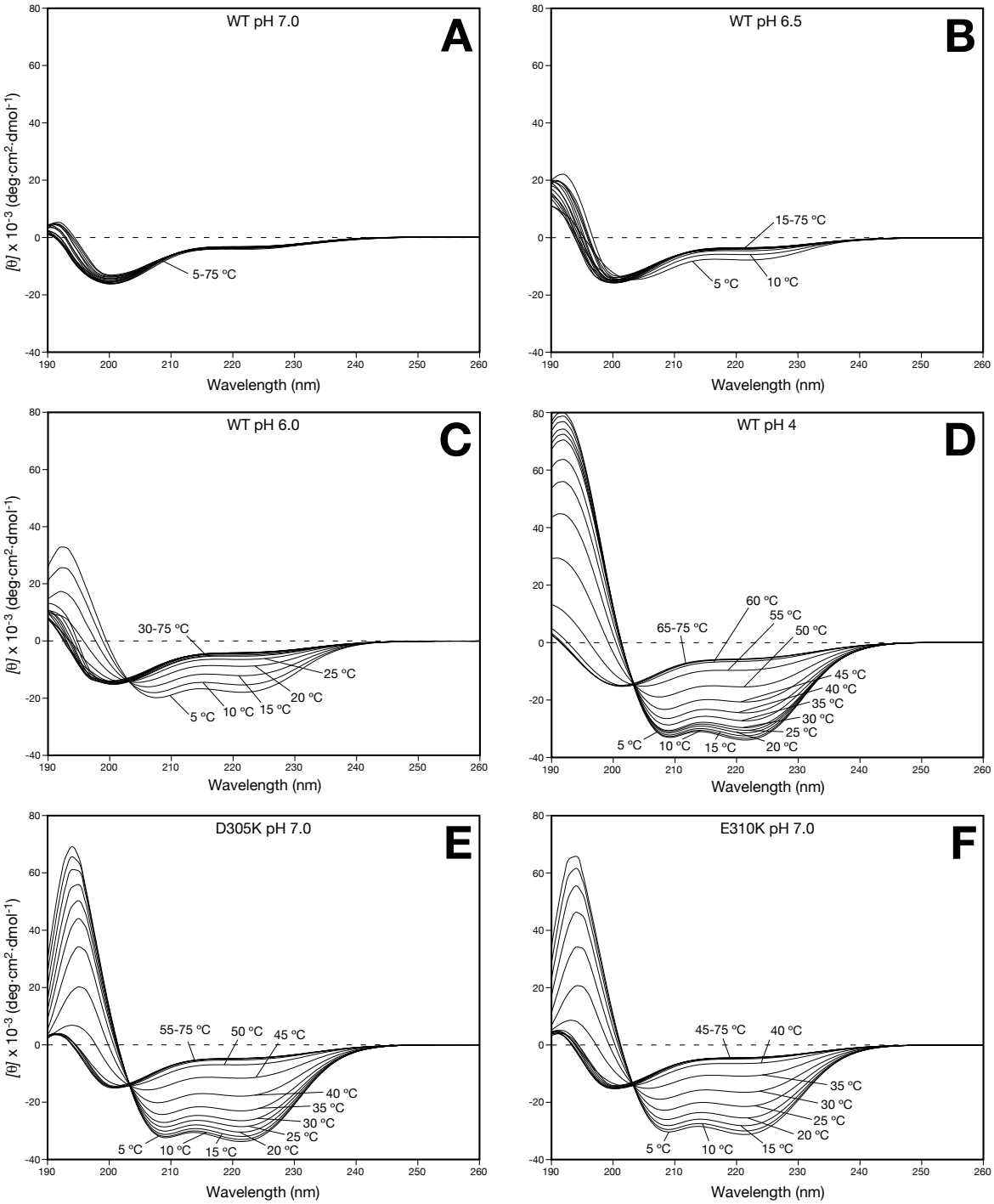

Figure 4.2 *− CD spectropolarimetry of Par-4 LZ peptides. Temperature dependence of the CD spectra of (A) rrPar-4LZ at pH 7.0 (B) rrPar-4LZ at pH 6.5 (C) rrPar-4LZ at pH 6.0 (D) rrPar-4LZ at pH 4 (E) rrPar-4LZD305K at pH 7.0 and (F) rrPar-4LZE310K at pH 7.0. Sample conditions are given in Table 4.2 and acquisition parameters are listed in Appendix F. The abbreviations WT, D305K and E310K denote rrPar-4LZ, rrPar-4LZD305K and rrPar-4LZE310K, respectively.*

This additional leucine residue also appears to have negatively influenced the solubility of rrPar-4LZ at low pH. No solubility limitations at pH 6.0 were reported previously [184]. Furthermore, CD spectra could be recorded down to pH values of 5.5. For rrPar-4LZ the

precipitation between pH 5.0 and 6.0 is almost quantitative and no reliable spectra could be recorded below pH 6.0. Conversely, around and below pH 4.0 the solubility of rrPar-4LZ improves. The theoretical pI of rrPar-4LZ is calculated as 4.5. However, it is likely that the pI is actually higher possibly due to the influence of coiled coil formation on the pKa values of acidic residues [135]. Hence, it is not surprising then that the solubility of rrPar-4LZ is reduced between pH 5.0 and 6.0. It is further possible that some of the observed differences to the previous study are an artefact resulting from the freeze-drying process. It has been reported previously that lyophilisation of proteins results in conformational changes, especially a reduction of the α-helical content, and promotion of aggregation [245]. However, the results for rrPar-4LZD305K and rrPar-4LZE310K were largely identical to previous results even though these peptides were freeze-dried. It should also be mentioned that despite the negative effects lyophilisation may have on the Par-4 LZ peptides, it proved to be a reliable method for obtaining stable peptides and consistent results.

Due to solubility limitations in the previous study, no CD spectra could be recorded below pH 5.5 [184]. A CD series of rrPar-4LZ at pH 4 is shown in Figure 4.2D. This series of rrPar-4LZ at pH 4 displays strong α-helical character and is indicative of a coiled coil with a $[\theta]_{222}/[\theta]_{208}$ ratio of 1.04. Noteworthy is the high thermal stability ($T_m \approx 50$ ºC) of rrPar-4LZ at pH 4 (Figs. 4.3A and B), which is higher than obtained previously for other Par-4(286-332) peptides [184,185]. This is consistent with the possible mitigation of repulsive electrostatic interactions due to partial protonation of acidic residues in the Par-4LZ domain (Chapter 4.1.2.). The high stability of rrPar-4LZ at pH 4 may be favoured as the sample is only dissolved in H_2O. It was previously shown that salt marginally disfavours helix formation at acidic pH [184]. Despite this increased thermal stability, stable supercoiling is only indicated until 25 ºC with $[\theta]_{222}/[\theta]_{208}$ ratios above one. The observed isodichroic point at 203 nm further suggests a two-state transition between coiled coil and unfolded states. The decreasing $[\theta]_{222}/[\theta]_{208}$ ratios may therefore suggest that the equilibrium between coiled coils and unfolded monomers shifts towards monomers with increasing temperatures.

CD spectropolarimetry results for the LZ point mutants rrPar-4LZD305K and rrPar-4LZE310K are virtually identical to previous results [185]. Consistent with their pH-independent folding, both mutants display coiled coil conformations at 5 ºC and neutral pH with $[\theta]_{222}/[\theta]_{208}$ ratios above one (Figs. 4.2E and F). As noticed previously [185], rrPar-4LZD305K ($T_m \approx 45$ ºC) is slightly more stable than rrPar-4LZE310K ($T_m \approx 35$ ºC) (Fig. 4.3B). Consistent with these results, a stable coiled coil with $[\theta]_{222}/[\theta]_{208}$ ratios above one is indicated until 25 ºC

for rrPar-4LZD305K and only until 15 ºC for rrPar-4LZE310K (Figs. 4.2E and F). Coiled coil formation at neutral pH is probably due to abrogation of the repulsive electrostatic interaction between Asp 305 and Glu 310' [185]. However, both mutants are less stable than rrPar-4LZ at pH 4 (Fig. 4.3B). This suggests that other electrostatic interactions such as the aspartate patch (Chapter 4.1.2.) are involved in the Par-4 LZ stability and that partial protonation of these amino acids results in slightly increased LZ stability. This is consistent with previous results, which show an increase in thermal stability of rrPar-4LZE310K with decreasing pH [185].

The thermal stability of both LZ point mutants was further analysed by CD spectro-polarimetry under denaturing conditions. It was repeatedly noticed for both peptides that they aggregate and precipitate at higher (> 300 μM) protein concentration (Chapter 2.12.1.). Urea was included in this study of rrPar-4LZD305K and rrPar-4LZE310K as it was shown to disrupt a polymeric state of rrPar-4FL, but still allow for self-association (Chapter 3.6.). The rationale was therefore to include 1 M urea to dissociate possible aggregates, but still be able to analyse a folded conformation. Urea concentrations of 6 M were used particularly with respect to DLS as a reference state for a mostly unfolded conformation of rrPar-4LZD305K and rrPar-4LZE310K.

Due to buffer absorption, the spectral width of the CD spectra is reduced from 190-260 nm in native buffer (20 mM NaCl, 10 mM Tris, pH 7.0) to 200-260 nm in native buffer + 1 M urea, and to 210-260 nm in native buffer + 6 M urea. Therefore, only the thermal stability as a change in $[\theta]_{222}$ is shown for rrPar-4LZD305K and rrPar-4LZE310K under these conditions (Figs. 4.3C and D). As was expected, under the strong denaturing conditions of 6 M urea both peptides are mostly unfolded (Figs. 4.3C and D). In contrast, in the presence of 1 M urea, CD spectropolarimetry results show that both LZ point mutants maintain an α-helical fold. However, the thermal stability of this helical conformation is reduced (Figs. 4.3C and D). Relative to native buffer without urea the T_m values decrease from 45 ºC to 35 ºC and from 35 ºC to 23 ºC for rrPar-4LZD305K and rrPar-4LZE310K. Note that no accurate information about the supercoiling status can be gained due to buffer absorption preventing collection of reliable CD data below 210 nm at urea concentrations above 1 M. Hence, the $[\theta]_{222}/[\theta]_{208}$ ratio cannot be determined accurately and no correlation between supercoiling and thermal stability can be made.

For rrPar-4LZD305K the destabilising effect of urea is less pronounced at low temperatures and thus similar $[\theta]_{222}$ values are obtained at 5 ºC in native buffer and native buffer + 1 M urea (Fig. 4.3C). The $[\theta]_{222}/[\theta]_{208}$ ratio above one at 5 ºC for rrPar-4LZD305K in native buffer + 1 M urea further suggests a supercoiled oligomeric state [141], indicating similar conformations under both conditions. Note that buffer absorption is decreased at lower temperature allowing the

collection of data down to ~207 nm, however, this value should be considered with caution. At 25 ºC the destabilising effect of 1 M urea is greater and a $[\theta]_{222}$ value is obtained that is more similar to the value obtained for rrPar-4LZE310K at 25 ºC in native buffer (Figs. 4.3C and D).

The rrPar-4LZE310K mutant was shown to be less stable than rrPar-4LZD305K [185]. Not surprisingly, the destabilising effect of 1 M urea is more pronounced for this mutant. At 5 ºC a partial α-helical character is observed that is significantly less helical than in native buffer. At 25 ºC rrPar-4LZE310K in 1 M urea is to a great extent unfolded (Fig. 4.3D). These results indicate that using both LZ point mutants and increasing concentrations of urea, coiled coil and α-helical states of different stabilities can be probed that are similar to the results of rrPar-4LZ at various pH values. However, no precipitation was observed for both LZ mutants under these conditions allowing measurements at higher peptide concentration.

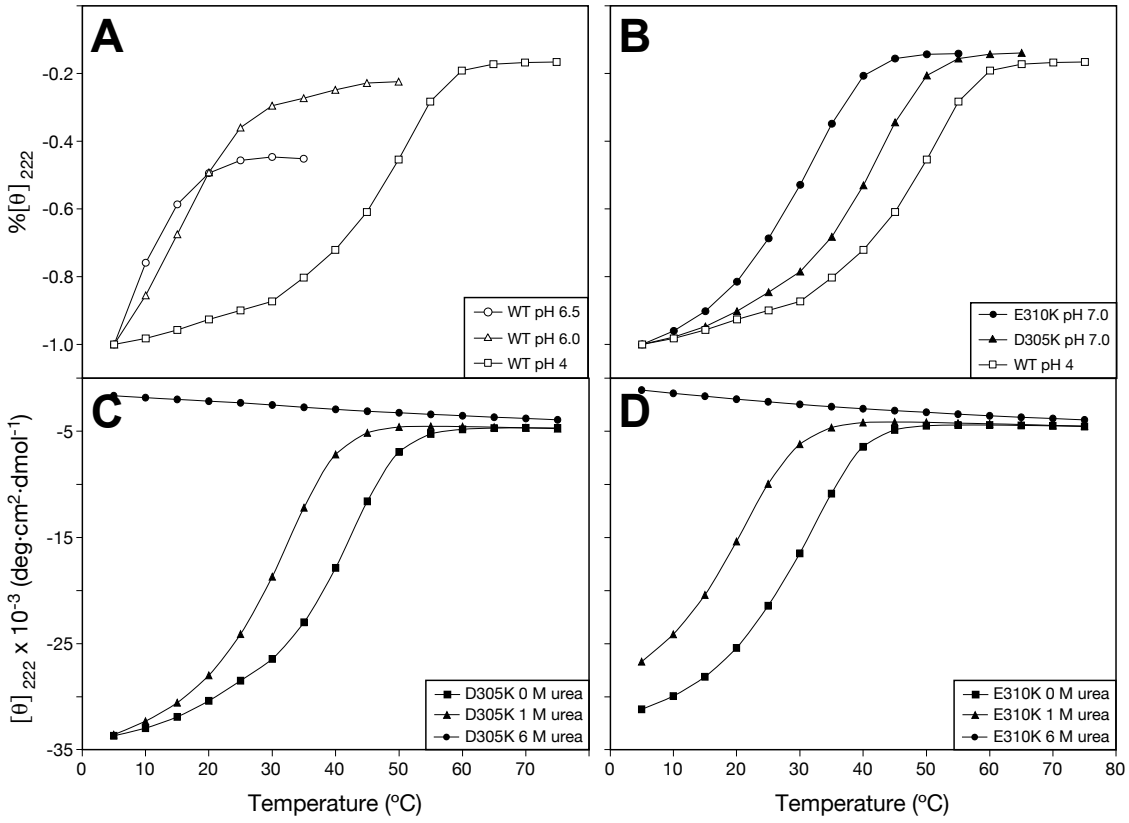

Figure 4.3 *− Thermal stability of Par-4 LZ peptides. (A) Melting curves of rrPar-4LZ at pH 6.5, 6.0 and 4, and of (B) rrPar-4LZ at pH 4, rrPar-4LZD305K at pH 7.0 and rrPar-4LZE310K at pH 7.0. The* $\%[\theta]_{222}$ *values are displayed as a function of temperature. The* $\%[\theta]_{222}$ *values were obtained by normalising the* $[\theta]_{222}$ *values at each temperature to the corresponding* $[\theta]_{222}$ *value at 5 ºC. Thermal stability of (C) rrPar-4LZD305K at pH 7.0 and (D) rrPar-4LZE310K at pH 7.0 under native conditions (0 M urea) and increasing denaturing conditions of 1 M and 6 M urea. The loss in α-helicity by thermal denaturation from 5-75 ºC was monitored as a change in* $[\theta]_{222}$*. Sample conditions are given in Table 4.2 and acquisition parameters are listed in Appendix F. The abbreviations WT, D305K and E310K denote rrPar-4LZ, rrPar-4LZD305K and rrPar-4LZE310K, respectively.*

It is interesting to note here that both LZ point mutants are less stable than previously described leucine zippers. For comparison, two leucine zippers of similar length, GCN4p1 [109] and rJun [246], have T_m values of 53 ºC (pH 7.0, 10 µM peptide concentration) and 52 ºC (pH 3.6, 15 µM peptide concentration), respectively. In contrast, the LZ point mutants rrPar-4LZD305K and rrPar-4LZE310K have T_m values of 45 ºC and 35 ºC (Fig. 4.3B), which are still below the 53 ºC and 52 ºC observed for GCN4p1 and rJun. Unlike GCN4p1 and rJun, which contain only one asparagine residue at position *a*, the LZ point mutants contain two asparagine residues at position *a*. As discussed in Chapter 4.1.2, this suggest that the two asparagine residues within the Par-4 LZ domain are detrimental for coiled coil stability resulting in less thermal stability compared to well-characterised leucine zipper model systems. To summarise this sub-section, using a new protein purification protocol did not significantly affect the CD spectroscopic properties of the Par-4 LZ peptides and results are comparable to previous studies [184,185]. Consistent with these studies the isolated wild-type Par-4 LZ domain (rrPar-4LZ) displays a highly pH and temperature dependent coiled coil formation. This pH dependence is mainly caused by repulsive electrostatic interactions between Asp 305 and Glu 310 residues, but other charged residues appear to contribute as well.

b) SEC and MALLS

Even though SEC was of limited use as a purification method for the Par-4 LZ peptides (Chapter 2.11.1.), the information gained about the hydrodynamic properties of the Par-4 constructs is, in most cases, comparable to DLS results (see below). The greatest hydrodynamic size at 4 ºC is obtained for rrPar-4LZD305K at pH 7.0, an intermediate size for rrPar-4LZ at pH 6.0 and the smallest size for rrPar-4LZ at pH 7.0 (Fig. 4.4A). The results obtained for rrPar-4LZE310K are virtually identical to rrPar-4LZD305K (data not shown). For comparison, volume distributions for these three peptides obtained by DLS are shown in Figure 4.4B, and will be discussed in more detail further below. Conversion of the retention times to *MWs* yields 28 kDa, 23 kDa and 21 kDa for rrPar-4LZD305K at pH 7.0, rrPar-4LZ at pH 6.0 and rrPar-4LZ at pH 7.0, respectively. MALLS results, obtained under similar conditions but higher temperature, suggest *MWs* of 11.5 and 5.8 kDa for rrPar-4LZD305K and rrPar-4LZ, both at pH 7.0 (Fig. 4.4C).

A retention time corresponding to an apparent *MW* of ~21 kDa is very large for the 6.0 kDa peptide rrPar-4LZ (Fig. 4.4A). This suggests that the high apparent *MW* is due to non-globular shapes or oligomerisation. However, a *MW* of 5.8 kDa is determined by MALLS for rrPar-4LZ

at pH 7.0 and 22 ºC (Fig. 4.4C). This is consistent with a monomeric conformation and thus indicates that the high apparent *MW* is due to non-globular shapes. CD spectropolarimetry indicates that rrPar-4LZ at pH 7.0 is disordered between 5 and 25 ºC (Fig. 4.2A). The similar CD results at 5 and 25 ºC therefore allow the comparison of the SEC results obtained at 4 and 22 ºC. Using the theoretical R_S values given in Table 4.3 for a 6 kDa protein in either a spherical (14.0 Å) or random coil state (20.5 Å), a three times increased hydrodynamic volume is expected for the random coil conformation relative to the globular conformation. Thus the SEC results are consistent with a monomeric, disordered coil-like conformation for rrPar-4LZ at pH 7.0 (DOM = disordered monomer). The hydrodynamic volume is calculated by $V_S = {}^4/_3\pi R_S^3$ [145].

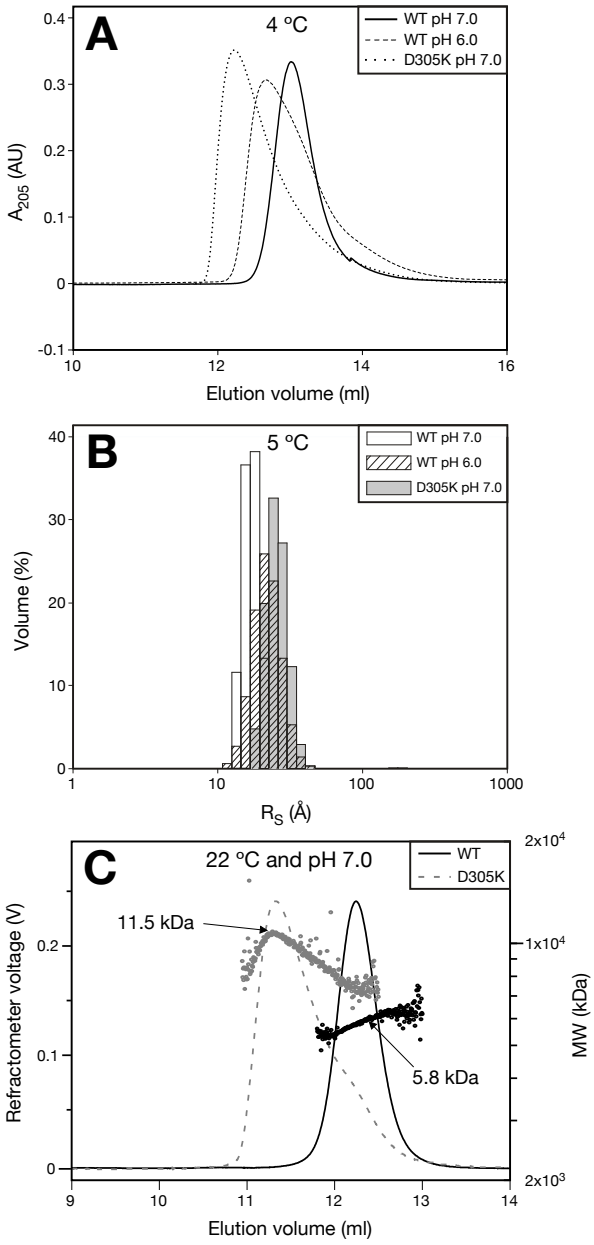

Figure 4.4 *– SEC and DLS of Par-4 LZ peptides. (A) The Par-4 LZ peptides elute from the SEC column in the order rrPar-4LZD305K at pH 7.0, rrPar-4LZ at pH 6.0 and rrPar-4LZ at pH 7.0. The estimated sizes correspond to spherical proteins with MWs of 28 kDa, 23 kDa and 21 kDa, respectively. The rrPar-4LZE310K peptide at pH 7.0 runs virtually identical to rrPar-4LZD305K (data not shown). Data have been normalised to present similar peak heights. (B) DLS results for the same three samples as in panel (A). Results are consistent with SEC results. (C) SEC-MALLS results of Par-4 LZ peptides at pH 7.0 and ambient temperature. Solid and dashed traces are the elution profiles of rrPar-4LZ and rrPar-4LZD305K recorded with the refractive index detector (left scale). Circles show the MW profile (right scale). To match data from the two detectors the elution volumes of the refractive index detector were subtracted by 0.14 ml to omit the dead volumes. Data have been normalised to present similar peak heights.*

For both mutants rrPar-4LZD305K and rrPar-4LZE310K, the *MWs* estimated by SEC are also high with ~28 kDa (Fig. 4.4A). MALLS results indicate a *MW* of 11.5 kDa for rrPar-4LZD305K at 22 ºC (Fig. 4.4C). This suggests a dimeric state for rrPar-4LZD305K, which is consistent with CD results indicating a coiled coil

conformation under these conditions (Fig. 4.2E). As similar CD spectra are obtained for rrPar-4LZD305K at 5 and 25 ºC, comparison of the SEC results obtained at 4 and 22 ºC is allowed. The high apparent *MWs* obtained for both LZ point mutants are not unusual, as the elongated rod-like shape of coiled coils is known to produce larger apparent *MWs* by SEC than are expected from the amino acid sequence [247]. As was discussed above, the coiled coil conformation of both LZ point mutants is less stable relative to other well-characterised leucine zippers [109,246]. Together with other experiments that will be presented below, this suggests that both LZ point mutants obtain an ordered dimeric conformation (with typical characteristics of a coiled coil), which, however, displays a certain degree of flexibility. The dimeric conformation of both rrPar-4LZD305K and rrPar-4LZE310K will be described from here on as a predominantly ordered dimer (POD).

Interestingly, a peak with intermediate retention time relative to rrPar-4LZ and rrPar-4LZD305K, both peptides at pH 7.0, is obtained for rrPar-4LZ at pH to 6.0 (Fig. 4.4A). These results suggest that under the SEC conditions disordered monomeric and ordered dimeric conformations are in fast interconversion. This is consistent with CD results at pH 6.0 and 5 ºC indicating 56% α-helicity (Fig. 4.2C). It was mentioned in Chapter 1.4. that the existence of isolated α-helices in solution is unlikely. Together with the SEC results, the moderate α-helical content may therefore indicate an interconversion between DOMs and PODs under these conditions. The isodichroic point at 203 nm further suggests a two-state transition between these two states with no significantly populated intermediates.

		Calculated R_S				
Oligomeric state	***MW***	**S**	**MG**	**PMG**	**RC**	**U**
Monomer	6.0	14.0	16.2	18.7	20.5	20.9
Dimer	12.0	17.9	20.4	24.5	28.8	29.9
Trimer	18.0	20.7	23.3	28.7	35.2	37.0
Tetramer	24.0	22.9	25.7	32.1	40.6	43.0

Table 4.3 *− Hydrodynamic properties of various oligomers of a 6 kDa peptide. Theoretical values of Stoke's radii (R_S) calculated for various oligomeric and folding states of a 6 kDa peptide using the mean values from equations given in [181] for spherical (S), molten globule (MG), pre-molten globule (PMG), random coil (RC) and urea-denatured (U) states. The MW is given in kDa and the R_S in Å.*

Another interesting SEC result is the peak shape of the Par-4 LZ proteins. Whereas a fairly symmetric peak shape is observed for rrPar-4LZ at pH 7.0 (Fig. 4.4A, solid trace), tails are evident for the peaks of rrPar-4LZ at pH 6.0, rrPar-4LZD305K at pH 7.0 and rrPar-4LZE310K at pH 7.0 (Fig. 4.4A, results for rrPar-4LZE310K not shown). A symmetric peak shape suggests a single molecular species [247] that is in the case of rrPar-4LZ at pH 7.0 a mostly disordered conformation. A tail may indicate structural interconversion between various molecular species [211,212], which is consistent with the previous interpretation for rrPar-4LZ at pH 6.0. These results therefore suggest that also rrPar-4LZD305K and rrPar-4LZE310K interconvert between DOMs and PODs. However, the POD state represents the major population for both LZ point mutants. Interestingly, a shoulder is observed for rrPar-4LZD305K at 22 ºC (Fig. 4.4C), and the elution time of this shoulder corresponds well with the elution time of the DOM (rrPar-4LZ at pH 7.0). This may indicate that exchange between DOM and POD states is slow under the SEC conditions for rrPar-4LZD305K resulting in separate peaks for POD and DOM. Similarly, the downward curving plots of *MW* versus elution time observed for rrPar-4LZD305K (Fig. 4.4C) are characteristic of a complex dissociating in response to dilution. Conversely, for rrPar-4LZ at pH 6.0 POD and DOM states appear to be equally populated resulting in an intermediate elution time. The elution time for rrPar-4LZ at pH 6.0 may further suggest that interconversion between DOM and CCD states is fast under the conditions of the SEC. Additional SEC experiments with varying peptide concentrations may be necessary for rrPar-4LZ at pH 6.0 and both LZ point mutants at pH 7.0. The analysis of the concentration dependency of the elution time may allow a better understanding of the involved dynamic processes. To summarise this sub-section, SEC and MALLS results indicate that rrPar-4LZ at pH 7.0 is a DOM. Conversely, results for rrPar-4LZD305K at pH 7.0 are consistent with a POD conformation that is in slow exchange with a DOM conformation. For rrPar-4LZ at pH 6.0 a dynamic interconversion between DOM and POD states is suggested with an approximately equal population in both states.

c) Dynamic light scattering

DLS was used to determine the hydrodynamic properties of the Par-4 LZ peptides under the same buffer conditions and with the same peptide concentration as used for CD spectropolarimetry and NMR (Chapter 4.3.2.). It was also assumed that DLS might allow the determination of the oligomeric state of coiled coil LZ peptides. However, as will be discussed below DLS did not have the high enough resolution and in most cases only allowed the exclusion of aggregated species under the studied conditions.

The results of DLS experiments are summarised in Table 4.4. For comparative purposes, the equation $\log(R_S) = 0.357*\log(MW)-0.204$ [181] was used to convert the experimentally determined R_S values to *MWs*. For rrPar-4LZ the obtained R_S values at various pH and temperatures (hence disordered and coiled coil states) are all similar (15.6-20.9 Å) but not indicative of aggregates (Table 4.4). For example, the presence of high molecular weight species is estimated to be below 1% for rrPar-4LZ at pH 4 (Fig. 4.5C). Similarly, the R_S values for rrPar-4LZD305K and rrPar-4LZE310K also show only slight differences (24.2-28.1 Å) under native and denaturing conditions. Interestingly, the R_S values for rrPar-4LZD305K and rrPar-4LZE310K are larger compared to rrPar-4LZ but also not indicative of aggregation. These results indicate that a differentiation between folded coiled coil states (rrPar-4LZ at pH 4, rrPar-4LZD305K at pH 7.0) and unfolded states (rrPar-4LZ at pH 7.0, rrPar-4LZD305K at pH 7.0 + 6 M urea) by DLS is not possible (Table 4.4). However, the DLS results are consistent with SEC results (see above), as larger R_S values are obtained for the Par-4 LZ peptides than are expected from their amino acid sequence (Table 4.4). It was previously mentioned that this is a typical observation for disordered and coiled coil proteins [145,181,226,248].

DLS determination of the oligomeric state of the Par-4 LZ peptides in coiled coil conformations was not possible. For comparative purposes the theoretical R_S values of different oligomeric states of a 6 kDa monomer are estimated using mean values from equations given in Ref. [181] (Table 4.3). Oligomeric states are approximated by increasing molecular weights of 12 kDa (dimer), 18 kDa (trimer) and 24 kDa (tetramer). As can be seen from these calculations, the differences in R_S values of various oligomers in a folded spherical conformation are larger relative to the variation observed in the data for the Par-4 LZ peptides (Table 4.4). Differences in R_S values of potential coiled coil dimers, trimers or tetramers may be even smaller than for spherical proteins [249]. A folded coiled coil itself is a rod-like structure (Fig. 4.1C). Due to their rod-like structures, different types of oligomers (up to tetramers as suggested by simulations) are most likely of similar length but different width. It is likely that the length of the molecule as the longest axis is more critical for the observed R_S value than the width of the molecule. This seems likely as the 66-residue coiled coil domain of rinderpest virus Phosphoprotein P forms a homotetramer and was shown to have an R_S of approximately 28 Å [250]. A value that is close to the values observed for rrPar-4LZD305K and rrPar-4LZE310K (Table 4.4). Even though the exact oligomeric state cannot be determined by DLS, a dimeric conformation, as indicated by sequence analysis (Chapter 4.1.2.), is consistent with the current data. Interestingly, there is a slight difference in the R_S values between rrPar-4LZ at various pH values and the LZ point

mutants rrPar-4LZD305K and rrPar-4LZE310K at pH 7.0 and increasing concentrations of urea (Table 4.4). This difference is also observed by SEC (Fig. 4.4A), however, the cause for this difference has not been determined yet.

			5 ºC		25 ºC	
Construct	**pH**	**Urea**	***MW***	***R_S***	***MW***	***R_S***
rrPar-4 LZ peptides	N/A	N/A	6.0	14.0	6.0	14.0
rrPar-4LZ	7.0	0 M	12.4	18.1	12.4	18.1
	6.5	0 M	N/A	N/A	12.4	18.1
	6.0	0 M	18.7	20.9	12.4	18.1
	4	0 M	12.4	18.1	8.2	15.6
rrPar-4LZD305K	7.0	0 M	28.0	24.2	28.0	24.2
	7.0	1 M	N/A	N/A	42.6	28.1
	7.0	6 M	N/A	N/A	28.0	24.2
rrPar-4LZE310K	7.0	0 M	28.0	24.2	42.6	28.1
	7.0	1 M	N/A	N/A	28.0	24.2
	7.0	6 M	N/A	N/A	42.6	28.1

Table 4.4 *− DLS-determined hydrodynamic properties of Par-4 LZ peptides. MW (kDa) and R_S (Å) values were calculated using the equation $\log(R_S) = 0.357*\log(MW) - 0.204$ in reference to a spherical conformation [181]. The mode R_S values of each measurement are shown. For comparison, theoretical values of a spherical conformation calculated from the amino acid sequence of rrPar-4LZ are also provided. Sample conditions are given in Table 4.2.*

The volume distributions for the Par-4 LZ peptides are shown in Figure 4.5. Relative narrow volume distributions are observed for Par-4 LZ peptides in a mostly coiled coil conformation (e.g. rrPar-4LZ at pH 4, rrPar-4LZD305K at pH 7.0) consistent with a predominantly single conformation (Fig. 4.5C). Compared to these relative narrow distributions, samples with partial α-helical character (e.g. rrPar-4LZ at pH 6.0 and 5 ºC, rrPar-4LZD305K at pH 7.0 + 1 M urea, rrPar-4LZE310K at pH 7.0 and 25 ºC) display significantly broader distributions (Figs. 4.5A, B and D). As was proposed for the SEC results, this observation is consistent with interconverting conformations. The volume distributions observed under 6 M urea concentrations are narrower relative to distributions under 1 M urea concentrations (Figs. 4.5E and H), suggesting that exchange between folded and unfolded conformations is reduced as the peptides are mostly

unfolded. For rrPar-4LZD305K, the volume distribution under 6 M urea is further slightly broader than in the absence of urea (Fig. 4.5F) consistent with an increased flexibility in the urea denatured state relative to the POD conformation.

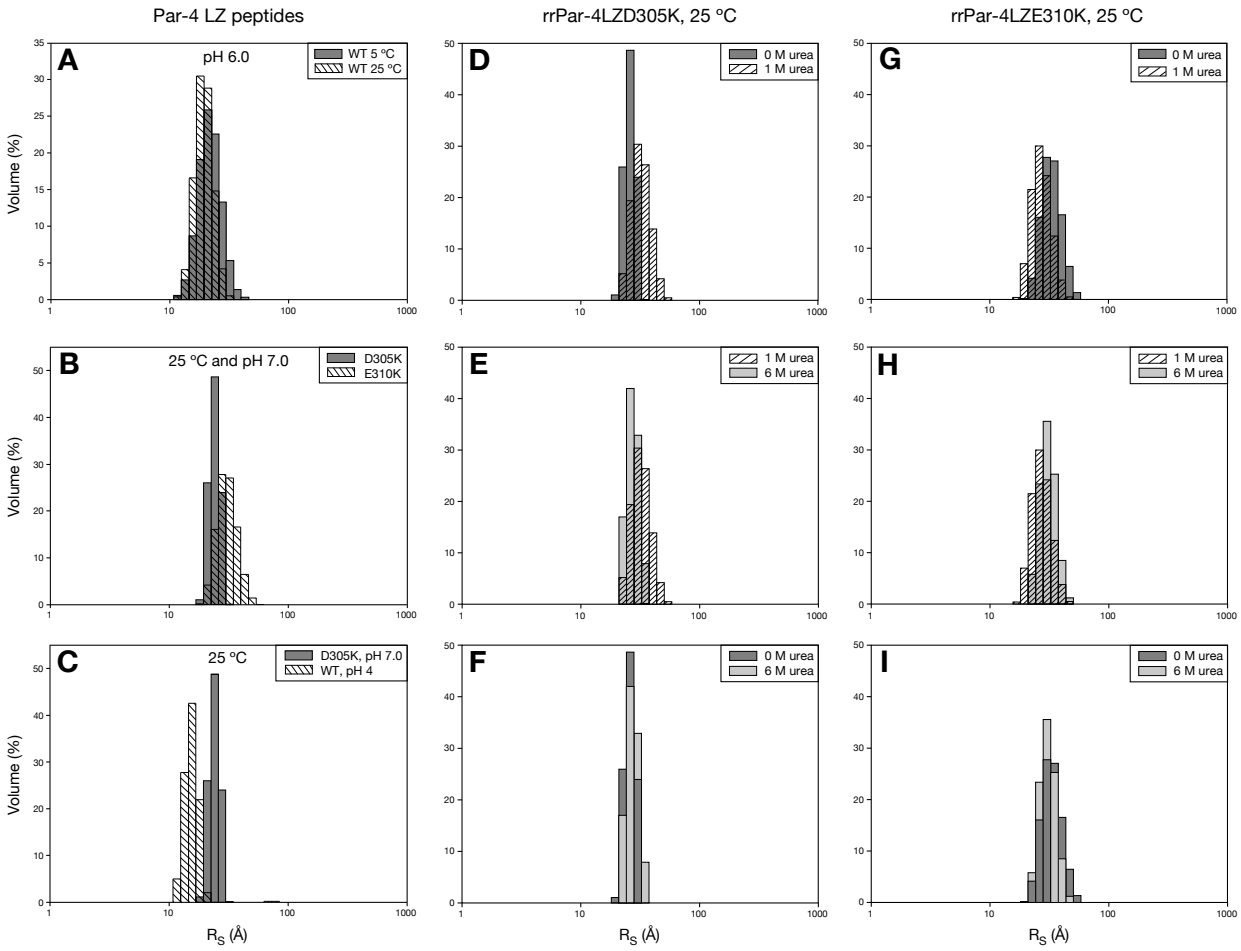

Figure 4.5 *− DLS of Par-4 LZ peptides. Volume distribution representation of DLS results showing the apparent hydrodynamic radius (R_S). (A) R_S of rrPar-4LZ at pH 6.0 for temperatures of 5 and 25 ºC. (B) R_S of rrPar-4LZD305K and rrPar-4LZE310K at 25 ºC and pH 7.0. (C) R_S at 25 ºC of rrPar-4LZ at pH 4 and rrPar-4LZD305K at pH 7.0. Volume distributions of rrPar-4LZD305K (D-F) and rrPar-4LZE310K (G-I) at pH 7.0 and 25 ºC under increasing concentrations of urea. Panels D and G compare results without urea with 1 M urea, panels E and H compare 1 M urea with 6 M urea, and panels F and I compare results without urea with 6 M urea. Results are summarised in Table 4.4. The abbreviations WT, D305K and E310K denote rrPar-4LZ, rrPar-4LZD305K and rrPar-4LZE310K, respectively.*

Even though an accurate control of the concentration of the Par-4 proteins during SEC was not possible due to dilution effects upon loading the samples on the SEC column, the SEC results are consistent with DLS measurements. It should be noted that the salt concentration is 2.5 fold increased for SEC relative to DLS to prevent non-specific interactions with the gel matrix. This suggests that SEC and DLS results do not change significantly within the analysed peptide and salt concentration range. It is possible that these results may hold true at higher protein and salt

concentrations, which have yet to be tested. To summarise this subsection, DLS results are consistent with disordered or coiled coil states of the Par-LZ peptides, and further with structural interconversion. Both of these observations are consistent with SEC results. Importantly, no significantly aggregated species were detected by DLS for the Par-4 LZ peptides.

d) Par-4 LZ Crosslinking

The crosslinker EDC is used to initiate the formation of amide bonds between free carboxylic and amino groups (Fig. 4.6). Assuming a parallel dimer as suggested by the amino acid sequence, the interhelical salt bridge between Glu 312 and Lys 317' (the prime indicating the second helical molecule) could be involved in amide bond formation, resulting in the covalent connection of two monomers. For the mutants rrPar-4LZD305K and rrPar-4LZE310K the interhelical salt bridges between Lys 305 and Glu 310' and between Asp 305 and Lys 312', respectively, may also be involved in crosslinking reactions.

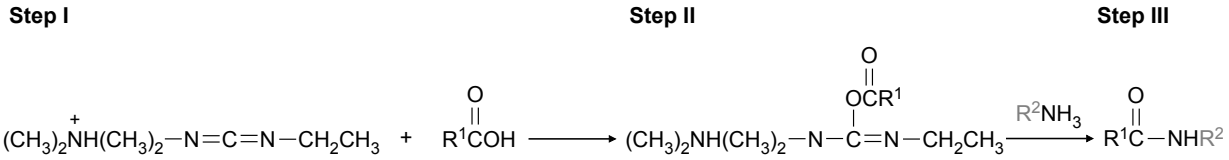

Figure 4.6 *– Crosslinking mechanism of EDC. EDC reacts with a carboxylic acid (Step I) to form an O-acylisourea intermediate (Step II). An amide bond is formed through the reaction of a primary amine with this O-acylisourea intermediate (Step III). For simplicity the leaving group of the former EDC is omitted in Step III.*

The results of Par-4 LZ crosslinking studies are shown in Figure 4.7. For each of the Par-4 LZ peptides, two predominant bands are seen. Molecular weight markers identify the most intense band as monomers (6 kDa), and the secondary band as a dimers (12 kDa). The appearance of the secondary band is consistent with the formation of a parallel dimeric conformation. Similar results are obtained for rrPar-4LZ at pH 4 and rrPar-4LZE310K at pH 7.0 (data not shown). It should be noted that other possibilities such as amide bond formation between the free amino and carboxylic groups at the N- and C-termini, respectively, cannot be excluded. However, control experiments with the spherical protein aprotinin (6.5 kDa) show that such crosslinking reactions do not occur efficiently (data not shown). For rrPar-4LZ at pH 6.0, faint additional bands above 21 kDa were detected, but are hardly visible in Figure 4.7B, that may result from non-specific crosslinking. Their relevance is currently unclear, but could be an indication of transient higher oligomer formation. Higher oligomer formation may be possible, as rrPar-4LZ

was shown to precipitate at pH values below 6.0. However, such transient complexes may not be detectable by DLS or SEC. Note however, that no stable high molecular weight complexes could be identified by crosslinking reactions.

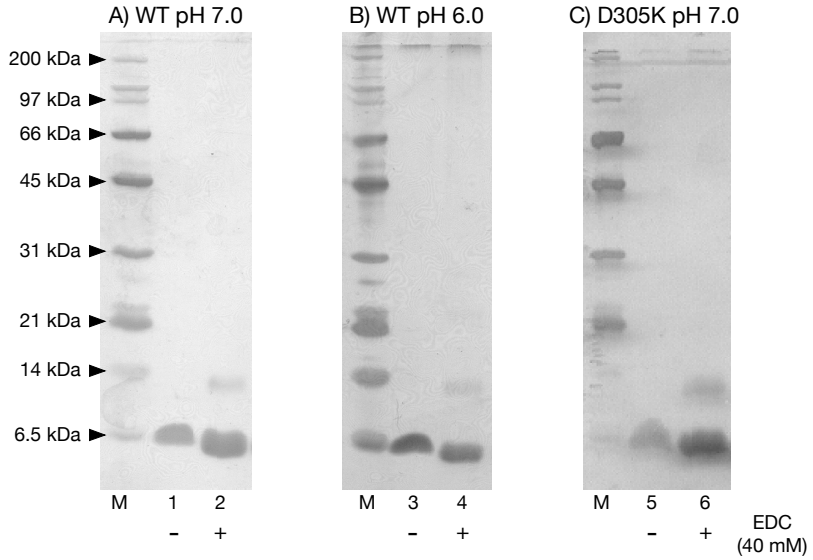

Figure 4.7 *– Crosslinking of Par-4 LZ peptides. The Par-4 LZ peptides (A) rrPar-4LZ at pH 7.0, (B) rrPar-4LZ at pH 6.0 and (C) rrPar-4LZD305K at pH 7.0 were incubated for 1 h on ice with either water as negative control (lanes 1, 3 and 5) or with 40 mM EDC (lanes 2, 4 and 6). Crosslinking reactions were analysed by 10% Tricine-PAGE. The control lanes identify the intense bands as monomers. The secondary bands in the EDC treated samples correspond to dimers as indicated by the molecular weight markers. Sample conditions prior to addition of EDC were 75 µM rrPar-4LZ in 20 mM NaCl, 10 mM Tris, pH 7.0, 40 µM rrPar-4LZ in 20 mM NaCl, 10 mM Mes, pH 6.0 and 75 µM rrPar-4LZD305K in 20 mM NaCl. The abbreviations WT and D305K denote rrPar-4LZ and rrPar-4LZD305K, respectively.*

Interestingly, also for rrPar-4LZ at pH 7.0 the appearance of dimers is observed. This seems to be in contradiction with CD (Fig. 4.2A) and SEC-MALLS (Fig. 4.4C) results indicating that rrPar-4LZ is mostly disordered at pH 7.0. This suggests that there is some interaction between rrPar-4LZ monomers at pH 7.0. It is possible that this interaction is localised to the proposed trigger site of rrPar-4LZ (Chapter 4.3.2.), but that this interaction does not result in full coiled coil formation due to electrostatic repulsion. Note that the proposed trigger site comprises Glu 312 and Lys 317. It is interesting to note here that the downward slope of *MW* towards shorter elution times observed for rrPar-4LZ at pH 7.0 by SEC-MALLS is unusual. It is not clear if this increase in *MW* from 5.4 kDa (leading edge) to 6.2 kDa (trailing edge) is significant (Fig. 4.4C). However, it may be indicative of transient association of a small proportion of the rrPar-4LZ ensemble resulting in a more compact conformation and thus later elution time and thus in a slightly increased *MW*. It is also possible that the observed crosslinking of rrPar-4LZ at pH 7.0 is an artefact of the crosslinking reaction itself. The crosslinking reaction is initiated by the formation of an O-acylisourea intermediate between EDC and a free carboxylic group

(Fig. 4.6). Such a reaction may mask the electrostatic repulsion between Asp 305 and Glu 310 residues and thus result in coiled coil formation with subsequent crosslinking. Taken together, crosslinking experiments suggest that the Par-4 LZ peptides form primarily monomers and dimers and that the observed NMR line broadening (Chapter 4.3.2.) is not due to aggregation.

e) Future directions

As was already mentioned above, the concentration dependency of the elution times of the Par-4 LZ peptides should be established by SEC. This will allow a better understanding of the involved exchange processes and confirm a dimeric state for the Par-4 LZ mutants at pH 7.0. The analysis of rrPar-4LZ at pH 6.0 by SEC-MALLS should also be helpful for the analysis of the equilibrium of DOM and POD conformations, as this peptide shows an elution time intermediate to DOMs and PODs. To further asses the exchange rate between DOMs and PODs additional analytical methods were started, such as AU (analytical ultracentrifugation). As conclusive results are pending possible advantages and limitations of AU will be discussed here. This system has the advantage that it is compatible with a variety of buffer conditions and also allows a temperature control. Therefore, various Par-4 peptides may be studied under different buffer (pH) conditions. However, as the Par-4 LZ peptides lack aromatic residues, the detection of the peptides by AU is limited to the A_{214} absorbance. The AU set-up further requires a maximum absorbance of one. Detection at 214 nm limits the useful concentration range for the Par-4 LZ peptides to below 15 μM. Therefore comparison of the AU results with other results at higher peptide concentration presented in this document has to be done with caution.

To summarise DLS, SEC and crosslinking results, a differentiation between coiled coil and unfolded states of the Par-4 LZ peptides by DLS was not possible due small differences in the measured R_S values. SEC results of coiled coil and disordered states were also found to be similar. However, both DLS and SEC results are consistent with elongated conformations as expected for either disordered or coiled coil states. SEC-MALLS results suggest dimeric states for the coiled coil peptides, as is suggested by the amino acid sequence, and monomeric states for the disordered peptides. A dimeric state of the coiled coil Par-4 LZ peptides is further confirmed by crosslinking results. Importantly, none of the here presented methods showed indications for large aggregates under the analysed conditions.

4.3. Coiled coil formation of the Par-4 LZ domain analysed by NMR spectroscopy

4.3.1. Materials and Methods

a) Chemical shift assignment and CSI calculation

The wild-type Par-4 LZ chemical shifts were assigned by Dr. Kaushik Dutta (New York Structural Biology Center, New York, USA) using $^{1}H,^{15}N$-HSQC, HNCO, HNCACB, CBCA(CO)NH (backbone) and H(CC)(CO)NH-TOCSY, (H)CC(CO)NH-TOCSY, HC(CO)NH, C(CO)NH, and HBHA(CO)NH (side chain) experiments. Typical number of complex points per dimension were 1024 x 128 x 64 (^{1}H x ^{13}C x ^{15}N). Data were processed with NMRPipe [251] and analysed with NMRView [252]. Spectra were acquired at 5 ºC on a Varian Inova 600 MHz spectrometer with an ambient temperature probe on a $^{13}C,^{15}N$-labelled 51-residue peptide in 20 mM NaCl, 12 mM Na_2HPO_4/NaH_2PO_4, pH 6.5. This 51-residue peptide was expressed and purified as described previously [187]. It was used for sequential assignments and CSI calculations presented in this chapter. The rrPar-4LZ peptide (52 residues), used for all other experiments described in this chapter, differs from this 51-residue peptide by an additional N-terminal leucine residue present in the vestigial protease cleavage site of rrPar-4LZ. Chemical shift dispersion of the 51-residue peptide is virtually identical to the rrPar-4LZ construct, except for one extra peak stemming from the leucine in the N-terminal vestigial protease cleavage site (data not shown). Assignments of the 51-residue peptide were therefore adopted for rrPar-4LZ for residues that have identical chemical shifts. Chemical Shift Indexing (CSI) [253] was performed using the C^{α}, C^{β} and C' chemical shift values from Par-4 LZ at pH 6.5 and 5 ºC (Appendix H). C' chemical shifts were corrected as described in Ref. [254].

b) $^{1}H,^{15}N$-SOFAST-HMQC spectra of Par-4LZ peptides

All NMR experiments are recorded on a Bruker Avance 700 MHz spectrometer as described in Chapter 3.4.1.b. $^{1}H,^{15}N$-SOFAST-HMQC spectra were acquired on 300 µl samples in D_2O matched Shigemi NMR tubes. Sample conditions are given in Table 4.2. All spectra were recorded at 5 ºC and 25 ºC with the following settings: 24 transients, 800 x 128 points (^{1}H x ^{15}N) and spectral widths of 10 and 30 ppm for ^{1}H and ^{15}N, respectively. Soft proton pulses with a bandwith of 3 ppm were centred at 7.8 ppm. The carrier was set to the frequency of the water resonance in the ^{1}H and to 119 ppm in the ^{15}N dimension. For rrPar-4LZ at pH 6.0, an additional spectrum with 512 transients, but otherwise identical conditions, was recorded. Acquisition parameters are given in Appendix G.

c) ^{15}N-relaxation measurements of rrPar-4LZ at pH 6.0

^{15}N-relaxation studies [255] and $^{3}J_{HNH\alpha}$ coupling constant measurements were performed at 5 ºC on a 300 µl sample in a D_2O matched Shigemi NMR tube. The sample contained 100 µM rrPar-4LZ in 20 mM NaCl, 10 mM Mes, pH 6.0 and 5% D_2O ($^{v}/_{v}$). *T_1* spectra were recorded with τ delays of 30.92, 90.35, 179.51, 298.38, 417.25, 595.56, 773.87 and 892.74 ms, while the *T_2* measurements used values of 16.32, 32.64, 48.96, 81.6, 114.24, 146.88, 179.52, 212.16 and 244.8 ms. The recycle delay was set to two seconds. {^{1}H}^{15}N steady state NOEs were obtained by recording spectra with and without ^{1}H presaturation at a duration of three seconds. The recycle delay was set to six seconds. *T_1*, *T_2* and {^{1}H}^{15}N-NOE experiments were acquired with the following settings: 24 transients, 2048 x 256 points (^{1}H x ^{15}N) and spectral widths of 10 and 25 ppm for ^{1}H and ^{15}N, respectively. A 3D-HNHA [256] experiment for the measurement of $^{3}J_{HNH\alpha}$ coupling constants was acquired with 24 transients, 2048 x 76 x 48 points (^{1}H x ^{1}H x ^{15}N) and spectral widths of 10 and 25 ppm for ^{1}H and ^{15}N, respectively. The carrier frequency was set to the frequency of the water resonance in the ^{1}H and to 119 ppm in the ^{15}N dimension, respectively.

Cross-correlated relaxation rates (η_{xy}) were acquired at 5 ºC as described in Ref. [257] on a 300 µl sample in a D_2O matched Shigemi NMR tube. The sample contained 60 µM rrPar-4LZ in 20 mM NaCl, 10 mM Mes, pH 6.0 and 5% D_2O ($^{v}/_{v}$). The following settings were used: 48 transients, 1024 x 256 points (^{1}H x ^{15}N) and spectral widths of 10 and 25 ppm for ^{1}H and ^{15}N, respectively. The carrier frequency was set to the frequency of the water resonance in the ^{1}H and to 119 ppm in the ^{15}N dimension, respectively. The recycle delay was set to 2.5 s.

d) NMR spectroscopy of REDPRO rrPar-4LZE310K

^{1}H,^{15}N-TROSY-HSQC and {^{1}H}^{15}N steady state NOE experiments of REDPRO rrPar-4LZE310K were acquired on a 300 µl sample in a D_2O matched Shigemi NMR tube, and contained 0.3 mM peptide in 20 mM NaCl, 10 mM Tris, pH 7.0 and 5% D_2O ($^{v}/_{v}$). ^{1}H,^{15}N-TROSY-HSQC and ^{1}H,^{15}N-HSQC spectra were recorded at 5 ºC with the following settings: 48 transients, 2048 x 256 points (^{1}H x ^{15}N) and spectral widths of 10 and 30 ppm for ^{1}H and ^{15}N. The carrier was set to the frequency of the water resonance in the ^{1}H and to 119 ppm in the ^{15}N dimension. {^{1}H}^{15}N steady-state NOEs were obtained by recording spectra with and without ^{1}H presaturation at a duration of six seconds. The recycle delay was set to six seconds. Spectra were recorded with the following settings: 72 transients, 2048 x 256 points (^{1}H x ^{15}N) and spectral

widths of 10 and 30 ppm for ^{1}H and ^{15}N, respectively. The carrier was set to the frequency of the water resonance in the ^{1}H and to 119 ppm in the ^{15}N dimensions.

e) NMR spectra processing and analysis

All data sets were linear predicted (32 prediction coefficients), apodised and zero-filled once in the indirect dimensions before Fourier transformation and final processing. Unless stated otherwise a shifted (π/2) squared sinusoidal bell function was used for apodisation. TopSpin 2.1 (Bruker BioSpin GmbH, Rheinstetten, Germany) was used for spectral processing and lineshape analysis. The ^{1}H and ^{15}N chemical shifts were referenced to the water signal [216]. Cross peak intensities, $^{3}J_{HNH\alpha}$ coupling constants, T_1 and T_2 rates were calculated using the program Analysis 2.0 [258].

4.3.2. Results and Discussion

CD spectropolarimetry shows that rrPar-4LZ at pH 6.5 and 5 ºC is mostly disordered, but also displays weak α-helicity (Fig. 4.2B). Consistent with this result, a weak, but significant, α-helical character is evident by CSI for the Par-4 LZ domain under similar conditions (Fig. 4.8), with the Glu 312-Lys 321 sequence displaying the highest degree of α-helicity. CSI calculations were performed with the C^{α}, C^{β} and C' chemical shift values obtained from the assignment process of Par-4(286-332)WT at pH 6.5 and 5 ºC. A fully formed α-helix, typically produces CSI values near +10 [253]. The modest CSI magnitudes observed for Par-4 indicate fluctuating torsion angles sampling regions typical for α-helical conformations [176] that may or may not be accompanied by intermittent formation of short or long helical stretches.

It is possible that the Glu 312-Lys 321 region may represent a trigger site for the LZ domain. Trigger sites were proposed as autonomous helical folding units, which are necessary for coiled coil formation and are stabilised by inter- and intrahelical salt bridges [259,260]. Residues Glu 312-Lys 321 comprise the fourth heptad of the Par-4 LZ domain and contain a potential intrahelical *i* to *i+3* salt bridge between Glu 314 and Lys 317 and a potential interhelical *i* to *i'+5* salt bridge between Glu 312 and Lys 317' that could help to stabilise this motif [261] (Figs. 4.1B and E). The occurrence of two asparagine residues (Asn 313, Asn 320) at position *a* within this region (Fig. 4.1B) appears to be in contradiction with the trigger site proposal, as these residues are usually detrimental for coiled coil stability [243]. However, monomer helix stability is a more critical factor for a trigger site [261] and additionally asparagines were shown not to be involved in the association step of coiled coil formation [242].

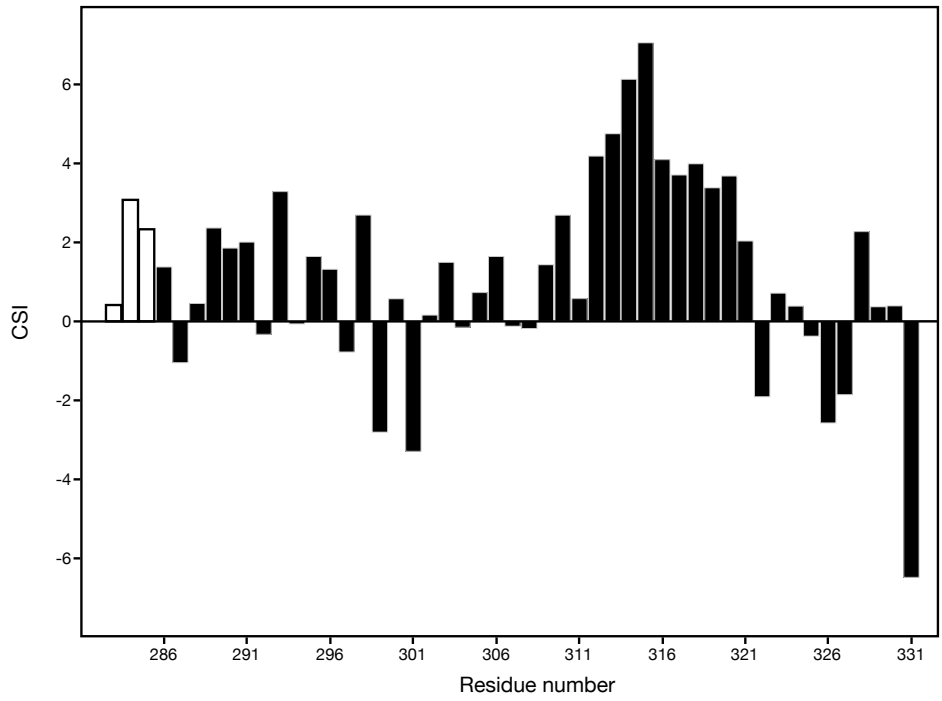

Figure 4.8 *– CSI for the Par-4 LZ domain. The Par-4 LZ sequence (black bars) begins at residue Gln 286. Residues N-terminal to Gln 286 (white bars) stem from the vestigial protease cleavage site. A moderate preference for α-helix is evident for the Glu 312-Lys 321 sequence.*

After confirming in the previous chapter that CD spectropolarimetry results of rrPar-4LZ at different pH values are comparable to previous results [184], rrPar-4LZ was subjected to NMR spectroscopy. The NMR spectra at temperatures of 5 and 25 ºC for rrPar-4LZ at pH 7.0, 6.0 and 4 are shown in Figure 4.9. The virtually complete resonance assignment of the LZ domain obtained by Dr. Dutta is shown in Figure 4.9A and plotted onto the pH 7.0 $^{1}H,^{15}N$-SOFAST-HMQC spectrum. Sequential assignment was achieved at pH 6.5 and 5 ºC, however, the NMR spectra at 5 ºC of rrPar-4LZ at pH 7.0 and 6.5 are virtually identical (data not shown), allowing the transfer of the assignments to the pH 7.0 spectrum. These NMR results are not surprising as CD spectropolarimetry indicates mostly unfolded conformations under both conditions (Figs. 4.2A and B).

A significant difference in the CD spectra of rrPar-4LZ is observed between pH 7.0 and 6.0. In contrast to the mostly disordered conformation (~18% of combined regular and distorted α-helicity) observed at pH 7.0, the pH 6.0 spectrum at 5 ºC displays α-helical (~56% α-helicity) yet not coiled coil character (Figs. 4.2A and C). Despite this clear increase in α-helicity at pH 6.0, the 5 ºC NMR spectra of rrPar-4LZ at pH 7.0 and 6.0 are virtually identical and no obvious signs of structure are observed under the experimental conditions used (Fig. 4.9A). Apart from relatively minor changes mostly confined to charged residues (e.g. Glu 297, Asp 305, Glu 308,

Glu 310, or Glu 312), only the appearance of additional peaks for Leu -3, Gly -2, Ser -1 and Gln 286 (marked by asterisks) is observed at pH 6.0. Note that residues with negative numbers stem from the vestigial protease cleavage at the N-terminus. A possible explanation for the occurrence of these peaks will be discussed below. A similar global conformational change is observed by CD spectropolarimetry for rrPar-4LZ at pH 6.0 between 5 and 25 ºC (Fig. 4.2C). However, neglecting temperature induced shifts, the NMR spectra at 5 and 25 ºC (pH 6.0) are similar and show no obvious signs of structure. Note that the additional peaks (marked by asterisks) at pH 6.0 are more prominent at 5 ºC than at 25 ºC (Fig. 4.9B).

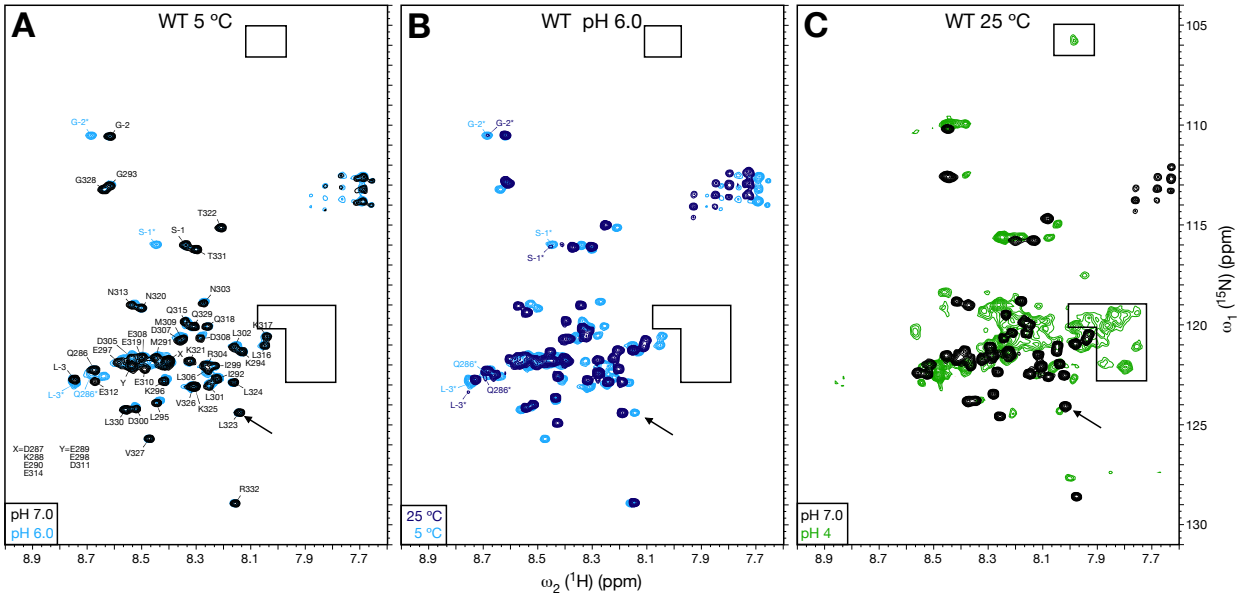

Figure 4.9 *– Influence of pH on the $^{1}H,^{15}N$-SOFAST-HMQC spectra of rrPar-4LZ. (A) Pairwise comparison of the NMR spectra at 5 ºC of rrPar-LZ at pH 7.0 (black contours) and pH 6.0 (blue contours). Assignments of the Par-4 LZ domain at 5 ºC are shown, starting with Gln 286. Negative residue numbers indicate amino acids originating from the protease cleavage site. X and Y denote overlapped peaks consisting of Asp 287, Lys 288, Glu 290, Asp 314 (X) and Glu 289, Glu 298, Asp 311 (Y). Additional peaks that arise at pH 6.0 (see text) are labelled in blue and marked by asterisks. (B) Overlay of the HMQC spectra at pH 6.0 for rrPar-4LZ at 5 ºC (blue contours) and 25 ºC (dark blue contours). Labelled peaks are as described in the legend to part (A). (C) Comparison of the NMR spectra at 25 ºC of rrPar-4LZ at pH 7.0 (black contours) and rrPar-4LZ at pH 4 (green contours). Selected peaks with an increased chemical shift dispersion are marked by black boxes. The black arrow indicates representative peaks that do not significantly change their position in response to decreasing pH. Sample conditions were 75 µM rrPar-4LZ in 20 mM NaCl, 10 mM Tris, pH 7.0; 40 µM rrPar-4LZ in 20 mM NaCl, 10 mM Mes, pH 6.0; and 50 µM rrPar-4LZ in MQ-H_2O pH 4. All samples were uniformly ^{15}N-labelled and contained 5% D_2O (v/v) in the sample buffer. All spectra were recorded with 24 transients, further acquisition parameters are listed in Appendix G. The spectrum of rrPar-4LZ at pH 4 was apodised using a shifted (π/5) sinusoidal function in F2 and a shifted (π/2) squared sinusoidal bell function in F1.*

Common to all rrPar-4LZ NMR spectra at pH values greater or equal to pH 6.0 is therefore the display of sharp peaks and of narrow ^{1}H chemical shift dispersions, which as discussed in Chapter 1.6.4. are characteristics of protein disorder. These features were observed for all rrPar-4LZ spectra at 5 and 25 ºC, and did not significantly change between pH 7.0 and 6.0. Conversely, rrPar-4LZ at pH 4 displays a distinct NMR spectrum at 25 ºC with a slightly increased ^{1}H chemical shift dispersion. For clarity, representative peaks with an increased dispersion are marked by black boxes in Figure 4.9C. As mentioned earlier, CD spectropolarimetry shows that rrPar-4LZ at pH 4 adopts a coiled coil conformation (Fig. 4.2D) and is more thermo-stable (Fig. 4.3A) than other rrPar-4LZ samples at higher pH. However, the NMR spectrum is complicated by a reduced signal intensity and severe line broadening with an average ^{1}H line width and standard deviation of 38.5 ± 43.9 Hz. Loss of signal intensity and line broadening is further enhanced at 5 ºC resulting in a sharp reduction in signal intensity (data not shown). The importance of these facts will be discussed further below.

The absence of NMR observable secondary structure for rrPar-4LZ at pH 6.0 and 5 ºC is further corroborated by ^{15}N-relaxation studies (Fig. 4.10). The central residues Met 291-Val 327 show R_1 rates of 2.78 ± 0.14 s^{-1} and R_2 rates of 7.03 ± 1.08 s^{-1} (Fig. 4.10A). In contrast, R_2 rates of approximately 14 s^{-1} were observed for the dimeric state of the 46-residue rJunLZ [262]. This suggests that under these conditions, the rrPar-4LZ peaks correspond to a flexible non-folded state. The rrPar-4LZ N- and C-termini show greater flexibility than the central residues, marked by lower R_2 relaxation rates without significant lowering of R_1 rates (Fig. 4.10A). The termini also have negative or weakly positive $\{^{1}H\}^{15}N$-NOE (Fig. 4.10B). To determine the contribution of chemical exchange processes to the apparent R_2 rates, the exchange rate (R_{ex}) was calculated from η_{xy} [183]. R_{ex} contributions are suggested for residues Gly 293-Leu 301 (Fig. 4.10C).

Values of 0.8 ± 0.1 for $\{^{1}H\}^{15}N$ steady-state NOEs are usually observed for residues in regular secondary structure (e.g. α-helices and β-sheets), whereas negative values are observed for residues in highly flexible regions like the N- or C-terminal ends of proteins [263]. For the central residues Met 291-Val 327 of rrPar-4LZ, $\{^{1}H\}^{15}N$-NOE values of 0.41 ± 0.09 (Fig. 4.10B) were obtained, which is typically interpreted as an intermediate state between rigid secondary structure and high flexibility [146,263]. Similar $\{^{1}H\}^{15}N$-NOE values, R_1, and R_2 rates were obtained for rrPar-4LZ at pH 7.0 and 5 ºC consistent with an unfolded conformation (data not shown). Additional evidence for the absence of stable secondary structures at 5 ºC and pH 6.0 comes from $^{3}J_{HNH\alpha}$ coupling constant measurements. The calculated values of approximately 6.4 ± 0.8 Hz are characteristic of a mostly disordered conformation (Fig. 4.10D). For

comparison, coupling constants for the α-helical rJunLZ dimer were approximately 4-5 Hz [246]. Note that NOESY spectra also show no indications of secondary structure within rrPar-4LZ at pH 6.0 (data not shown). As only rrPar-4LZ samples at pH values greater or equal to pH 6.0 were amenable to NMR relaxation studies, no ^{15}N-relaxation data was acquired for the coiled coil rrPar-4LZ at pH 4 (Fig. 4.2A) due to insufficient signal intensity and severe line broadening.

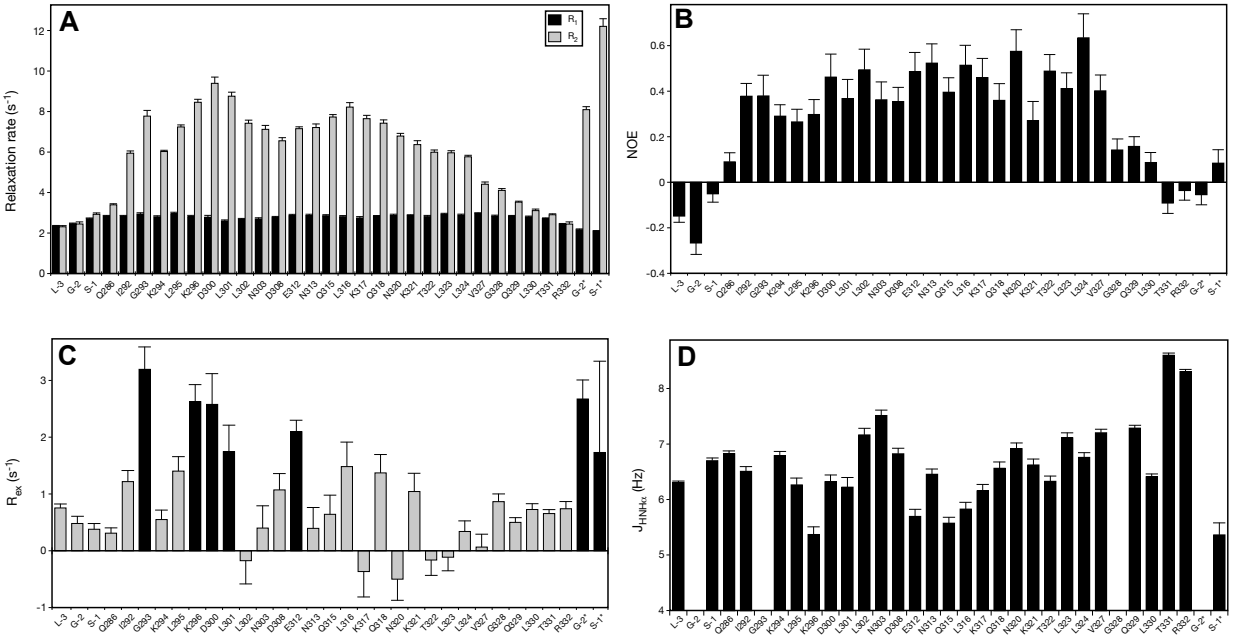

Figure 4.10 *– ^{15}N-relaxation and J-coupling of rrPar-4LZ at pH 6.0 and 5 ºC. (A) R_1 (black bars) and R_2 (grey bars) rates, (B) {^{1}H}^{15}N-NOE and (C) R_{ex} rates [183,257] of not significantly overlapped peaks. Black bars in part (C) indicate R_{ex} contributions > 1.5 s^{-1}. (D) $^3J_{HNH\alpha}$ coupling constants for the same residues. Coupling constants for glycine residues are not shown. ^{15}N-relaxation rates, {^{1}H}^{15}N-NOE and $^3J_{HNH\alpha}$ coupling constants were acquired with a 100 µM sample in 20 mM NaCl, 10 mM Mes, pH 6.0 at 5 ºC and R_{ex} rates with a 60 µM sample.*

Only minor differences are observed at the first glance in the NMR spectra of rrPar-4LZ at 5 ºC and pH values of 7.0 and 6.0 (Fig. 4.9A), however, significant differences between these NMR spectra are observed for the HMQC cross peak intensities. After correcting for concentration differences, a decrease in signal intensity for the majority of peaks of 45-65% is evident at pH 6.0 relative to pH 7.0, with intermediate intensities at pH 6.5 (Fig. 4.11A). At pH 4 the decrease is even more pronounced than at pH 6.0 (Fig. 4.11B). However, due to line broadening only a few resonances could be identified that overlay with peaks of the mostly unfolded rrPar-4LZ at pH 7.0 (a representative peak is marked by a black arrow in Figure 4.9C).

The cross peak intensities of rrPar-4LZ at pH 4 and 5 ºC were not analysed due to insufficient signal intensity.

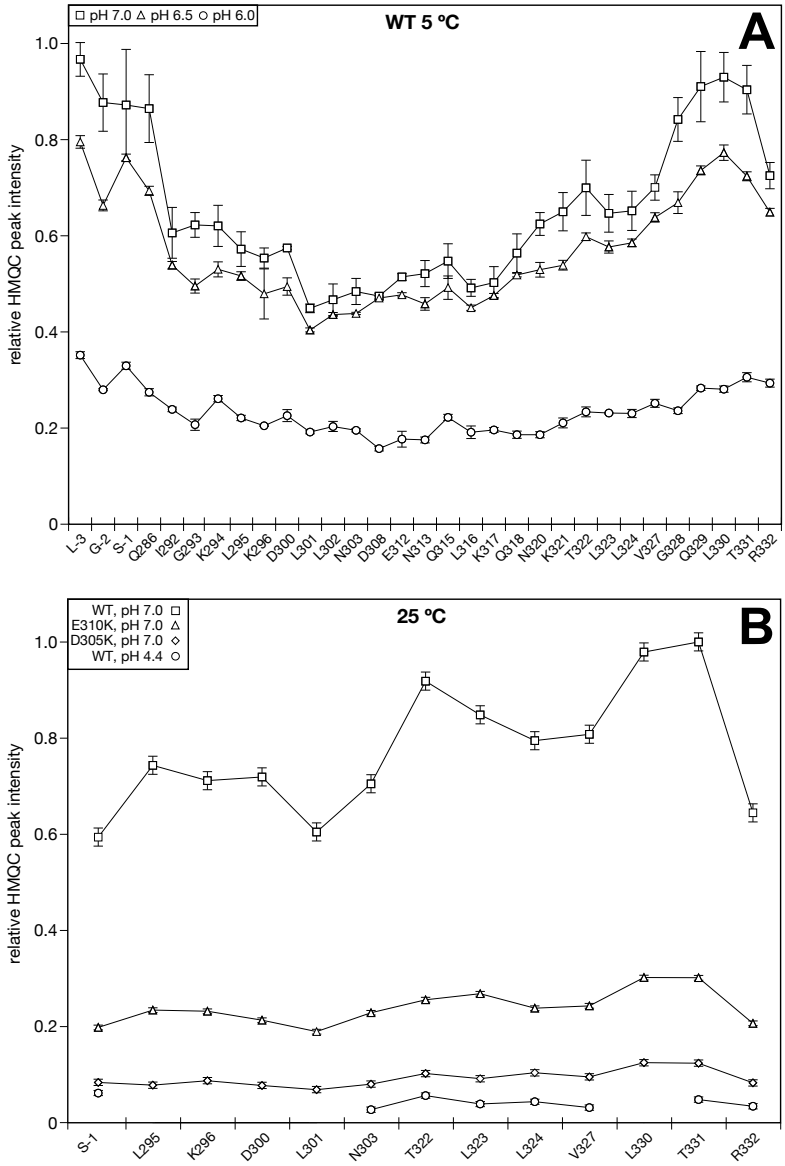

Figure 4.11 *− NMR peak intensity of Par-4 LZ peptides. (A) $^{1}H,^{15}N$-SOFAST-HMQC peak intensity of rrPar-4LZ at 5 ºC as a function of pH. Displayed are the normalised peak heights at pH 7.0, pH 6.5 and pH 6.0. Intensities at pH 6.0 were acquired with a 60 µM rrPar-4LZ sample and were adjusted by a factor of 1.25 for comparison with the intensities at pH 7.0 and pH 6.5 acquired with 75 µM samples. (B) $^{1}H,^{15}N$-SOFAST-HMQC peak intensities at 25 ºC for rrPar-4LZ at pH 7.0 and 4, rrPar-4LZE310K at pH 7.0 and rrPar-4LZD305K at pH 7.0. Intensities of rrPar-4LZ at pH 4 were acquired with a 50 µM sample and were adjusted by a factor of 1.5 for comparison with the intensities of the other peptides acquired with 75 µM samples. Only resonances not significantly overlapped in each spectrum were analysed. Gaps for rrPar-4LZ at pH 4 indicate residues that could not be identified in the corresponding spectrum. Intensities were measured as peak heights. No significantly different results are obtained using peak volumes. Intensities in both panels were normalised to the highest peak intensity for comparison. The abbreviations WT, D305K and E310K denote rrPar-4LZ, rrPar-4LZD305K and rrPar-4LZE310K, respectively.*

As mentioned in the previous chapter, a drop in pH is associated with an increase in α-helicity (Fig. 4.2). Based on SEC and MALLS results, a structural interconversion between DOM and POD fractions of the Par-4 LZ peptides was proposed in the previous chapter. The observed decrease in cross peak signal intensity of 45-65% for rrPar-4LZ at pH 6.0 (Fig. 4.11A) correlates well with the observed α-helicity of 56% (Fig. 4.2C). This signal intensity decrease and the chemical shift similarities of the analysed peaks suggest that the observable NMR cross peaks represent the DOM fraction. The reduced cross peak intensities are consistent with CD spectropolarimetry results suggesting that the DOM fraction is the minor population under acidic conditions (Figs. 4.2C and D). The assignment of these peaks to the DOM fractions is further consistent with the ^{15}N-relaxation data (Fig. 4.10) and other indications for protein disorder, such as sharp peaks, a narrow ^{1}H chemical shift dispersion and chemical shift values close to random coil shifts (Fig. 4.9A).

The results shown in Figures 4.9 and 4.11 also suggest that peaks of the POD fraction are not accessible by NMR at the used NMR parameters with 24 transients per increments. A possible explanation is that peaks of the POD fraction are line broadened resulting in a signal intensity decrease beyond detection limits. Line broadening has been repeatedly observed for coiled coils and representative examples are given below. Relative to residues of the flexible and disordered C-Terminus of HSBP1 (heat shock binding protein 1), residues that were part of the helical domain, which forms a coiled coil, were broad and of low intensity [247]. It was proposed by the authors that line broadening is due to oligomerisation and/or non-globular shapes affecting the tumbling rate of the molecule. The contribution from non-globular shapes to the observed line broadening for the Par-4 LZ peptides is questionable, as NMR spectra with reasonably sharp lines have been obtained for coiled coils of similar length (e.g. rJun leucine zipper [246], FIP2 [264], or the N-terminus of the nucleocapsid protein of the Andes Hantavirus[265]). Additionally, line broadening may be due to chemical exchange processes as described for the coiled coil domain of FIP2 [264]. In complex with Rab11 a stable coiled coil is observed for FIP2. However, when unbound to Rab11 internal motions within FIP2 result in a fraying of the helices at the C-terminal end of the FIP2 coiled coil [264]. The observed line broadening for rrPar-4LZ at pH 4 indicates that similar mechanisms exist for the Par-4 LZ peptides resulting in the inaccessibility of the POD fraction. However, DLS results (Chapter 4.2.2.c) argue against aggregation.

As the DOM peaks are observed as a separate set of peaks this suggests that chemical exchange between DOM and POD fractions is slow on the NMR time scale. A slow chemical

exchange process is likely as exchange rates for model leucine zippers were found to be in the order of 10 s^{-1} [138]. This value is relatively small compared to the chemical shift difference observed for folded and unfolded leucine zippers [266]. Further indications for a slow exchange come from four additional peaks (marked by asterisks in Fig. 4.9A) observed for rrPar-4LZ at pH 6.0 and 5 ºC. Sequential assignment of these peaks is difficult, as they only become suitably intense under low pH conditions where solubility becomes limited. However, based on the chemical shifts, two of these peaks must arise from a glycine and either a serine or a threonine. The only sequential Gly-Ser or Gly-Thr pair within the rrPar-4LZ sequence is Gly -2 and Ser -1 (negative numbers indicate residues from the protease cleavage site). Additionally, the previously assigned Gly -2 and Ser -1 peaks show nearly identical nitrogen chemical shifts as these two additional peaks (Fig. 4.9A). Therefore, these two peaks were denoted Gly -2* and Ser -1*. The other two additional peaks were denoted Leu -3* and Gln 286* due to their proximity to the N-terminal residues Leu -3 and Gln 286. The asterisks denote a second conformation arising as pH is decreased, which is likely the POD conformation.

As the 11 N-terminal residues are not likely to form a coiled coil (Chapter 4.1.2.), they are probably mostly disordered independent of pH. This is consistent with a maximum of 70-85% α-helicity for the Par-4 LZ peptides [184,185]. The intensity of these four additional peaks at pH 6.0 is significantly greater at 5 ºC than at 25 ºC (Fig. 4.9B), corroborating that these peaks stem from the N-terminus of the POD fraction, which is more populated at 5 ºC than at 25 ºC (Fig. 4.2C). Relative to Gly -2 and Ser -1 of the DOM fraction, Gly -2* and Ser -1* have similar R_1 rates of approximately 2 s^{-1}, but four to six times higher R_2 rates (Fig. 4.10A). The increased R_2 rates are partly due to an increase in R_{ex} (Fig. 4.10C). Furthermore, the $\{^1H\}^{15}N$-NOE are slightly larger than for the peaks of the DOM fraction (Fig. 4.10B). Taken together, these data suggest that Gly -2* and Ser -1* are relatively unstructured regions of the POD fraction. Relative to the ordered section of the POD fraction, these four additional peaks are more flexible and thus have sharper and more intense lines. Other peaks arising from residues of the POD fraction are either exchange broadened as described above, and/or are of to low intensity for detection under the conditions used. Otherwise peaks could be overlapped by the more intense peaks stemming from the DOM fraction.

A similar dynamic exchange between a dimeric coiled coil state and a monomeric less structured state was recently described for the GCN4 leucine zipper [266]. In contrast to the present study, the monomeric form predominated at low pH. The monomeric state of GCN4 is in many ways consistent with the disordered rrPar-4LZ fraction. Both peptides display similar

chemical shift dispersions and each provides indications of residual α-helical structure (see above). In both cases, central residues displayed $\{^1H\}^{15}N$-NOE near 0.4, and in the case of GCN4, this was explained by the proposal of a structural core. Conversely, the $\{^1H\}^{15}N$-NOE for urea unfolded GCN4 were mostly negative. It was suggested that this monomeric form of GCN4 represents a stable folding intermediate that facilitates dimerisation; a proposal that is not inconsistent with the data for the Par-4 LZ domain. A further analysis of the coiled coil state of rrPar-4LZ was difficult due to its poor NMR spectroscopic properties. At pH 6.0 the solubility of rrPar-4LZ is limited and at pH 4 the NMR spectra are affected by severe line broadening. Therefore, NMR spectroscopy was focussed on the LZ point mutants rrPar-4LZD305K and rrPar-4LZE310K, which form a coiled coil independent of pH [185], but also display a better solubility than rrPar-4LZ at pH 6.0.

The NMR spectra of the LZ point mutants rrPar-4LZD305K and rrPar-4LZE310K at 25 ºC and pH 7.0 are very similar to the spectrum of rrPar-4LZ at pH 4 (Figs. 4.12A and B), with all spectra displaying a similar ^1H chemical shift dispersion. Additionally, broad lines are evident for rrPar-4LZD305K and some less pronounced line broadening also occurs for rrPar-4LZE310K. The average ^1H line widths for various Par-4 LZ peptides at 25 ºC are 17.5 ± 2.8 Hz (rrPar-4LZ, pH 7.0), 32.5 ± 11.1 Hz (rrPar-4LZE310K, pH 7.0) 43.7 ± 27.8 Hz (rrPar-4LZD305K, pH 7.0) and 38.5 ± 43.9 Hz (rrPar-4LZ, pH 4). The large standard deviation of rrPar-4LZD305K and rrPar-4LZ (pH 4) line widths is a result from the broadest line widths. The observed line broadening for the latter three peptides is even more pronounced at 5 ºC (data not shown). Interestingly, this increase in ^1H line widths for the Par-4 LZ peptides appears to be correlated with an increase in thermal stability and coiled coil formation (Figs. 4.3A and B). Line broadening is probably not due to high molecular weight complex formation, as aggregation is not suggested by DLS or SEC for these NMR samples (Chapters 4.2.2.b and c). Consistent with the NMR signal intensity decrease observed for rrPar-4LZ with decreasing pH, rrPar-4LZD305K and rrPar-4LZE310K at pH 7.0 and 25 ºC display a pronounced loss in HMQC cross peak intensity (Fig. 4.11B). The more stable rrPar-4LZD305K displays a lower signal intensity at pH 7.0 than rrPar-4LZE310K. Analysis of the cross peak intensity at 5 ºC of both these peptides was not done due to insufficient signal intensity. As was proposed for rrPar-4LZ, these results suggest that the analysed peaks, which overlay with peaks of rrPar-4LZ at pH 7.0 (marked by black arrows in Figs. 4.12A and B), represent the DOM fraction. As the DOM fraction is the minor population for both LZ point mutants at 25 ºC (Figs. 4.2E and F) a significantly reduced intensity for these peaks is expected relative to the disordered rrPar-4LZ at pH 7.0.

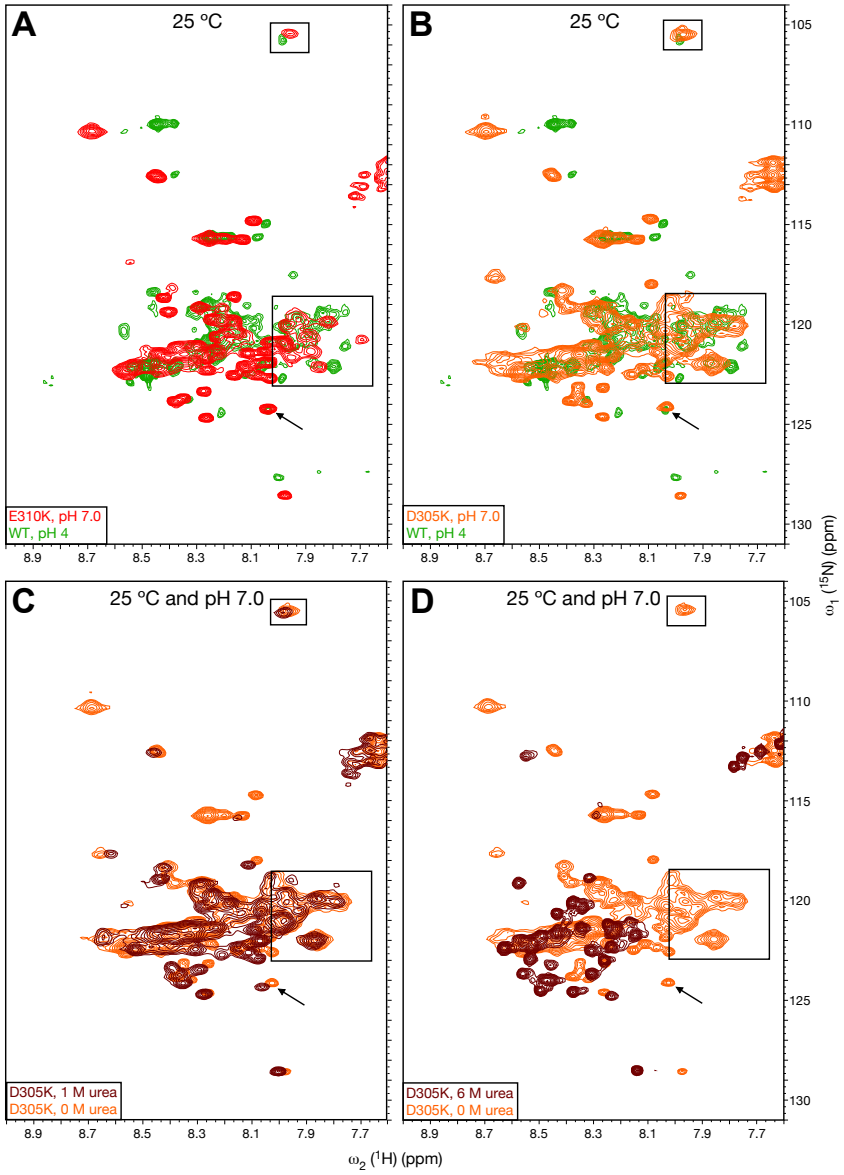

Figure 4.12 *– $^{1}H,^{15}N$-SOFAST-HMQC spectra of the Par-4 LZ point mutants. Overlay of the NMR spectra of rrPar-4LZ at pH 4 (green contours) and (A) rrPar-4LZE310K at pH 7.0 (red contours) or (B) rrPar-4LZD305K at pH 7.0 (orange contours). The influence of increasing concentrations of the denaturant urea on the $^{1}H,^{15}N$-SOFAST-HMQC spectra of rrPar-4LZD305K at pH 7.0 is shown in Figures (C) and (D). Compared are the spectra in the absence of urea (orange contours) with the spectra in the presence of (C) 1 M urea (brown contours) and (D) 6 M urea (brown contours). Selected peaks associated with the POD conformation are marked by black boxes. The black arrow indicates representative peaks that are associated with the DOM conformation. All samples were uniformly ^{15}N-labelled and contained 5% D_2O ($^{v}/_{v}$) in the sample buffer. Sample conditions were 50 µM rrPar-4LZ in MQ-H_2O, pH 4; 75 µM rrPar-4LZE310K in 20 mM NaCl, 10 mM Tris, pH 7.0; and 75 µM rrPar-4LZD305K in 20 mM NaCl, 10 mM Tris, pH 7.0, with 0 M, 1 M and 6 M urea, respectively. All spectra were acquired at 25 °C with 24 transients, further acquisition parameters are given in Appendix G. All spectra except for rrPar-4LZD305K in 6 M urea were apodised using a shifted (π/5) sinusoidal function in F2 and a shifted (π/2) squared sinusoidal bell function in F1. The abbreviations WT, D305K and E310K denote rrPar-4LZ, rrPar-4LZD305K and rrPar-4LZE310K, respectively.*

A similar degree of line broadening at 25 ºC is observed for rrPar-4LZD305K at pH 7.0 in the presence of 1 M urea relative to the spectrum without urea (Fig. 4.12C). Both spectra are very similar apart from minor shift differences for some of the peaks. The shift differences may be due to the loss of secondary structure as observed by CD spectropolarimetry (Fig. 4.3C). As aggregation is disfavoured in the presence of 1 M urea and no aggregated species could be detected by DLS (Fig. 4.5D), this suggests that the observed line broadening is due to dynamic exchange processes within the POD fraction of rrPar-4LZD305K. Significantly sharper lines are observed for rrPar-4LZD305K at 25 ºC and pH 7.0 in the presence of 6 M urea (Fig. 4.12D). Additionally, a significant reduction in the ^{1}H chemical shift dispersion is evident. This is consistent with a urea unfolded state as indicated by CD spectropolarimetry (Fig. 4.3C). Note that similar results were obtained for rrPar-4LZE310K in 6 M urea (data not shown).

These results indicate that the observed line broadening in the NMR spectra of the Par-4 LZ peptides (Figs. 4.9C and 4.12) reflects the coiled coil formation observed by CD spectropolarimetry. A slow exchange mechanism between POD and DOM states was proposed above for rrPar-4LZ, with the equilibrium between PODs and DOMs depending on the pH. A similar exchange process is likely for the LZ point mutants, and peaks affected by line broadening are probably associated with the POD fraction. $^{1}H,^{15}N$-HSQC spectra of both LZ point mutants further suggest the existence of two separate sets of peaks (data not shown). However, analysis of the $^{1}H,^{15}N$-HSQC spectra of rrPar-4LZD305K was still difficult due to line broadening. With the aim of reducing line broadening contributions from oligomerisation, a partially deuterated REDPRO sample of rrPar-4LZE310K was prepared (Chapter 2.11.8.). This peptide was chosen due to its ability to form a coiled coil (Fig. 4.2F) with only minor line broadening at relatively high concentration (Fig. 4.12A). In particular the broad peaks (marked by black boxes in Fig. 4.13A) of REDPRO rrPar-4LZE310K at pH 7.0 and 5 ºC displayed an improvement in line shape and peak intensity using a $^{1}H,^{15}N$-TROSY-HSQC sequence. These results allowed a characterisation of some of the POD-associated peaks by ^{15}N-relaxation measurements (see below).

The $^{1}H,^{15}N$-TROSY-HSQC spectrum of REDPRO rrPar-4LZE310K at pH 7.0 and 5 ºC clearly shows the existence of two separate sets of peaks (Fig. 4.13A). A conservative peak count results in approximately 26 peaks with sharp lines and approximately 38 peaks with broad lines. The average ^{1}H line widths of these peaks were 6.4 ± 2.1 Hz for the sharp peaks, and 26.1 ± 2.1 Hz for the broad peaks. Only the ^{1}H line widths of well resolved peaks were analysed (Fig. 4.13A). Analysis of well resolved peaks further indicates a volume ratio of 1:3 between

sharp and broad peaks. Furthermore, $\{^1H\}^{15}N$ NOE values of the broad peaks are slightly increased (0.60 ± 0.07) relative to the $\{^1H\}^{15}N$ NOE values of the sharp peaks (0.34 ± 0.25). The large standard deviation for the sharp peaks arises due to negative values from residues probably located at the C-terminus of rrPar-4LZE310K. The majority of the sharp peaks overlay with peaks of rrPar-4LZ at pH 7.0 and 5 ºC (a representative peak is marked by a black arrow in Fig. 4.13A). This suggests a similar chemical environment for these residues in both peptides and thus indicates that these residues are associated with the DOM fraction. In contrast, the three times increased volume of the broad peaks of REDPRO rrPar-4LZE310K suggest that the broad peaks represent the major population, which under these conditions is the POD fraction as indicated by CD spectropolarimetry (Fig. 4.2F). In addition, this set of broad peaks displays a wider chemical shift dispersion relative to the set of sharp peaks. For clarity, representative POD-associated peaks are marked by black boxes in Figure 4.13A. Furthermore, the $\{^1H\}^{15}N$ steady state NOE values of ~0.6 for the broad peaks of rrPar-4LZE310K confirm their assignment to the POD fraction, and indicates that residues of the POD fraction are in a slightly more rigid conformation than residues of the DOM fraction with $\{^1H\}^{15}N$ NOEs of ~0.34. However, a $\{^1H\}^{15}N$ NOE value of 0.6 is still not indicative of rigid secondary structure [263] as expected for a coiled coil, and hence only suggests a predominantly ordered state. This suggests that internal factors within the Par-4 LZ sequence contribute to a less rigid conformation than is expected for stable leucine zippers, such as GCN4 or rJun [262].

Similarly, two sets of peaks appear to exist for rrPar-4LZD305K at pH 7.0 (Fig. 4.12B) and rrPar-4LZ at pH 4 (Fig. 4.9C). However, artificially broad lines due to short acquisition times in the SOFAST-HMQC sequence make the difference in line widths less apparent. As the broader peaks have shorter proton T_2 relaxation times, it is expected that a significant amount of NMR signal intensity is lost for these peaks during the evolution periods of the $^1H,^{15}N$-correlation experiment relative to the signal intensity of the sharp peaks. The DOM and POD fractions are approximately equally populated for rrPar-4LZ at pH 6.0 and 5 ºC, as is indicated by an α-helicity of 56% (Fig. 4.2C). A more accurate description of the population state between PODs and DOMs is not possible. The observed CD signal is an averaged signal and contains protein disorder contributions from the dynamic interconversion between DOMs and PODs, and from disordered segments at the N-terminus of rrPar-4LZ (see above). Considering the potential loss in NMR signal intensity during the evolution periods of the NMR experiment and assuming equal populations of DOMs and PODs for rrPar-4LZ at pH 6.0 and 5 ºC, it is expected that the (broad) peaks associated with the ordered region of the POD conformation are significantly less

intense than the peaks associated with the DOM fraction. The acquisition of a $^{1}H,^{15}N$-SOFAST-HMQC spectrum of rrPar-4LZ at pH 6.0 and 5 ºC with 512 transients shows the existence of a second set of peaks with greatly reduced signal intensity (Fig. 4.13B). These peaks display similar chemical shifts than the second set of peaks observed for REDPRO rrPar-4LZ (Fig. 4.13B), rrPar-4LZD305K (Fig. 4.12B) or rrPar-4LZ at pH 4 (Fig. 4.9C). For clarity, these peaks are marked by black boxes in the corresponding spectra. These observations are consistent with the above proposed slow chemical exchange between DOM and POD conformations.

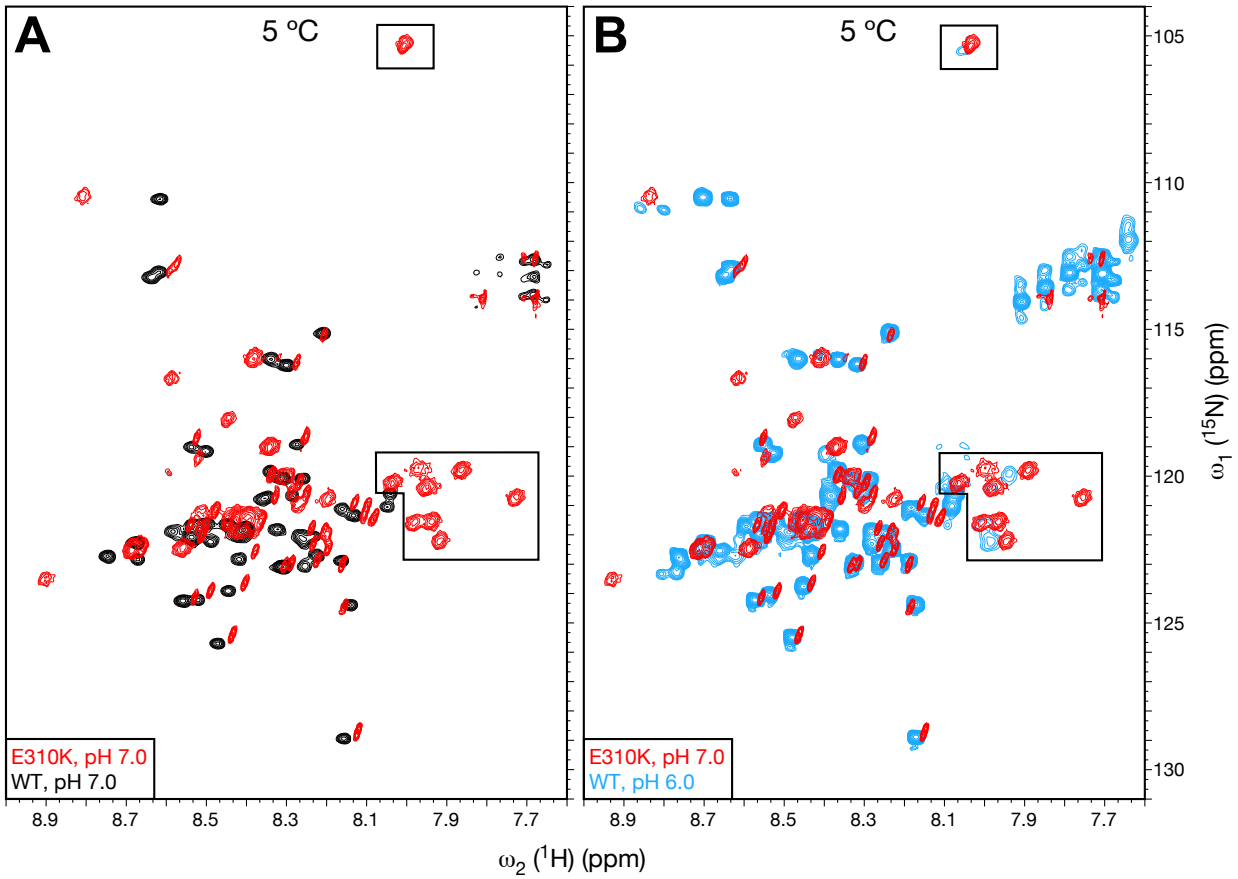

Figure 4.13 *– A second set of peaks exist in the NMR spectra of the Par-4 LZ peptides. (A) Pairwise overlay of the $^{1}H,^{15}N$-SOFAST-HMQC spectrum of rrPar-4LZ at pH 7.0 (black contours) and the $^{1}H,^{15}N$-TROSY-HSQC spectrum of rrPar-4LZE310K at pH 7.0 (red contours) (B) Comparison of the $^{1}H,^{15}N$-TROSY-HSQC spectrum of rrPar-4LZE310K at pH 7.0 (red contours) and the $^{1}H,^{15}N$-SOFAST-HMQC spectrum of rrPar-4LZ at pH 6.0 acquired with 512 transients (blue contours). Selected peaks associated with the POD conformation are marked by black boxes. The black arrow indicates representative peaks associated with the DOM conformation. All samples were uniformly ^{15}N-labelled and contained 5% D_2O (v/v) in the sample buffer. Sample conditions were 75 µM rrPar-4LZ in 20 mM NaCl, 10 mM Tris, pH 7.0; 40 µM rrPar-4LZ in 20 mM NaCl, 10 mM Mes, pH 6.0; and 300 µM rrPar-4LZE310K in 20 mM NaCl, 10 mM Tris, pH 7.0. All spectra were acquired at 5 ºC, further acquisition parameters are given in Appendix G. The spectrum of REDPRO rrPar-4LZE310K at pH 7.0 was apodised using a shifted (π/5) sinusoidal function in F2 and a shifted (π/2) squared sinusoidal bell function in F1. The abbreviations WT, D305K and E310K denote rrPar-4LZ, rrPar-4LZD305K and rrPar-4LZE310K, respectively.*

The total peak number for REDPRO rrPar-4LZE310K was estimated with 64 peaks (see above). Since rrPar-4LZE310K contains only 51 residues, this suggests that only some residues are in slow exchange with a second conformation. However, an isodichroic point is observed for this peptide by CD spectropolarimetry (Fig. 4.2F), indicating that interconversion is only between two states without significantly populated intermediates. This implies that separate sets of peaks arise from the DOM and POD fractions. However, spectral overlap may masks some peaks from both fractions. The N-terminus of the Par-4 LZ peptides is predicted to be disordered and may thus possess distinct NMR properties relative to the C-terminal residues involved in coiled coil formation. It is therefore possible that some of the observed peaks are not in a slow exchange between DOM and POD conformations, but in an intermediate to fast exchange. This may result in missing peaks due to line broadening or in averaged NMR signals. It may therefore be necessary to assign the additional peaks and also obtain additional ^{15}N-relaxation experiments for a better characterisation of the involved exchange processes. However, chemical shift assignment of these additional peaks appears to be a challenging task, due to the narrow chemical shift dispersion of the Par-4 LZ peptides, resulting in peak overlap. The low signal intensity of the POD-associated peaks (rrPar-4LZ at pH 6.0 and 5 ºC) and a low resolution due to severe line broadening (e.g. rrPar-4LZ at pH 4.4, rrPar-4LZD305K at pH 7.0) are further factors limiting an assignment approach. Furthermore, it may be necessary to obtain kinetic data for the strand exchange rates of the Par-4 LZ coiled coils. This kinetic data should then be analysed for consistency with the proposed slow exchange process between DOMs and PODs.

The {^{1}H,^{15}N}-NOEs of ~0.6 obtained for the broad peaks of the POD fraction of REDPRO rrPar-4LZE310K indicate that the backbone of the respective residues is of moderate rigidity. For stable secondary structure, and usually for coiled coils, {^{1}H}^{15}N-NOEs of approximately 0.8 are observed [262,263]. These results are in contrast to CD spectropolarimetry results indicating a stable coiled coil conformation (Fig. 4.2F). Consistent with a less rigid coiled coil, peaks of the coiled coil POD fraction are affected by line broadening (Fig. 4.13A). It is not known what causes the line broadening, but together with the {^{1}H}^{15}N-NOE values these results suggest that the coiled coil dimer experiences some kind of destabilisation. This destabilisation may be a result of internal motions within the coiled coil fraction. Various residues within the Par-4 LZ sequence have been described in Chapter 4.1.2. to be detrimental for coiled coil stability. The decrease in stability conferred by these residues may allow for internal motions and may thus cause the peaks of the POD fraction to broaden. As such important residues two asparagine residues (Asn 313 and Asn 320, Fig. 4.1) were identified. The influence of Asn 313 on coiled

coil stability will be described in Chapter 4.5.2. However, other acidic residues, such as the aspartate patch (Fig. 4.1E), may also be critical for the coiled coil destabilisation, as the LZ point mutants show a slight increase in stability with decreasing pH [185]. One may propose that the coiled coil conformation of the Par-4 LZ peptides displays properties of a molten-globule. Like a molten-globule, coiled coil Par-4 LZ peptides contain secondary structure, but also possess a significant degree of flexibility. However, the current data is not sufficient to call the coiled coil state of rrPar-4LZE310K a molten-globule, and hence this conformation is described in this document as a predominantly ordered dimer (POD).

In summary, while coiled coil formation of the Par-4 LZ domain is observed by CD spectropolarimetry, NMR spectroscopy and other techniques suggest that the formed coiled coils are, at least under certain conditions, transient in nature and in equilibrium with disordered monomers. However, the coiled coil dimers are less stable relative to well-characterised leucine zipper model peptides, and are therefore more appropriately described as predominantly ordered. Destabilisation of the Par-4 LZ coiled coil is probably related to sequence peculiarities within the Par-4 LZ sequence. The data further suggest that chemical exchange between DOMs and PODs is slow on the NMR time scale.

4.4. The effect of TFE on coiled coil formation of rrPar-4LZ

4.4.1. Materials and Methods

a) Sample preparation

Samples of rrPar-4LZ were prepared at neutral pH with increasing concentrations of d^3-TFE from 10-30% ($^v/_v$) (Table 4.5). As described in Chapter 4.2.1.a, the H_2O-dissolved rrPar-4LZ was diluted in appropriate buffer to give a final peptide concentration of 75 µM. Addition of d^3-TFE to 20 mM NaCl, 10 mM Tris, pH 7.0 resulted in a pH decrease to approximately 5. Therefore buffer and TFE were mixed in advance, neutralised and than used to dilute the rrPar-4LZ aliquot. For sterility reasons, pH values were measured with suitable pH paper strips. The same samples were used for CD and NMR spectroscopy.

b) Circular Dichroism

CD spectra were recorded in 1 nm steps from 260 to 190 nm as described in Chapter 3.4.1.a. Acquisition parameters are given in Appendix F. Spectral deconvolution was performed with the algorithms Selcon3 [267] and CONTIN-LL [213] through the DICHROWEB interface.

	rrPar-4LZ peptide concentration	Buffer composition
a)	75 µM	20 mM NaCl, 10 mM Tris, pH 7 + 10% d^3-TFE ($^v/_v$)
b)	75 µM	20 mM NaCl, 10 mM Tris, pH 7 + 20% d^3-TFE ($^v/_v$)
c)	75 µM	20 mM NaCl, 10 mM Tris, pH 7 + 30% d^3-TFE ($^v/_v$)
d)	75 µM	20 mM NaCl, 10 mM Tris, pH 5 + 30% d^3-TFE ($^v/_v$)

Table 4.5 *− Sample conditions of rrPar-4LZ with increasing concentrations of TFE.*

c) NMR spectroscopy

NMR experiments were performed on a Bruker Avance 700 MHz spectrometer as described in Chapter 3.4.1.b. ^1H,^{15}N-correlation spectra are acquired on 300 µl samples in D_2O matched Shigemi NMR tubes. All samples were uniformly ^{15}N-labelled and contained 5% D_2O ($^v/_v$) in the sample buffer. All spectra were recorded at 5 ºC and 25 ºC. The carrier frequency was set to the frequency of the water resonance in the ^1H dimension. Further acquisition parameters are given in Appendix G. Spectra were processed and referenced as described in Chapter 3.4.1.b. using a shifted (π/2) squared sinusoidal bell function for apodisation.

4.4.2. Results and Discussion

Due to the problems associated with conformational exchange in the NMR spectra of the Par LZ peptides (see previous chapter), alternative methods were sought to stabilise the coiled coil conformation. The additive TFE has been described to stabilise secondary structures such as α-helices [140]. Under certain conditions TFE was able to induce dimerisation and trimerisation of amphipathic α-helical peptides [268]. It was therefore thought that TFE might stabilise the α-helical coiled coil fraction, and also reduce exchange with the disordered fraction. However, it was demonstrated previously that TFE is able to disrupt tertiary and quaternary structures. Dependent on the concentration, TFE can dissociate coiled coils into monomeric forms [142,269]. The rationale was therefore to test if TFE can induce a transition from the disordered to an α-helical state of rrPar-4LZ. It was further interesting to analyse if TFE would allow for self-association of rrPar-4LZ, or conversely would disrupt the coiled coils. As TFE has also been described to affect conformational exchange equilibria and shift these to time scales that may allow structural characterisation by NMR [140,223], a potential improvement of the NMR spectra was another rationale for using TFE.

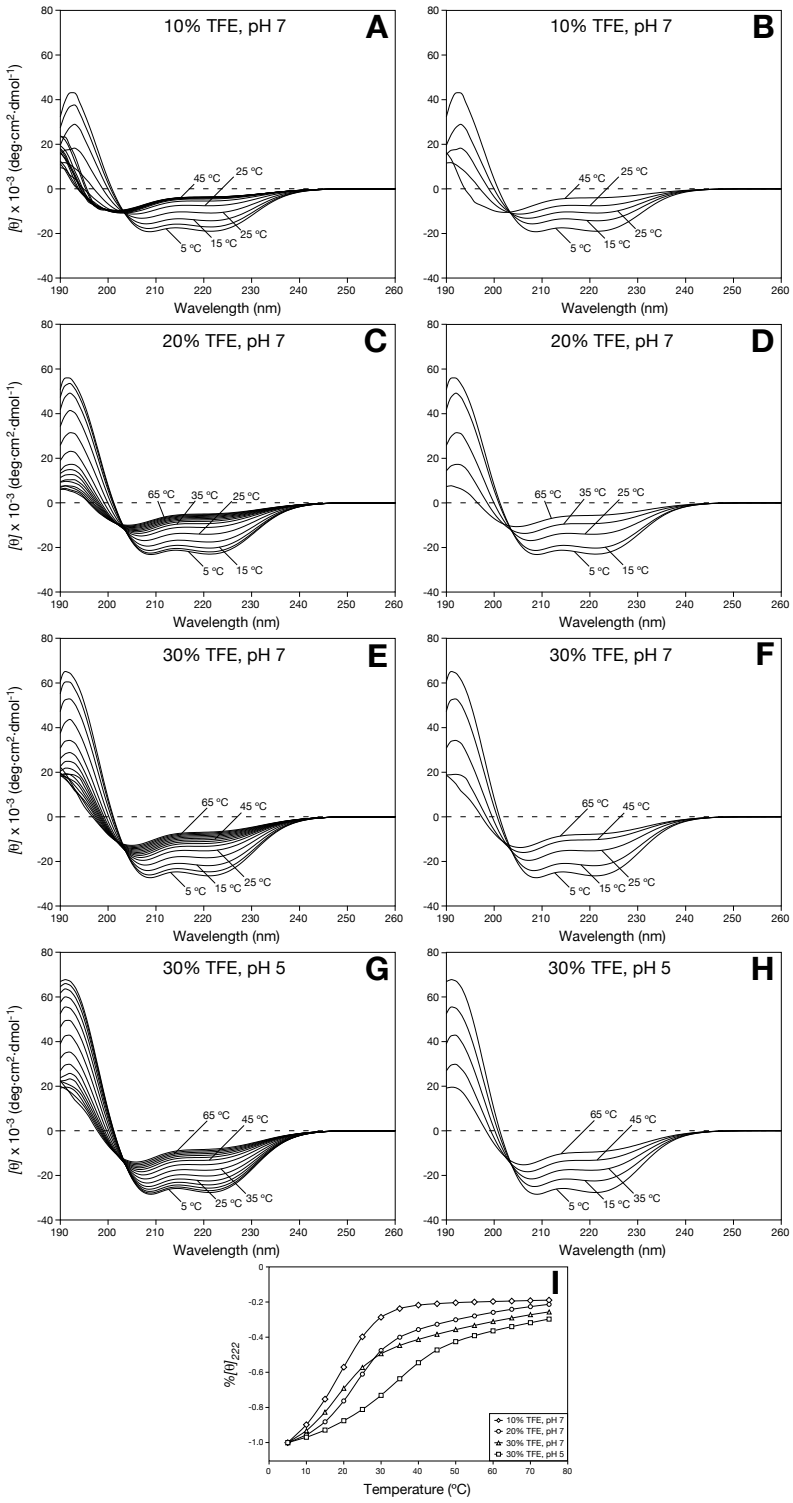

Figure 4.14 *− CD spectropolarimetry of rrPar-4LZ under various TFE concentrations. Temperature dependence of the CD spectra of rrPar-4LZ at pH 7 with (A, B) 10% d³-TFE (v/v), (C, D) 20% d³-TFE (v/v), and (E, F) 30% d³-TFE (v/v). The influence of pH on the CD spectrum at 30% d³-TFE (v/v) at pH 5 is shown in panels (G) and (H). All spectra were acquired in 5 ºC intervals over a temperature range of 5-75 ºC and traces for each temperature are shown in panels A, C, E and G. For clarity panels B, D, F and H show traces of five evenly spaced temperatures. (I) Thermal stability of rrPar-4LZ under various TFE concentrations showing the %$[\theta]_{222}$ values as a function of temperature. The %$[\theta]_{222}$ values were obtained by normalising the $[\theta]_{222}$ values at each temperature to the corresponding $[\theta]_{222}$ value at 5 ºC. Acquisition parameters are given in Appendix F. Sample concentrations are listed in Table 4.5.*

CD spectra of rrPar-4LZ in TFE are shown in Figure 4.14. Significant α-helical character is obvious at 5 ºC under all TFE concentrations. However, at 25 ºC α-helicity is only observed for 30% TFE, pH 5 (Fig. 4.14G). The spectrum at 10% TFE, pH 7 and 25 ºC suggests a mostly disordered state (Fig. 4.14A), with moderate α-helicities at 20% and 30% TFE at pH 7 (Figs. 4.14C-F). This indicates that TFE stabilises an α-helical conformation of rrPar-4LZ at neutral pH as opposed to similar conditions without TFE (Fig. 4.2A). Spectral deconvolution further demonstrates an increase in α-helicity with increasing TFE concentrations and decreasing temperatures (Table 4.6). The Selcon3 algorithm suggests an increase in α-helicity at 5 ºC from 58% (10% TFE, pH 7) to 82% (30% TFE, pH 5). Similarly at 25 ºC, the α-helical content increases from 23% (10% TFE, pH 7) to 69% (30% TFE, pH 5). It is further evident from these results that under identical TFE concentrations an acidic pH contributes to increased stability over neutral pH values. This is consistent with the previous notion that acidic residues within the Par-4 LZ domain are critical for coiled coil stability. It should be noted that for the Selcon3 algorithm the fits between calculated and experimental data are not optimal. NRMSD values above 0.25 are usually regarded as to constitute an error in the analysis procedure and values less than 0.1 should be aimed for [182]. Better NRMSD values are obtained using the CONTIN-LL algorithm (Table 4.6). Apart from slight differences at 25 ºC and for 10% TFE, pH 7 the deconvolution results from the CONTIN-LL algorithm are similar to the results from the Selcon3 algorithm. Note that the overall increase in α-helicity with increasing TFE concentrations is not as well reflected in the deconvolution results from the CONTIN-LL algorithm.

Despite this clear increase in α-helicity with increasing TFE concentration, the gain in thermal stability is only small (Fig. 4.14I). At neutral pH the T_m value increases from 20 ºC (10% TFE) to 25 ºC (20% TFE) (Table 4.7). Interestingly, at pH 7 rrPar-4LZ is more stable in 20% TFE than in 30% TFE. A further increase is observed at 30% TFE, pH 5 with a T_m value of 35 ºC (Table 4.7). However, these values are significantly lower than the thermal stabilities observed for rrPar-4LZ at pH 4 ($T_m \approx 50$ ºC) and rrPar-4LZD305K at pH 7.0 ($T_m \approx 45$ ºC) (Fig. 4.3B). This indicates that the latter two conditions are more stable and probably better suited for structural analysis than rrPar-4LZ in TFE. This is corroborated by the supercoiling status. The $[\theta]_{222}/[\theta]_{208}$ ratios of rrPar-4LZ in TFE are shown in Table 4.7. No stable supercoiling is indicated for all tested TFE concentrations. In particular at 25 ºC, the $[\theta]_{222}/[\theta]_{208}$ ratios suggest mainly monomeric states. Again this indicates that addition of TFE does not result in a greater stability of the coiled coil relative to rrPar-4LZ at pH 4 or rrPar-4LZD305K at pH 7.0 (Figs. 4.2D and E). As mentioned earlier, $[\theta]_{222}/[\theta]_{208}$ ratios above one indicate supercoiling whereas values below 0.9 are usually

interpreted as non-interacting helices (see Ref. [142] and references therein). Therefore, the observed $[\theta]_{222}/[\theta]_{208}$ ratios at 5 ºC, which are close to 1, suggest a more dynamic equilibrium between α-helical and disordered states relative to rrPar-4LZ at pH 4 and rrPar-4LZD305K. Note that rrPar-4LZ in 30% TFE has a similar helical content to rrPar-4LZ at pH 4 or rrPar-4LZD305K at pH 7.0 (compare Figs. 4.2D and E with Figs. 4.14E and G). However, the $[\theta]_{222}/[\theta]_{208}$ ratios between 1.0 and 0.9 suggest a more dynamic interconversion between disordered and α-helical states for rrPar-4LZ in 30% TFE. Additionally, in the presence of TFE the transition between α-helical and unfolded states appears to be of complex nature, as no well-defined isodichroic points are observed (Figs. 4.14E and G).

	α-helix (NRMSD)			
	Selcon3		CONTIN-LL	
Buffer composition	**5 ºC**	**25 ºC**	**5 ºC**	**25 ºC**
0% TFE, pH 7.0	18% (0.172)	13% (2.103)	18% (0.058)	9% (0.63)
0% TFE, pH 6.0	53% (0.219)	22% (0.258)	74% (0.082)	22% (0.058)
10% TFE, pH 7.0	58% (0.157)	23% (0.373)	71% (0.077)	24% (0.084)
20% TFE, pH 7.0	68% (0.121)	46% (0.256)	69% (0.030)	56% (0.084)
30% TFE, pH 7.0	79% (0.120)	49% (0.280)	83% (0.023)	60% (0.097)
30% TFE, pH 5.0	82% (0.096)	69% (0.121)	81% (0.014)	74% (0.023)

Table 4.6 *– Influence of increasing TFE concentrations on the α-helicity of rrPar-4LZ. Spectral deconvolution was performed using the algorithms Selcon3 [267] and CONTIN-LL [213]. For simplicity, only the combined percentage of regular and distorted α-helix is shown. The NRMSD value is given in brackets as a quality parameter for each deconvolution. The corresponding CD spectra are shown in Fig. 4.14 and sample concentrations are given in Table 4.5. The results of rrPar-4LZ at pH 7.0 and 6.0 without TFE are used for comparison. The corresponding CD spectra are shown in Figs. 4.2A and C. Sample concentrations for these two peptides were 75 µM rrPar-4LZ in 20 mM NaCl, 10 mM Tris, pH 7.0 and 40 µM rrPar-4LZ in 20 mM NaCl, 10 mM Mes, pH 6.0.*

TFE can dissociate coiled coils into monomers, and CD data suggests that TFE concentrations of 30% start to disrupt the coiled coil state of rrPar-4LZ at pH 7. Thermal stabilities and $[\theta]_{222}/[\theta]_{208}$ ratios are reduced in the presence of 30% TFE relative to 20% TFE (Table 4.7). DLS measurements to determine the hydrodynamic properties of rrPar-4LZ in TFE were performed; however, measurements were unstable and the results of poor quality. This also indicates a very dynamic behaviour of rrPar-4LZ in TFE. Due to the poor quality and great uncertainties in the

data, no DLS results are shown here. However, using TFE had another potentially positive outcome. Previous attempts to study rrPar-4LZ at pH 5 resulted in protein precipitation. Due to the well known ability of TFE in solubilising proteins and peptides [140], no precipitation was observed allowing the analysis of rrPar-4LZ at pH 5 by CD and NMR spectroscopy. This ability of TFE may prove useful for other possibly coiled coil Par-4 constructs that are prone to precipitate. However, suitable TFE concentrations need to be tested that do not completely disrupt the oligomeric state.

		$[\theta]_{222}/[\theta]_{208}$ ratio	
Buffer composition	T_m	**5 ºC**	**25 ºC**
no TFE, pH 7.0	N/A	0.45	0.40
no TFE, pH 6.0	18 ºC	0.91	0.59
10% TFE, pH 7	20 ºC	0.99	0.72
20% TFE, pH 7	25 ºC	1.00	0.83
30% TFE, pH 7	22 ºC	0.97	0.78
30% TFE, pH 5	35 ºC	0.98	0.90

Table 4.7 *– Thermal stability and supercoiling of rrPar-4LZ under various TFE concentrations. Influence of increasing TFE concentrations on the T_m value and the $[\theta]_{222}/[\theta]_{208}$ ratio of rrPar-4LZ. Ratios above 1.0 are indicative of supercoiling. T_m values and $[\theta]_{222}/[\theta]_{208}$ ratios were calculated from the CD spectra shown in Figure 4.14. Protein concentrations and buffer conditions are given in the legend to Table 4.5. The results of rrPar-4LZ at pH 7.0 and 6.0 without TFE are used for comparison. The corresponding CD spectra are shown in Fig. 4.2A and C. Sample concentrations for these two peptides were 75 µM rrPar-4LZ in 20 mM NaCl, 10 mM Tris, pH 7.0 and 40 µM rrPar-4LZ in 20 mM NaCl, 10 mM Mes, pH 6.0.*

Despite the increase in α-helicity with TFE, an improvement of the NMR spectra could not be achieved. The deconvolution algorithms predict a similar α-helical content for rrPar-4LZ in 10% TFE, pH 7 and for rrPar-4LZ at pH 6.0 without TFE (Table 4.6). Apart from slight shift differences, which are probably due to TFE, almost identical NMR spectra are obtained under both conditions at 5 ºC (Fig. 4.15A) and 25 ºC (data not shown). As was discussed for rrPar-4LZ at pH 6.0 in the previous chapter, the NMR spectrum of rrPar-4LZ in 10% TFE, pH 7 displays no obvious signs of secondary structure. Interestingly, the additional peaks Gly -2* and Ser -1* (Fig. 4.9A) are also visible in the 10% TFE, pH 7 spectrum at 5 ºC. These peaks have been discussed above as belonging to the N-terminus of the POD conformation. As observed for

rrPar-4LZ at pH 6.0, the intensity of these two peaks is temperature dependent and thus significantly decreased at 25 ºC (data not shown). These results suggests that the majority of the peaks observed for rrPar-4LZ in 10% TFE, pH 7 represent the DOM fraction, and most peaks of the POD conformation are of low intensity, and therefore hidden in the noise.

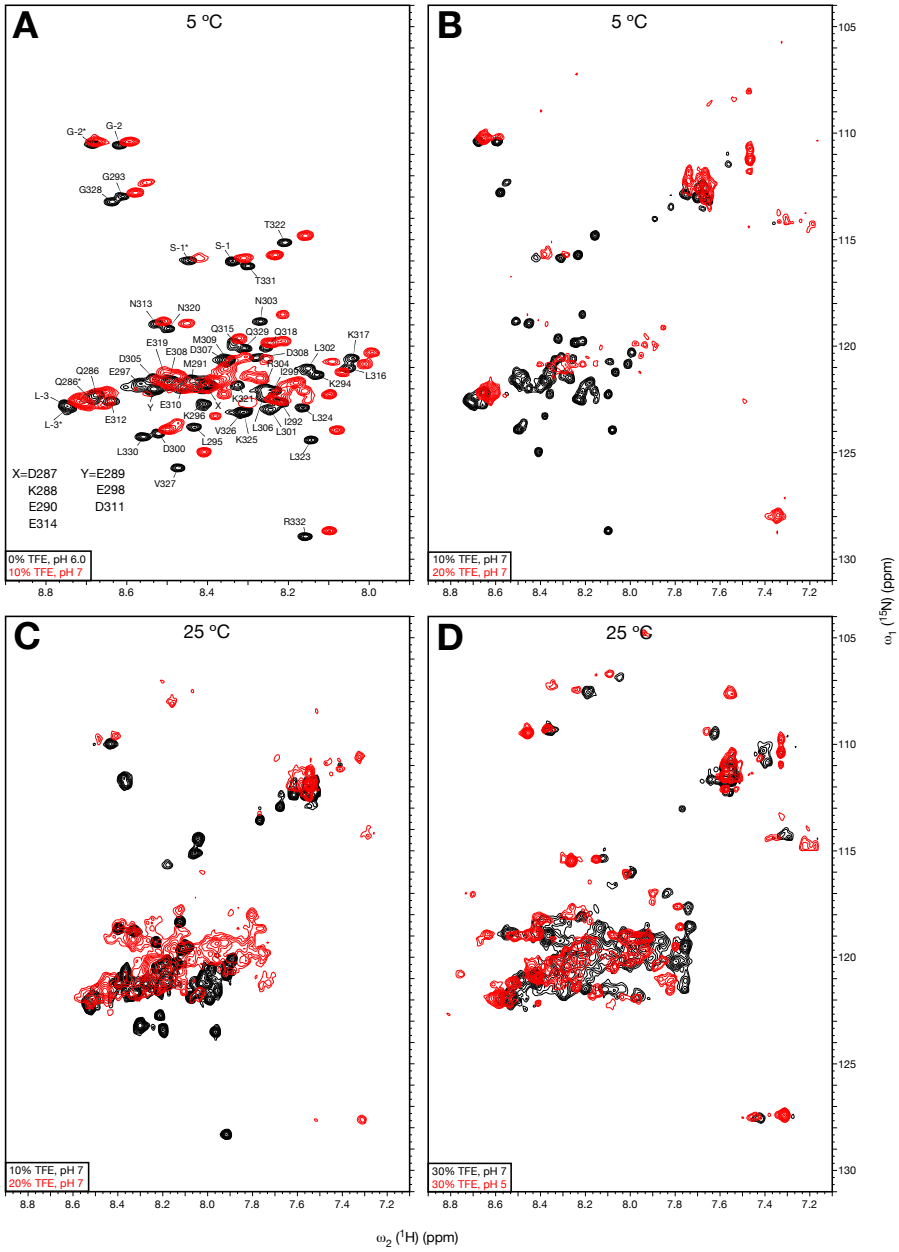

Figure 4.15 *– $^{1}H,^{15}N$-SOFAST-HMQC spectra of rrPar-4LZ at various TFE concentrations. (A) Pairwise overlay of the NMR spectra at 5 ºC of rrPar-4LZ at pH 6.0 (black contours) and rrPar-4LZ at pH 7 + 10% TFE (v/v) (red contours). Assignments are shown for rrPar-4LZ at pH 6.0. (B) Comparison of the NMR spectra at 5 ºC of rrPar-4LZ at pH 7 + 10% TFE (v/v) (black contours) with rrPar-4LZ at pH 7 + 20% TFE (v/v) (red contours) (C) Comparison of the same peptides as in panel (B) but at 25 ºC. (D) Overlay of the NMR spectra at 25 ºC of rrPar-4LZ + 30% TFE (v/v) at pH 7 (black contours) and pH 5 (red contours). All samples were uniformly ^{15}N-labelled and contained 5% D_2O (v/v) in the sample buffer. Sample conditions were 40 µM rrPar-4LZ in 20 mM NaCl, 10 mM Mes, pH 6.0; conditions for the other peptides are given in Table 4.5. Acquisition parameters are given in Appendix G.*

As higher TFE concentrations of 20% and 30% were shown to increase the α-helical content of rrPar-4LZ (Fig. 4.14), better quality NMR spectra were expected. However, as higher TFE concentrations do not confer increased stability, these NMR spectra are severely affected by line broadening and decreased signal intensity. At 5 ºC, where CD spectropolarimetry indicates significant α-helical character, very little signal is detected by NMR (Fig. 4.15B). Not surprisingly, the most intense peaks probably belong to the N- and C-terminal residues Leu -3, Gly -2, Ser -1 and Arg 322, which are probably more flexible than other residues of rrPar-4LZ. Interestingly, Gly -2* and Ser -1* appear to be more intense than Gly -2 and Ser -1 (Fig. 4.15B, for assignments see panel A). The increase in signal intensity at 25 ºC is probably due to a population increase of the DOM fraction (Fig. 4.15C). The peaks are further severely line broadened, but the cause for this line broadening cannot be fully explained at this time. It is possible that line broadening is related to the viscosity increase at higher TFE concentrations [270] affecting the tumbling rate of the molecule. Interestingly, no significant differences are observed in the NMR spectra for rrPar-4LZ in 30% TFE at pH 7 and 5 (Fig. 4.15D). The increased thermal stability observed at pH 5 (Fig. 4.14I) therefore does not result in an improved spectrum. Even though some peaks display an increased chemical shift dispersion and may thus be associated with the ordered fraction, the overall spectral quality is not suitable for further analysis.

In summary, an α-helical fold, as judged by CD spectropolarimetry, is induced by TFE at neutral pH. The α-helical content is dependent on the TFE concentration, but a higher α-helical content does not result in an increased stability of the ordered state. The results further suggest a very dynamic behaviour between disordered and ordered conformations in the presence of TFE. Overall no significant improvement in the NMR spectra was obtained that allowed a structure determination of the Par-4 LZ domain.

4.5. Asparagine residue contributions to Par-4 LZ stability

4.5.1. Materials and Methods

a) Sample preparation

The rrPar-4LZN313I peptide was expressed and purified as described in Chapter 2.11.9. Samples at various pH values were prepared by diluting H_2O-dissolved rrPar-4LZN313I with appropriate buffers (Table 4.8). For samples with pH values below or equal to pH 6.0 the solubility of rrPar-4LZN313I was reduced and precipitation occurred. The precipitate was removed by centrifugation in a tabletop centrifuge and the protein concentration was

remeasured. The same samples were used for CD, DLS and NMR spectroscopy. Sample d (Table 4.8) was only used for NMR spectroscopy.

	rrPar-4LZN313I peptide concentration	Buffer composition
a)	50 µM	20 mM NaCl, 10 mM Tris, pH 7.0
b)	7 µM	20 mM NaCl, 10 mM Mes, pH 6.0
c)	40 µM	H_2O, pH 4
d)	2.5 mM	H_2O, pH 4

Table 4.8 *– Sample conditions of rrPar-4LZN313I at various pH values.*

b) Circular Dichroism

CD spectra were recorded in 1 nm steps from 260 to 190 nm as described in Chapter 3.4.1.a. Acquisition parameters are given in Appendix F. Spectral deconvolution was performed using the algorithms Selcon3 and CONTIN-LL through the DICHROWEB interface.

c) Dynamic Light Scattering

DLS measurements were performed as described in Chapter 3.2.1.a.

d) NMR spectroscopy

NMR experiments were performed on a Bruker Avance 700 MHz spectrometer as described in Chapter 3.4.1.b. ^{1}H,^{15}N-correlation spectra were acquired on 300 µl samples in D_2O matched Shigemi NMR tubes. All samples were uniformly ^{15}N-labelled and contained 5% D_2O ($^{v}/_{v}$) in the sample buffer. All spectra were recorded at 5 ºC and 25 ºC. The carrier frequency was set to the frequency of the water resonance in the ^{1}H dimension. Further acquisition parameters are given in Appendix G. The spectra were processed and referenced as described in Chapter 3.4.1.b. using a shifted ($\pi/2$) squared sinusoidal bell function for apodisation.

4.5.2. Results and Discussion

Despite clear indications of coiled coil formation by CD spectropolarimetry, the poor quality of the NMR spectra of the Par-4 LZ did not allow a structure determination of the coiled coil conformation. In Chapter 4.2.2.b an interconversion between DOM and POD conformations was proposed, and the equilibrium between DOM and POD conformations was shown to be pH dependent. The DOM conformation dominates at neutral pH and the POD conformation at pH 4

(Chapter 4.3.2.). However, NMR spectra at pH 4 showed severe line broadening for the majority of the POD-associated peaks, which prevented a more detailed analysis by NMR. It was suggested that line broadening is due to internal motions within the POD fraction (Chapter 4.3.2.). Stabilisation of the POD conformation, and thus a reduction in line broadening, was investigated as an approach that would allow structure determination. However, a stabilisation of the POD conformation could not be achieved by simple means such as addition of TFE. Therefore, other measures became necessary to stabilise the coiled coil fraction of the Par-4 LZ peptides.

Unlike most other LZ-families (except for the Oasis family) [117] the Par-4 LZ domain contains two asparagine residues at position *a* within its heptad repeats (Figs. 4.1B and C). These residues are proposed to contribute to conformational exchange. Previously, it was demonstrated that asparagine residues contribute to coiled coil stability, not by affecting the association step, but mainly by controlling the dissociation rate of the oligomer [242]. Furthermore, the influence of asparagine residues on coiled coil stability depends on their position in the coiled coil, with asparagine residues at the N-terminus having a greater destabilising effect than asparagine residues at the C-Terminus [243]. Also increasing numbers of asparagines result in decreased coiled coil stability [243]. To test whether the internal asparagine residues contribute to Par-4 LZ stability, the more N-terminal asparagine at position 313 (Fig. 4.1C) was mutated to an isoleucine residue. To preserve the proposed dimeric state (Chapter 4.1.2.) only one of the asparagine residues was mutated at a time. The remaining asparagine would further maintain the specificity of coiled coil formation and prevent the formation of coiled coils in different registers. Isoleucine was preferred over other hydrophobic residues as it strongly promotes a dimeric coiled coil conformation [129]. Unlike valine, which also promotes dimeric conformations, isoleucine contributes to an increased thermal stability due to additional van der Waals interactions between methylene groups of residues at position *a* and *d* [109,129]. The rationale of this mutation approach was to create a Par-4 LZ peptide with a stable coiled coil conformation that would allow structure determination. A stable coiled coil conformation would further serve as a reference state for additional biophysical methods. Analysis of the Par-4 LZ peptides by various techniques, such as SEC or DLS, has been complicated by the conformational exchange between dimeric and monomeric conformations (Chapter 4.2.2.).

As was observed for the Par-4 LZ wild-type rrPar-4LZ, rrPar-4LZN313I is mostly insoluble at pH values below or equal to pH 6.0, but solubility improves around pH 4.0 or below. Not surprisingly, DLS indicates high molecular weight species at pH 6.0 suggesting aggregation

under these conditions (Table 4.9). Aggregation may occur as the pH approaches the pI value of rrPar-4LZN313I. Interestingly, even at pH 7.0 high molecular weight species were detected with approximate R_S values between 32.5-121.8 Å. The species with smaller R_S values predominate at 5 ºC (~80%), whereas at 25 ºC this proportion decreases to ~40%, indicating that at 25 ºC the aggregated species predominate (Table 4.9). In contrast, DLS results obtained at pH 4 are of similar magnitude as observed for rrPar-4LZ (Table 4.4) and indicate low molecular weight species. As mentioned for rrPar-4LZ (Chapter 4.2.2.c), the oligomeric state of the rrPar-4LZN313I coiled coil could not be assessed by DLS. The high R_S values observed at neutral pH may be an artefact of the substitution of the polar asparagine for the hydrophobic isoleucine. Thus, the increased hydrophobic surface might result in non-specific hydrophobic interactions of rrPar-4LZN313I molecules that are not accompanied by coiled coil formation (Fig. 4.16). This indicates that asparagine residues may also be important regulators of aggregation in non-coiled coil conformations preventing the formation of insoluble aggregates *in vivo* [131]. This is consistent with previous notions that substitution of asparagine residues can result in the formation of higher order oligomers [109].

	5 ºC		**25 C**	
Sample condition	***MW***	***R_S***	***MW***	***R_S***
rrPar-4LZN313I peptide	6.0	20.9	6.0	20.9
rrPar-4LZN313I at pH 7.0	64.0/2590	32.5/121.8	97.0/1720	37.7/105.2
rrPar-4LZN313I at pH 6.0	N/A	4125	N/A	13350
rrPar-4LZN313I at pH 4	8.2	15.6	N/A	N/A

Table 4.9 *– DLS-determined hydrodynamic properties of rrPar-4LZN313I. MW (kDa) and R_S (Å) values were calculated using the equation $\log(R_S) = 0.357*\log(MW) - 0.204$ in reference to a spherical conformation [181]. The mode R_S values of each measurement are shown. For comparison, theoretical values for a* ***urea unfolded state*** *of rrPar-4LZN313I calculated from the amino acid sequence are also provided. Sample conditions are given in Table 4.8. Note that calculated MWs for rrPar-4LZN313I at pH 6.0 are in the GDa range and therefore omitted.*

Coiled coil formation of rrPar-4LZN313I is strongly suggested by CD spectropolarimetry (Fig. 4.16). As was observed for rrPar-4LZ, coiled coil formation occurred predominantly at acidic pH and low temperature. Consistent with these results, only weak α-helical character of approximately 40% (average of both deconvolution algorithms) is observed at neutral pH and

5 ºC for rrPar-4LZN313I (Fig. 4.16A). This character is significantly stronger than observed for the wild-type rrPar-4LZ (Fig. 4.2A) suggesting that Asn 313 significantly affects coiled coil formation. In contrast to rrPar-4LZ where no T_m value could be estimated, a T_m value of ~15 ºC is determined for rrPar-4LZN313I at neutral pH (Fig. 4.16G). Consistent with the increased α-helicity of rrPar-4LZN313I at pH 7.0, a significantly increased α-helical content and thermal stability is observed at pH 6.0 (Fig. 4.16C) relative to rrPar-4LZ (Fig. 4.2C). However, DLS indicates large soluble aggregates under these conditions suggesting that the increased stability may be related to aggregation.

Strong α-helical character and a greatly increased thermal stability are also observed at pH 4 (Fig. 4.16E). The α-helical content under these conditions is estimated at approximately 90%. A T_m value could not be determined as it is outside the probed temperature range of 5-75 ºC (Fig. 4.16G). Note that DLS indicates that this increased thermal stability is not due to aggregation. The CD spectrum further suggests coiled coil formation with $[\theta]_{222}/[\theta]_{208}$ ratios above one until 25 ºC. This is somewhat surprising as it is similar to the behaviour observed for rrPar-4LZ at pH 4 (Fig. 4.2D) despite a greatly increased thermal stability. However, for rrPar-4LZN313I this ratio remains above 0.9 until 65 ºC thus suggesting an equilibrium between disordered and ordered conformations under these conditions, with the ordered fraction representing the major population. The well-defined isodichroic point at 203 nm further suggests a two-state transition (Fig. 4.16E).

CD spectropolarimetry shows that at 5 ºC and pH 7.0 both rrPar-4LZ (Fig. 4.2A) and rrPar-4LZN313I (Fig. 4.16A) are mostly disordered. As expected, the corresponding NMR spectra are almost identical (Fig. 4.17A). Shift differences for residues neighbouring Asn 313 (e.g. Glu 312, Gln 315 or Leu 316) probably arise due to substitution of the polar asparagine residue by the hydrophobic isoleucine residue. Due to aggregation (see above) and resulting sensitivity limitations spectra of rrPar-4LZN313I at pH 6.0 are not shown. Despite the clear increase in thermal stability of rrPar-4LZN313I at pH 4 relative to rrPar-4LZ, the corresponding NMR spectrum at 25 ºC is still affected by severe line broadening and low sensitivity. Relative to the wild-type rrPar-4LZ at pH 4 the ^{1}H chemical shift dispersion is only marginally increased, however, the intensity for the majority of peaks is further deceased. Interestingly, two sets of peaks seem to exist for Gly -2, Ser -1 and Arg 322 (Fig. 4.17B, for assignments compare with panel A) suggesting that at least two different conformations exist under these conditions. These two separate sets may be due to exchange of ordered and disordered conformations on a slow NMR time scale or alternatively due to the formation of a non-symmetric dimer/oligomer.

However, a more definitive analysis would require a chemical shift assignment, which was not possible due to the poor quality of the NMR spectra.

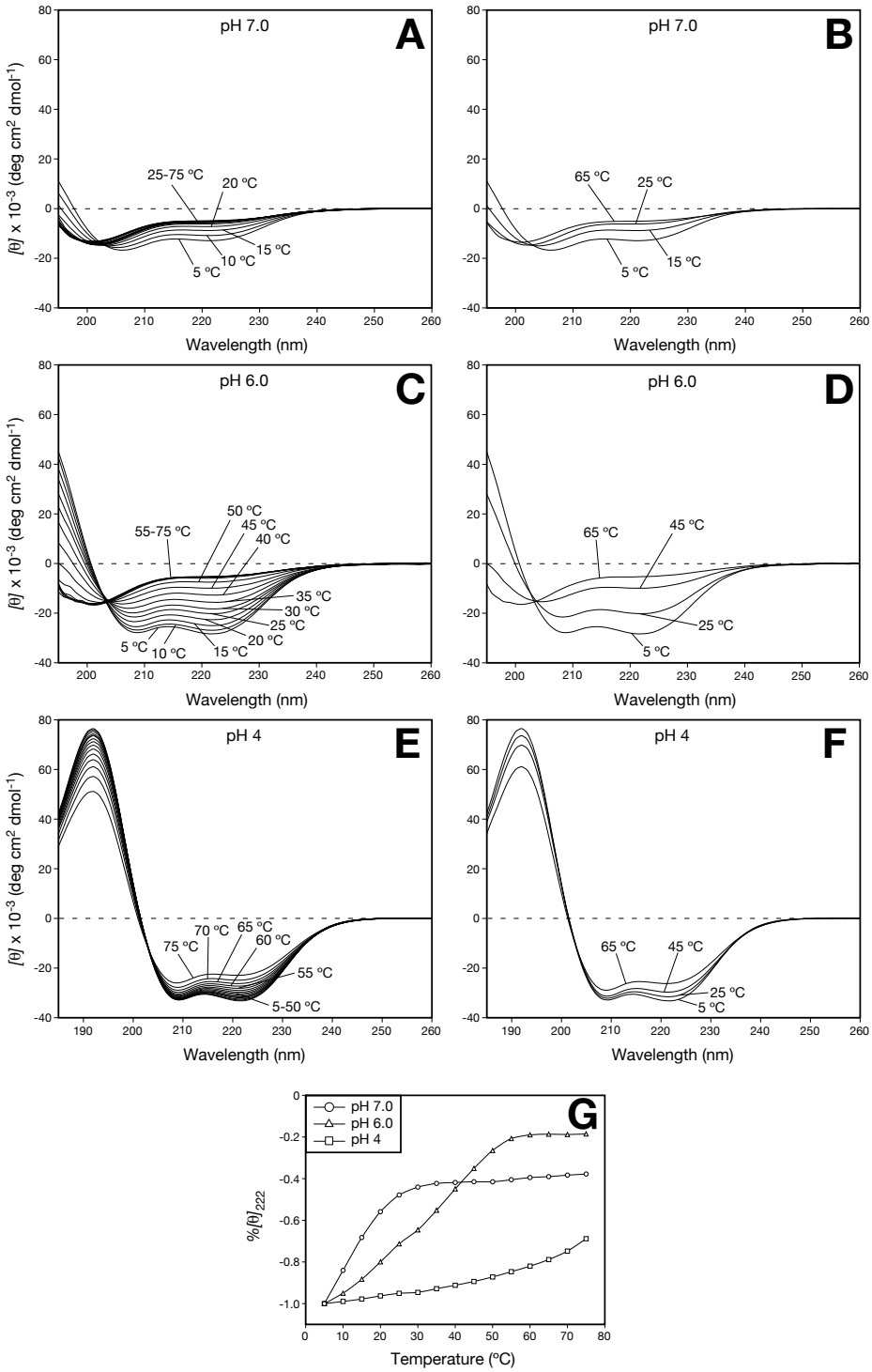

Figure 4.16 *− CD spectropolarimetry of rrPar-4LZN313I. Temperature dependence of the CD spectra of rrPar-4LZN313I at (A, B) pH 7.0, (C, D) pH 6.0, and (E, F) pH 4. The complete temperature series is shown in panels A, C, and E. For clarity, four evenly spaced temperature series are shown in panels B, D, and F. (G) Thermal stability of rrPar-4LZ at various pH values showing the %$[\theta]_{222}$ values as a function of temperature. The %$[\theta]_{222}$ values were obtained by normalising the $[\theta]_{222}$ values at each temperature to the corresponding $[\theta]_{222}$ value at 5 ºC. Sample conditions are given in Table 4.8. Acquisition parameters are given in Appendix F.*

To circumvent the sensitivity problem, an additional sample of rrPar-4LZN313I at pH 4 with a concentration of 2.5 mM was prepared. The corresponding spectrum shows an improved sensitivity (Fig. 4.17C), but is otherwise still of poor quality. At 25 ºC, a significant peak overlap is observed and a conservative peak counts estimates at least 120 peaks. The situation is further worsened by line broadening. Eventual NMR experiments such as chemical shift assignment or relaxation measurements would be extremely challenging under such conditions. Note that no DLS data is available for this sample and some of the observed problems may be attributed to aggregation, which cannot be excluded at the high Par-4 LZ concentration, in particular for rrPar-4LZN313I which is prone to aggregate. However, it is possible that spectra of higher quality are obtained at an intermediate concentration and that NMR spectra of rrPar-4LZN313I benefit from deuteration.

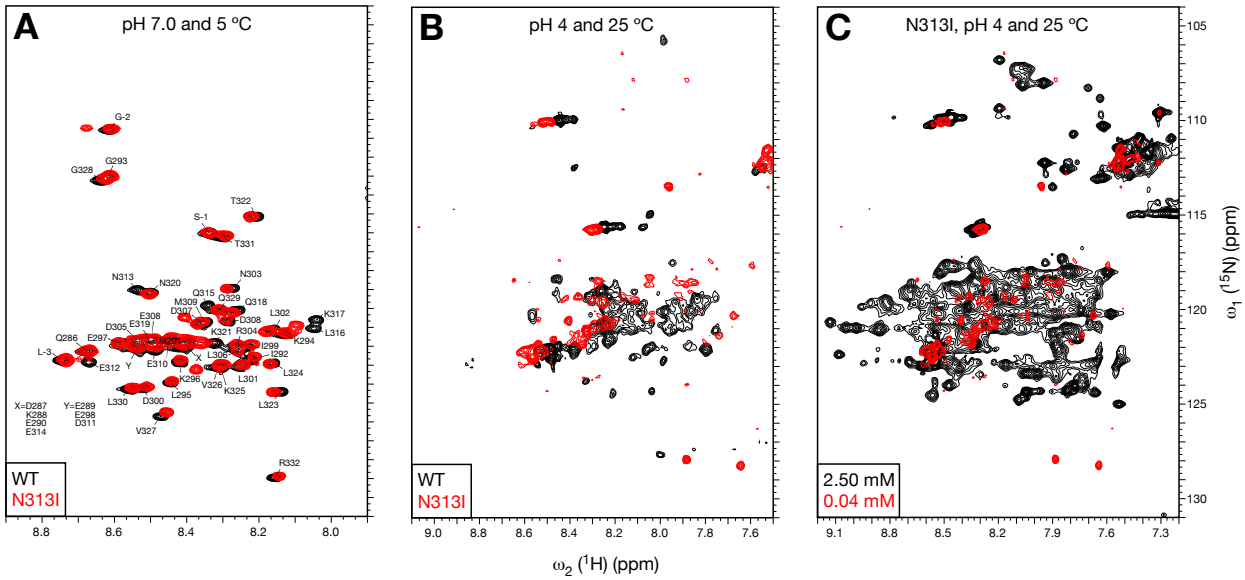

Figure 4.17 *– NMR spectroscopy of rrPar-4LZN313I. Pairwise overlay of the $^{1}H,^{15}N$-SOFAST-HMQC spectra of rrPar-4LZ (black contours) and rrPar-4LZN313I (red contours) at (A) 5 ºC and pH 7.0, and (B) 25 ºC and pH 4. (C) Concentration dependence of the $^{1}H,^{15}N$-correlation spectra of rrPar-4LZN313I at 25 ºC and pH 4. Displayed are the $^{1}H,^{15}N$-HSQC spectrum acquired at a concentration of 2.5 mM (black contours) and the $^{1}H,^{15}N$-SOFAST-HMQC spectrum acquired at a concentration 40 µM (red contours). All samples were uniformly ^{15}N-labelled and contained 5% D_2O (v/v) in the sample buffer. Sample conditions were 75 µM rrPar-4LZ in 20 mM NaCl, 10 mM Tris, pH 7.0 and 50 µM rrPar-4LZ in MQ-H_2O, pH 4. For rrPar-4LZN313I conditions see Table 4.8. Acquisition parameters are given in Appendix G.*

Data presented here suggest that the asparagine residue at position *a* within rrPar-4LZ affects coiled coil stability, resulting in decreased thermal stability relative to hydrophobic residues such as isoleucine. For rrPar-4LZ at pH 4, a T_m value of approximately 50 ºC (Fig. 4.3A) is obtained

that is significantly lower than the T_m value (> 75 ºC) for rrPar-4LZN313I (Fig.4.16G). Despite this clear difference in thermal stability, the corresponding NMR spectra of both peptides are very similar and of poor quality. It is currently not known what causes the poor NMR spectroscopic properties of the Par-4 LZ peptides, as NMR solution structures of coiled coils of similar length have been described in the literature (e.g. rJun leucine zipper [246], FIP2 [264], or the N-terminus of the nucleocapsid protein of the Andes Hantavirus [265]). These peptides produce sharper and better dispersed $^{1}H,^{15}N$-correlation spectra relative to the Par-4 LZ peptides. However, the lack of chemical shift dispersion for Par-4 may be related to the absence of aromatic residues that could induce a greater dispersion due to ring current effects. Interestingly, for the rJun leucine zipper a similar T_m value of 52 ºC relative to rrPar-4LZ at pH 4 was determined. Note that this T_m value was measured on a four to five times less concentrated sample (pH 3.6, 15 µM rJun concentration). It is possible that rJun produces better NMR spectra than rrPar-4LZ, as the rJun dimer was stabilised through an intermolecular disulfide bond at the N-terminus [246]. This covalent linkage of the rJun dimer may reduce the conformational exchange between disordered monomers and ordered dimers. Such a conformational exchange was proposed above for rrPar-4LZ and rrPar-4LZN313I. Mutation of asparagine residues at position *a* of the heptad to hydrophobic residues has been demonstrated to decrease conformational exchange [138], and an improvement of the NMR spectra was therefore expected. However, the observed line broadening for rrPar-4LZN313I indicates that conformational exchange continues. Also the low pH conditions should have resulted in a decrease in conformational exchange, as pH 4 was shown to be more stabilising than mutation of either Asp 305 or Glu 310 to lysine residues in mitigating the repulsive electrostatic interactions (Fig. 4.3B). An alternative explanation for the observed line broadening may be that due the propensity of rrPar-4LZN313I to aggregate it is in exchange between different oligomeric coiled coil states (e.g. between dimer and tetramers).

Taken together, more than three and a half years were spent on trying to optimise the NMR conditions for the Par-4(286-332) peptide with little success. Even the latest N313I mutant, which showed favourable stability by CD spectropolarimetry, was not amenable to NMR. It is questionable if further improvements can be achieved by mutation such as an N313I, D305K double mutant. Such constructs may profit from additional van der Waals interactions[185], but should still be analysed at acidic pH to mitigate destabilising interactions from an aspartate patch in the Par-4 LZ domain (Chapter 4.1.2.). These aspartate residues are therefore also prime candidates for mutation. Substitution of aspartates such as Asp 307 or Asp 311 by arginine could

increase the stability of the Par-4 LZ domain by introducing new intrahelical salt bridges and mitigating some of the intrahelical electrostatic repulsion. Also the helix-forming propensity of arginine is higher than for aspartate [241]. It is further possible to remove the Met 309 residue by mutation and replace it by a leucine to increase coiled coil stability. Methionine is occasionally found at position *d* [117], but might interfere with packing of the side chains in the hydrophobic interface. However, any mutation will lead further away from the wild-type sequence. It was demonstrated in Chapter 1.2.1 that the Par-4 LZ domain is highly conserved in vertebrates (Fig. 1.1). This suggests that most residues are essential for the Par-4 function, even though some of them may be detrimental to coiled coil formation. The D305K, E310K and N313I mutants were created to stabilise the coiled coil fraction and allow structure determination of the Par-4 LZ domain. To the knowledge of the author these mutants have no physiological relevance, nor have Par-4 mutants with these mutations tested for their pro-apoptotic potential *in vivo*. Similarly, additional mutations described above would also only serve to stabilise the coiled coil fraction, but have no biological relevance.

A different approach to reduce conformational exchange between disordered monomers and ordered dimers could be the introduction of cysteine residues a suitable positions within the heptad. Disulfide bond formation between opposing cysteine residues may stabilise the dimeric conformation. This may allow the determination of the NMR solution structure as seems to be suggested by the results of the rJun leucine zipper [246]. An alternative way to continue from here is to change the construct length. The Par-4(286-332) constructs were created to comprise the Par-4 LZ domain. Only Par-4 constructs with residues Gln 286-Arg 332 were, to a certain extent, soluble upon heterologous expression in *E. coli*. However, as the LZ domain is predicted to start with Ile 292, these constructs contain eleven residues (Gln 286-Met 291 + five residues from the protease cleavage site Gly -5 - Ser -1) that are not likely to be involved in coiled coil formation. A disordered conformation for these 11 residues is corroborated by deconvolution results, usually predicting 20-30% of the Par-4 LZ peptide sequence not to be in an α-helical conformation (i.d. β-sheet, β-turn or disordered). These deconvolution results are taken from the Par-4 LZ peptides in their most stable condition at 5 ºC, e.g rrPar-4LZ at pH 4, rrPar-4LZD305K at pH 7.0 or rrPar-4LZE310K at pH 7.0 (Figs. 4.2D-F). This suggests that 20-30% of the residues of the Par-4 LZ peptides are freely accessible for other interactions, which could involve transient associations with other Par-4 LZ molecules. It is possible that such transient associations may also negatively affect the NMR spectra. It should be noted here that for the majority of the Par-4 LZ peptides in a mostly coiled coil state only Leu -3, Gly -2 and Ser -1

(and sometimes Arg 332) are observed by NMR as sharp and intense peaks, whereas all other resonances appear to be broad (e.g. Fig. 4.17B). Hence, it is likely that some of the N-terminal residues (e.g. Gln 286-Met 291), which are not predicted to be part of a coiled coil, may be involved in other interactions. It should therefore be considered to create new Par-4 LZ constructs with shorter N-terminii. The Gln 286-Met 291 stretch was supposedly necessary for the solubility of the Par-4 LZ peptides, however, with the here described denaturing protocol it should be possible to purify even N-terminally truncated Par-4 LZ peptides with lower solubility. To further reduce the length of this unfolded stretch at the N-terminus it is possible to switch to the pCFE-GST-TEV/2 expression vectors that allow for a shorter protease cleavage site (Chapter 2.3.2, Appendix B). Finally, another way could involve increasing the length of the Par-4 construct. Introducing additional heptad repeats could thus increase the coiled coil stability [136,224]. This approach is corroborated by initial results from the analysis of the Par-4 CC domain, which will be presented in the following chapter.

4.6. Structural characterisation of the Par-4 Coiled Coil domain

4.6.1. Materials and Methods

a) Sample preparation

rrPar-4CC was expressed and purified as described in Chapter 2.10. Samples with increasing concentrations of urea were prepared by diluting H_2O-dissolved rrPar-4CC with appropriate buffers (Table 4.10). For samples at neutral pH and with urea concentrations below or equal to 1 M, the solubility of rrPar-4CC was reduced and precipitation occurred. The precipitate was removed by centrifugation in a tabletop centrifuge and the protein concentration was remeasured. The same samples were used for CD and DLS spectroscopy.

	rrPar-4LZN313I peptide concentration	Buffer composition
a)	7 µM	20 mM NaCl, 10 mM Tris, pH 7.0 + 1M urea
b)	25 µM	20 mM NaCl, 10 mM Tris, pH 7.0 + 6 M urea
c)	25 µM	H_2O, pH 4

Table 4.10 *– Sample conditions of rrPar-4CC used for DLS and CD spectropolarimetry.*

b) Circular Dichroism

CD spectra were recorded as described in Chapter 3.4.1.a. Acquisition parameters are given in Appendix F. Due to buffer absorption the spectral width of the CD spectra was reduced from 190-260 nm (native buffer) to 205-260 nm (native buffer + 1 M urea) and 210-260 nm (native buffer + 6 M urea). Spectral deconvolution was performed using the algorithms Selcon3 and CONTIN-LL through the DICHROWEB interface.

c) Dynamic Light Scattering

DLS measurements were performed as described in Chapter 3.2.1.a. R_S values obtained from measurements in urea were corrected using the Dispersion Technology Software 5.1 to account for the increased solvent viscosity and the increased refractive index.

d) Crystallisation trials

Crystal screenings were performed using the HR2-110 Crystal Screen and the HR2-112 Crystal Screen 2 (Hampton Research). The concentration of H_2O-dissolved rrPar-4CC used for crystal screening was approximately 12 mg/ml (~1 mM). Sitting drops were set up as a 1:1 dilution of 0.5 µl rrPar-4CC and 0.5 µl of mother liquor. Crystal Screens were incubated at temperatures of 4 ºC and 21 ºC.

4.6.2. Results and Discussion

Spectral deconvolution suggests that approximately 30% of the residues of rrPar-4FL adopt an α-helical conformation (Chapter 3.4.2.). It was further proposed that the majority of this α-helical character can be attributed to the coiled coil formation observed for rrPar-4FL (Chapter 3.6.) due to the presence of the LZ domain. As the Par-4 LZ domain only comprises 40 residues (Fig. 1.1) this indicates that other residues are involved in self-association. The most likely candidates are the residues of the Par-4 CC domain (residues 254-332, Fig. 1.1). This domain has been discussed above as an N-terminal extension of the Par-4 LZ domain (Chapter 4.1.2.). It was proposed that this extension might increase the stability of the Par-4 coiled coil due to formation of additional heptad repeats. However, it was also noted that this domain contains characteristics that would be in contrast with a stable coiled coil. But as CD spectropolarimetry suggests, the additional heptad repeats in rrPar-4FL have overcome these destabilising factors. Similarly, it was previously shown that increasing the chain length of C-terminal Par-4 peptides resulted in a

more pronounced self-association [54]. Note that this assumption does not exclude that other regions of Par-4 may contribute to the α-helical signal and/or are involved in self-association.

To analyse the coiled coil forming propensity of the Par-4 CC domain the Par-4(240-332)WT construct (rrPar-4CC) was used, which contains the full Par-4 CC domain. This construct is of particular interest as this protein was shown to act in a dominant-negative manner, blocking the pro-apoptotic activity of full-length Par-4 in PC-3 cell cultures [55]. Assuming that the Par-4 CC domain forms a coiled coil, it was proposed that this construct inhibits Par-4 through direct association via the CC domain with full-length Par-4 itself, or through direct binding to Par-4 effector proteins. As described in Chapter 2.6, self-association of full-length Par-4 (rrPar-4FL) results in decreased solubility and hence a denaturing purification protocol became necessary. Therefore, a denaturing purification protocol was applied for rrPar-4CC, and it was noticed during purification that this protein behaves very similar to rrPar-4FL.

Unlike rrPar-4FL, rrPar-4CC is not stable in native buffer (20 mM NaCl, 10 mM Tris, pH 7.0). The majority of rrPar-4CC precipitated reducing the concentration from 25 µM to ~1 µM. The concentration was estimated from A_{205} absorbance readings acquired parallel with the CD spectrum. The solubility of rrPar-4CC is also reduced in native buffer + 1 M urea and the concentration was estimated at ~8 µM. Not surprisingly, no solubility limitations are observed in native buffer + 6 M urea. As noticed for other Par-4 peptides (Chapter 4.2.2.a), the most stable tested condition for rrPar-4CC, with no apparent solubility limitations in the absence of urea, was detected in MQ-H_2O at an acidic pH of approximately 4. For sterility reason the pH was only assessed with suitable pH paper strips. Like rrPar-4LZ, the stock solutions can be easily diluted with MQ-H_2O for the final CD samples and both rrPar-4CC and rrPar-4LZ are stable under these conditions.

The CD spectrum of rrPar-4CC in MQ-H_2O at pH 4 (Fig. 4.18A) is characteristic of a well defined and thermo-stable coiled coil. The α-helical content at 5 and 25 ºC is predicted with ~89% (average of both deconvolution algorithms). The T_m value is estimated at ~70 ºC (Fig. 4.19A), which is significantly greater relative to rrPar-4LZ ($T_m \approx 50$ ºC) under similar conditions at pH 4 (Fig. 4.19B). This suggests that the increased chain length in rrPar-4CC confers an increased stability of the coiled coil. Accordingly, the $\theta_{222}/\theta_{208}$ ratio remains above 1.0 till 35 ºC in contrast to rrPar-4LZ with only 25 ºC (Chapter 4.2.2.a). Due to the low concentration of rrPar-4CC in native buffer at pH 7.0 the resulting CD spectrum is very noisy (Fig. 4.18C). However, even at that low concentration the spectrum would suggest that rrPar-4CC forms a coiled coil at pH 7.0. Coiled coil formation of rrPar-4CC at pH 7.0 and 5 ºC is

also indicated in the presence of 1 M urea (Fig. 4.18E). The α-helical conformation under these conditions is relatively stable with a T_m value of approximately 40 ºC (Fig. 4.19A). In native buffer + 6 M urea some α-helicity is evident at temperatures below 15 ºC (Fig. 4.18G), however, above 15 ºC rrPar-4CC is mostly disordered. The observation of coiled coil conformations at neutral pH is consistent with the earlier proposed coiled coil state of rrPar-4FL (Chapter 3.6.). This strongly suggests that the increased chain length of rrPar-4CC, relative to rrPar-4LZ, is sufficient for self-association at pH 7.0. rrPar-4LZ is probably too short to overcome the repulsive electrostatic interaction between Asp 305 and Glu 310 residues that has been identified as the main destabilising factor for rrPar-4LZ at neutral pH [185]. The observed pH dependence for rrPar-4LZ therefore appears to be an experimental artefact as coiled coil formation is observed for the whole CC domain. Decreasing pH may stabilise the coiled coil through protonation of acidic residues that were shown to decrease Par-4 coiled coil stability (Chapter 4.2.2.a). However, most of the characterised Par-4 interactions take place in the cytoplasm or nucleoplasm at physiological pH. The commonly observed decrease in pH during apoptosis is probably not low enough to significantly alter the self-association properties of Par-4 as, in most cases, this drop does not fall below pH 6.5 [11].

It was already mentioned that the properties of rrPar-4CC are very similar to rrPar-4FL. Not surprisingly, a polymeric state of rrPar-4CC at pH 4 (R_S ~1500 Å at 25 ºC) is detected by DLS (Table 4.11). It is possible that the increased thermal stability relative to rrPar-LZ can, in part, be attributed to aggregation. This is consistent with the absence of an isodichroic point, thus suggesting a more complex folding behaviour than a simple two-state transition. Note that the traces in Figures 4.18A and B do not converge in one single point. The R_S values of rrPar-4CC in the presence of urea are greatly reduced and no significant difference (R_S ~32.5 Å at 25 ºC) is observed between 1 and 6 M urea (Table 4.11). It is not clear if the slight difference of 5 Å at 5 and 25 ºC is significant (Table 4.11). These results therefore suggest a disruption of the polymeric complex under denaturing conditions. Interestingly, in 1 M urea coiled coil formation is still observed (Fig. 4.18E). Using the equation given in Ref. [181] an R_S value of approximately 29.1 Å is calculated for rrPar-4CC in a urea denatured coil-like conformation. This theoretical value is similar to the experimentally determined R_S value of 32.5 Å in 6 M urea at 25 ºC (Table 4.11) and suggests that the R_S values obtained in 1 and 6 M urea are associated with low molecular weight species. As mentioned earlier, the high apparent *MWs* obtained for rrPar-4CC in 1 or 6 M urea (Table 4.11) are consistent with proteins in coil-like or coiled coil

conformations. Note that *MWs* calculated for rrPar-4CC at pH 4 according to the equation given in Ref. [181] are in the GDa range and are therefore omitted in Table 4.11.

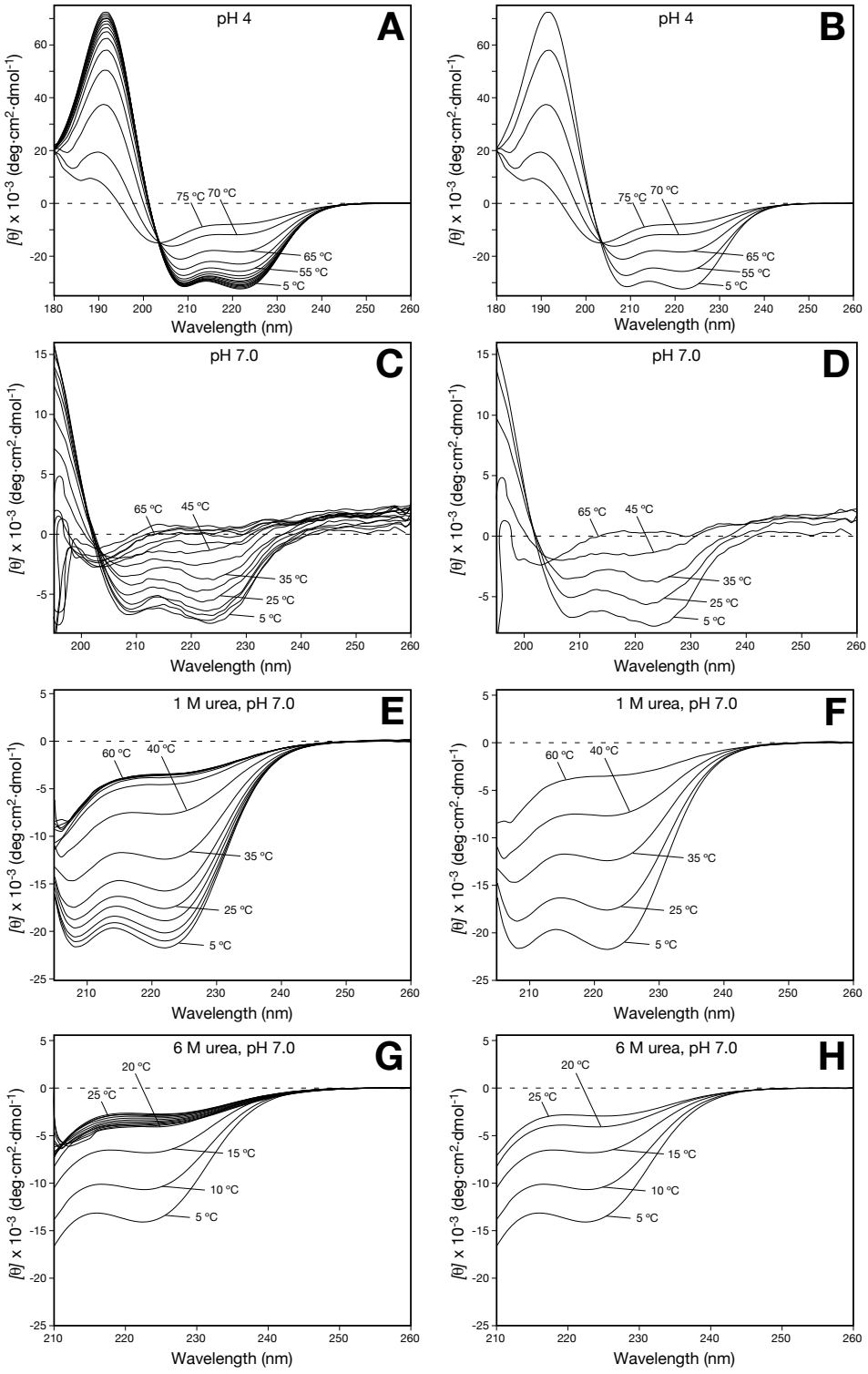

Figure 4.18 *− CD spectropolarimetry of rrPar-4CC. CD spectra of rrPar-4CC as a function of temperature are shown for various conditions: (A, B) at pH 4, (C, D) at pH 7.0, (E, F) at pH 7.0 + 1 M urea, and (G, H) at pH 7.0 + 6 M urea. The complete temperature series are shown in panels A, C, E and G. For clarity, five evenly spaced temperature series are shown in panels B, D, F and H. Sample conditions are listed in Table 4.10. The concentration of rrPar-4CC in 20 mM NaCl, 10 mM Tris, pH 7.0 (panel C and D) was estimated at ~1 µM. Acquisition parameters are given in Appendix F.*

Polymerisation of α-helical proteins such as rrPar-4CC is not uncommon. It was for instance shown recently that the tau protein can, under certain conditions, form α-helical fibrillar aggregates, which have spectroscopic features of α-helical coiled coils [271]. Similar polymeric states were usually not observed for rrPar-4LZ, except under special conditions. Particularly rrPar-4LZ is predominantly in a low oligomeric state in MQ-H_2O at pH 4 (Fig. 4.5C). This suggests that the additional N-terminal residues in rrPar-4CC create a surface that allows for polymerisation. It is also possible that rrPar-4LZ is not stable enough to allow for polymerisation as lower oligomeric complexes may dissociate at a much faster rate. In contrast, rrPar-4CC displays an increased thermal stability (Fig. 4.19B) and low order oligomeric complexes may be stable enough to polymerise. Note that the thermally more stable rrPar-4LZN313I also displayed a propensity for polymerisation (Table 4.9). The interactions involved in polymerisation appear to be of weak nature as polymerisation is to a certain extent suppressed in 1 M urea (Table 4.11).

	5 ºC		25 C	
Sample condition	***MW***	***R_S***	***MW***	***R_S***
rrPar-4CC peptide	11.4	29.1	11.4	29.1
rrPar-4CC at pH 4, 0 M urea	N/A	1275/3076	N/A	1477
rrPar-4CC at pH 7.0, 1 M urea	97.0	37.7	64.0	32.5
rrPar-4CC at pH 7.0, 6 M urea	97.0	37.7	64.0	32.5

Table 4.11 *− DLS-determined hydrodynamic properties of rrPar-4CC. MW (kDa) and R_S (Å) values were calculated using the equation log(R_S) = 0.357*log(MW) − 0.204 in reference to a spherical conformation [181]. This equation was used to display that the degree of extended structure is very high for the rrPar-4CC proteins in urea. The mode R_S values of each measurement are shown. For comparison, theoretical values for a* ***urea unfolded state*** *of rrPar-4CC calculated from the amino acid sequence are also provided. Calculated MWs for rrPar-4CC at pH 4 are in the GDa range and therefore omitted. Sample conditions are given in Table 4.10.*

For full-length rrPar-4FL polymerisation is also observed, but to a significantly lesser extent (R_S ~189 Å, Table 3.1). This indicates that Par-4 segments N-terminal to the CC domain may prevent higher order polymerisation of the CC domain in the context of full-length Par-4. This would further indicate that polymerisation is an artefact of the experimental conditions and may not represent the biologically active state. Post-translational modifications in mammalian cells may also regulate the oligomeric state of the CC domain and may thus prevent polymerisation *in vivo*. For instance, phosphorylation of laminins during mitosis results in their depolymerisation

triggering the disassembly of the nuclear lamina[272]. It should be noted that the first 19 N-terminal residues of rrPar-4CC (Gly 240-Asn 253 + five residues of the protease cleavage site) are not predicted to be part of a coiled coil (Fig. 4.1A) and may therefore contribute to polymerisation in an unknown way. These residues may be removed for future studies of the CC domain. Due to the propensity of the CC domain to polymerise it may be helpful to include additives that prevent oligomerisation, but still allow for coiled coil formation. Urea did not give the best results, as rrPar-4CC was still fairly insoluble in 1 M urea. Thus acetonitrile or TFE may be alternative candidates. In particular TFE was shown to have a favourable solubilising property at pH 5 for rrPar-4LZ (Chapter 4.4.2.). However, for both additives optimal concentrations need to be determined that allow further structural characterisations of the coiled coil state.

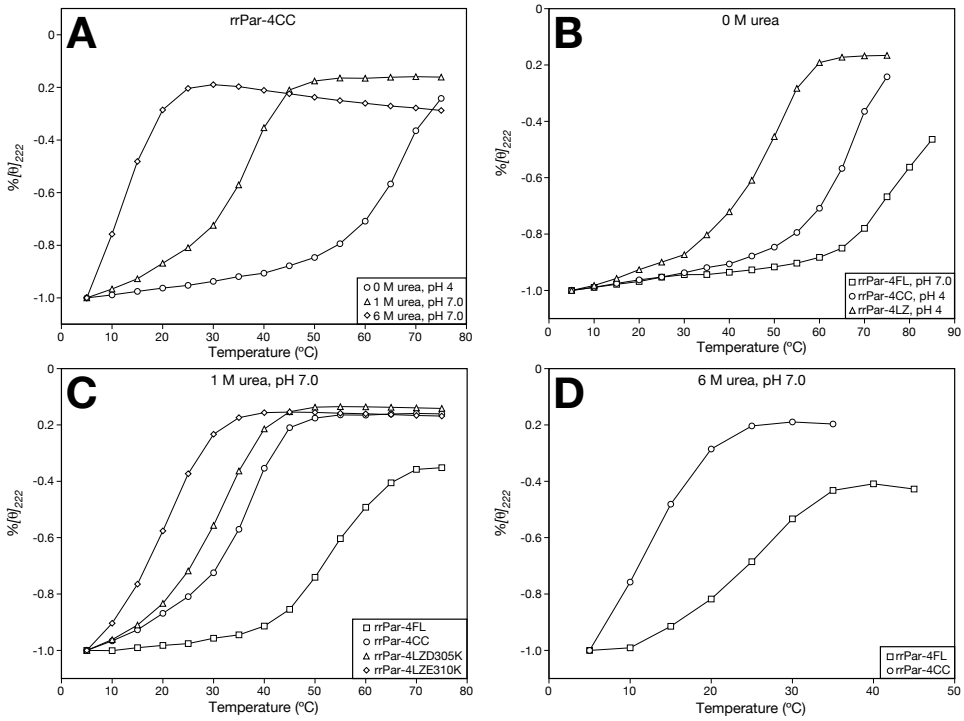

Figure 4.19 *– Thermal stability of various Par-4 constructs. Temperature dependence of the molar ellipticity measured at 222 nm for (A) rrPar-4CC under denaturing and non-denaturing conditions, (B) various Par-4 constructs under non-denaturing conditions, (C) various Par-4 constructs in native buffer (20 mM NaCl, 10 mM Tris, pH 7.0) + 1 M urea and (D) two Par-4 constructs in native buffer + 6 M urea. Displayed are the* $\%[\theta]_{222}$ *value of (A) 25 µM rrPar-4CC in MQ-*H_2O*, pH 4 (open circles); 8 µM rrPar-4CC in native buffer + 1 M urea (open triangles); and 25 µM rrPar-4CC in native buffer + 6 M urea (open diamonds); in (B) 8 µM rrPar-4FL in native buffer (open squares); 25 µM rrPar-4CC in MQ-*H_2O*, pH 4 (open circles); and 75 µM rrPar-4LZ in MQ-*H_2O*, pH 4 (open triangles); in (C) 8 µM rrPar-4FL (open squares); 8 µM rrPar-4CC (open circles); 75 µM rrPar-4LZD305K (open triangles); and 75 µM rrPar-4LZD305K (open diamonds) all four in native buffer + 1 M urea; and in (D) 8 µM rrPar-4FL (open squares); and 25 µM rrPar-4CC (open circles) both in native buffer + 6 M urea. The* $\%[\theta]_{222}$ *values were obtained by normalising the* $[\theta]_{222}$ *values at each temperature to the corresponding* $[\theta]_{222}$ *value at 5 ºC.*

As rrPar-4CC was not ^{15}N-labelled and due to its low concentration, NMR spectroscopy was not a suitable method for further structural characterisation. However, the concentration of the rrPar-4CC stock solution (~12 mg/ml) was sufficient for crystallisation trials. After approximately 6 weeks crystals were obtained at 21 ºC (Fig. 4.20). Based on the mother liquor, which contained 0.2 mM sodium citrate, 0.1 mM HEPES, pH 7.5 and 20% isopropanol ($^{v}/_{v}$), additional screenings were prepared as hanging drops. For these screenings the drop volume was increased, and the rrPar-4CC and precipitant concentration was varied in a sensible manner. These additional screenings were further seeded with crystals from the first screening plate and left at 21 ºC for crystal growth. So far no crystals at a suitable size for X-ray diffraction have been obtained. However, given the morphology and three-dimensional nature of these crystals, crystallisation of rrPar-4CC remains a promising lead.

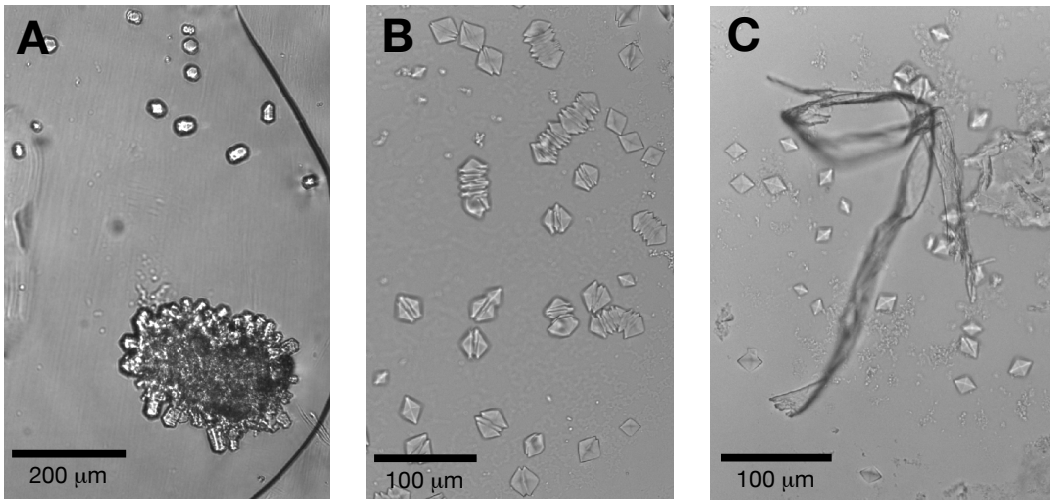

Figure 4.20 *– Crystallisation trials of rrPar-4CC. Crystals of rrPar-4CC obtained with A) the original screening in 0.2 mM sodium citrate, 0.1 mM HEPES, pH 7.5 and 20% isopropanol ($^{v}/_{v}$). Crystals obtained after optimisation with decreasing concentration of isopropanol are shown in B) with 15% isopropanol ($^{v}/_{v}$) and C) with 10% isopropanol ($^{v}/_{v}$).*

A comparison of thermal stabilities of various Par-4 constructs under denaturing and non-denaturing conditions is shown in Figures 4.19B-D. As noted above rrPar-4CC displays an increased stability over rrPar-4LZ (Fig. 4.19B). Interestingly, even in their most stable state at pH 4 both rrPar-4LZ and rrPar-4CC are not as stable as rrPar-4FL under non-denaturing conditions (Fig. 4.19B). Similar trends are observed in native buffer + 1 M urea and in native buffer + 6 M urea (Figs. 4.19C and D). In each case rrPar-4FL displays a greater thermal stability over rrPar-4CC and the Par-4 LZ peptides. Under non-denaturing conditions the high thermal stabilities of rrPar-4FL and rrPar-4CC (Fig. 4.19B) can be partly attributed to polymerisation (see above). However, disruption of the polymeric state by urea results in a similar order of

stabilities (Figs. 4.19C and D). Note that rrPar-4LZD305K and rrPar-4LZE310K are displayed in Figure 4.19C for comparative purposes, as the wild-type rrPar-4LZ does not adopt a coiled conformation at neutral pH (Fig. 4.2A). However, they are omitted from Figure 4.19D as they are mostly unfolded in native buffer + 6 M urea.

It is interesting to note that rrPar-4FL and rrPar-4CC display distinct stabilities under denaturing and non-denaturing conditions. As both proteins contain the whole CC domain, this suggests that other factors contribute to the stability difference. An increased thermal stability due to an increased concentration of rrPar-4FL is unlikely, as rrPar-4FL (8 µM) was used in a lower concentration than rrPar-4CC (25 µM) (Figs. 4.19B and D), except for conditions in native buffer + 1 M urea where both proteins are at a concentration of 8 µM (Fig. 4.19C). In addition, polymerisation of both proteins under non-denaturing conditions may interfere with thermal stabilities, but to what extent is currently unknown. It is therefore likely that other segments of Par-4 N-terminal to the CC domain, and thus absent in rrPar-4CC, contribute to coiled coil stability. As mentioned earlier (Chapter 1.2.1.), the N-terminal region of Par-4 was shown to interact with the CC domain, however, this interaction was proposed to prevent coiled coil formation rather than enhance it [54]. Thus other regions of Par-4 between the N-Terminus and the CC domain are potentially involved in the stabilisation.

rrPar-4CC displays a relatively high thermal stability at pH 4 with an T_m value of ~70 ºC (Fig. 4.19A). The $\theta_{222}/\theta_{208}$ ratio that is close to one further suggests a stable coiled coil at the physiological temperature of 35 ºC (Fig. 4.18A). Based on the presented data it is reasonable to assume that at physiological pH the stability of the coiled coil is reduced. Furthermore, polymerisation may artificially increase coiled coil stability. Hence, it is possible that under physiological conditions (pH 7.0 and 37 ºC) a similar interconversion between coiled coil and disordered conformations exists, as is observed for the Par-4 LZ peptides (Chapter 4.3.2.). This is not surprising as the Par-4 CC domain contains various highly conserved residues that are detrimental to coiled coil stability (Fig. 1.1). These conserved residues include Asp 305 and Glu 310, and the repulsive electrostatic interaction between them, the aspartate patch within the LZ domain, three asparagine residues at position *a* and two charged residues at position *d* of the heptad (Fig. 4.1B-E). Even though, these residues may not prevent coiled coil formation in the context of the whole CC domain under physiological conditions, they may destabilise it resulting in transient coiled coil formation or allowing for strand exchange. It is interesting to note, in this context, that for the trimeric Heat Shock Factor-binding Protein 1 (HSBP1) motional processes on the millisecond time scale were detected by NMR. Other NMR data indicated an otherwise

stable coiled coil conformation with a rigid peptide backbone. CD spectropolarimetry further indicated a moderate melting temperature of 48 ºC [247]. It is possible that similar motions on the millisecond time scale are possible for the Par-4 CC domain under physiological conditions.

In summary, additional heptad repeats present in rrPar-4CC are sufficient to overcome destabilising factors that prevent coiled coil formation of the Par-4 LZ domain at neutral pH. This provides evidence that the pH dependent coiled coil formation of rrPar-4LZ may not be physiologically relevant as the peptide is probably too short to stabilise a coiled coil conformation. The full Par-4 CC domain may therefore represent the physiologically relevant domain for self-association. However, evolutionary conserved residues, which confer to a decreased stability of the Par-4 coiled coil, suggest that *in vivo* self-association through the coiled coil domain may be transient.

4.7. The advantage of transient coiled coil formation in Par-4

The highly conserved sequence of the Par-4 CC domain displays features that are commonly considered to be detrimental to coiled coil stability (Chapter 4.1.2.). Based on these observations and the observed order-disorder equilibrium for rrPar-4LZ (Chapter 4.3.2.) it is proposed here that also full-length Par-4 may display a dynamic equilibrium between ordered oligomers and disordered monomers. However, great caution should be taken when transferring *in vitro* results obtained from an isolated domain (Par-4 LZ domain) to the full-length protein (Par-4). Such results may not necessarily have a physiological relevance for the full-length protein and the observed disorder-order equilibria may only apply for the Par-4 LZ constructs. Possible models how such a dynamic exchange behaviour could be advantageous for the function of Par-4 are shown in Figure 4.21. These models are based on the current literature and the results presented in this document, however, they are speculative and experimentally unproven. They may be useful for the design of future experiments to determine which models are appropriate. A coiled coil with high thermal stability and hardly any strand exchange may not be desirable from a regulatory point of view. Buried asparagine residues have long been considered to weaken coiled coil stability [129] and to tune strand exchange rates in coiled coils [138]. It has therefore been suggested that reduced coiled coil stability conferred by the presence of asparagine residues at position *a* and/or other factors can facilitate readily reversible homo- and heterodimerisation [107]. For leucine zipper-containing transcription factors [117,118], this would allow formation of different arrays of homo- and heterodimers, thereby modulating DNA affinity and hence the

range of affected genes [273,274]. A similar mechanism for sampling of effector molecules might be possible for Par-4.

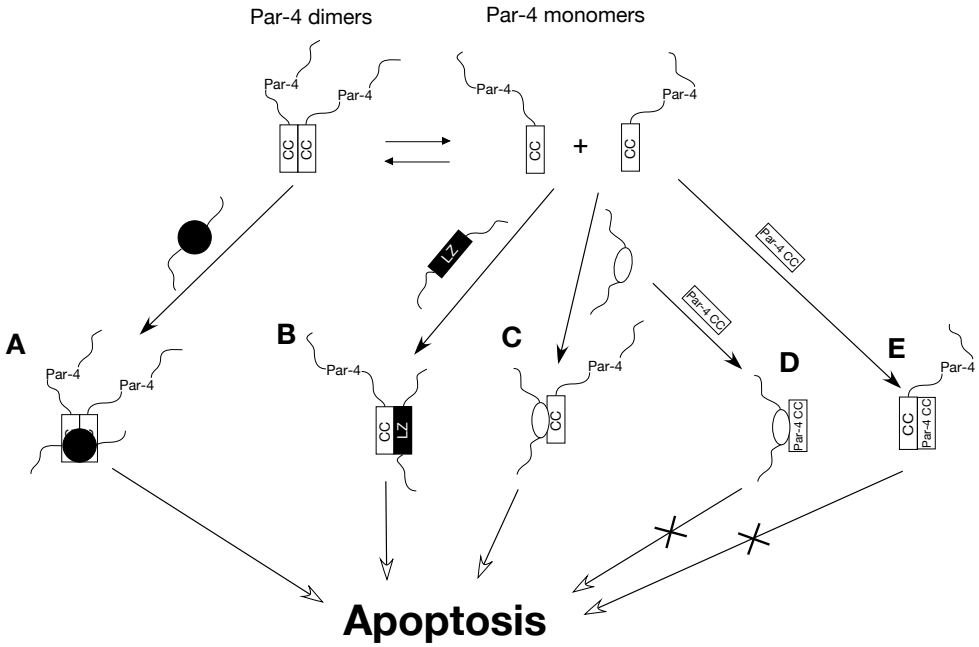

Figure 4.21 *− Potential order-disorder equilibria may be necessary for the function of Par-4. The displayed models are hypothetical and not confirmed by experiments. Par-4 was shown to self-associate through the CC domain. It is likely that in vivo Par-4 exists in an equilibrium between disordered monomers and self-associated ordered oligomers. Based on the analysis of the amino acid sequence, self-associated Par-4 is displayed as dimers. (A) Due to inherent destabilising factors self-association of Par-4 is of transient nature and the dimer rapidly dissociates. Binding of an effector protein to the dimerised Par-4 CC domain results in stabilisation of the dimer. This newly formed complex is then able to induce apoptosis. (B) A disordered Par-4 monomer is bound by a coiled coil or leucine zipper domain containing effector protein (e.g. AATF (Chapter 1.3.4.m)) possibly forming a heterodimeric coiled coil. (C) The binding domain of an effector protein, which is not a coiled coil or leucine zipper domain (e.g. the zinc-finger domain of aPKCζ (Chapter 1.3.4.a)), can provide a surface that better accommodates potentially destabilising residues in a homodimeric Par-4 coiled coil. As for model (B), the newly formed heterodimer is stable enough to induce apoptosis. Potential modes for CC domain containing Par-4 deletion mutants (e.g. rrPar-4CC) acting in a dominant-negative manner are shown in panels (D) and (E). These mutants may titrate Par-4 effector proteins (D) or titrate full-length Par-4 trough heterodimerisation via the CC domain (E).*

In one possible model Par-4 may bind its effector molecules through the CC domain as a monomer (Figs. 4.21B and C). Potential dynamic exchange properties of Par-4 may allow reversible homo- and heterodimerisation (or oligomerisation) as proposed above for leucine zipper-containing transcription factors (Fig. 4.21B). For instance, it has been demonstrated that the Par-4 CC domain is essential for the interaction with the leucine zipper domain of AATF and

probably of Dlk (Chapter 1.3.4.) suggesting the formation of a hetero-oligomeric coiled coil. Dynamic exchange would therefore offer a simple regulatory mechanism controlling the function, cellular localisation and turnover of Par-4. Binding partners of Par-4 may further provide a binding surface that can better accommodate residues that would be destabilising in the homo-oligomeric coiled coil conformation. This may result in an increased stability of the heterodimer, relative to the Par-4 homodimer (Fig. 4.21C). A dynamic exchange behaviour may further be necessary for the regulation of Par-4. As mentioned above, ectopic overexpression of rrPar-4CC was shown to abolish the pro-apoptotic function of Par-4, indicating that this construct can act in a dominant negative manner. It was shown above that rrPar-4CC is less stable than full-length Par-4 suggesting that self-association of rrPar-4CC may be disfavoured relative to rrPar-4FL. Opportunities for heterodimerisation with full-length Par-4 may thus be enhanced (Fig. 4.21E), making rrPar-4CC an effective inhibitor of Par-4. The potentially more dynamic exchange behaviour of rrPar-4CC may also interfere with the binding of full-length Par-4 to its effector proteins (Fig. 4.21D). The same considerations can be applied to a physiologically more relevant splice isoform of Par-4. This naturally occurring 33 kDa splice variant of Par-4 lacks exon 3, which contains amino acids necessary for nuclear translocation of Par-4, and shows no nuclear localisation [47]. It was therefore proposed that this variant may associate with full-length Par-4 via the CC domain, which is still present in this splice variant, and prevent nuclear translocation of full-length Par-4. In this way, it may inhibit Par-4's pro-apoptotic function and thus act as a naturally occurring dominant negative splice variant [47]. Possible order-disorder equilibria in the context of the full-length Par-4 protein may therefore allow reversible association with this splice variant.

Self-association of Par-4 through the CC domain may be a prerequisite for binding to its effector molecule (Fig. 4.21A). Several cases have been described where a coiled coil domain provides the binding surface for interaction with other proteins (e.g the binding of Rab11 to the FIP2 coiled coil [264], the binding of ARF6 to the JIP4 coiled coil [275] or association of the coiled coil domain of NEMO with ubiquitin [276]). Such a binding mode for Par-4 is corroborated by recent findings demonstrating that substitution of three leucine residues at position *d* within the Par-4 LZ domain to alanines abrogates binding to Amida [53]. The proposed dynamic exchange of Par-4 between disordered monomers and ordered dimers may therefore represent another regulatory switch for the pro-apoptotic function of Par-4. Homodimerisation of Par-4 may occur *in vivo,* but is of transient nature preventing a sensitisation of cells to apoptosis. However, binding of Par-4 effector molecules to the coiled coil

CC domain strengthens the self-association of Par-4, resulting in a stable hetero-oligomer consisting of a Par-4 dimer and the effector protein(s) (Fig. 4.21A). This stable hetero-complex is then able to promote apoptosis. It has also been shown in a previous work that association with effector proteins can result in structural rearrangement of a coiled coil. Binding of DNA-ligase IV to Xrcc4 was shown to induce a local unwinding of the coiled coil of Xrcc4 and thereby flattening the binding surface [277]. Reduced coiled coil stability in Par-4 could therefore potentially facilitate local structural rearrangements upon association with effector molecules. It is also possible that a combination of the above described mechanisms apply for Par-4 depending on the Par-4 association partner.

It was suggested that the full-length Par-4 forms a very thermo-stable coiled coil under physiological conditions (Figs. 3.11A and 4.19B). This high stability may not allow for a readily reversible and dynamic association behaviour as described above. As CD spectropolarimetry only measures the average of all conformations in solution, a rapid exchange between monomers and oligomers may not be detected under the current conditions. The strong coiled coil character obtained for rrPar-4FL is probably overemphasised by the subtraction of the CD spectrum of rrPar-4ΔLZ (Fig. 3.11). As mentioned earlier, rrPar-4ΔLZ lacks the complete LZ domain (residues 291-332) and shows no significant α-helical character (Fig. 3.7B). In contrast, full-length Par-4 displays α-helicity that can be attributed to the LZ domain and to regions N-terminal to it, such as the remainder of the CC domain (Fig. 3.7A and Chapter 3.6.). These N-terminal regions adopt an α-helical fold only in conjunction with the LZ domain as observed for rrPar-4FL, but not in the absence of the LZ domain as in rrPar-4ΔLZ. Thus, the subtraction shown in Figure 3.11A is likely to be skewed to more negative θ_{222} values relative to θ_{208} values due to α-helical regions in rrPar-4FL not formed in rrPar-4ΔLZ. This suggests that the coiled coil proposed for rrPar-4FL may not be as stable as Figure 3.11A implies.

NMR spectra of full-length Par-4 show that approximately 50% of the expected peaks are missing (Fig. 3.8), which may be considered as another indication for the existence of exchange processes. Whether the missing peaks are due to an exchange process between disordered and ordered states was not determined. Note that the earlier proposal in Chapter 3.4.2, that peaks of the CC domain are broadened beyond detection due to formation of a higher molecular weight complex of non-globular shape, is also consistent with the data. However, as these results were obtained *in vitro* with heterologously expressed Par-4, the properties of Par-4 may be different *in vivo*. Post-translational modifications such as phosphorylation were shown to interfere with coiled coil formation, either abrogating or in some cases promoting self-association [278,279]. A

few phosphorylation sites in the Par-4 C-terminus have been predicted most notably a casein kinase II site within the CC domain at Ser 258, which is highly conserved among mammals [27] (Fig. 1.1). Additionally, recent *in vivo* NMR studies suggest that proteins may not be as rigid as the results of *in vitro* NMR studies suggest [280]. Thus, *in vivo* self-association of Par-4 may be more dynamic than results presented here indicate.

The highly conserved polar residues that may be detrimental for coiled coil stability may not only facilitate order-disorder equilibria, but could also be important regulators of protein solubility. In Chapter 4.5.2. the contribution of a buried asparagine residue to the stability of the Par-4 LZ domain was demonstrated. Substitution of this residue by an isoleucine was not sufficient to induce self-association at neutral pH, probably as electrostatic repulsion between Asp 305 and Glu 310‘ was the dominating factor for coiled coil stability under these conditions. However, under acidic pH conditions a significant increase in thermal stability was observed. Interestingly, an increased propensity to aggregate was observed for this peptide. This may be just an artefact of the *in vitro* studies; however, it may also be important for the *in vivo* function of Par-4. It is possible that more canonical stabilising residues within the Par-4 CC domain would result in higher order complex formation and aggregation [131], rendering Par-4 biologically inactive. Accumulation of (Par-4) protein aggregates within the cell could trigger stress responses that may lead to cellular damage (Chapter 1.3.1.).

The high conservation of polar residues at positions *a* and *d* within the Par-4 CC domain suggests that these residues are essential for the biological function of Par-4, even though they are commonly considered to destabilise a coiled coil. It was proposed above that these conserved residues are necessary to prevent *in vivo* aggregation of Par-4 resulting in the loss of Par-4 activity. It was also proposed that conserved polar residues facilitate a dynamic exchange behaviour between Par-4 monomers and oligomers that may be essential for Par-4 to function as an effective regulator of apoptosis.

5. Conclusions and Future work

5.1. Conclusions

(i) The first conclusion to be drawn from the presented data is that Par-4 can be classified as an IDP (Chapters 3.2.2. and 3.4.2.). Apart from the C-terminus that self-associates possibly via coiled coil formation (Chapter 3.6.), the majority of the Par-4 sequence adopts an elongated coil-like conformation in solution. The α-helical character observed for full-length Par-4 by CD spectropolarimetry was mostly attributed to coiled coil formation of the C-terminus, but may also involve other regions of Par-4 (Chapters 3.4.2.). It was further shown that the isolated Par-4 SAC domain, despite being primarily disordered, displays indications for residual structure. Interestingly, the isolated SAC domain possess distinct NMR spectroscopic properties compared to the SAC domain in the context of full-length Par-4 (Chapter 3.4.2.).

(ii) Deletion studies suggest that the entire Par-4 CC domain (residues 254-332) is necessary for coiled coil formation under physiological conditions (Chapter 4.6.2.). Neither the isolated LZ domain as in rrPar-4LZ (residues 292-332) (Chapter 4.2.2.) nor the five N-terminal heptads of the CC domain as in rrPar-4ΔLZ (residues 254-290) (Chapter 3.4.2.) are sufficient, in isolation, to adopt a coiled coil conformation at neutral pH. However, both sub-domains together as part of the entire CC domain, as in rrPar-4FL or rrPar-4CC, are sufficient for coiled coil formation (Chapters 3.6. and 4.6.2.). Despite the presence of the first five heptad repeats of the CC domain, rrPar-4ΔLZ displays no α-helical character and shows no indications for self-association. In contrast to this, rrPar-4FL that contains the whole CC domain, including the LZ domain, self-associates (Chapter 3.6.).

(iii) Consistent with the previous conclusion, the five additional heptad repeats of the Par-4 CC domain relative to the LZ domain are sufficient for coiled coil formation at physiological pH (Chapter 4.6.2.), despite inherent factors that are commonly considered to be detrimental to coiled coil stability. The interhelical charge-charge repulsion between residues Asp 305 and Glu 310‘ was identified as the main destabilising factor that prevents coiled coil formation of the Par-4 LZ domain at neutral pH [184]. The destabilising effect of this interaction is probably outweighed by the gain in stability through additional heptad repeats. It should be noted that other factors that potentially interfere with coiled coil stability, such as asparagine residues at position *a*, charged residues at position *d* and the aspartate patch within the LZ domain, appear also to be compensated for by the increased chain length. Especially the charged residues at position *d* within the hydrophobic interface, make this coiled coil structure an interesting target for structural characterisation.

(iv) The fourth conclusion arises from the previous conclusions. The pH dependence of coiled coil formation for rrPar-4LZ (Chapter 4.2.2.) is probably not physiologically relevant. The chain length of rrPar-4LZ is probably too short to overcome coiled coil destabilising factors. In contrast, the increased chain length of rrPar-4CC with additional heptad repeats is sufficient for coiled coil formation at neutral pH. This highlights an interesting point about the danger of studying protein domains *in vitro* and in isolation. Therefore, caution should be taken when transferring results obtained from isolated domains to the full-length protein. Nonetheless, the peculiar NMR spectroscopic properties of the coiled coil Par-4 LZ peptides make these peptides interesting academic targets.

To summarise the conclusions, Par-4 is a highly conserved protein indicating that the majority of residues are essential for the biological function. While the N-terminus of Par-4 displays a high degree of ID, the C-terminus of Par-4 was shown to self-associate through coiled coil formation at neutral pH. However, a pH dependency of coiled coil formation for Par-4 as observed for the isolated Par-4 LZ domain is questionable.

5.2. Contributions to the current knowledge

Despite great problems with the purification of the Par-4 proteins, some interesting results could be obtained that help to better understand the properties of Par-4. Intrinsic disorder in Par-4 and coiled coil formation of the Par-4 C-terminus could be predicted from the amino acid sequence and verified by various biophysical methods. The advantages of IDPs for regulatory processes have been discussed in (Chapter 1.5.) and clarify how Par-4 may act as an effective regulator of apoptosis, in particular as a hub protein integrating pro- and anti-apoptotic signals. The problems observed during purification and biophysical characterisation of Par-4 described in this study, and by other research groups, can be attributed to a great extent to the ID nature and self-association of Par-4.

The results further suggest that Par-4 self-associates at neutral pH through coiled coil formation, which is localised to the Par-4 C-terminus. Despite being essential for self-association, the LZ domain is not the biologically relevant domain. Self-association depends on an intact CC domain including the LZ domains. This indicates that previous results demonstrating a pH dependence of coiled formation are an experimental artefact of the LZ construct itself. Even though this pH dependence may be of academic interest, the biological relevance is questionable especially in context of the biological function of Par-4. This information may, however, be of great importance for the design of inhibitory peptides that

specifically associate with full-length Par-4 and block its function. Peptides may be designed in such a way that homodimerisation is disfavoured, but heterodimerisation with full-length Par-4 occurs with high affinity.

Substitution of a polar asparagine within the oligomeric interface by a hydrophobic isoleucine resulted in an increased thermal stability of the coiled coil, however, also resulted in an increased propensity to aggregate (Chapter 4.5.2.). This suggests that polar residues within the oligomeric interface, even though they are detrimental for coiled coil stability, are important regulators of protein solubility, and thus important for the biologic activity [131].

5.3. Future work

Like many PhDs, this thesis produces more new question than it answers. Probably one of the most interesting questions that arose from this thesis is what residues are visible in the NMR spectra of rrPar-4FL and rrPar-4ΔLZ. Therefore chemical shift assignment of both proteins should be one of the major next steps. Especially for rrPar-4FL it would be interesting to know if peaks from the CC domain can be observed. In addition to the assignments, ^{15}N-relaxation measurements may be recorded, which would further allow conclusions about the dynamics of the involved residues to be drawn. It may be beneficial to perform these NMR measurements on (partially) deuterated proteins, as rrPar-4FL is likely to contain non-globular shaped domains that may not be detected in non-deuterated samples. Similar NMR experiments could be performed for rrPar-4SAC. This domain shows some indication of residual secondary or tertiary structure and further displays distinct NMR properties than the SAC domain in the context of full-length Par-4. Additional NMR experiments may therefore be useful to clarify some of the observed differences.

As isolation of rat full-length Par-4 and its analysis by NMR proved to be a challenging task, expression of Par-4 orthologues from different species, such as human or zebrafish, may produce proteins that are more amenable to NMR studies. Furthermore, bioassays should be developed to confirm that the heterologously expressed Par-4 proteins are biologically functional. A simple test could demonstrate that the isolated Par-4 proteins still bind their effector proteins.

The Par-4 LZ peptides displayed peculiar NMR spectroscopic properties that were difficult to analyse. However, their physiological relevance is questionable as the whole CC domain is likely to be the biologically functional unit. Analysing their folding behaviour may be of academic interest, however, results cannot be easily transferred to the CC domain, as it probably shows different structural properties. It is therefore in my opinion not worth continuing with Par-4 LZ

peptides in their current form and work should rather focus on the entire CC domain. This may involve new constructs with greater solubility, and the optimisation of experimental conditions. The CC domain offers the advantage to study coiled coil formation under almost physiological conditions and removes pH as a critical factor for oligomerisation. As a highly non-globular shape can be expected, CC constructs may benefit from deuterium labelling.

Par-4 CC constructs may further be necessary for the analysis of association with Par-4 interaction partners. Previous results (Chapter 1.3.4.) suggest that a functional Par-4 CC domain is necessary for binding to its effector proteins. LZ peptides may show only weak binding relative to CC constructs. This is corroborated by initial interaction studies showing that the wild-type Par-4 LZ domain only interacts with the zinc-finger domain of aPKCζ at pH 6.0 (personal communication with Dr. K. Dutta). Analysis of Par-4 in complex with other proteins is therefore another important aim for future studies. So far, work was mainly concentrated on the aPKCζ zinc-finger domain, however, this domain is highly insoluble and could not be isolated in a stable soluble form (personal communication with H. Prasad). Therefore other Par-4 interaction partners need to be screened.

To assess the oligomeric state of the Par-4 constructs, methods other than NMR may be necessary. It was already mentioned that characterisation of Par-4 LZ peptides by MALLS and AU have begun. Similar experiments may be performed with full-length Par-4 and constructs comprising the CC domain. A different method that may be approached is SAXS, which could also provide information about the oligomeric state of Par-4. Also FT-IR spectroscopy(Fourier transform - infrared spectroscopy) is a possible method to study the oligomeric state of coiled coils. Vibrational bands obtained for coiled coils depend on the pitch value of the supercoil and therefore may allow differentiation between dimers, trimers or tetramers [281].

It is further necessary to analyse the strand exchange rates in the Par-4 constructs to better understand the existing dynamics. Possible methods to measure strand exchange rates have been described in Ref. [138] and involve fluorescence labelling techniques. The easiest experiment probably involves the labelling of peptides with two different fluorescence labels. Labels should be chosen so that close proximity of the two different labels results in quenching of the fluorescence. Mixing of these two differently labelled peptide species and measuring the fluorescence decay over time should allow the determination of the strand exchange rates within the coiled coils. These experiments could be performed with full-length Par-4 and Par-4 CC constructs. Similar types of fluorescence experiments should be performed in (cancer) cells mainly to study the oligomeric state of Par-4 in its native environment. These experiments are

further necessary to clarify if Par-4 homodimerisation (-oligomerisation) is physiologically relevant.

NMR results of the Par-4 LZ peptides indicate a dynamic equilibrium between disordered monomers and coiled coil dimers (Chapter 4.3.2.). Due to the sequence peculiarities of the Par-4 CC domain similar equilibria may exist for full-length Par-4 or isolated Par-4 CC constructs. It was proposed in Chapter 4.7. that such equilibria may be necessary for the biologic function of Par-4 facilitating hetero-oligomerisation with Par-4 effector proteins. Identification of such equilibria and analysis of the underlying factors causing the equilibrium is therefore another potential aim. This should help to understand if coiled coil stabilising and destabilising factors are balanced in such a way in Par-4 that self-association occurs, but still allow hetero-oligomerisation.

Crystallisation trials showed that it is possible to obtain crystals for the Par-4 CC domain. Therefore crystallisation trials may be intensified to obtain crystals that would allow structure determination. As rrPar-4CC contained a stretch of disordered residues at the N-terminus, a further optimisation of the Par-4 construct and the crystallisation conditions may be necessary.

Appendices

Appendix A: List of Suppliers

^{15}N-ammonium chloride (99%)	Cambridge Isotope Lab., Andover, USA
Amylose resin High Flow	New England Biolabs, Ipswich, USA
Restriction Endonuclease *BamH* I	New England Biolabs, Ipswich, USA
BL21(DE3) CodonPlus E. coli strain	Stratagene, La Jolla, USA
BSA	Sigma-Aldrich, St. Louis, USA
Chelating Sepharose Fast Flow	GE Healthcare, Uppsala, Sweden
CM-sephadex	Sigma Chemical Co., St. Louis, USA
Crystal Screen, HR2-110	Hampton Research, Aliso Viejo, USA
Crystal Screen 2, HR2-112	Hampton Research, Aliso Viejo, USA
Cuvette, plastic, 1 cm path-length	Sarstedt, Nürnbrecht, Germany
Cuvette, quartz, 0.1 cm path-length	Hellma, Müllheim, Germany
Delta Pak 15u C18-300Å, 300 x 3.9 mm column	Waters Corporation, Milford, USA
Deuterium oxide (99.9%)	Cambridge Isotope Lab., Andover, USA
DH5α E. coli strain	Invitrogen, Carlsbad, USA
EDC	Sigma-Aldrich, St. Louis, USA
Restriction Endonuclease *EcoR* I	Roche Applied Science, Penzberg, Germany
Gel Filtration Calibration Kit (6.5-75 kDa)	GE Healthcare, Uppsala, Sweden
U13C6–D-glucose (99%)	Cambridge Isotope Lab., Andover, USA
Glutaraldehyde (25%)	Ajax Finechem, Taren Point, Australia
Glutathione Sepharose 4 Fast Flow	GE Healthcare, Uppsala, Sweden
Restriction Endonuclease *Hind* III	Roche Applied Science, Penzberg, Germany
HiTrap Q FF, 1 ml column	GE Healthcare, Uppsala, Sweden
HiTrap SP FF, 1 ml column	GE Healthcare, Uppsala, Sweden
Isopropyl-β-D-thiogalactopyranoside	Probiogen Biochemicals, Milton, Australia
Jupiter 5u C18 300Å, 250 x 10 mm column	Phenomenex Inc., Torrance, USA
KOD Hot Start DNA Polymerase	Merck Biosciences, Darmstadt, Germany
Maltoheptaose agarose	Sigma-Aldrich, St. Louis, USA
Molecular Weight Marker Kit (12-200 kDa)	Sigma-Aldrich, St. Louis, USA
Restriction Endonuclease *Nde* I	Roche Applied Science, Penzberg, Germany
pET23a/pET32a	Merck Biosciences, Darmstadt, Germany
pH paper strips, pH-Fix 0-14	Macherey-Nagel, Düren, Germany
pH paper strips, Special indicator (5.2-7.2)	Merck KGaA, Darmstadt, Germany

pGex-4T-3/pGex-6P-3	GE Healthcare, Uppsala, Sweden
pProEX-HTb	Invitrogen, Carlsbad, USA
Protease inhibitor cocktail set III	Merck Biosciences, Darmstadt, Germany
Restriction Endonuclease *Pst* I	Roche Applied Science, Penzberg, Germany
Pwo DNA Polymerase	Roche Applied Science, Penzberg, Germany
QAE-sephadex	Sigma-Aldrich, St. Louis, USA
Rosetta(DE3) E. coli strain	Merck Biosciences, Darmstadt, Germany
Restriction Endonuclease *Sal* I	Roche Applied Science, Penzberg, Germany
Superdex 75 10/300 GL column	GE Healthcare, Uppsala, Sweden
Superdex 200 10/300 GL column	GE Healthcare, Uppsala, Sweden
Syringe filter, 0.2 µm pore size, sterile	Advantec Toyo Kaisha, Tokyo, Japan
Syringe filter, 0.8 µm pore size, non-sterile	Sartorius AG, Göttingen, Germany
T4 DNA Ligase	Roche Applied Science, Penzberg, Germany
TALON cobalt affinity resin	BD Biosciences, Palo Alto, USA
Thrombin	Sigma-Aldrich, St. Louis, USA
TOP10 E.coli strain	Invitrogen, Carlsbad, USA
2,2,2-Trifluoroethanol-d^3 (99,5%)	Sigma-Aldrich, St. Louis, USA
Trypsin	Sigma-Aldrich, St. Louis, USA
Ultrafree-MC Centrifugal Filter (0.22 µm)	Millipore Corporation Billerica, USA
Vivaspin 20	Vivascience AG, Hannover, Germany
Restriction Endonuclease *Xba* I	Roche Applied Science, Penzberg, Germany

Appendix B: Plasmid maps of cell free expression vectors

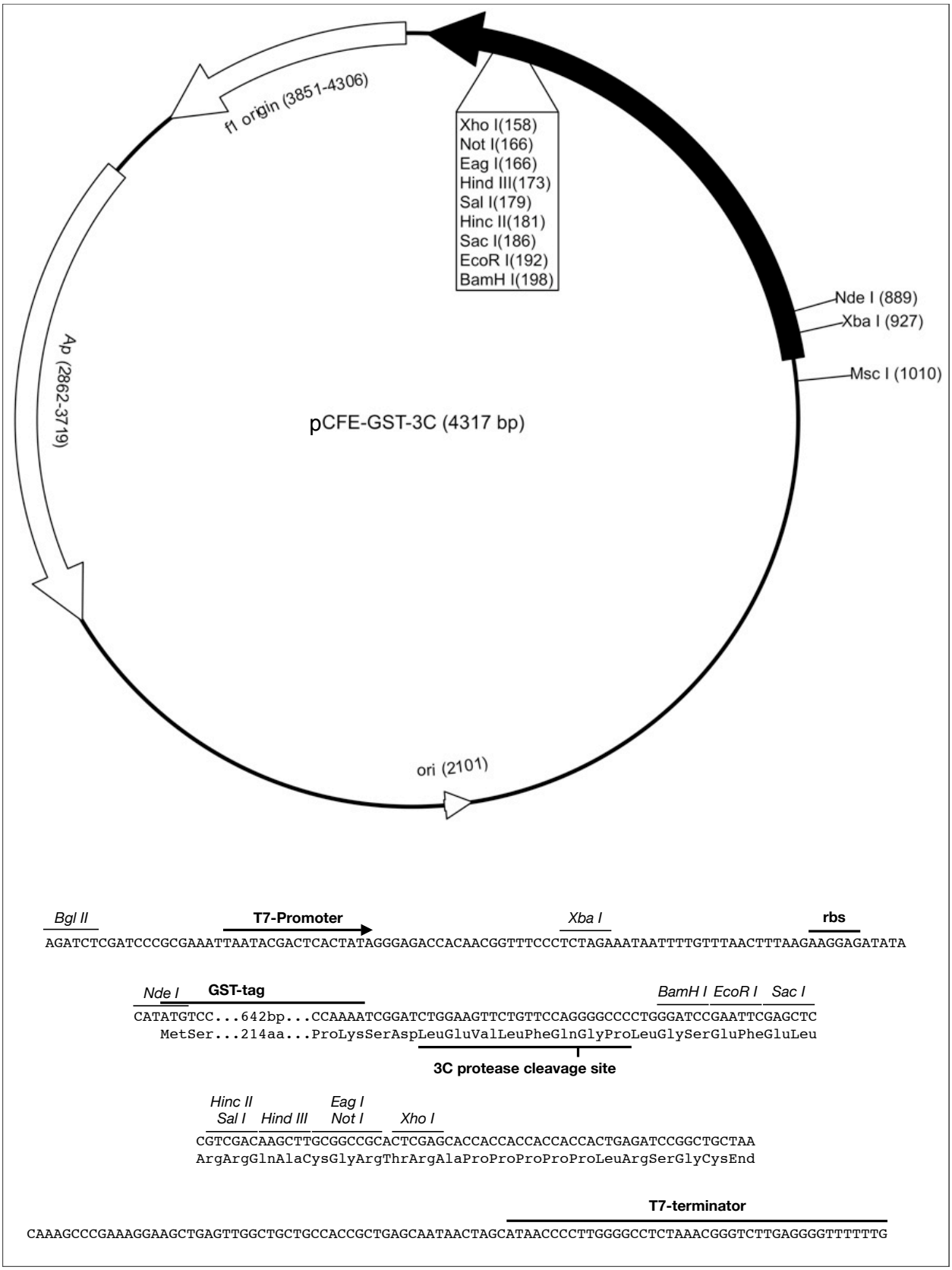

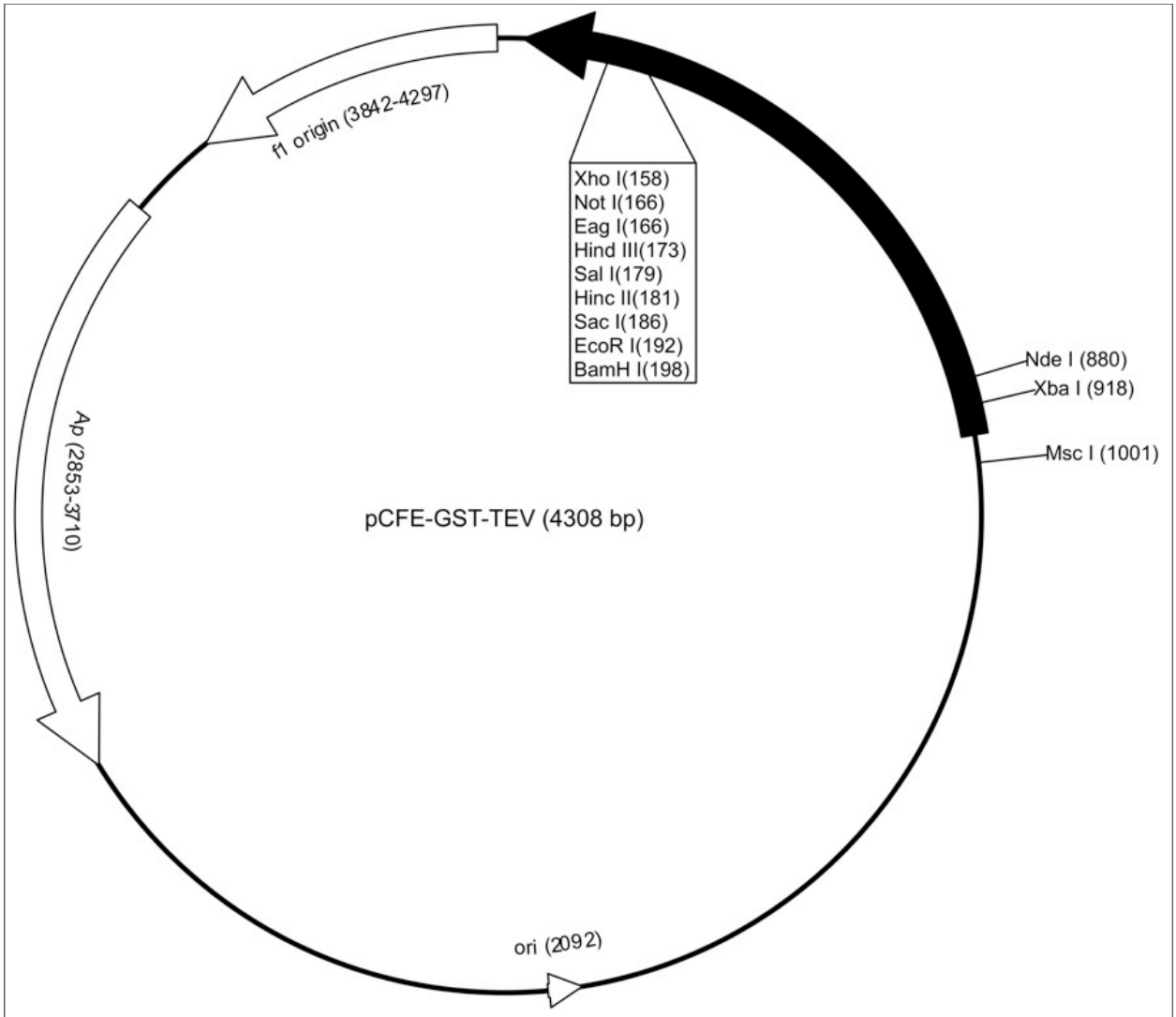

Bgl II **T7-Promoter** *Xba I* **rbs**

AGATCTCGATCCCGCGAAATTAATACGACTCACTATAGGGAGACCACAACGGTTTCCCTCTAGAAATAATTTTGTTTAACTTTAAGAAGGAGATATA

Nde I **GST-tag** *BamH I* *EcoR I* *Sac I*

CATATGTCC...642bp...CCAAAATCGGATGAAAACCTGTATTTTCAGGGATCCGAATTCGAGCTC

MetSer...214aa...ProLysSerAspGluAsnLeuTyrPheGlnGlySerGluPheGluLeu

rTEV cleavage site

Hinc II *Sal I* *Hind III* *Eag I* *Not I* *Xho I*

CGTCGACAAGCTTGCGGCCGCACTCGAGCACCACCACCACCACCACTGAGATCCGGCTGCTAA

ArgArgGlnAlaCysGlyArgThrArgAlaProProProProProLeuArgSerGlyCysEnd

T7-terminator

CAAAGCCCGAAAGGAAGCTGAGTTGGCTGCTGCCACCGCTGAGCAATAACTAGCATAACCCCTTGGGGCCTCTAAACGGGTCTTGAGGGGTTTTTTG

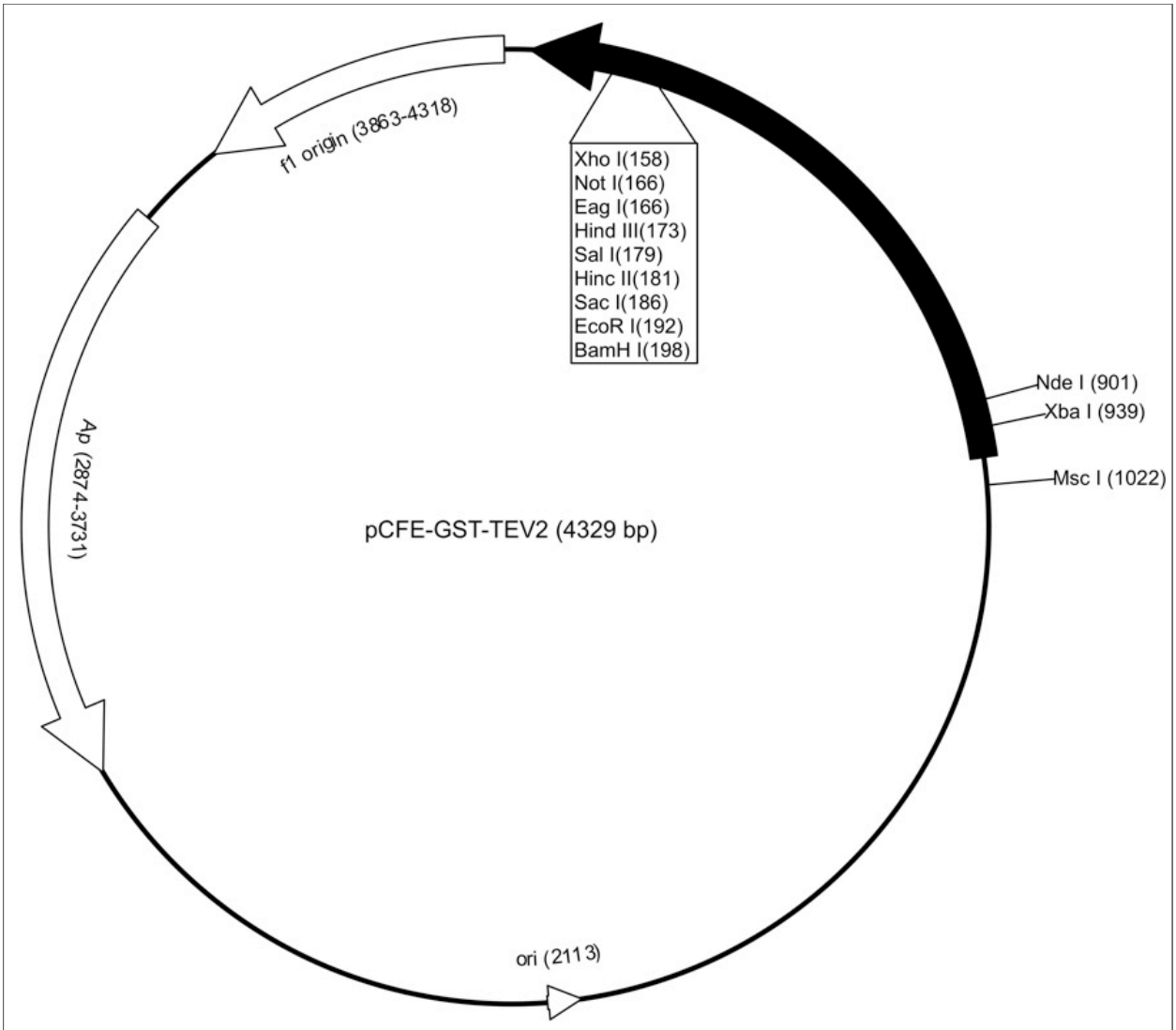

Bgl II **T7-Promoter** *Xba I* **rbs**

AGATCTCGATCCCGCGAAATTAATACGACTCACTATAGGGAGACCACAACGGTTTCCCTCTAGAAATAATTTTGTTTAACTTTAAGAAGGAGATATA

Nde I **GST-tag** *BamH I* *EcoR I* *Sac I*

CATATGTCC...642bp...CCAAAATCGGATGATTACGATATCCCAACGACCGAAAACCTGTATTTTCAGGGATCCGAATTCGAGCTC

MetSer...214aa...ProLysSerAspAspTyrAspIleProThrThrGluAsnLeuTyrPheGlnGlySerGluPheGluLeu

rTEV cleavage site

Hinc II *Sal I* *Hind III* *Eag I* *Not I* *Xho I*

CGTCGACAAGCTTGCGGCCGCACTCGAGCACCACCACCACCACCACTGAGATCCGGCTGCTAA

ArgArgGlnAlaCysGlyArgThrArgAlaProProProProProLeuArgSerGlyCysEnd

T7-terminator

CAAAGCCCGAAAGGAAGCTGAGTTGGCTGCTGCCACCGCTGAGCAATAACTAGCATAACCCCTTGGGGCCTCTAAACGGGTCTTGAGGGGTTTTTTG

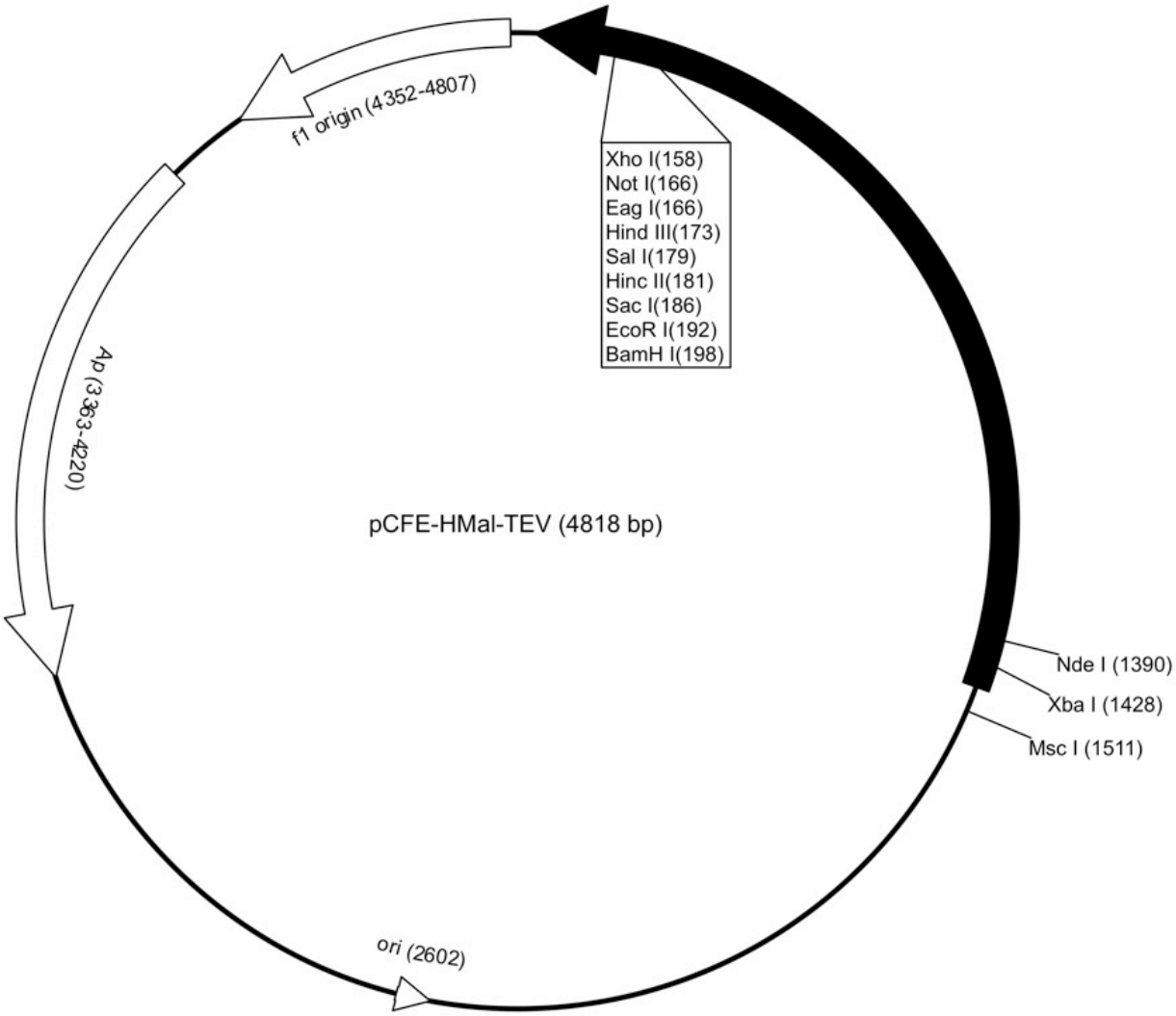

Bgl II **T7-Promoter** *Xba I* **rbs**

AGATCTCGATCCCGCGAAATTAATACGACTCACTATAGGGAGACCACAACGGTTTCCCTCTAGAAATAATTTTGTTTAACTTTAAGAAGGAGATATA

Nde I **HMBP-tag**

CATATGCATCACCATCACCATCACATGAAA..1089bp...CAGACTAATTCGAGCTCGAACAACAACAACAATAACAATAACAACAACCTCGGG

MetHisHisHisHisHisHisMetLys...363aa...GlnThrAsnSerSerSerAsnAsnAsnAsnAsnAsnAsnAsnAsnLeuGly

BamH I *EcoR I* *Sac I* *Hinc II* *Sal I* *Hind III* *Eag I* *Not I* *Xho I*

GAAAACCTGTATTTTCAGGGCGGATCCGAATTCGAGCTCCGTCGACAAGCTTGCGGCCGCACTCGAGCACCACCACCACCACCACTGAGATCCGGCTGCTAA

GluAsnLeuTyrPheGlnGlyGlySerGluPheGluLeuArgArgGlnAlaCysGlyArgThrArgAlaProProProProProLeuArgSerGlyCysEnd

rTEV cleavage site

T7-terminator

CAAAGCCCGAAAGGAAGCTGAGTTGGCTGCTGCCACCGCTGAGCAATAACTAGCATAACCCCTTGGGGCCTCTAAACGGGTCTTGAGGGGTTTTTTG

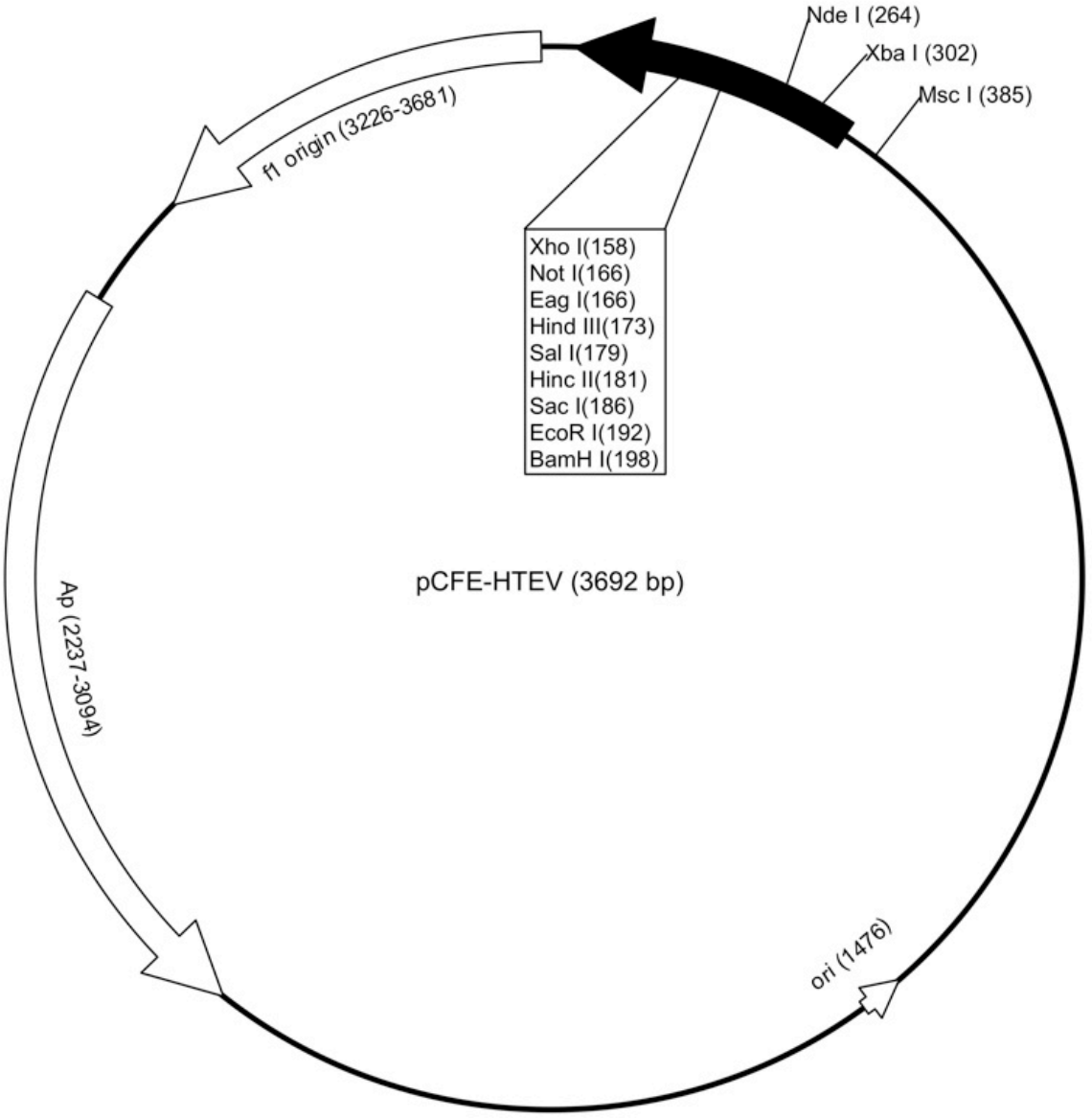

Bgl II **T7-Promoter** *Xba I* **rbs**

```
AGATCTCGATCCCGCGAAATTAATACGACTCACTATAGGGAGACCACAACGGTTTCCCTCTAGAAATAATTTTGTTTAACTTTAAGAAGGAGATATA
```

Nde I **His-tag**

```
CATATGTCGTACTACCATCACCATCACCATCACGATTACGATATCCCAACGACCGAAAACCTGTATTTTCAGTCC
   MetSerTyrTyrHisHisHisHisHisHisAspTyrAspIleProThrThrGluAsnLeuTyrPheGlnGly
```

rTEV cleavage site

BamH I *EcoR I* *Sac I* *Hinc II* *Sal I* *Hind III* *Eag I* *Not I* *Xho I*

```
GGATCCGAATTCGAGCTCCGTCGACAAGCTTGCGGCCGCACTCGAGCACCACCACCACCACCACTGAGATCCGGCTGCTAA
GlySerGluPheGluLeuArgArgGlnAlaCysGlyArgThrArgAlaProProProProProLeuArgSerGlyCysEnd
```

T7-terminator

```
CAAAGCCCGAAAGGAAGCTGAGTTGGCTGCTGCCACCGCTGAGCAATAACTAGCATAACCCCTTGGGGCCTCTAAACGGGTCTTGAGGGGTTTTTTG
```

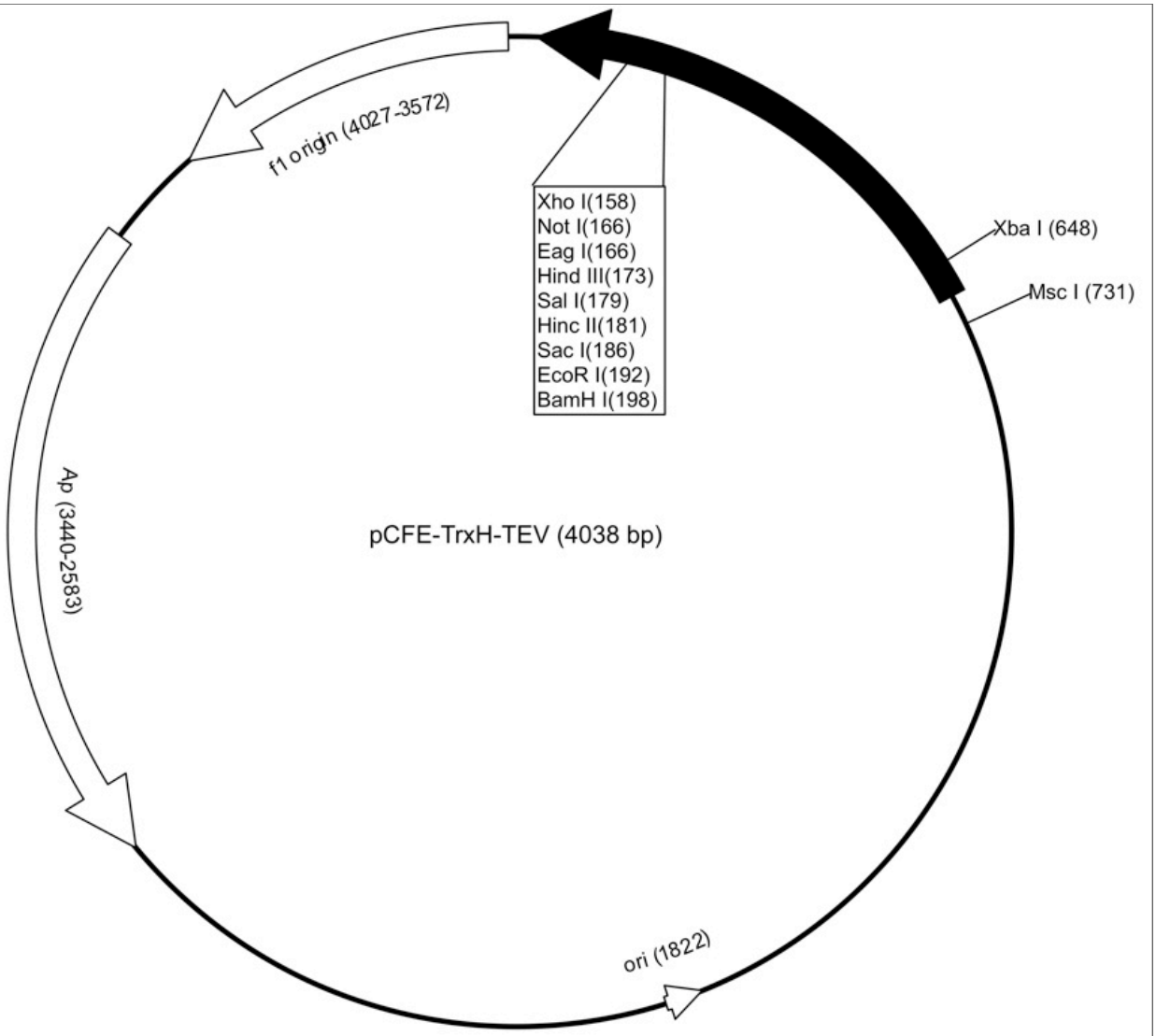

Bgl II **T7-Promoter** *Xba I* **rbs**

AGATCTCGATCCCGCGAAATTAATACGACTCACTATAGGGAGACCACAACGGTTTCCCTCTAGAAATAATTTTGTTTAACTTTAAGAAGGAGATATA

Nde I **Trx-tag** *Msc I* *Nde I* **His-tag**

CATATGAGC...315bp...CTGGCCGGTTCTGGTTCTGGCCATATGCATCACCATCACCATCACGATTACGATATCCCAACGACC

MetSer...105aa...LeuAlaGlySerGlySerGlyHisMetHisHisHisHisHisHisAspTyrAspIleProThrThr

BamH I *EcoR I* *Sac I* *Hinc II* *Sal I* *Hind III* *Eag I* *Not I* *Xho I*

GAAAACCTGTATTTTCAGGGCGGATCCGAATTCGAGCTCCGTCGACAAGCTTGCGGCCGCACTCGAGCACCACCACCACCACCACTGAGATCCGGCTGCTAA

GluAsnLeuTyrPheGlnGlyGlySerGluPheGluLeuArgArgGlnAlaCysGlyArgThrArgAlaProProProProProLeuArgSerGlyCysEnd

rTEV cleavage site

T7-terminator

CAAAGCCCGAAAGGAAGCTGAGTTGGCTGCTGCCACCGCTGAGCAATAACTAGCATAACCCCTTGGGGCCTCTAAACGGGTCTTGAGGGGTTTTTTG

Appendix C: Initial NMR spectroscopic characterisation of Par-4(286-332)WT

As discussed in Chapter 2.12.2, Par-4(286-332) constructs purified according to the original protocol described in Chapter 2.11.1. were unstable and displayed a poor spectral quality. In comparison to the more stable RP-HPLC purified rrPar-4LZ, Par-4(286-332)WT purified with original protocol displays a multitude of additional peaks at neutral pH (Fig. A.1A). As the Par-4 LZ domain is disordered under these conditions only 49 peaks are expected (51 residues - 1 N-terminal residue - 1 prolyl residue). With decreasing pH the number of additional peaks increases (Fig. A.1B and C). It was therefore assumed that this increase in peak number is associated with an increase in secondary structural content, as is suggested by CD spectroscopy for a decreasing pH [184].

Interestingly, a Par-4(286-332)WT sample that went through the whole pH titration process from pH 7.5 immediately down to 3.4 and then stepwise back to 7.5 (Fig. A.1C and D) shows a significant difference in peak numbers between the start and end point of the titration process (Fig. A.1D). To obtain spectra at intermediate pH values around pH 5 it was necessary to drop the pH first below 4 and then steadily increase it back to 7.5. Otherwise, if the pH is decreased stepwise from neutral pH precipitation occurred below pH 6.0. Note that the spectra in Figure A.1D are from two different NMR samples but from the same stock solution. A spectrum at neutral pH was not acquired prior to the pH titration as this was done with the previous sample shown in black contours in Figure A.1D. The observed difference between both spectra suggests that the increase in additional peak numbers is a time dependent process probably due to degradation. It should be noted that between individual measurements at each pH value several days passed allowing for degradation (Fig. A.1). Similar spectra were obtained for Par-4 (286-332)D305K and Par-4(286-332)E310K also suggesting degradation. Both LZ point mutants were purified with the same original protocol as Par-4(286-332)WT.

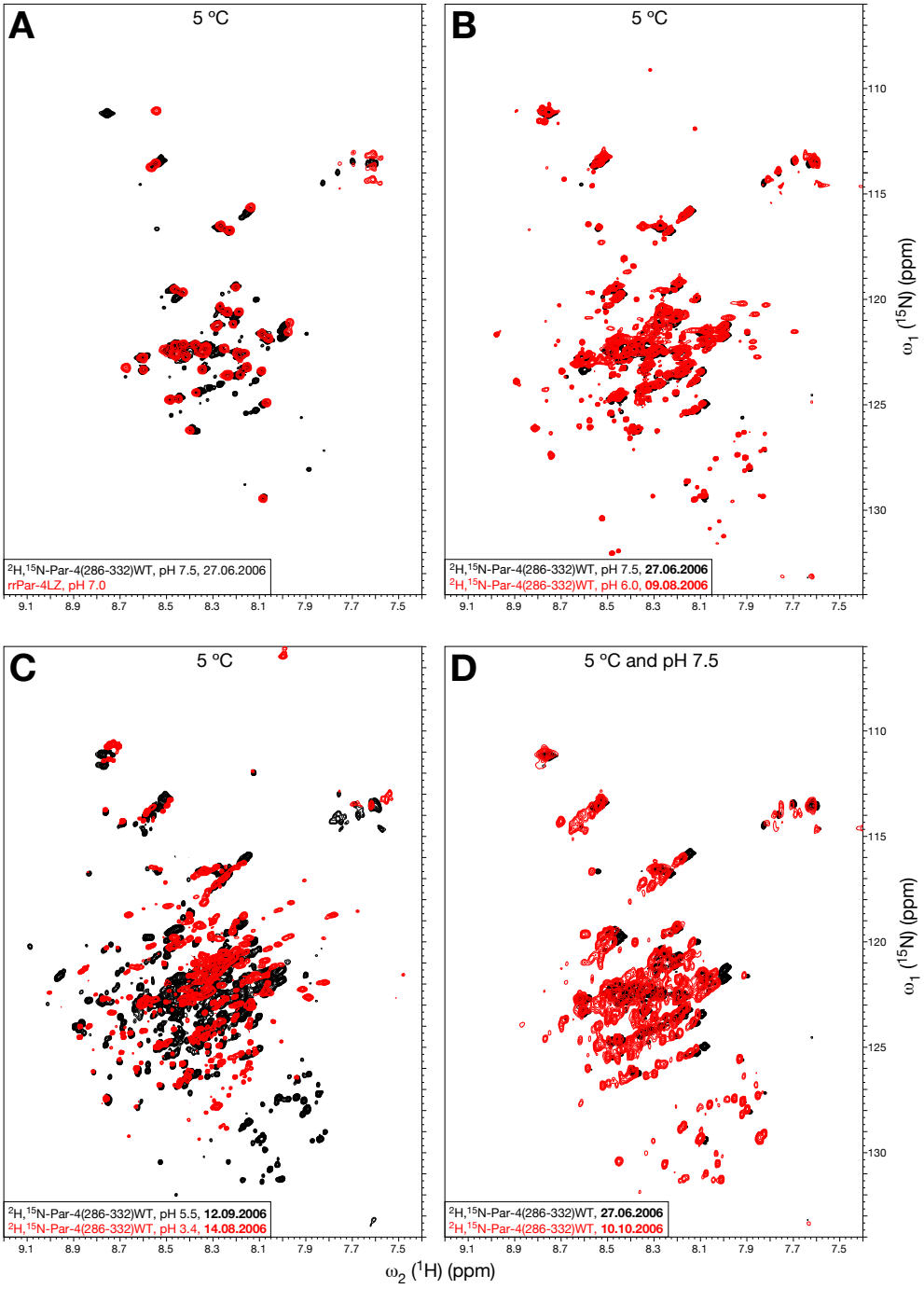

Figure A.1 *– ^{1}H,^{15}N-TROSY-HSQC spectra of Par-4(286-332)WT. (A) Pairwise comparison of the ^{1}H,^{15}N-TROSY-HSQC spectrum of Par-4(286-332)WT at pH 7.5 (black contours) with the ^{1}H,^{15}N-SOFAST-HMQC spectrum of rrPar-4LZ at pH 7.0 (red contours). (B) Overlay of the ^{1}H,^{15}N-TROSY-HSQC spectra of Par-4(286-332)WT at pH 7.5 (black contours) and pH 5.8 (red contours); (C) at pH 5.5 (black contours) and pH 3.4 (red contours); and (D) at pH 7.5. Spectra in D were acquired with two NMR samples at different dates before and after the pH titration. All spectra were acquired at 5 °C. Further acquisition parameters are given in Appendix G. Par-4(286-332)WT was uniformly ^{2}H,^{15}N-labelled; rrPar-4LZ was uniformly ^{15}N-labelled. Sample conditions were 200 µM Par-4(286-332)WT in 20 mM Na_2HPO_4/NaH_2PO_4, pH 7.5, 6.0, 5.5 or 3.4, respectively, and 5% D_2O ($^v/_v$); 75 µM rrPar-4LZ in 20 mM NaCl, 10 mM Tris, pH 7.0 and 5% D_2O ($^v/_v$). The rationale for using a deuterated Par-4(286-332)WT sample was to reduce line broadening contributions arising due to aggregation.*

Appendix D: NMR spectroscopy of the Par-4 LZ domain as GST fusion protein

a) Materials and Methods

The GST-Par-4(286-332)WT fusion protein (GST-LZ) was purified as described in Chapter 2.11.4. After adding D_2O to 5% ($^v/_v$) the sample was used for NMR spectroscopy. The GST-LZ concentration was 30 µM. After acquisition of an $^1H,^{15}N$-HSQC reference spectrum, half of the NMR sample was dialysed overnight at 4 ºC to 500 ml 50 mM NaCl, 1 mM DTT and 20 mM Na_2HPO_4/NaH_2PO_4, pH 5.5. The final NMR sample had a concentration of ~15 µM GST-LZ and contained 5% D_2O ($^v/_v$). $^1H,^{15}N$-HSQC spectra were recorded and processed as described in Chapter 3.4.1.b. Acquisition parameters are given in Appendix G.

b) Results and Discussion

Due to the stability problems of the Par-4 LZ peptides mentioned in Chapter 2.12.2, alternative methods to analyse the Par-4 LZ domain were sought. As mentioned in Chapter 3.6, for small GST-fusion proteins signals in $^1H,^{15}N$-HSQC spectra almost exclusively arise from the target protein [230]. It was proposed that signals of the GST-tag are probably broadened beyond observable limits due to dimerisation of GST. As the target protein is attached to GST through a linker sequence, it retains a certain degree of flexibility allowing rapid reorientation that results in observable peaks. Since the Par-4(286-332)WT construct is 5.9 kDa in size it seemed likely that it can be studied in this way. It was further thought that the GST tag might also increase the stability of the LZ construct and prevent proteolytic degradation to a certain extent. Furthermore, non-specific aggregation may be minimised in the presence of the bulky GST-tag. As mentioned in Chapter 2.12.2, these two factors are likely to be related to the poor quality of the initial NMR spectra. Even though these considerations made the study of GST-LZ an interesting target, other factors limiting this approach were considered as well. The presence of the bulky GST tag may interfere or prevent oligomerisation of the attached LZ domain. Also oligomerisation of the LZ domain may affect the tumbling rate and hence lead to line broadening of the peaks associated with the LZ domain.

For comparative purposes $^1H,^{15}N$-HSQC spectra of GST-LZ were acquired at pH 7.0 and 25 ºC as a reference for a disordered conformation. As mentioned earlier, coiled coil formation of the Par-4 LZ domain is pH and temperature dependent [184]. An NMR buffer at pH 5.5 was therefore used to study GST-LZ under conditions where the LZ tag is supposed to be mostly folded. Comparison of the NMR spectrum of GST-LZ at pH 7.0 and 25 ºC with rrPar-4LZ at

pH 7.0 and 25 ºC shows that both spectra are similar (Fig. A.2A). The spectrum of rrPar-4LZ at pH 7.0 and 25 ºC serves as an example for a mostly disordered conformation of the isolated (non-GST-tagged) Par-4 LZ domain (Chapter 4.3.2.). As expected, the narrow ^{1}H chemical shift dispersion and the sharp peaks observed for the GST-LZ spectrum are consistent with an unfolded conformation for the LZ tag under these conditions. Approximately 56 peaks are counted for GST-LZ consistent with the assumption that next to the resonances from the LZ tag (52 residues) also signals from the linker sequence are visible. An exact peak count is difficult due to significant signal overlap in the centre of the spectrum. Note that no assignments were made for this spectrum.

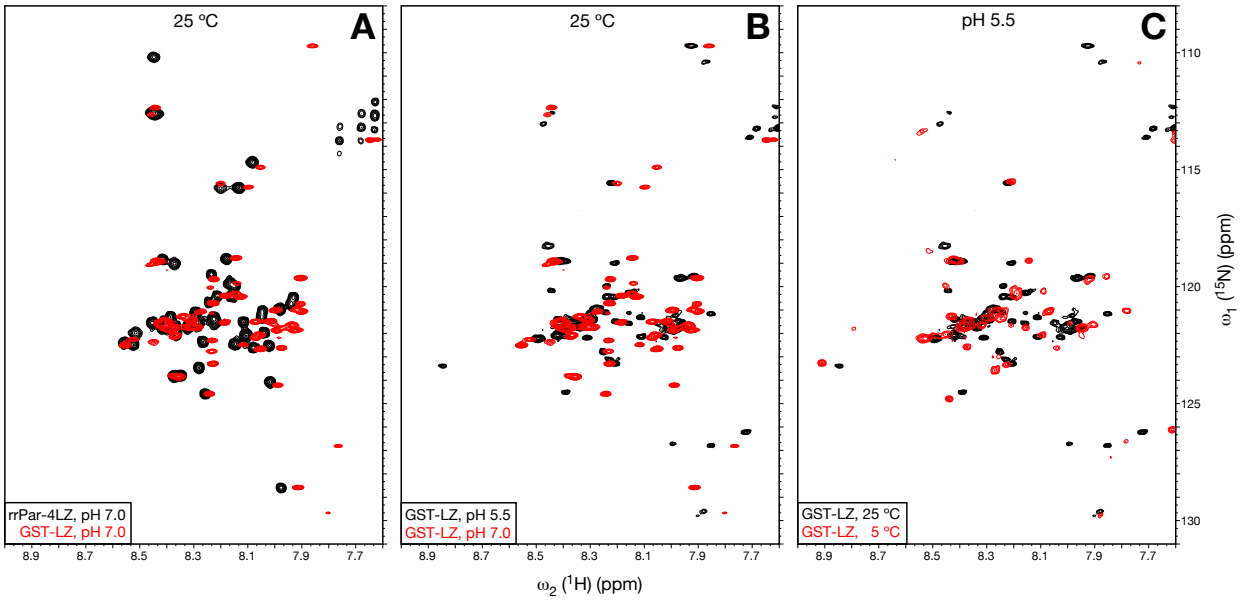

Figure A.2 *– NMR spectroscopy of the Par-4 LZ domain as a GST-fusion protein. (A) Pairwise comparison of the $^{1}H,^{15}N$-SOFAST-HMQC spectrum of rrPar-4LZ at pH 7.0 (black contours) with the $^{1}H,^{15}N$-HSQC spectrum of GST-LZ at pH 7.0 (red contours). Both spectra were acquired at 25 ºC. (B) Overlay of the $^{1}H,^{15}N$-HSQC spectra at 25 ºC of GST-LZ at pH 7.0 (red contours) and pH 5.5 (black contours). (C) Temperature dependance of the $^{1}H,^{15}N$-HSQC spectra of GST-LZ at pH 5.5. Displayed are the spectra recorded at 5ºC (red contours) and 25 ºC (black contours). Sample concentration were 75 µM rrPar-4LZ in 20 mM NaCl, 10 mM Tris, pH 7.0 and 5% D_2O (v/v); 30 µM GST-LZ in 50 mM NaCl, 1 mM DTT and 20 mM Na_2HPO_4/NaH_2PO_4, pH 7.0 and 5% D_2O (v/v), and 15 µM GST-LZ in 50 mM NaCl, 1 mM DTT and 20 mM Na_2HPO_4/NaH_2PO_4, pH 5.5 and 5% D_2O (v/v). Acquisition parameters are given in Appendix G.*

A drop in pH to 5.5 results only in minor changes for GST-LZ at 25 ºC (Fig. A.2B). Some shifted resonances are visible at pH 5.5 relative to pH 7.0, however, the overall spectrum is still indicative of a disordered conformation. The peak number seems to be unchanged with 51 easily identified peaks. Again spectral overlap prevents an exact peak count. Note that the pH decrease

to 5.5 did not resulted in protein precipitation as was observed for the isolated rrPar-4LZ constructs indicating that GST improved the solubility at pH 5.5. A decrease in temperature to further stabilise the coiled coil conformation at pH 5.5 does not result in significant changes of the NMR spectrum (Fig. A.2C). A notable difference between the two spectra at pH 5.5 is the intensity decrease for some of the resonances at 5 ºC relative to 25 ºC. This seems to be related to the slightly decreased peak number of approximately 46 peaks. A similar cross peak intensity decrease that accompanied a drop in pH was observed for rrPar-4LZ (Chapter 4.3.2.). Coiled coil formation of GST-LZ could not be verified as a CD spectrometer was not available at this time. It is therefore possible that the presence of a GST tag prevented coiled coil formation. However, SEC indicated a self-association of the GST-LZ beyond the expected dimeric state of GST (data not shown).

Taken together, an improvement in the NMR spectra that would allow a structural characterisation of the Par-4(286-332)WT construct at various pH values could not be achieved using a GST fusion protein of Par-4(286-332)WT. Since the results of RP-HPLC purified rrPar-4LZ showed no stability problems or signs of excessive aggregation, analysis of the GST-LZ fusion protein was not pursued further. This approach, however, may prove useful for the study of binding partners of the LZ domain. Various conditions for protein-protein interactions such as pH or protein concentration can be easily screened in this way [230].

Appendix E: Calibration curves for size exclusion chromatography

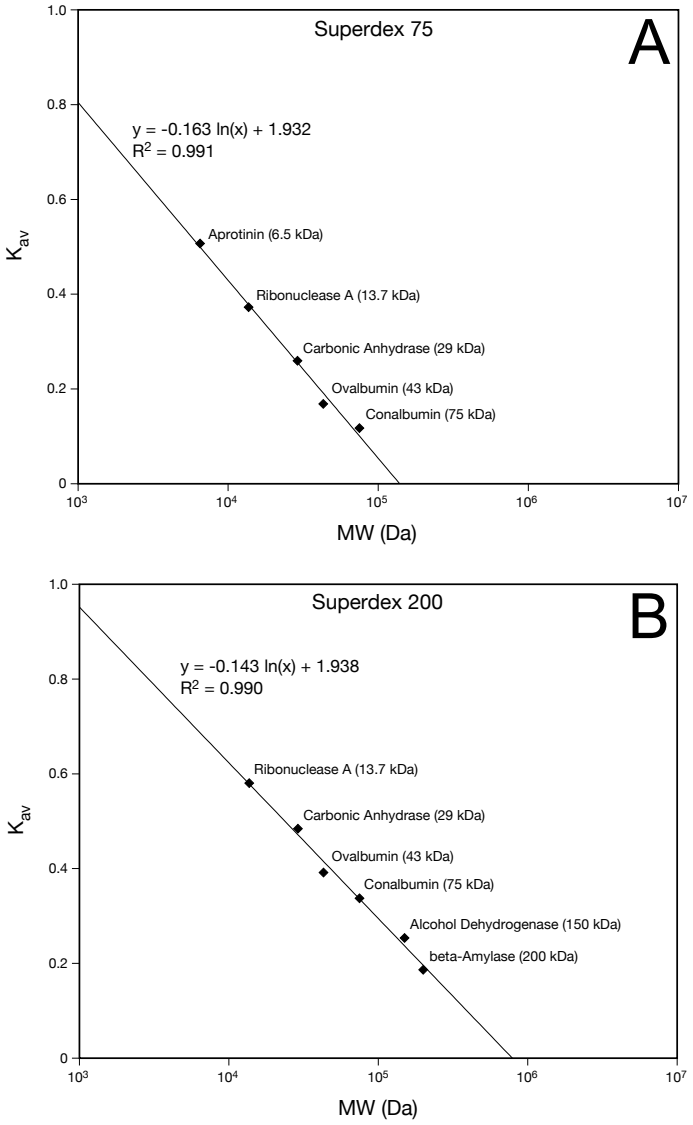

Calibration curves were established with Superdex 75 and 200 columns connected to the BioLogic DuoFlow System and using isocratic flow of 0.4 ml/min at 4 ºC. The K_{av} value is defined as $K_{av} = (V_e-V_0)/(V_c-V_0)$, where V_c is the geometric column volume, V_0 is the column void volume and V_e is the elution volume of the molecular weight marker. Trend line equations and R^2 values are given for each column.

Appendix F: CD spectropolarimetry acquisition parameters

Figure (page)	Construct	Concentration[1]	Buffer	SW[2]	SS[3]	IT[4]	TR[5]	TI[6]
Figure 3.7A and B (101), Figure 3.11B (110), Figure 4.19B (176)	rrPar-4FL	0.30 (8)	20 mM NaCl, 10 mM Tris, pH 7.0	180 - 260	0.5	1.0	5 - 85	5
Figure 3.7C and D (101)	rrPar-4ΔLZ	0.30 (10)	20 mM NaCl, 10 mM Tris, pH 7.0	180 - 260	0.5	1.0	5 - 75	5
Figure 3.7E and F (101)	rrPar-4SAC	0.30 (43)	20 mM NaCl, 10 mM Tris, pH 7.0	180 - 260	0.5	1.0	5 - 75	5
Figure 3.9A and B (105)	rrPar-4SAC	0.30 (43)	20 mM NaCl, 10 mM Tris, pH 7.0	185 - 260	1.0	1.0	5 - 75	10
Figure 3.9C and D (105)	rrPar-4SAC	0.30 (43)	20 mM NaCl, 10 mM Mes, pH 6.0	185 - 260	1.0	1.0	5 - 75	5
Figure 3.9E and F (105)	rrPar-4SAC	0.30 (43)	20 mM NaCl, 10 mM NaAc, pH 5.0	185 - 260	1.0	1.0	5 - 75	5
Figure 3.9G and H (105)	rrPar-4SAC	0.30 (43)	20 mM NaCl, 10 mM NaAc, pH 4.0	185 - 260	1.0	1.0	5 - 75	5
Figure 3.9I and J (105)	rrPar-4SAC	0.30 (43)	20 mM NaCl, 10 mM Tris, pH 5 + 30% d^3-TFE (v/v)	185 - 260	1.0	1.0	5 - 75	5
Figure 3.11B (105), Figure 4.19C (176)	rrPar-4FL	0.30 (8)	20 mM NaCl, 10 mM Tris, pH 7.0 + 1 M urea	210 - 260	0.5	1.0	5 - 75	5
Figure 3.11B (105), Figure 4.19D (176)	rrPar-4FL	0.30 (8)	20 mM NaCl, 10 mM Tris, pH 7.0 + 6 M urea	210 - 260	0.5	1.0	5 - 75	5
Figure 4.2A (124)	rrPar-4LZ	0.45 (75)	20 mM NaCl, 10 mM Tris, pH 7.0	185 - 260	1.0	1.0	5 - 75	5
Figure 4.2B (124), Figure 4.3A (127)	rrPar-4LZ	0.45 (75)	20 mM NaCl, 10 mM Mes, pH 6.5	185 - 260	1.0	1.0	5 - 75	5
Figure 4.2C (124), Figure 4.3A (127)	rrPar-4LZ	0.24 (40)	20 mM NaCl, 10 mM Mes, pH 6.0	185 - 260	1.0	1.0	5 - 75	5
Figure 4.2D (124), Figure 4.3A and B (127), Figure 4.19B (176)	rrPar-4LZ	0.30 (50)	H_2O, pH 4	175 - 260	1.0	1.0	5 - 75	5
Figure 4.2E (124), Figure 4.3B and C (127)	rrPar-4LZD305K	0.45 (75)	20 mM NaCl, 10 mM Tris, pH 7.0	185 - 260	1.0	1.0	5 - 75	5
Figure 4.2F (124), Figure 4.3B and D (127)	rrPar-4LZE310K	0.45 (75)	20 mM NaCl, 10 mM Tris, pH 7.0	185 - 260	1.0	1.0	5 - 75	5
Figure 4.3C (127), Figure 4.19C (176)	rrPar-4LZD305K	0.45 (75)	20 mM NaCl, 10 mM Tris, pH 7.0 + 1 M urea	200 - 260	1.0	1.0	5 - 75	5
Figure 4.3C (127)	rrPar-4LZD305K	0.45 (75)	20 mM NaCl, 10 mM Tris, pH 7.0 + 6 M urea	210 - 260	1.0	1.0	5 - 75	5
Figure 4.3C (127), Figure 4.19C (176)	rrPar-4LZE310K	0.45 (75)	20 mM NaCl, 10 mM Tris, pH 7.0 + 1 M urea	200 - 260	1.0	1.0	5 - 75	5
Figure 4.3C (127)	rrPar-4LZE310K	0.45 (75)	20 mM NaCl, 10 mM Tris, pH 7.0 + 6 M urea	205 - 260	1.0	1.0	5 - 75	5
Figure 4.14A, B and I (156)	rrPar-4LZ	0.45 (75)	20 mM NaCl, 10 mM Tris, pH 7 + 10% d_3-TFE (v/v)	185 - 260	1.0	1.0	5 - 75	5
Figure 4.14C, D and I (156)	rrPar-4LZ	0.45 (75)	20 mM NaCl, 10 mM Tris, pH 7 + 20% d^3-TFE (v/v)	185 - 260	1.0	1.0	5 - 75	5
Figure 4.14E, F and I (156)	rrPar-4LZ	0.45 (75)	20 mM NaCl, 10 mM Tris, pH 7 + 30% d^3-TFE (v/v)	185 - 260	1.0	1.0	5 - 75	5
Figure 4.14G, H and I (156)	rrPar-4LZ	0.45 (75)	20 mM NaCl, 10 mM Tris, pH 5 + 30% d^3-TFE (v/v)	185 - 260	1.0	1.0	5 - 75	5
Figure 4.16A, B and G (166)	rrPar-4LZN313I	0.30 (50)	20 mM NaCl, 10 mM Tris, pH 7.0	190 - 260	1.0	1.0	5 - 75	5
Figure 4.16C, D and G (166)	rrPar-4LZN313I	0.04 (7)	20 mM NaCl, 10 mM Mes, pH 6.0	190 - 260	1.0	1.0	5 - 75	5
Figure 4.16E, F and G (166)	rrPar-4LZN313I	0.24 (40)	H_2O, pH 4	180 - 260	1.0	1.0	5 - 75	5
Figure 4.18A and B (174), Figure 4.19A and B (176)	rrPar-4CC	0.30 (25)	H_2O, pH 4	175 - 260	1.0	1.0	5 - 75	5
Figure 4.18C and D (174), Figure 4.19A and C (176)	rrPar-4CC	0.08 (7)	20 mM NaCl, 10 mM Tris, pH 7.0 + 1 M urea	205 - 260	1.0	1.0	5 - 75	5
Figure 4.18E and F (174), Figure 4.19A and D (176)	rrPar-4CC	0.3 (25)	20 mM NaCl, 10 mM Tris, pH 7.0 + 6 M urea	210 - 260	1.0	1.0	5 - 75	5

[1] Concentration in mg/ml (μM)
[2] SW - Spectral width (nm)
[3] SS - Step size (nm)
[4] IT - Integration time (s)
[5] TR - Temperature range (°C)
[6] TI - Temperature intervall (°C)

Appendix G: NMR spectroscopy acquisition parameters

Figure (page)	Construct	Concentration	Buffer[1]	Experiment	Temperature	SFRQ[2]	Transients	SW[3] (^{1}H)	SW[3] (^{15}N)	NP[4] (^{1}H)	NI[5] (^{15}N)	CF[6] (^{15}N)	D1[7]	BW SP[8]	offset SP[9]
Figure 3.8A and C (102)	rrPar-4FL	480 µM	20 mM NaCl, 10 mM Tris, pH 7.0	{^{1}H, ^{15}N}-HSQC	5 ºC	700.25	200	11.98	30.0	2048	128	119.0	2.0	N/A	N/A
Figure 3.8A and B (102)	{^{15}N} rrPar-4ΔLZ	90 µM	100 mM NaCl, 1 mM DTT, 20 mM Na_2HPO_4/NaH_2PO_4, pH 7.5	{^{1}H, ^{15}N}-HSQC	5 ºC	700.25	20	11.98	30.0	2048	128	120.0	1.5	N/A	N/A
Figure 3.8B and C (102), Figure 3.10A and B (107)	{^{15}N} rrPar-SAC	340 µM	20 mM NaCl, 10 mM Tris, pH 7.0	{^{1}H, ^{15}N}-HSQC	5 ºC	700.25	24	11.98	40.0	2048	256	120.0	1.0	N/A	N/A
Figure 3.10A (107)	{^{15}N} rrPar-SAC	500 µM	PBS, pH 7.4	{^{1}H, ^{15}N}-HSQC	5 ºC	700.25	8	11.98	30.0	2048	256	119.0	1.0	N/A	N/A
Figure 3.10B (107)	{^{15}N } rrPar-SAC	43 µM	20 mM NaCl, 10 mM Tris, pH 5 + 30% d^3-TFE (v/v)	{^{1}H, ^{15}N}-SOFAST-HMQC	5 ºC	700.25	24	10.00	30.0	800	128	119.0	0.1	3.0	8.0
Figure 4.9A (142), Figure 4.13A (153), Figure 4.17A (167), Figure A.1A (167)	{^{15}N } rrPar-4LZ	75 µM	20 mM NaCl, 10 mM Tris, pH 7.0	{^{1}H, ^{15}N}-SOFAST-HMQC	5 ºC	700.25	24	10.00	30.0	800	128	119.0	0.1	2.0	7.8
Figure 4.9A and B (142), Figure 4.15A (161)	{^{15}N } rrPar-4LZ	40 µM	20 mM NaCl, 10 mM Mes, pH 6.0	{^{1}H, ^{15}N}-SOFAST-HMQC	5 ºC	700.25	96	10.00	30.0	800	128	119.0	0.1	2.0	7.8
Figure 4.9A and B (142)	{^{15}N } rrPar-4LZ	40 µM	20 mM NaCl, 10 mM Mes, pH 6.0	{^{1}H, ^{15}N}-SOFAST-HMQC	25 ºC	700.25	96	10.00	30.0	800	128	119.0	0.1	2.0	7.8
Figure 4.9C (142), Figure A.2A (201)	{^{15}N } rrPar-4LZ	75 µM	20 mM NaCl, 10 mM Tris, pH 7.0	{^{1}H, ^{15}N}-SOFAST-HMQC	25 ºC	700.25	24	10.00	30.0	800	128	119.0	0.1	2.0	7.8
Figure 4.9C (142), Figure 4.12A and B (149), Figure 4.17B (167)	{^{15}N } rrPar-4LZ	50 µM	H_2O, pH 4	{^{1}H, ^{15}N}-SOFAST-HMQC	25 ºC	700.25	24	10.00	30.0	800	128	119.0	0.1	3.0	7.8
Figure 4.12A (149)	{^{15}N } rrPar-4LZE310K	75 µM	20 mM NaCl, 10 mM Tris, pH 7.0	{^{1}H, ^{15}N}-SOFAST-HMQC	25 ºC	700.25	24	10.00	30.0	800	128	119.0	0.1	2.0	7.8
Figure 4.12B, C and D (149)	{^{15}N } rrPar-4LZD305K	75 µM	20 mM NaCl, 10 mM Tris, pH 7.0	{^{1}H, ^{15}N}-SOFAST-HMQC	25 ºC	700.25	24	10.00	30.0	800	128	119.0	0.1	2.0	7.8
Figure 4.12C (149)	{^{15}N } rrPar-4LZD305K	75 µM	20 mM NaCl, 10 mM Tris, pH 7.0 + 1 M urea	{^{1}H, ^{15}N}-SOFAST-HMQC	25 ºC	700.25	24	10.00	30.0	800	128	119.0	0.1	2.0	8.0
Figure 4.12D (149)	{^{15}N } rrPar-4LZD305K	75 µM	20 mM NaCl, 10 mM Tris, pH 7.0 + 6 M urea	{^{1}H, ^{15}N}-SOFAST-HMQC	25 ºC	700.25	24	10.00	30.0	800	128	119.0	0.1	3.0	8.0
Figure 4.13A and B (153)	{^{2}H, ^{13}C, ^{15}N } rrPar-4LZE310K	75 µM	20 mM NaCl, 10 mM Tris, pH 7.0	{^{1}H, ^{15}N}-TROSY-HSQC	5 ºC	700.25	48	10.00	30.0	2048	256	119.0	1.5	N/A	N/A
Figure 4.13B (153)	{^{15}N } rrPar-4LZ	40 µM	20 mM NaCl, 10 mM Mes, pH 6.0	{^{1}H, ^{15}N}-SOFAST-HMQC	5 ºC	700.25	512	10.00	30.0	800	128	119.0	0.1	3.0	7.8
Figure 4.15A and B (161)	{^{15}N } rrPar-4LZ	75 µM	20 mM NaCl, 10 mM Tris, pH 7 + 10% d^3-TFE (v/v)	{^{1}H, ^{15}N}-SOFAST-HMQC	5 ºC	700.25	24	10.00	30.0	800	128	119.0	0.1	3.0	7.8
Figure 4.15B (161)	{^{15}N } rrPar-4LZ	75 µM	20 mM NaCl, 10 mM Tris, pH 7 + 20% d^3-TFE (v/v)	{^{1}H, ^{15}N}-SOFAST-HMQC	5 ºC	700.25	24	10.00	30.0	800	128	119.0	0.1	3.0	7.8
Figure 4.15C (161)	{^{15}N } rrPar-4LZ	75 µM	20 mM NaCl, 10 mM Tris, pH 7 + 10% d^3-TFE (v/v)	{^{1}H, ^{15}N}-SOFAST-HMQC	25 ºC	700.25	24	10.00	30.0	800	128	119.0	0.1	3.0	7.8
Figure 4.15D (161)	{^{15}N } rrPar-4LZ	75 µM	20 mM NaCl, 10 mM Tris, pH 7 + 30% d^3-TFE (v/v)	{^{1}H, ^{15}N}-SOFAST-HMQC	25 ºC	700.25	24	10.00	30.0	800	128	119.0	0.1	3.0	8.0
Figure 4.17A (167)	{^{15}N } rrPar-4LZN3131	50 µM	20 mM NaCl, 10 mM Tris, pH 7.0	{^{1}H, ^{15}N}-SOFAST-HMQC	5 ºC	700.25	24	10.00	30.0	800	128	119.0	0.1	3.0	7.8
Figure 4.17B and C (167)	{^{15}N } rrPar-4LZN3131	40 µM	H_2O, pH 4	{^{1}H, ^{15}N}-SOFAST-HMQC	25 ºC	700.25	24	10.00	30.0	800	128	119.0	0.1	3.0	7.8
Figure 4.17C (167)	{^{15}N } rrPar-4LZN3131	2.5 mM	H_2O, pH 4	{^{1}H, ^{15}N}-HSQC	25 ºC	700.25	24	11.98	30.0	2048	256	119.0	2.0	N/A	N/A
Figure A.1A, B and D (199)	{^{2}H, ^{15}N} Par-4(286-332)WT	200 µM	20 mM Na_2HPO_4/NaH_2PO_4, pH 7.5	{^{1}H, ^{15}N}-TROSY-HSQC	5 ºC	700.25	112	11.98	30.0	2048	256	120.5	1.5	N/A	N/A
Figure A.1B (199)	{^{2}H, ^{15}N} Par-4(286-332)WT	200 µM	20 mM Na_2HPO_4/NaH_2PO_4, pH 6.0	{^{1}H, ^{15}N}-TROSY-HSQC	5 ºC	700.25	112	11.98	30.0	2048	256	120.5	1.5	N/A	N/A
Figure A.1C (199)	{^{2}H, ^{15}N} Par-4(286-332)WT	200 µM	20 mM Na_2HPO_4/NaH_2PO_4, pH 5.5	{^{1}H, ^{15}N}-TROSY-HSQC	5 ºC	700.25	112	11.98	40.0	2048	256	115.5	1.5	N/A	N/A
Figure A.1C (199)	{^{2}H, ^{15}N} Par-4(286-332)WT	200 µM	20 mM Na_2HPO_4/NaH_2PO_4, pH 3.4	{^{1}H, ^{15}N}-TROSY-HSQC	5 ºC	700.25	112	11.98	30.0	2048	256	120.5	1.5	N/A	N/A
Figure A.1D (199)	{^{2}H, ^{15}N} Par-4(286-332)WT	200 µM	20 mM Na_2HPO_4/NaH_2PO_4, pH 7.5	{^{1}H, ^{15}N}-TROSY-HSQC	5 ºC	700.25	40	11.98	30.0	2048	128	120.5	1.0	N/A	N/A
Figure A.2A and B (201)	{^{15}N} GST-LZ	30 µM	50 mM NaCl, 1 mM DTT, 20 mM Na_2HPO_4/NaH_2PO_4, pH 7.0	{^{1}H, ^{15}N}-HSQC	25 ºC	700.25	64	11.98	25.0	2048	256	119.0	2.0	N/A	N/A
Figure A.2B and C (201)	{^{15}N} GST-LZ	15 µM	50 mM NaCl, 1 mM DTT, 20 mM Na_2HPO_4/NaH_2PO_4, pH 5.5	{^{1}H, ^{15}N}-HSQC	25 ºC	700.25	128	11.98	25.0	2048	256	119.0	2.0	N/A	N/A
Figure A.2C (201)	{^{15}N} GST-LZ	15 µM	50 mM NaCl, 1 mM DTT, 20 mM Na_2HPO_4/NaH_2PO_4, pH 5.5	{^{1}H, ^{15}N}-HSQC	5 ºC	700.25	128	11.98	25.0	2048	128	119.0	2.0	N/A	N/A

[1] all buffers contained 5% D_2O (v/v)
[2] SFRQ - Spectrometer frequency (^{1}H) in MHz
[3] SW - Sweep width in ppm
[4] NP - Number of points per increment
[5] NI - Number of increments
[6] CF - Carrier frequency in ppm
[7] D1 - Recycle delay in s
[8] BW SP - Band with of soft proton pulse
[9] offset SP - offset of soft proton pulse

Appendix H: Chemical Shifts for Par-4(286-332)WT

Residue	H^{α} (ppm)	C^{α} (ppm)	C^{β} (ppm)	C' (ppm)
Gly -4	4.01	43.25	N/A	N/A
Pro -3	4.50	63.52	32.31	177.63
Gly -2	4.03	45.25	N/A	174.47
Ser -1	4.45	58.61	63.76	174.93
Gln 286	4.37	55.99	29.34	175.86
Asp 287	4.57	54.74	41.13	176.45
Lys 288	N/A	56.85	33.01	176.83
Glu 289	4.26	56.95	30.31	176.89
Glu 290	4.25	56.84	30.34	176.78
Met 291	N/A	55.71	32.65	176.55
Ile 292	N/A	61.88	38.50	177.78
Gly 293	3.94	45.45	N/A	174.24
Lys 294	4.32	56.39	33.31	176.91
Leu 295	4.35	55.43	42.30	177.72
Lys 296	N/A	57.04	32.97	176.78
Glu 297	4.25	56.64	30.41	176.59
Glu 298	4.28	56.88	30.29	176.96
Ile 299	4.08	61.77	38.93	176.32
Asp 300	4.26	54.66	41.00	176.55
Leu 301	4.24	55.86	42.21	174.93
Leu 302	N/A	55.65	42.07	176.55
Asn 303	N/A	53.35	38.80	175.26
Arg 304	N/A	56.38	30.97	176.16
Asp 305	4.58	54.73	40.98	176.55
Leu 306	4.30	55.49	42.23	177.60
Asp 307	N/A	54.75	41.13	176.19
Asp 308	4.59	54.49	41.00	176.42
Met 309	4.48	55.64	32.83	176.62
Glu 310	4.24	56.87	30.27	176.96
Asp 311	4.58	54.55	41.38	176.90
Glu 312	4.21	57.58	29.99	176.98
Asn 313	4.67	54.15	38.88	176.33
Glu 314	4.14	58.04	29.77	177.68
Gln 315	4.18	57.39	28.77	177.33

Residue	H^{α} (ppm)	C^{α} (ppm)	C^{β} (ppm)	C' (ppm)
Leu 316	4.18	56.16	41.98	178.20
Lys 317	4.22	57.37	32.81	177.63
Gln 318	4.26	56.42	29.21	176.83
Glu 319	4.21	57.35	30.16	176.82
Asn 320	4.70	53.68	38.57	175.88
Lys 321	4.31	57.13	32.88	177.34
Thr 322	N/A	62.94	69.52	174.70
Leu 323	4.34	55.40	42.24	177.29
Leu 324	4.32	55.22	42.25	177.26
Lys 325	4.32	56.28	33.07	176.45
Val 326	4.11	62.33	32.91	176.40
Val 327	4.09	62.87	32.77	176.84
Gly 328	3.96	45.21	N/A	173.93
Gln 329	4.33	55.77	29.78	176.08
Leu 330	4.44	55.29	42.45	177.62
Thr 331	4.36	61.84	70.08	173.64
Arg 332	N/A	57.483	31.471	N/A

Appendix I: Bibliography

1. Thompson CB. Apoptosis in the pathogenesis and treatment of disease. *Science* 1995; 267 (5203); 1456-1462
2. Danial NN, Korsmeyer SJ. Cell Death: Critical Control Points. Cell 2004; 116 (2); 205-219
3. Lockshin RA, Williams CM. Programmed cell death--II. Endocrine potentiation of the breakdown of the intersegmental muscles of silkmoths. *J Insect Physiol* 1964; 10 (4); 643-649
4. Hanahan D, Weinberg RA. The Hallmarks of Cancer. *Cell* 2000; 100 (1); 57-70
5. Evan GI, Vousden KH. Proliferation, cell cycle and apoptosis in cancer. *Nature* 2001; 411 (6835); 342-348
6. Croce CM. Oncogenes and Cancer. *N Engl J Med* 2008; 358 (5); 502-511
7. Leist M, Jäättelä M. Four deaths and a funeral: from caspases to alternative mechanisms. *Nat Rev Mol Cell Biol* 2001; 2 (8); 589-598
8. Zhao Y, Rangnekar VM. Apoptosis and tumor resistance conferred by Par-4. *Cancer Biol Ther* 2008; 7 (12); 1867-1874
9. Kyprianou N, English HF, Isaacs JT. Programmed Cell Death during Regression of PC-82 Human Prostate Cancer following Androgen Ablation. *Cancer Res* 1990; 50 (12); 3748-3753
10. Rangnekar VM. Apoptosis Mediated by a Novel Leucine Zipper Protein Par-4. *Apoptosis* 1998; 3 (2); 61-66
11. Matsuyama S, Reed JC. Mitochondria-dependent apoptosis and cellular pH regulation. *Cell* Death Differ 2000; 7; 1155-1165
12. Martikainen P, Kyprianou N, Tucker RW, Isaacs JT. Programmed Death of Nonproliferating Androgen-independent Prostatic Cancer Cells. *Cancer Res* 1991; 51 (17); 4693-4700
13. Sells SF, Wood DP, Jr., Joshi-Barve SS, Muthukumar S, Jacob RJ, Crist SA, Humphreys S, Rangnekar VM. Commonality of the gene programs induced by effectors of apoptosis in androgen-dependent and -independent prostate cells. *Cell Growth Differ* 1994; 5 (4); 457-466
14. Johnstone RW, See RH, Sells SF, Wang J, Muthukkumar S, Englert C, Haber DA, Licht JD, Sugrue SP, Roberts T, Rangnekar VM, Shi Y. A novel repressor, par-4, modulates transcription and growth suppression functions of the Wilms' tumor suppressor WT1. *Mol Cell Biol* 1996; 16 (12); 6945-6956
15. Boghaert ER, Sells SF, Walid AJ, Malone P, Williams NM, Weinstein MH, Strange R, Rangnekar VM. Immunohistochemical analysis of the proapoptotic protein Par-4 in normal rat tissues. *Cell* Growth Differ 1997; 8 (8); 881-890
16. Page G, Kögel D, Rangnekar V, Scheidtmann KH. Interaction partners of Dlk/ZIP kinase: co-expression of Dlk/ZIP kinase and Par-4 results in cytoplasmic retention and apoptosis. *Oncogene* 1999; 18 (51); 7265-7273
17. Paige AJW. Redefining tumour suppressor genes: exceptions to the two-hit hypothesis. *Cell Mol Life Sci* 2003; 60 (10); 2147-2163
18. Cook J, Krishnan S, Ananth S, Sells SF, Shi Y, Walther MM, Linehan WM, Sukhatme VP, Weinstein MH, Rangnekar VM. Decreased expression of the pro-apoptotic protein Par-4 in renal cell carcinoma. *Oncogene* 1999; 18 (5); 1205-1208

19. Kogel D, Reimertz C, Mech P, Poppe M, Fruhwald MC, Engemann H, Scheidtmann KH, Prehn JHM. Dlk/ZIP kinase-induced apoptosis in human medulloblastoma cells: requirement of the mitochondrial apoptosis pathway. *Br J Cancer* 2001; 85 (11); 1801-1808
20. Boehrer S, Chow KU, Puccetti E, Ruthardt M, Godzisard S, Krapohl A, Schneider B, Hoelzer D, Mitrou PS, Rangnekar VM, Weidmann E. Deregulated expression of prostate apoptosis response gene-4 in less differentiated lymphocytes and inverse expressional patterns of par-4 and bcl-2 in acute lymphocytic leukemia. *Hematol J* 2001; 2 (2); 103-107
21. Joshi J, Fernandez-Marcos PJ, Galvez A, Amanchy R, Linares JF, Duran A, Pathrose P, Leitges M, Canamero M, Collado M, Salas C, Serrano M, Moscat J, Diaz-Meco MT. Par-4 inhibits Akt and suppresses Ras-induced lung tumorigenesis. *EMBO J* 2008; 27 (16); 2181-2193
22. Moreno-Bueno G, Fernandez-Marcos PJ, Collado M, Tendero MJ, Rodriguez-Pinilla SM, Garcia-Cao I, Hardisson D, Diaz-Meco MT, Moscat J, Serrano M, Palacios J. Inactivation of the Candidate Tumor Suppressor Par-4 in Endometrial Cancer. *Cancer Res* 2007; 67 (5); 1927-1934
23. Johnstone RW, Tommerup N, Hansenb C, Vissingc H, Shi Y. Mapping of the Human PAWR (par-4) Gene to Chromosome 12q21. *Genomics* 1998; 53 (2); 241-243
24. Murty VVVS, Renault B, Falk CT, Bosl GJ, Kpati R, Chaganti RSK. Physical Mapping of a Commonly Deleted Region, the Site of a Candidate Tumor Suppressor Gene, at 12q22 in Human Male Germ Cell Tumors. *Genomics* 1996; 35 (3); 562-570
25. Azmi AS, Wang Z, Burikhanov R, Rangnekar VM, Wang G, Chen J, Wang S, Sarkar FH, Mohammad RM. Critical role of prostate apoptosis response-4 in determining the sensitivity of pancreatic cancer cells to small-molecule inhibitor-induced apoptosis. *Mol Cancer Ther* 2008; 7 (9); 2884-2893
26. Gurumurthy S, Goswami A, Vasudevan KM, Rangnekar VM. Phosphorylation of Par-4 by Protein Kinase A Is Critical for Apoptosis. *Mol Cell Biol* 2005; 25 (3); 1146-1161
27. El-Guendy N, Rangnekar VM. Apoptosis by Par-4 in cancer and neurodegenerative diseases. *Exp Cell Res* 2003; 283 (1); 51-66
28. Bos JL. ras Oncogenes in Human Cancer: A Review. *Cancer Res* 1989; 49 (17); 4682-4689
29. Barradas M, Monjas A, Diaz-Meco MT, Serrano M, Moscat J. The downregulation of the pro-apoptotic protein Par-4 is critical for Ras-induced survival and tumor progression. *EMBO J* 1999; 18 (22); 6362-6369
30. Taglialatela G, Gegg M, Perez-Polo JR, Williams LR, Rose GM. Evidence for DNA fragmentation in the CNS of aged Fischer-344 rats. *Neuroreport* 1996; 7 (5); 977-980
31. Bieberich E, MacKinnon S, Silva J, Noggle S, Condie BG. Regulation of cell death in mitotic neural progenitor cells by asymmetric distribution of prostate apoptosis response 4 (PAR-4) and simultaneous elevation of endogenous ceramide. *J Cell Biol* 2003; 162 (3); 469-479
32. Loo DT, Copani A, Pike CJ, Whittemore ER, Walencewicz AJ, Cotman CW. Apoptosis is induced by beta-amyloid in cultured central nervous system neurons. *Proc Natl Acad Sci USA* 1993; 90 (17); 7951-7955

33. Duan W, Zhang Z, Gash DM, Mattson MP. Participation of prostate apoptosis response-4 in degeneration of dopaminergic neurons in models of Parkinson's disease. *Ann Neurol* 1999; 46 (4); 587-597
34. Duan W, Guo Z, Mattson MP. Participation of Par-4 in the Degeneration of Striatal Neurons Induced by Metabolic Compromise with 3-Nitropropionic Acid. *Exp Neurol* 2000; 165 (1); 1-11
35. Pedersen WA, Luo H, Kruman I, Kasarskis E, Mattson MP. The prostate apoptosis response-4 protein participates in motor neuron degeneration in amyotrophic lateral sclerosis. *FASEB J* 2000; 14 (7); 913-924
36. Kruman II, Nath A, Maragos WF, Chan SL, Jones M, Rangnekar VM, Jakel RJ, Mattson MP. Evidence that Par-4 Participates in the Pathogenesis of HIV Encephalitis. *Am J Pathol* 1999; 155 (1); 39-46
37. Bredesen DE, Rao RV, Mehlen P. Cell death in the nervous system. *Nature* 2006; 443 (7113); 796-802
38. Mattson M, Duan W, Chan S, Camandola S. Par-4: an emerging pivotal player in neuronal apoptosis and neurodegenerative disorders. *J Mol Neurosci* 1999; 13 (1); 17-30
39. Duan W, Rangnekar V, M. , Mattson M, P. . Prostate Apoptosis Response-4 Production in Synaptic Compartments Following Apoptotic and Excitotoxic Insults. *J Neurochem* 1999; 72 (6); 2312-2322
40. Guo Q, Fu W, Xie J, Luo H, Sells SF, Geddes JW, Bondada V, Rangnekar VM, Mattson MP. Par-4 is a mediator of neuronal degeneration associated with the pathogenesis of Alzheimer disease. *Nat Med* 1998; 4 (8); 957-962
41. Vetterkind S, Morgan KG. The pro-apoptotic protein Par-4 facilitates vascular contractility by cytoskeletal targeting of ZIPK. *J Cell Mol Med* 2009; 13 (5); 887-895
42. Lafuente MJ, Martin P, Garcia-Cao I, Diaz-Meco MT, Serrano M, Moscat J. Regulation of mature T lymphocyte proliferation and differentiation by Par-4. *EMBO J* 2003; 22 (18); 4689-4698
43. Xie J, Guo Q. Par-4 Inhibits Choline Uptake by Interacting with CHT1 and Reducing Its Incorporation on the Plasma Membrane. *J Biol Chem* 2004; 279 (27); 28266-28275
44. Guo Q, Xie J, Chang X, Zhang X, Du H. Par-4 is a synaptic protein that regulates neurite outgrowth by altering calcium homeostasis and transcription factor AP-1 activation. *Brain Res* 2001; 903 (1-2); 13-25
45. Park SK, Nguyen MD, Fischer A, Luke MP-S, Affar EB, Dieffenbach PB, Tseng H-C, Shi Y, Tsai L-H. Par-4 Links Dopamine Signaling and Depression. *Cell* 2005; 122 (2); 275-287
46. Libich DS, Schwalbe M, Kate S, Venugopal H, Claridge JK, Edwards PJ, Dutta K, Pascal SM. Intrinsic Disorder and Coiled-coil formation in Prostate Apoptosis Response Factor 4. *FEBS J* 2009; 276 (14); 3710-3728
47. Wang G, Silva J, Krishnamurthy K, Bieberich E. A novel isoform of prostate apoptosis response 4 (PAR-4) that co-distributes with F-actin and prevents apoptosis in neural stem cells. *Apoptosis* 2006; 11 (3); 315-325

48. Diaz-Meco MT, Municio MM, Frutos S, Sanchez P, Lozano J, Sanz L, Moscat J. The Product of par-4, a Gene Induced during Apoptosis, Interacts Selectively with the Atypical Isoforms of Protein Kinase C. *Cell* 1996; 86 (5); 777-786
49. Valmiki M, Ramos J. Death Effector Domain-Containing Proteins. *Cell Mol Life Sci* 2009; 66 (5); 814-830
50. El-Guendy N, Zhao Y, Gurumurthy S, Burikhanov R, Rangnekar VM. Identification of a Unique Core Domain of Par-4 Sufficient for Selective Apoptosis Induction in Cancer Cells. *Mol Cell Biol* 2003; 23 (16); 5516-5525
51. Altschul SF, Madden TL, Schaffer AA, Zhang J, Zhang Z, Miller W, Lipman DJ. Gapped BLAST and PSI-BLAST: a new generation of protein database search programs. *Nucleic Acids Res* 1997; 25 (17); 3389-3402
52. Thompson JD, Higgins DG, Gibson TJ. CLUSTAL W: improving the sensitivity of progressive multiple sequence alignment through sequence weighting, position-specific gap penalties and weight matrix choice. *Nucleic Acids Res* 1994; 22 (22); 4673-4680
53. Boosen M, Vetterkind S, Koplin A, Illenberger S, Preuss U. Par-4-mediated recruitment of Amida to the actin cytoskeleton leads to the induction of apoptosis. *Exp Cell Res* 2005; 311 (2); 177-191
54. Gao S, Wang H, Lee P, Melamed J, Li CX, Zhang F, Wu H, Zhou L, Wang Z. Androgen receptor and prostate apoptosis response factor-4 target the c-FLIP gene to determine survival and apoptosis in the prostate gland. *J Mol Endocrinol* 2006; 36 (3); 463-483
55. Sells SF, Han SS, Muthukkumar S, Maddiwar N, Johnstone R, Boghaert E, Gillis D, Liu G, Nair P, Monnig S, Collini P, Mattson MP, Sukhatme VP, Zimmer SG, Wood DP, Jr., McRoberts JW, Shi Y, Rangnekar VM. Expression and function of the leucine zipper protein Par-4 in apoptosis. *Mol Cell Biol* 1997; 17 (7); 3823-3832
56. Goswami A, Burikhanov R, de Thonel A, Fujita N, Goswami M, Zhao Y, Eriksson JE, Tsuruo T, Rangnekar VM. Binding and Phosphorylation of Par-4 by Akt Is Essential for Cancer Cell Survival. *Mol Cell* 2005; 20 (1); 33-44
57. Ranganathan P, Rangnekar VM. Regulation of Cancer Cell Survival by Par-4. *Ann N Y Acad Sci* 2005; 1059; 76-85
58. Anrather J, Csizmadia V, Soares MP, Winkler H. Regulation of NF-kB RelA Phosphorylation and Transcriptional Activity by p21ras and Protein Kinase Cζ in Primary Endothelial Cells. *J Biol Chem* 1999; 274 (19); 13594-13603
59. Chakraborty M, Qiu SG, Vasudevan KM, Rangnekar VM. Par-4 Drives Trafficking and Activation of Fas and FasL to Induce Prostate Cancer Cell Apoptosis and Tumor Regression. *Cancer Res* 2001; 61 (19); 7255-7263
60. Nalca A, Qiu SG, El-Guendy N, Krishnan S, Rangnekar VM. Oncogenic Ras Sensitizes Cells to Apoptosis by Par-4. *J Biol Chem* 1999; 274 (42); 29976-29983
61. Park HH, Wu H. Crystal Structure of RAIDD Death Domain Implicates Potential Mechanism of PIDDosome Assembly. *J Mol Biol* 2006; 357 (2); 358-364

62. Scott FL, Stec B, Pop C, Dobaczewska MK, Lee JJ, Monosov E, Robinson H, Salvesen GS, Schwarzenbacher R, Riedl SJ. The Fas-FADD death domain complex structure unravels signalling by receptor clustering. *Nature* 2009; 457 (7232); 1019-1022
63. Balducci L, Beghe C. Cancer and age in the USA. *Crit Rev Oncol Hematol* 2001; 37 (2); 137-145
64. Tyner SD, Venkatachalam S, Choi J, Jones S, Ghebranious N, Igelmann H, Lu X, Soron G, Cooper B, Brayton C, Hee Park S, Thompson T, Karsenty G, Bradley A, Donehower LA. p53 mutant mice that display early ageing-associated phenotypes. *Nature* 2002; 415 (6867); 45-53
65. Maier B, Gluba W, Bernier B, Turner T, Mohammad K, Guise T, Sutherland A, Thorner M, Scrable H. Modulation of mammalian life span by the short isoform of p53. *Genes Dev* 2004; 18 (3); 306-319
66. Zhao Y, Burikhanov R, Qiu S, Lele SM, Jennings CD, Bondada S, Spear B, Rangnekar VM. Cancer Resistance in Transgenic Mice Expressing the SAC Module of Par-4. *Cancer Res* 2007; 67 (19); 9276-9285
67. Levi-Montalcini R. The nerve growth factor: its mode of action on sensory and sympathetic nerve cells. *Harvey Lect* 1966; 60; 217-259
68. Kerr JF, Wyllie AH, Currie AR. Apoptosis: a basic biological phenomenon with wide-ranging implications in tissue kinetics. *Br J Cancer* 1972; 26 (239-257)
69. Dal Canto MC, Gurney ME. Development of central nervous system pathology in a murine transgenic model of human amyotrophic lateral sclerosis. *Am J Pathol* 1994; 145 (6); 1271-1279
70. Li J, Yuan J. Caspases in apoptosis and beyond. *Oncogene* 2008; 27 (48); 6194-6206
71. Jin Z, El-Deiry WS. Overview of cell death signaling pathways. *Cancer Biol Ther* 2005; 4 (2); 139-163
72. Fuentes-Prior P, Salvesen GS. The protein structures that shape caspase activity, specificity, activation and inhibition. *Biochem J* 2004; 384 (2); 201-232
73. Galvan V, Gorostiza OF, Banwait S, Ataie M, Logvinova AV, Sitaraman S, Carlson E, Sagi SA, Chevallier N, Jin K, Greenberg DA, Bredesen DE. Reversal of Alzheimer's-like pathology and behavior in human APP transgenic mice by mutation of Asp664. *Proc Natl Acad Sci USA* 2006; 103 (18); 7130-7135
74. Graham RK, Deng Y, Slow EJ, Haigh B, Bissada N, Lu G, Pearson J, Shehadeh J, Bertram L, Murphy Z, Warby SC, Doty CN, Roy S, Wellington CL, Leavitt BR, Raymond LA, Nicholson DW, Hayden MR. Cleavage at the caspase-6 site is required for neuronal dysfunction and degeneration due to mutant huntingtin. *Cell* 2006; 125 (6); 1179-1191
75. Burikhanov R, Zhao Y, Goswami A, Qiu S, Schwarze SR, Rangnekar VM. The Tumor Suppressor Par-4 Activates an Extrinsic Pathway for Apoptosis. *Cell* 2009; 138 (2); 377-388
76. Xiong ZG, Chu XP, Simon RP. Ca2+-Permeable Acid-sensing Ion Channels and Ischemic Brain Injury. *J Membr Biol* 2006; 209 (1); 59-68
77. Yang L, Mei Y, Xie Q, Han X, Zhang F, Gu L, Zhang Y, Chen Y, Li G, Gao Z. Acidification induces Bax translocation to the mitochondria and promotes ultraviolet light-induced apoptosis. *Cell Mol Biol Lett* 2008; 13 (1); 119-129

78. Matsuyama S, Llopis J, Deveraux QL, Tsien RY, Reed JC. Changes in intramitochondrial and cytosolic pH: early events that modulate caspase activation during apoptosis. *Nat Cell Biol* 2000; 2 (6); 318-325

79. Jochum W, Passegue E, Wagner EF. AP-1 in mouse development and tumorigenesis. *Oncogene* 2001; 20 (19); 2401-2412

80. de Thonel A, Bettaieb A, Jean C, Laurent G, Quillet-Mary A. Role of protein kinase C zeta isoform in Fas resistance of immature myeloid KG1a leukemic cells. *Blood* 2001; 98 (13); 3770-3777

81. Chen L-F, Greene WC. Shaping the nuclear action of NF-κB. *Nat Rev Mol Cell Biol* 2004; 5 (5); 392-401

82. Diaz-Meco MT, Lallena M-J, Monjas A, Frutos S, Moscat J. Inactivation of the Inhibitory kappa B Protein Kinase/Nuclear Factor kappa B Pathway by Par-4 Expression Potentiates Tumor Necrosis Factor alpha -induced Apoptosis. *J Biol Chem* 1999; 274 (28); 19606-19612

83. Pikarsky E, Porat RM, Stein I, Abramovitch R, Amit S, Kasem S, Gutkovich-Pyest E, Urieli-Shoval S, Galun E, Ben-Neriah Y. NF-kB functions as a tumour promoter in inflammation-associated cancer. *Nature* 2004; 431 (7007); 461-466

84. Sakurai H, Chiba H, Miyoshi H, Sugita T, Toriumi W. IkB Kinases Phosphorylate NF-kB p65 Subunit on Serine 536 in the Transactivation Domain. *J Biol Chem* 1999; 274 (43); 30353-30356

85. Leitges M, Sanz L, Martin P, Duran A, Braun U, GarcIa JF, Camacho F, Diaz-Meco MT, Rennert PD, Moscat J. Targeted Disruption of the ζPKC Gene Results in the Impairment of the NF-kB Pathway. *Mol Cell* 2001; 8 (4); 771-780

86. Moscat J, Diaz-Meco MT, Wooten MW. Of the atypical PKCs, Par-4 and p62: recent understandings of the biology and pathology of a PB1-dominated complex. *Cell Death Differ* 2009; 16 (11); 1426-1437

87. Sanchez P, De Carcer G, Sandoval IV, Moscat J, Diaz-Meco MT. Localization of Atypical Protein Kinase C Isoforms into Lysosome-Targeted Endosomes through Interaction with p62. *Mol Cell Biol* 1998; 18 (5); 3069-3080

88. Chang S, Kim JH, Shin J. p62 forms a ternary complex with PKCζ and PAR-4 and antagonizes PAR-4-induced PKCζ inhibition. *FEBS Lett* 2002; 510 (1-2); 57-61

89. Kawai T, Akira S, Reed JC. ZIP Kinase Triggers Apoptosis from Nuclear PML Oncogenic Domains. *Mol Cell Biol* 2003; 23 (17); 6174-6186

90. Boosen M, Vetterkind S, Kubicek J, Scheidtmann K-H, Illenberger S, Preuss U. Par-4 Is an Essential Downstream Target of DAP-like Kinase (Dlk) in Dlk/Par-4-mediated Apoptosis. *Mol Biol Cell* 2009; 20 (18); 4010-4020

91. Vetterkind S, Illenberger S, Kubicek J, Boosen M, Appel S, Naim HY, Scheidtmann K-H, Preuss U. Binding of Par-4 to the actin cytoskeleton is essential for Par-4/Dlk-mediated apoptosis. *Exp Cell Res* 2005; 305 (2); 392-408

92. Roussigne M, Cayrol C, Clouaire T, Amalric F, Girard J-P. THAP1 is a nuclear proapoptotic factor that links prostate-apoptosis-response-4 (Par-4) to PML nuclear bodies. *Oncogene* 2003; 22 (16); 2432-2442

93. Richard DJ, Schumacher V, Royer-Pokora B, Roberts SGE. Par4 is a coactivator for a splice isoform, specific transcriptional activation domain in WT1. *Genes Dev* 2001; 15 (3); 328-339

94. Cheema SK, Mishra SK, Rangnekar VM, Tari AM, Kumar R, Lopez-Berestein G. Par-4 Transcriptionally Regulates Bcl-2 through a WT1-binding Site on the bcl-2 Promoter. *J Biol Chem* 2003; 278 (22); 19995-20005

95. Qiu G, Ahmed M, Sells SF, Mohiuddin M, Weinstein MH, Rangnekar VM. Mutually exclusive expression patterns of Bcl-2 and Par-4 in human prostate tumors consistent with down-regulation of Bcl-2 by Par-4. *Oncogene* 1999; 18 (3); 623-631

96. Boehrer S, Chow KU, Beske F, Kukoc-Zivojnov N, Puccetti E, Ruthardt M, Baum C, Rangnekar VM, Hoelzer D, Mitrou PS, Weidmann E. In Lymphatic Cells Par-4 Sensitizes to Apoptosis by Down-Regulating Bcl-2 and Promoting Disruption of Mitochondrial Membrane Potential and Caspase Activation. *Cancer Res* 2002; 62 (6); 1768-1775

97. Lu C, Chen JQ, Zhou GP, Wu SH, Guan YF, Yuan CS. Multimolecular complex of Par-4 and E2F1 binding to Smac promoter contributes to glutamate-induced apoptosis in human- bone mesenchymal stem cells. *Nucleic Acids Res* 2008; 36 (15); 5021-5032

98. Goswami A, Qiu S, Dexheimer TS, Ranganathan P, Burikhanov R, Pommier Y, Rangnekar VM. Par-4 Binds to Topoisomerase 1 and Attenuates Its DNA Relaxation Activity. *Cancer Res* 2008; 68 (15); 6190-6198

99. Xie J, Guo Q. PAR-4 Is Involved in Regulation of β-Secretase Cleavage of the Alzheimer Amyloid Precursor Protein. *J Biol Chem* 2005; 280 (14); 13824-13832

100. Guo Q, Xie J, Chang X, Du H. Prostate apoptosis response-4 enhances secretion of amyloid beta peptide 1-42 in human neuroblastoma IMR-32 cells by a caspase-dependent pathway. *J Biol Chem* 2001; 276 (19); 16040-16044

101. Guo Q, Xie J. AATF Inhibits Aberrant Production of Amyloid β Peptide 1-42 by Interacting Directly with Par-4. *J Biol Chem* 2004; 279 (6); 4596-4603

102. Masters SL, Yao S, Willson TA, Zhang J-G, Palmer KR, Smith BJ, Babon JJ, Nicola NA, Norton RS, Nicholson SE. The SPRY domain of SSB-2 adopts a novel fold that presents conserved Par-4-binding residues. *Nat Struct Mol Biol* 2006; 13 (1); 77-84

103. Boehrer S, Kukoc-Zivojnov N, Nowak D, Bergmann M, Baum C, Puccetti E, Weidmann E, Hoelzer D, Mitrou PS, Chow KU. Upon Drug-Induced Apoptosis Expression of Prostate-apoptosis-response-gene-4 Promotes Cleavage of Caspase-8, Bid and Mitochondrial Release of Cytochrome c. *Hematol* 2004; 9 (5); 425-431

104. Liu J, Rost B. Comparing function and structure between entire proteomes. *Protein Sci* 2001; 10 (10); 1970-1979

105. Burkhard P, Stetefeld J, Strelkov SV. Coiled coils: a highly versatile protein folding motif. *Trends Cell Biol* 2001; 11 (2); 82-88

106. Mason JM, Arndt KM. Coiled Coil Domains: Stability, Specificity, and Biological Implications. *Chembiochem* 2004; 5 (2); 170-176

107. O'Shea EK, Klemm JD, Kim PS, Alber T. X-ray structure of the GCN4 leucine zipper, a two-stranded, parallel coiled coil. *Science* 1991; 254 (5031); 539-544

108. Junius FK, O'Donoghue SI, Nilges M, Weiss AS, King GF. High Resolution NMR Solution Structure of the Leucine Zipper Domain of the c-Jun Homodimer. *J Biol Chem* 1996; 271 (23); 13663-13667
109. Harbury PB, Zhang T, Kim PS, Alber T. A switch between two-, three-, and four-stranded coiled coils in GCN4 leucine zipper mutants. *Science* 1993; 262 (5138); 1401-1407
110. Kammerer RA, Kostrewa D, Zurdo J, Detken A, Garcia-Echeverria C, Green JD, Muller SA, Meier BH, Winkler FK, Dobson CM, Steinmetz MO. Exploring amyloid formation by a de novo design. *Proc Natl Acad Sci USA* 2004; 101 (13); 4435-4440
111. Deng Y, Liu J, Zheng Q, Eliezer D, Kallenbach NR, Lu M. Antiparallel Four-Stranded Coiled Coil Specified by a 3-3-1 Hydrophobic Heptad Repeat. *Structure* 2006; 14 (2); 247-255
112. Liu J, Deng Y, Zheng Q, Cheng C-S, Kallenbach NR, Lu M. A Parallel Coiled-Coil Tetramer with Offset Helices. *Biochemistry* 2006; 45 (51); 15224-15231
113. Liu J, Zheng Q, Deng Y, Kallenbach NR, Lu M. Conformational Transition between Four and Five-stranded Phenylalanine Zippers Determined by a Local Packing Interaction. *J Mol Biol* 2006; 361 (1); 168-179
114. Liu J, Zheng Q, Deng Y, Cheng C-S, Kallenbach NR, Lu M. A seven-helix coiled coil. *Proc Natl Acad Sci USA* 2006; 103 (42); 15457-15462
115. Rose A, Meier I. Scaffolds, levers, rods and springs: diverse cellular functions of long coiled-coil proteins. *Cell Mol Life Sci* 2004; 61 (16); 1996-2009
116. Rose A, Schraegle S, Stahlberg E, Meier I. Coiled-coil protein composition of 22 proteomes - differences and common themes in subcellular infrastructure and traffic control. *BMC Evol Biol* 2005; 5 (1); 66
117. Vinson C, Myakishev M, Acharya A, Mir AA, Moll JR, Bonovich M. Classification of Human B-ZIP Proteins Based on Dimerization Properties. *Mol Cell Biol* 2002; 22 (18); 6321-6335
118. Murre C, McCaw PS, Vaessin H, Caudy M, Jan LY, Jan YN, Cabrera CV, Buskin JN, Hauschka SD, Lassar AB, Weintraub H, Baltimore D. Interactions between heterologous helix-loop-helix proteins generate complexes that bind specifically to a common DNA sequence. *Cell* 1989; 58 (3); 537-544
119. Obrdlik P, Neuhaus G, Merkle T. Plant heterotrimeric G protein β subunit is associated with membranes via protein interactions involving coiled-coil formation. *FEBS Lett* 2000; 476 (3); 208-212
120. Moffett P, Farnham G, Peart J, Baulcombe DC. Interaction between domains of a plant NBS-LRR protein in disease resistance-related cell death. *EMBO J* 2002; 21 (17); 4511-4519
121. Wang Y, Gao R, Lynn DG. Ratcheting Up vir Gene Expression in Agrobacterium tumefaciens: Coiled Coils in Histidine Kinase Signal Transduction. *Chembiochem* 2002; 3 (4); 311-317
122. Strelkov SV, Hermann H, Aebi U. Molecular architecture of intermediate filaments. *Bioessays* 2003; 25 (3); 243-251
123. Kammerer RA. Alpha-helical coiled-coil oligomerization domains in extracellular proteins. *Matrix Biol* 1997; 15 (8-9); 555-565
124. Schliwa M, Woehlke G. Molecular motors. *Nature* 2003; 422 (6933); 759-765

125. Landschulz WH, Johnson PF, McKnight SL. The leucine zipper: a hypothetical structure common to a new class of DNA binding proteins. *Science* 1988; 240 (4860); 1759-1764

126. O'Shea EK, Rutkowski R, Kim PS. Evidence that the leucine zipper is a coiled coil. *Science* 1989; 243 (4890); 538-542

127. Moitra J, Szilak L, Krylov D, Vinson C. Leucine Is the Most Stabilizing Aliphatic Amino Acid in the d Position of a Dimeric Leucine Zipper Coiled Coil. *Biochemistry* 1997; 36 (41); 12567-12573

128. Grigoryan G, Keating AE. Structural specificity in coiled-coil interactions. *Curr Opin Struct Biol* 2008; 18 (4); 477-483

129. Acharya A, Rishi V, Vinson C. Stability of 100 Homo and Heterotypic Coiled-Coil a-a' Pairs for Ten Amino Acids (A, L, I, V, N, K, S, T, E, and R). *Biochemistry* 2006; 45 (38); 11324-11332

130. Lumb KJ, Kim PS. A Buried Polar Interaction Imparts Structural Uniqueness in a Designed Heterodimeric Coiled Coil. *Biochemistry* 1995; 34 (27); 8642-8648

131. Hartmann MD, Ridderbusch O, Zeth K, Albrecht R, Testa O, Woolfson DN, Sauer G, Dunin-Horkawicz S, Lupas AN, Alvarez BH. A coiled-coil motif that sequesters ions to the hydrophobic core. *Proc Natl Acad Sci USA* 2009; 106 (40); 16950-16955

132. McLachlan AD, Stewart M. Tropomyosin coiled-coil interactions: evidence for an unstaggered structure. *J Mol Biol* 1975; 98 (2); 293-304

133. Zhou NE, Kay CM, Hodges RS. The net energetic contribution of interhelical electrostatic attractions to coiled-coil stability. *Protein Eng* 1994; 7 (11); 1365-1372

134. Krylov D, Mikhailenko I, Vinson C. A thermodynamic scale for leucine zipper stability and dimerization specificity: e and g interhelical interactions. *EMBO J* 1994; 13 (12); 2849-2861

135. Bosshard HR, Marti DN, Jelesarov I. Protein stabilization by salt bridges: concepts, experimental approaches and clarification of some misunderstandings. *J Mol Recognit* 2004; 17 (1); 1-16

136. Kohn WD, Monera OD, Kay CM, Hodges RS. The Effects of Interhelical Electrostatic Repulsions between Glutamic Acid Residues in Controlling the Dimerization and Stability of Two-stranded alpha-Helical Coiled-coils. *J Biol Chem* 1995; 270 (43); 25495-25506

137. Yadav MK, Leman LJ, Price DJ, Brooks CL, Stout CD, Ghadiri MR. Coiled Coils at the Edge of Configurational Heterogeneity. Structural Analyses of Parallel and Antiparallel Homotetrameric Coiled Coils Reveal Configurational Sensitivity to a Single Solvent-Exposed Amino Acid Substitution. *Biochemistry* 2006; 45 (14); 4463-4473

138. Wendt H, Berger C, Baici A, Thomas RM, Bosshard HR. Kinetics of Folding of Leucine Zipper Domains. *Biochemistry* 1995; 34 (12); 4097-4107

139. Jelesarov I, Durr E, Thomas RM, Bosshard HR. Salt Effects on Hydrophobic Interaction and Charge Screening in the Folding of a Negatively Charged Peptide to a Coiled Coil (Leucine Zipper). *Biochemistry* 1998; 37 (20); 7539-7550

140. Buck M. Trifluoroethanol and colleagues: cosolvents come of age. Recent studies with peptides and proteins. *Q Rev Biophys* 1998; 31; 297-355

141. Cooper TM, Woody RW. The effect of conformation on the CD of interacting helices: a theoretical study of tropomyosin. *Biopolymers* 1990; 30 (7-8); 657-676

142. Su JY, Hodges RS, Kay CM. Effect of Chain Length on the Formation and Stability of Synthetic .alpha.-Helical Coiled Coils. *Biochemistry* 1994; 33 (51); 15501-15510
143. Uversky VN, Oldfield CJ, Dunker AK. Intrinsically Disordered Proteins in Human Diseases: Introducing the D2 Concept. *Annu Rev Biophys* 2008; 37 (1); 215
144. Dunker AK, Lawson JD, Brown CJ, Williams RM, Romero P, Oh JS, Oldfield CJ, Campen AM, Ratliff CM, Hipps KW, Ausio J, Nissen MS, Reeves R, Kang C, Kissinger CR, Bailey RW, Griswold MD, Chiu W, Garner EC, Obradovic Z. Intrinsically disordered protein. *J Mol Graph Model* 2001; 19 (1); 26-59
145. Uversky VN. Natively unfolded proteins: A point where biology waits for physics. *Protein Sci* 2002; 11 (4); 739-756
146. Galea CA, Wang Y, Sivakolundu SG, Kriwacki RW. Regulation of Cell Division by Intrinsically Unstructured Proteins: Intrinsic Flexibility, Modularity, and Signaling Conduits. *Biochemistry* 2008; 47 (29); 7598-7609
147. Iakoucheva LM, Brown CJ, Lawson JD, Obradovic Z, Dunker AK. Intrinsic Disorder in Cell-signaling and Cancer-associated Proteins. *J Mol Biol* 2002; 323 (3); 573-584
148. Hartwell LH, Kastan MB. Cell cycle control and cancer. *Science* 1994; 266 (5192); 1821-1828
149. Uversky VN, Fink AL. Conformational constraints for amyloid fibrillation: the importance of being unfolded. *Biochim Biophys Acta* 2004; 1698 (2); 131-153
150. Eliezer D. Biophysical characterization of intrinsically disordered proteins. *Curr Opin Struct Biol* 2009; 19 (1); 23-30
151. Dunker AK, Obradovic Z, Romero P, Garner EC, Brown CJ. Intrinsic protein disorder in complete genomes. *Genome Inform Ser Workshop Genome Inform* 2000; 11; 161-171
152. Oldfield CJ, Cheng Y, Cortese MS, Romero P, Uversky VN, Dunker AK. Coupled Folding and Binding with α-Helix-Forming Molecular Recognition Elements. *Biochemistry* 2005; 44 (37); 12454-12470
153. Romero P, Obradovic Z, Li X, Garner EC, Brown CJ, Dunker AK. Sequence complexity of disordered protein. *Proteins* 2001; 42 (1); 38-48
154. Rucker AL, Creamer TP. Polyproline II helical structure in protein unfolded states: Lysine peptides revisited. *Protein Sci* 2002; 11 (4); 980-985
155. Receveur-Brechot V, Bourhis J-M, Uversky VN, Canard B, Longhi S. Assessing protein disorder and induced folding. *Proteins* 2006; 62 (1); 24-45
156. Ayed A, Mulder FAA, Yi G-S, Lu Y, Kay LE, Arrowsmith CH. Latent and active p53 are identical in conformation. *Nat Struct Mol Biol* 2001; 8 (9); 756-760
157. Wriggers W, Mehler E, Pitici F, Weinstein H, Schulten K. Structure and Dynamics of Calmodulin in Solution. *Biophys J* 1998; 74 (4); 1622-1639
158. Cheng EHY, Kirsch DG, Clem RJ, Ravi R, Kastan MB, Bedi A, Ueno K, Hardwick JM. Conversion of Bcl-2 to a Bax-like Death Effector by Caspases. *Science* 1997; 278 (5345); 1966-1968

159. Clem RJ, Cheng EHY, Karp CL, Kirsch DG, Ueno K, Takahashi A, Kastan MB, Griffin DE, Earnshaw WC, Veliuona MA, Hardwick JM. Modulation of cell death by Bcl-xL through caspase interaction. *Proc Natl Acad Sci USA* 1998; 95 (2); 554-559

160. Chang BS, Minn AJ, Muchmore SW, Fesik SW, Thompson CB. Identification of a novel regulatory domain in Bcl-xL and Bcl-2. *EMBO J* 1997; 16 (5); 968-977

161. Yamamoto K, Ichijo H, Korsmeyer SJ. BCL-2 Is Phosphorylated and Inactivated by an ASK1/Jun N-Terminal Protein Kinase Pathway Normally Activated at G2/M. *Mol Cell Biol* 1999; 19 (12); 8469-8478

162. Trombitas K, Greaser M, Labeit S, Jin J-P, Kellermayer M, Helmes M, Granzier H. Titin Extensibility In Situ: Entropic Elasticity of Permanently Folded and Permanently Unfolded Molecular Segments. *J Cell Biol* 1998; 140 (4); 853-859

163. Polverini E, Fasano A, Zito F, Riccio P, Cavatorta P. Conformation of bovine myelin basic protein purified with bound lipids. *Eur Biophys J* 1999; 28 (4); 351-355

164. He Z, Dunker AK, Wesson CR, Trumble WR. Ca(2+)-induced folding and aggregation of skeletal muscle sarcoplasmic reticulum calsequestrin. The involvement of the trifluoperazine-binding site. *J Biol Chem* 1993; 268 (33); 24635-24641

165. Craig TA, Veenstra TD, Naylor S, Tomlinson AJ, Johnson KL, Macura S, Juranic N, Kumar R. Zinc Binding Properties of the DNA Binding Domain of the 1,25-Dihydroxyvitamin D3 Receptor. *Biochemistry* 1997; 36 (34); 10482-10491

166. Meszaros B, Tompa P, Simon I, Dosztanyi Z. Molecular Principles of the Interactions of Disordered Proteins. *J Mol Biol* 2007; 372 (2); 549-561

167. Kriwacki RW, Hengst L, Tennant L, Reed SI, Wright PE. Structural studies of p21Waf1/Cip1/ Sdi1 in the free and Cdk2-bound state: conformational disorder mediates binding diversity. *Proc Natl Acad Sci USA* 1996; 93 (21); 11504-11509

168. Yusupov MM, Yusupova GZ, Baucom A, Lieberman K, Earnest TN, Cate JHD, Noller HF. Crystal Structure of the Ribosome at 5.5 A Resolution. *Science* 2001; 292 (5518); 883-896

169. Lewis M, Chang G, Horton NC, Kercher MA, Pace HC, Schumacher MA, Brennan RG, Lu P. Crystal Structure of the Lactose Operon Repressor and Its Complexes with DNA and Inducer. *Science* 1996; 271 (5253); 1247-1254

170. Slijper M, Boelens R, Davis AL, Konings RNH, van der Marel GA, van Boom JH, Kaptein R. Backbone and Side Chain Dynamics of lac Repressor Headpiece (1-56) and Its Complex with DNA. *Biochemistry* 1997; 36 (1); 249-254

171. Grimmler M, Wang Y, Mund T, Cilensek Z, Keidel E-M, Waddell MB, Jäkel H, Kullmann M, Kriwacki RW, Hengst L. Cdk-Inhibitory Activity and Stability of p27Kip1 Are Directly Regulated by Oncogenic Tyrosine Kinases. *Cell* 2007; 128 (2); 269-280

172. Shoemaker BA, Portman JJ, Wolynes PG. Speeding molecular recognition by using the folding funnel: The fly-casting mechanism. *Proc Natl Acad Sci USA* 2000; 97 (16); 8868-8873

173. Dunker AK, Cortese MS, Romero P, Iakoucheva LM, Uversky VN. Flexible nets. *FEBS J* 2005; 272 (20); 5129-5148

174. Schnell S, Fortunato S, Roy S. Is the intrinsic disorder of proteins the cause of the scale-free architecture of protein-protein interaction networks? *Proteomics* 2007; 7 (6); 961-964

175. Kim PM, Sboner A, Xia Y, Gerstein M. The role of disorder in interaction networks: a structural analysis. *Mol Syst Biol* 2008; 4; 179

176. Mittag T, Forman-Kay JD. Atomic-level characterization of disordered protein ensembles. *Curr Opin Struct Biol* 2007; 17 (1); 3-14

177. Li X, Romero P, Rani M, Dunker AK, Obradovic Z. Predicting Protein Disorder for N-, C- and Internal Regions. *Genome Inform Ser Workshop Genome Inform* 1999; 10; 30-40

178. Linding R, Jensen LJ, Diella F, Bork P, Gibson TJ, Russell RB. Protein Disorder Prediction: Implications for Structural Proteomics. *Structure* 2003; 11 (11); 1453-1459

179. Callebaut I, Labesse G, Durand P, Poupon A, Canard L, Chomilier J, Henrissat B, Mornon JP. Deciphering protein sequence information through hydrophobic cluster analysis (HCA): current status and perspectives. *Cell Mol Life Sci* 1997; 53 (8); 621-645

180. Uversky VN, Gillespie JR, Fink AL. Why are"natively unfolded" proteins unstructured under physiologic conditions? *Proteins* 2000; 41 (3); 415-427

181. Uversky VN. What does it mean to be natively unfolded? *Eur J Biochem* 2002; 269 (1); 2-12

182. Kelly SM, Jess TJ, Price NC. How to study proteins by circular dichroism. *Biochim Biophys Acta* 2005; 1751 (2); 119-139

183. Cavanagh J, Fairbrother WJ, Palmer AG, III, Skelton NJ, Rance M. Protein NMR spectroscopy: principles and practice - 2nd edn. Elsevier Academic Press, Amsterdam, Boston 2007; 702-704

184. Dutta K, Alexandrov A, Huang H, Pascal SM. pH-induced folding of an apoptotic coiled coil. *Protein Sci* 2001; 10 (12); 2531-2540

185. Dutta K, Engler FA, Cotton L, Alexandrov A, Bedi GS, Colquhoun J, Pascal SM. Stabilization of a pH-sensitive apoptosis-linked coiled coil through single point mutations. *Protein Sci* 2003; 12 (2); 257-265

186. Sambrook J, Fritsch EF, Maniatis T. Molecular cloning: a laboratory manual - 2nd edn. Cold Spring Harbor Laboratory Press, Plainview, New York, USA 1989.

187. Alexandrov A, Dutta K, Pascal SM. MBP fusion protein with a viral protease cleavage site: one-step cleavage/purification of insoluble proteins. *Biotechniques* 2001; 30 (6); 1194-1198

188. Staunton D, Schlinkert R, Zanetti G, Colebrook SA, Campbell ID. Cell-free expression and selective isotope labelling in protein NMR. *Magn Reson Chem* 2006; 44 (S1); S2-S9.

189. Shekhtman A, Ghose R, Goger M, Cowburn D. NMR structure determination and investigation using a reduced proton (REDPRO) labeling strategy for proteins. *FEBS Lett* 2002; 524 (1-3); 177-182

190. Scopes RK. Measurement of protein by spectrophotometry at 205 nm. *Anal Biochem* 1974; 59 (1); 277-282

191. Smith PK, Krohn RI, Hermanson GT, Mallia AK, Gartner FH, Provenzano MD, Fujimoto EK, Goeke NM, Olson BJ, Klenk DC. Measurement of protein using bicinchoninic acid. *Anal Biochem* 1985; 150 (1); 76-85

192. Schägger H, von Jagow G. Tricine-sodium dodecyl sulfate-polyacrylamide gel electrophoresis for the separation of proteins in the range from 1 to 100 kDa. *Anal Biochem* 1987; 166 (2); 368-379
193. Tompa P. Intrinsically unstructured proteins. *Trends Biochem Sci* 2002; 27 (10); 527-533
194. Dyson HJ, Wright PE. Intrinsically unstructured proteins and their functions. *Nat Rev Mol Cell Biol* 2005; 6 (3); 197-208
195. Uversky VN, Oldfield CJ, Dunker AK. Showing your ID: intrinsic disorder as an ID for recognition, regulation and cell signaling. *J Mol Recognit* 2005; 18 (5); 343-384
196. Garnier J, Gibrat JF, Robson B. GOR method for predicting protein secondary structure from amino acid sequence. *Computer Methods for Macromolecular Sequence Analysis* 1996; 266; 540-553
197. Demarest SJ, Martinez-Yamout M, Chung J, Chen H, Xu W, Dyson HJ, Evans RM, Wright PE. Mutual synergistic folding in recruitment of CBP/p300 by p160 nuclear receptor coactivators. *Nature* 2002; 415 (6871); 549-553
198. Richards JP, Bachinger HP, Goodman RH, Brennan RG. Analysis of the Structural Properties of cAMP-responsive Element-binding Protein (CREB) and Phosphorylated CREB. *J Biol Chem* 1996; 271 (23); 13716-13723
199. Radhakrishnan I, Perez-Alvarado GC, Parker D, Dyson HJ, Montminy MR, Wright PE. Solution Structure of the KIX Domain of CBP Bound to the Transactivation Domain of CREB: A Model for Activator:Coactivator Interactions. *Cell* 1997; 91 (6); 741-752
200. Hamiaux C, Perez J, Prange T, Veesler S, Ries-Kautt M, Vachette P. The BPTI decamer observed in acidic pH crystal forms pre-exists as a stable species in solution. *J Mol Biol* 2000; 297 (3); 697-712
201. Kabsch W, Mannherz HG, Suck D, Pai EF, Holmes KC. Atomic structure of the actin: DNase I complex. *Nature* 1990; 347 (6288); 37-44
202. Vijay-Kumar S, Bugg CE, Cook WJ. Structure of ubiquitin refined at 1.8 Å resolution. *J Mol Biol* 1987; 194 (3); 531-544
203. Matthews DA, Dragovich PS, Webber SE, Fuhrman SA, Patick AK, Zalman LS, Hendrickson TF, Love RA, Prins TJ, Marakovits JT, Zhou R, Tikhe J, Ford CE, Meador JW, Ferre RA, Brown EL, Binford SL, Brothers MA, DeLisle DM, Worland ST. Structure-assisted design of mechanism-based irreversible inhibitors of human rhinovirus 3C protease with potent antiviral activity against multiple rhinovirus serotypes. *Proc Natl Acad Sci USA* 1999; 96 (20); 11000-11007
204. Hu CC, Ghabrial SA. The conserved, hydrophilic and arginine-rich N-terminal domain of cucumovirus coat proteins contributes to their anomalous electrophoretic mobilities in sodium dodecylsulfate-polyacrylamide gels. *J Virol Methods* 1995; 55 (3); 367-379
205. Uversky VN. Use of fast protein size-exclusion liquid chromatography to study the unfolding of proteins which denature through the molten globule. *Biochemistry* 1993; 32 (48); 13288-13298
206. Tcherkasskaya O, Uversky VN. Denatured collapsed states in protein folding: Example of apomyoglobin. *Proteins* 2001; 44 (3); 244-254

207. Grzela R, Szolajska E, Ebel C, Madern D, Favier A, Wojtal I, Zagorski W, Chroboczek J. Virulence Factor of Potato Virus Y, Genome-attached Terminal Protein VPg, Is a Highly Disordered Protein. *J Biol Chem* 2008; 283 (1); 213-221

208. Spolaore B, Bermejo R, Zambonin M, Fontana A. Protein Interactions Leading to Conformational Changes Monitored by Limited Proteolysis: Apo Form and Fragments of Horse Cytochrome c. *Biochemistry* 2001; 40 (32); 9460-9468

209. Hubbard SJ. The structural aspects of limited proteolysis of native proteins. *Biochim Biophys Acta* 1998; 1382 (2); 191-206

210. Lacy ER, Wang Y, Post J, Nourse A, Webb W, Mapelli M, Musacchio A, Siuzdak G, Kriwacki RW. Molecular Basis for the Specificity of p27 Toward Cyclin-dependent Kinases that Regulate Cell Division. *J Mol Biol* 2005; 349 (4); 764-773

211. Batra-Safferling R, Abarca-Heidemann K, Korschen HG, Tziatzios C, Stoldt M, Budyak I, Willbold D, Schwalbe H, Klein-Seetharaman J, Kaupp UB. Glutamic Acid-rich Proteins of Rod Photoreceptors Are Natively Unfolded. *J Biol Chem* 2006; 281 (3); 1449-1460

212. De Biasio A, Guarnaccia C, Popovic M, Uversky VN, Pintar A, Pongor S. Prevalence of Intrinsic Disorder in the Intracellular Region of Human Single-Pass Type I Proteins: The Case of the Notch Ligand Delta-4. *J Proteome Res* 2008; 7 (6); 2496-2506

213. Provencher SW, Gloeckner J. Estimation of globular protein secondary structure from circular dichroism. *Biochemistry* 1981; 20 (1); 33-37

214. Whitmore L, Wallace BA. DICHROWEB, an online server for protein secondary structure analyses from circular dichroism spectroscopic data. *Nucleic Acids Res* 2004; 32; W668-673

215. Whitmore L, Wallace BA. Protein secondary structure analyses from circular dichroism spectroscopy: Methods and reference databases. *Biopolymers* 2008; 89 (5); 392-400

216. Wishart DS, Bigam CG, Yao J, Abildgaard F, Dyson HJ, Oldfield E, Markley JL, Sykes BD. 1H, 13C and 15N chemical shift referencing in biomolecular NMR. *J Biomol NMR* 1995; 6 (2); 135-140

217. Shi Z, Woody RW, Kallenbach NR, George DR. Is polyproline II a major backbone conformation in unfolded proteins? *Adv Protein Chem* 2002; 62; 163-240

218. Sreerama N, Venyaminov SYU, Woody RW. Estimation of the number of alpha-helical and beta-strand segments in proteins using circular dichroism spectroscopy. *Protein Science* 1999; 8 (2); 370-380

219. Dyson HJ, Wright PE. Elucidation of the protein folding landscape by NMR. *Methods Enzymol* 2005; 394; 299-321

220. Dyson HJ, Wright PE. Nuclear magnetic resonance methods for elucidation of structure and dynamics in disordered states. *Methods Enzymol* 2001; 339; 258-270

221. Dyson HJ, Wright PE. Unfolded Proteins and Protein Folding Studied by NMR. *Chem Rev* 2004; 104 (8); 3607-3622

222. Dyson HJ, Wright PE. Insights into the structure and dynamics of unfolded proteins from nuclear magnetic resonance. *Adv Protein Chem* 2002; 62; 311-340

223. Olofsson S, Baltzer L. Structure and dynamics of a designed helix-loop-helix dimer in dilute aqueous trifluoroethanol solution. A strategy for NMR spectroscopic structure determination of molten globules in the rational design of native proteins. *Fold Des* 1996; 1 (5); 347-356

224. Luo P, Baldwin RL. Mechanism of Helix Induction by Trifluoroethanol: A Framework for Extrapolating the Helix-Forming Properties of Peptides from Trifluoroethanol/Water Mixtures Back to Water. *Biochemistry* 1997; 36 (27); 8413-8421

225. Schanda P, Brutscher B. Very Fast Two-Dimensional NMR Spectroscopy for Real-Time Investigation of Dynamic Events in Proteins on the Time Scale of Seconds. *J Am Chem Soc* 2005; 127 (22); 8014-8015

226. Bada M, Walther D, Arcangioli B, Doniach S, Delarue M. Solution structural studies and low-resolution model of the Schizosaccharomyces pombe sap1 protein. *J Mol Biol* 2000; 300 (3); 563-574

227. Mosley CA, Taupenot L, Biswas N, Taulane JP, Olson NH, Vaingankar SM, Wen G, Schork NJ, Ziegler MG, Mahata SK, O'Connor DT. Biogenesis of the Secretory Granule: Chromogranin A Coiled-Coil Structure Results in Unusual Physical Properties and Suggests a Mechanism for Granule Core Condensation. *Biochemistry* 2007; 46 (38); 10999-11012

228. Marshall CB, Chakrabartty A, Davies PL. Hyperactive Antifreeze Protein from Winter Flounder Is a Very Long Rod-like Dimer of alpha-Helices. *J Biol Chem* 2005; 280 (18); 17920-17929

229. Wang X, Graveland-Bikker JF, De Kruif CG, Robillard GT. Oligomerization of hydrophobin SC3 in solution: From soluble state to self-assembly. *Protein Sci* 2004; 13 (3); 810-821

230. Liew CK, Gamsjaeger R, Mansfield RE, Mackay JP. NMR spectroscopy as a tool for the rapid assessment of the conformation of GST-fusion proteins. *Protein Sci* 2008; 17 (9); 1630-1635

231. Xie H, Vucetic S, Iakoucheva LM, Oldfield CJ, Dunker AK, Obradovic Z, Uversky VN. Functional Anthology of Intrinsic Disorder. 3. Ligands, Post-Translational Modifications, and Diseases Associated with Intrinsically Disordered Proteins. *J Proteome Res* 2007; 6 (5); 1917-1932

232. Wright PE, Dyson HJ. Intrinsically unstructured proteins: re-assessing the protein structure-function paradigm. *J Mol Biol* 1999; 293 (2); 321-331

233. Romero PR, Zaidi S, Fang YY, Uversky VN, Radivojac P, Oldfield CJ, Cortese MS, Sickmeier M, LeGall T, Obradovic Z, Dunker AK. Alternative splicing in concert with protein intrinsic disorder enables increased functional diversity in multicellular organisms. *Proc Natl Acad Sci USA* 2006; 103 (22); 8390-8395

234. Adzhubei AA, Sternberg MJE. Left-handed Polyproline II Helices Commonly Occur in Globular Proteins. *J Mol Biol* 1993; 229 (2); 472-493

235. Williamson MP. The structure and function of proline-rich regions in proteins. *Biochem J* 1994; 297 (2); 249-240

236. Reeves R. Chromatin changes during the cell cycle. *Curr Opin Cell Biol* 1992; 4 (3); 413-423

237. Reeves R, Beckerbauer L. HMGI/Y proteins: flexible regulators of transcription and chromatin structure. *Biochim Biophys Acta* 2001; 1519 (1-2); 13-29

238. Lupas A, Van Dyke M, Stock J. Predicting Coled Coils from Protein Sequences. *Science* 1991; 252; 1162-1164

239. Guex N, Peitsch MC. SWISS-MODEL and the Swiss-PdbViewer: an environment for comparative protein modeling. *Electrophoresis* 1997; 18 (15); 2714-2723

240. Meier M, Burkhard P. Statistical analysis of intrahelical ionic interactions in alpha-helices and coiled coils. *J Struct Biol* 2006; 155 (2); 116-129

241. Jiang B, Guo T, Peng L-W, Sun Z-R. Folding type-specific secondary structure propensities of amino acids, derived from α-helical, β-sheet, α/β, and α+β proteins of known structures. *Biopolymers* 1998; 45 (1); 35-49

242. Knappenberger JA, Smith JE, Thorpe SH, Zitzewitz JA, Matthews CR. A Buried Polar Residue in the Hydrophobic Interface of the Coiled-coil Peptide, GCN4-p1, Plays a Thermodynamic, not a Kinetic Role in Folding. *J Mol Biol* 2002; 321 (1); 1-6

243. Zhu H, Celinski SA, Scholtz JM, Hu JC. The contribution of buried polar groups to the conformational stability of the GCN4 coiled coil. *J Mol Biol* 2000; 300 (5); 1377-1387

244. Wyatt PJ. Light scattering and the absolute characterization of macromolecules. *Anal Chim Acta* 1993; 272 (1); 1-40

245. Roy I, Gupta MN. Freeze-drying of proteins: some emerging concerns. *Biotechnol Appl Biochem* 2004; 39 (Pt 2); 165-177

246. Junius FK, Mackay JP, Bubb WA, Jensen SA, Weiss AS, King GF. Nuclear Magnetic Resonance Characterization of the Jun Leucine Zipper Domain: Unusual Properties of Coiled-Coil Interfacial Polar Residues. *Biochemistry* 1995; 34 (18); 6164-6174

247. Tai L-J, McFall SM, Huang K, Demeler B, Fox SG, Brubaker K, Radhakrishnan I, Morimoto RI. Structure-Function Analysis of the Heat Shock Factor-binding Protein Reveals a Protein Composed Solely of a Highly Conserved and Dynamic Coiled-coil Trimerization Domain. *J Biol Chem* 2002; 277 (1); 735-745

248. Wilkins DK, Grimshaw SB, Receveur V, Dobson CM, Jones JA, Smith LJ. Hydrodynamic Radii of Native and Denatured Proteins Measured by Pulse Field Gradient NMR Techniques. *Biochemistry* 1999; 38 (50); 16424-16431

249. Masson S, Kern T, Le Goullec A, Giustini C, Simorre J-P, Callow P, Vernet T, Gabel F, Zapun A. Central Domain of DivIB Caps the C-terminal Regions of the FtsL/DivIC Coiled-coil Rod. *J Biol Chem* 2009; 284 (40); 27687-27700

250. Rahaman A, Srinivasan N, Shamala N, Subbarao Shaila M. Phosphoprotein of the Rinderpest Virus Forms a Tetramer through a Coiled Coil Region Important for Biological Function: A STRUCTURAL INSIGHT. *J Biol Chem* 2004; 279 (22); 23606-23614

251. Delaglio F, Grzesiek S, Vuister GW, Zhu G, Pfeifer J, Bax A. NMRPipe: A multidimensional spectral processing system based on UNIX pipes. *J Biomol NMR* 1995; 6 (3); 277-293

252. Johnson BA, Blevins RA. NMR View: A computer program for the visualization and analysis of NMR data. *J Biomol NMR* 1994; 4 (5); 603-614

253. Wishart DS, Sykes BD. The 13C Chemical-Shift Index: A simple method for the identification of protein secondary structure using 13C chemical-shift data. *J Biomol NMR* 1994; 4 (2); 171-180

254. Schwarzinger S, Kroon GJA, Foss TR, Chung J, Wright PE, Dyson HJ. Sequence-Dependent Correction of Random Coil NMR Chemical Shifts. *J Am Chem Soc* 2001; 123 (13); 2970-2978

255. Farrow NA, Muhandiram R, Singer AU, Pascal SM, Kay CM, Gish G, Shoelson SE, Pawson T, Forman-Kay JD, Kay LE. Backbone Dynamics of a Free and a Phosphopeptide-Complexed Src Homology 2 Domain Studied by 15N NMR Relaxation. *Biochemistry* 1994; 33 (19); 5984-6003

256. Vuister GW, Bax A. Quantitative J correlation: a new approach for measuring homonuclear three-bond J(HNH.alpha.) coupling constants in 15N-enriched proteins. *J Am Chem Soc* 1993; 115 (17); 7772-7777

257. Pelupessy P, Espallargas GM, Bodenhausen G. Symmetrical reconversion: measuring cross-correlation rates with enhanced accuracy. *J Magn Reson* 2003; 161 (2); 258-264

258. Vranken WF, Boucher W, Stevens TJ, Fogh RH, Pajon A, Llinas M, Ulrich EL, Markley JL, Ionides J, Laue ED. The CCPN data model for NMR spectroscopy: Development of a software pipeline. *Proteins* 2005; 59 (4); 687-696

259. Kammerer RA, Schulthess T, Landwehr R, Lustig A, Engel J, Aebi U, Steinmetz MO. An autonomous folding unit mediates the assembly of two-stranded coiled coils. *Proc Natl Acad Sci USA* 1998; 95 (23); 13419-13424

260. Steinmetz MO, Stock A, Schulthess T, Landwehr R, Lustig A, Faix J, Gerisch G, Aebi U, Kammerer RA. A distinct 14 residue site triggers coiled-coil formation in cortexillin I. *EMBO J* 1998; 17 (7); 1883-1891

261. Kammerer RA, Jaravine VA, Frank S, Schulthess T, Landwehr R, Lustig A, Garcia-Echeverria C, Alexandrescu AT, Engel J, Steinmetz MO. An Intrahelical Salt Bridge within the Trigger Site Stabilizes the GCN4 Leucine Zipper. *J Biol Chem* 2001; 276 (17); 13685-13688

262. Mackay JP, Shaw GL, King GF. Backbone Dynamics of the c-Jun Leucine Zipper: 15N NMR Relaxation Studies. *Biochemistry* 1996; 35 (15); 4867-4877

263. Lacy ER, Filippov I, Lewis WS, Otieno S, Xiao L, Weiss S, Hengst L, Kriwacki RW. p27 binds cyclin-CDK complexes through a sequential mechanism involving binding-induced protein folding. *Nat Struct Mol Biol* 2004; 11 (4); 358-364

264. Wei J, Liu Y, Bose K, Henry GD, Baleja JD. Disorder and Structure in the Rab11 Binding Domain of Rab11 Family Interacting Protein 2. *Biochemistry* 2009; 48 (3); 549-557

265. Wang Y, Boudreaux DM, Estrada DF, Egan CW, St. Jeor SC, De Guzman RN. NMR Structure of the N-terminal Coiled Coil Domain of the Andes Hantavirus Nucleocapsid Protein. *J Biol Chem* 2008; 283 (42); 28297-28304

266. Nikolaev Y, Pervushin K. NMR Spin State Exchange Spectroscopy Reveals Equilibrium of Two Distinct Conformations of Leucine Zipper GCN4 in Solution. *J Am Chem Soc* 2007; 129 (20); 6461-6469

267. Sreerama N, Woody RW. A Self-Consistent Method for the Analysis of Protein Secondary Structure from Circular Dichroism. *Anal Biochem* 1993; 209 (1); 32-44

268. MacPhee CE, Perugini MA, H. Sawyer W, Howlett GJ. Trifluoroethanol induces the self-association of specific amphipathic peptides. *FEBS Lett* 1997; 416 (3); 265-268

269. Zhou NE, Zhu BY, Sykes BD, Hodges RS. Relationship between amide proton chemical shifts and hydrogen bonding in amphipathic alpha-helical peptides. *J Am Chem Soc* 1992; 114 (11); 4320-4326

270. Yao S, Howlett GJ, Norton RS. Peptide self-association in aqueous trifluoroethanol monitored by pulsed field gradient NMR diffusion measurements. *J Biomol NMR* 2000; 16 (2); 109-119

271. Kunjithapatham R, Oliva FY, Doshi U, Perez M, Avila J, Munoz V. Role for the α-Helix in Aberrant Protein Aggregation. *Biochemistry* 2005; 44 (1); 149-156

272. Heitlinger E, Peter M, Haner M, Lustig A, Aebi U, Nigg EA. Expression of chicken lamin B2 in Escherichia coli: characterization of its structure, assembly, and molecular interactions. *J Cell Biol* 1991; 113 (3); 485-495

273. McKnight SL. Molecular zippers in gene regulation. *Sci Am* 1991; 264 (4); 54

274. Alber T. Structure of the leucine zipper. *Curr Opin Genet Dev* 1992; 2 (2); 205-210

275. Isabet T, Montagnac G, Regazzoni K, Raynal B, Khadali FE, England P, Franco M, Chavrier P, Houdusse A, Menetrey J. The structural basis of Arf effector specificity: the crystal structure of ARF6 in a complex with JIP4. *EMBO J* 2009; 28 (18); 2835-2845

276. Yoshikawa A, Sato Y, Yamashita M, Mimura H, Yamagata A, Fukai S. Crystal structure of the NEMO ubiquitin-binding domain in complex with Lys 63-linked di-ubiquitin. *FEBS Lett* 2009; 583 (20); 3317-3322

277. Sibanda BL, Critchlow SE, Begun J, Pei XY, Jackson SP, Blundell TL, Pellegrini L. Crystal structure of an Xrcc4-DNA ligase IV complex. *Nat Struct Mol Biol* 2001; 8 (12); 1015-1019

278. Szilak L, Moitra J, Krylov D, Vinson C. Phosphorylation destabilizes alpha-helices. *Nat Struct Mol Biol* 1997; 4 (2); 112-114

279. Szilak L, Moitra J, Vinson C. Design of a leucine zipper coiled coil stabilized 1.4 kcal mol-1 by phosphorylation of a serine in the e position. *Protein Sci* 1997; 6 (6); 1273-1283

280. Inomata K, Ohno A, Tochio H, Isogai S, Tenno T, Nakase I, Takeuchi T, Futaki S, Ito Y, Hiroaki H, Shirakawa M. High-resolution multi-dimensional NMR spectroscopy of proteins in human cells. *Nature* 2009; 458 (7234); 106-109

281. Heimburg T, Schunemann J, Weber K, Geisler N. FTIR-Spectroscopy of Multistranded Coiled Coil Proteins. *Biochemistry* 1999; 38 (39); 12727-12734